UNCLASSIFIED

AD NUMBER
AD868194

LIMITATION CHANGES

TO:

Approved for public release; distribution is unlimited.

FROM:

Distribution authorized to DoD only; Administrative/Operational Use; MAR 1970. Other requests shall be referred to Air Force Cambridge Research Laboratory, CRO, Hanscom AFB, MA 01730.

AUTHORITY

afcrl ltr, 19 mar 1974

THIS PAGE IS UNCLASSIFIED

AFCRL-69-0552

ATMOSPHERIC RADIANCE MODELS FOR LIMB-VIEWING GEOMETRY IN THE FIVE- TO TWENTY-FIVE-MICRON SPECTRAL REGION

by

Victor L. Corbin
Alexander Dalgarno
Thomas C. Deggs
Fred B. House
Pedro Lilienfeld
George Ohring
George E. Oppel

Honeywell Inc.
Aerospace Division
Minneapolis, Minnesota 55413

Scientific Report No. 1

March 1970

Contract Monitor: Randall E. Murphy
Optical Physics Laboratory

Prepared for:

AIR FORCE CAMBRIDGE RESEARCH LABORATORIES
OFFICE OF AEROSPACE RESEARCH
UNITED STATES AIR FORCE
BEDFORD, MASSACHUSETTS 01730

AFCRL-69-0552

ATMOSPHERIC RADIANCE MODELS FOR LIMB-VIEWING GEOMETRY IN THE FIVE- TO TWENTY-FIVE-MICRON SPECTRAL REGION

by

Victor L. Corbin
Alexander Dalgarno
Thomas C. Deggs
Fred B. House
Pedro Lilienfeld
George Ohring
George E. Oppel

Honeywell Inc.
Aerospace Division
Minneapolis, Minnesota 55413

Contract No. F19628-69-C-0258
Project No. 8692

Scientific Report No. 1

March 1970

Contract Monitor: Randall E. Murphy
Optical Physics Laboratory

Prepared for:

AIR FORCE CAMBRIDGE RESEARCH LABORATORIES
OFFICE OF AEROSPACE RESEARCH
UNITED STATES AIR FORCE
BEDFORD, MASSACHUSETTS 01730

ABSTRACT

The infrared radiance arising from the earth's limb for altitudes from sea level to 500 kilometers and within the spectral limits of 5 to 25 microns was determined from theoretical calculations. The atmosphere was divided into two altitude regimes: the lower atmosphere (below 70 kilometers) and the upper atmosphere (above 70 kilometers). The lower limb models were developed from the University of Michigan computer program with modifications, including the addition of a model for nitric acid. Spectral radiances were determined as a function of geometrical, geographical, and temporal parameters. Emphasis was placed on developing limb radiance models for the upper atmosphere, including identification of active molecular species in the infrared, the specification of their abundances and their wavelengths of emission. In addition, particulate material sources, including infrared radiation arising from dust particles and noctilucent clouds, and uncertainties in atmospheric parameters were considered.

FOREWORD

This special scientific report presents the results of a theoretical study of the emission properties of the earth's atmosphere. The study was performed jointly under contract F19628-69-C-0258 by Honeywell Inc. as prime contractor and GCA Corporation as subcontractor.

The study investigated the infrared radiance arising from the earth's limb from sea level to an altitude of 500 kilometers and within the electromagnetic spectral limits of 5 to 25 microns. The primary purpose of the study was to obtain first-order numerical estimates of horizon radiance for the design of a horizon experiment program. In many cases, the results were obtained without experimental verification; users are therefore cautioned on the limitations of the resulting data. For study purposes, the atmosphere was divided into two altitude regimes: the lower atmosphere (below 70 kilometers) and the upper atmosphere (above 70 kilometers).

The lower limb models were developed from the University of Michigan computer program with modifications, including the addition of a model for nitric acid. Spectral radiances were determined as a function of geometrical, geographical, and temporal parameters, taking into account the range of carbon dioxide, water vapor and ozone concentration, and temperature profile variations.

Emphasis was placed on developing limb radiance models for the upper atmosphere. This portion of the study included the identification of active molecular species in the infrared, the specification of their abundances, their wavelengths of emission and the development of a realistic physical model to perform theoretical radiance calculations. In addition, particulate material sources, including infrared radiation arising from dust particles and noctilucent clouds, and the variability of limb radiance due to the means, extremes, and uncertainties in atmospheric parameters were considered.

CONTENTS

CONTENTS (Continued)

ILLUSTRATIONS

ILLUSTRATIONS (Continued)

ILLUSTRATIONS (Continued)

xi

ILLUSTRATIONS (Continued)

TABLES

xii

SYMBOLS

Symbol	Definition	First used in Equation	on Page
a	Particle radius, cm	59	145
a_o	Minimum particle radius, cm	59	145
a_1	Maximum particle radius, cm	59	145
$A(\nu)$	Absorption at frequency ν	37	83
$A_{u \rightarrow \ell}$	Einstein coefficient for spontaneous emission	25	77
$B_{u \rightarrow \ell}$	Einstein coefficient for absorption	25	77
$B_{\ell \rightarrow u}$	Einstein coefficient for induced emission	26	77
B_λ	Planck function, watts/cm^2-ster-μm	59	145
B_v	Molecular rotational constant	46	87
C	Velocity of light, 2.9979×10^{10} cm/sec	28	77
C_λ	Absorption or emission cross section, cm^2	59	145
d	Particle diameter, cm	55	139
e	Charge on electron, 4.80298×10^{-10} ESU	29	78
$E(J)$	Rotational energy	46	87
f_o	Oscillator strength of resonance transition	31	78
$f_{\ell \rightarrow u}$	Oscillator strength in absorption	29	78
g	Gravitational acceleration, 980 cm/sec^2	1	14
g_ℓ	Statistical weight of lower state	26	77
g_u	Statistical weight of upper state	26	77
G	Rate at which single molecule absorbs energy from continuum flux I_o, watts	31	78

Symbol	Definition	First used in Equation	on Page
G'	Molecular cross section for absorption of radiative flux, G/I_o	54	91
h	Tangent height (closest approach of a ray path to the earth's surface), km	Fig. 9	32
h	Planck's constant, 6.6256×10^{-27} erg-sec	5	56
I_o	Flux from continuum source, watts/cm^2-μm	31	78
J	Rotational quantum number	46	87
J''	Rotational quantum number in lower vibrational state	48	87
k	Boltzmann constant, 1.38054×10^{-16} erg/°K	27	77
$k(\nu)$	Spectral absorption coefficient, frequency basis	36	83
K	Defined constant	55	139
k_{MV}	Rate coefficient for transfer of vibrational excitation from another molecular species	54	91
k_{VM}	Rate coefficient for transfer of vibrational excitation to another molecular species	54	91
k_{VT}	Rate coefficient for transfer of vibrational excitation to translational energy	53	90
k_{TV}	Rate coefficient for transfer of translational energy to vibrational excitation	53	90
ℓ	Subscript indicating lower state	25	77
ℓn	Natural logarithm	36	83
L	Path length, cm	56	140
$L(\kappa_o)$	Function used to obtain total absorption from continuum source by optically thick Doppler line	41	85
m	Mass of electron, 9.1091×10^{-28} ESU	29	78

xiv

SECTION I
INTRODUCTION

This study is concerned with the problem of investigating the natural infrared background of the earth in the 5 to 25 micrometer region of the electromagnetic spectrum. This general problem area is of interest from the standpoints of systems design, military surveillance and the advancement of scientific knowledge. The estimates of the infrared radiant background from physical models developed in the study are useful in these areas. Knowledge of the magnitude, extreme range and variability of the background radiances is important in defining the specifications of radiometer systems and the logic of developing optimum background measurement programs. In a similar manner, the background estimates are of interest in the areas of military surveillance and homing interception defense measures. Finally, the problem area is extremely interesting in terms of our scientific knowledge of the physical processes taking place in the atmosphere, especially in the altitude region above about 70 km.

The scope of the current effort is the development of physical models to estimate infrared radiation arising from active molecular gases and particulate material in the atmosphere from the surface to about 500 km. The effort is confined to viewing the atmosphere, geometrically speaking, against the relatively "cold" background of space, and viewing geometrics include exoatmospheric viewing where the reference frame is outside the earth's atmosphere (e.g., viewing the atmospheric limb from a satellite platform) and endoatmospheric viewing where the reference frame is imbedded within the atmosphere (e.g., viewing from the zenith to the horizon from a rocket platform). This study does not consider the infrared background of the earth-atmosphere system, where the atmosphere is viewed against the "hot" infrared source of the earth's surface, since the problem area has been investigated extensively by other researchers.

1

The basic physics of developing a realistic theoretical model to estimate radiance in the infrared spectrum are reasonably well known. Any theoretical model relies on a knowledge of atmospheric properties. Our knowledge of the physical properties of the atmosphere such as temperature and composition are quite certain from the surface to upper balloon altitudes of about 30 km, are less certain in the low altitude rocket range from 30 to 70 km, and become uncertain and sometimes speculative at altitudes about 70 km.

In much the same manner, the physical methods of treating the problem of computing background radiances may be divided into two altitude regions, a lower atmosphere from the surface to 70 km, and an upper atmosphere above 70 km. An extensive amount of theoretical modeling effort has been performed in the lower atmospheric region. Much less effort has been performed on the upper atmospheric region. The primary effort of the current study is directed toward the problem of developing a realistic physical model in the upper atmosphere.

For convenience in subsequent discussions, the atmosphere is divided into two regions, the lower atmosphere and the upper atmosphere. Some of the physical properties distinguishing these two regions are as follows:

Lower Atmosphere (surface to 70 km)

- Physical properties such as chemical composition, temperature and pressure are reasonably well known.

- Collision between molecules is rapid enough to maintain a thermal equilibrium population of vibrational states.

- Radiative transfer theory is well known and has been verified against observations.

2

- A mixed Lorentz-Doppler line shape is required in the treatment of atmospheric transmission properties.

Upper Atmosphere (above 70 km)

- Atmospheric properties such as chemical abundances and temperature are uncertain as to their magnitude, variability and even as to their identity in the case of minor atmospheric constituents.

- Collisions between molecules are less effective in maintaining excited vibrational states as compared to the lower atmosphere.

- Radiation excitation mechanisms become more important with increasing altitude.

- Radiative transfer theory is reasonably well known but has not been verified extensively against observations.

- A Doppler line shape is a good approximation in treating atmospheric transmission properties.

- Chemiluminescent and fluorescent processes become important.

In the problem of investigating the natural infrared background of the earth, the current study relies on the physical model developed by Anding (1968) in order to perform radiance calculations for the lower atmosphere. This model has been incorporated in a working computer program whose calculations have been verified against observations. The computational model for the upper atmosphere developed in this study represents an entirely new effort. All the properties mentioned in the physical description of the upper atmosphere above have been developed and incorporated into a computer program. The sophistication and accuracy of the physical model are commensurate with the uncertainties in the knowledge of the physical properties of the upper atmosphere.

3

The balance of the report summarizes the research effort performed under contract F19628-69-0258 and presents preliminary results of background radiance calculations for both the lower- and upper-atmospheric regions. Section II, for example, discusses the derivation of temperature, pressure and absorber profiles for the lower atmosphere. These represent the spatial and temporal variations of atmospheric properties, and the model atmospheres are used as input data to Anding's radiance synthesizer program. Section III presents the results of background radiances from the lower atmosphere in the 5 to 25 μm region, the variability, means and extremes of infrared limb radiances.

The effort directed towards the upper atmospheric portion of the problem is presented in Sections IV through VII. A discussion of infrared active gases, their abundances and wavelengths of emission is presented in Section IV. These data are input values to the computational model which is developed in Section V. Preliminary results of infrared background radiances are presented in Section VI, based upon the computational model. These results include examples of band radiances as viewed by exoatmospheric and endoatmospheric reference platforms. A detailed spectra from the H_2O rotational band is also included in the results. The discussion in Section VII concerns infrared radiation from particulate material such as clouds and dust in the upper atmosphere and from dust in interplanetary space. Consideration of both gaseous and particulate sources of infrared radiation provides a reasonably complete picture of the natural infrared radiant background of the near earth environment.

SECTION II

DERIVATION OF TEMPERATURE, PRESSURE, AND ABSORBER PROFILES FOR THE LOWER ATMOSPHERE (0 to 70 km)

Part of the research effort during the study was the derivation of models of the lower atmosphere in the altitude range from the surface to 70 km. These models include the altitude distribution of temperature, pressure, and important absorber gases in the 5 to 25 μm spectral region. The specification of these parameters and their distributions with altitude are used as input data to a radiation synthesizer program (Anding, 1969) which computes spectral radiances as a function of arbitrary view directions. The model atmospheres derived herein represent the spatial and temporal variations of atmospheric parameters about the earth. Extreme atmospheric conditions are also included as part of the data set. Spectral radiances computed from these models will give a good indication of the magnitude and variation of the earth's natural infrared background for altitudes up to about 70 km. These data are important in defining radiometer design specifications and spatial sampling requirements.

This section discusses the sources of information used to construct the model atmospheres, the uncertainties in our knowledge of parameters, variations as a function of time, latitude and longitude, and the methods used to interpolate parameters as a function of altitude. The parameter profiles derived in the study are tabulated in Appendix A, and Appendix B summarizes the identification of codes in A. Appendix C presents a selection of 47 model atmospheres that are representative of spatial and temporal variations, mean and extreme conditions about the earth.

A. APPROACH TO DERIVATION OF PROFILES

The infrared radiance is related to the atmospheric temperature, pressure, and absorber distributions. To obtain estimates of the mean radiance and its variability in time and space from theoretical calculations, one must have estimates of the mean vertical profiles of temperature, pressure, and absorbers, and the variations from the mean. The major meteorological variations in the 0 to 70 km region are the latitudinal and seasonal variations, and season and latitude are used as a basis for deriving a set of profiles representing atmospheric variability.

The computer program used to calculate radiances for the lower atmosphere is a modified version of the one developed by Anding (1968). The absorbing gases included in this program are H_2O vapor, CO_2, O_3, HNO_3, N_2O and CH_4. Only the first four of these gases are incorporated in the 5 to 25 micron region. Even though radiances from nitrous oxide are not computed in the spectral region of interest for the lower atmosphere, profiles of N_2O are derived below for the sake of completeness and use during future research efforts. Absorption constants for CH_4 are not presently available for the 7.6-micron band; however, its omission should not be significant in the lower atmosphere because of the heavy absorption due to the strong wing of the 6.3-band of water vapor.

Of the five gases mentioned, carbon dioxide and nitrous oxide are uniformly mixed up to the levels at which dissociation begins. Water vapor and ozone, on the other hand, vary vertically, horizontally, and with time. Thus, with respect to carbon dioxide and nitrous oxide, it is sufficient to specify a constant mixing ratio up to the levels of dissociation (for CO_2, ~100 km; for N_2O, ~30 km). For both water vapor and ozone, however, as with temperature and pressure, a number of different profiles are required to cover the range of observed variations. Nitric acid is also variable with altitude and is discussed in Appendix D.

All profiles cover the range from the surface to 90 km. For ease of tabulation and punching the data on cards, and to minimize sources of error, each profile is initially tabulated at the minimum number of heights necessary to portray

6

the main features of the particular profile. These heights may be called key heights. Appropriate interpolation schemes are contained in the computer program that prepares the initial profiles for input to the radiance calculations. The following sections discuss each atmospheric parameter individually and describe how vertical profiles representative of that parameter's mean state and variability are constructed.

1. Temperature

The U.S. Standard Atmosphere (1962) temperature profile is adopted as the mean temperature profile. The basic variations about the mean can be represented by several temperature profiles from the U.S. Standard Atmosphere Supplements (1966): The 15° latitude annual mean; 45° latitude January and July profiles; and 75° latitude January and July profiles. As presented in the U.S. Standard Atmosphere Supplements, the 75° latitude profiles extend only to 30 km. We have extended these profiles to 90 km as described below.

Observations of the summer temperature profile between 30 and 90 km at Barrow, Alaska (71°N) (Theon, et al., 1967; Theon, 1968) indicate little variability with time. Seven temperature profiles presented by Theon (1968; Figure 6) are averaged to extend our 75° July temperature profile to 90 km. Although the data are sparse for these altitudes in the arctic regions, the available information does indicate little variability in summer. Thus, the adopted profile, though based on few observations, should be representative of arctic summer conditions at these altitudes.

For arctic (75° latitude) winter conditions, the U.S. Standard Atmosphere Supplements contains three temperature profiles from the surface to 30 km. These three — a warm, cold, and mean profile — cover the range of thermal regimes that exist in the winter stratosphere. The cold regime is dominant over northeastern Canada and the warm regime is dominant over the Aleutian

7

area. The mean profile is extended to 52.5 km using the analyses of Kantor (1966). Kantor derives temperature at 75°N latitude between 25 and 55 km from radiosonde data for latitude 60°N, meteorological rocket wind and temperature observations at Fort Churchill, Canada (55°N) and Fort Greely, Alaska (64°N), and application of the thermal wind relationship. The warm and cold January, 75° profiles are extrapolated to 52.5 km by assuming that their temperatures at 52.5 km are ± 10°K from the mean temperature (see Figure 1). All three profiles are extrapolated to a common temperature of 210°K at 90 km, this temperature being based upon the few high latitude – high altitude rocket grenade observations (Theon, et al, 1967; Theon, 1968). It should be pointed out that, as opposed to summer conditions in the 50 to 90 km at high latitudes, the few available soundings indicate large variability in winter — up to 80°K temperature change in 3 hours.

The standard atmosphere, and January temperature profiles for 45°N and 75°N (mean) are plotted in Figure 2; the 15° annual mean, and July temperature profiles for 45° and 75° are plotted in Figure 3.

The temperature profiles assembled thus far should provide a reasonable estimate of the seasonal and latitudinal variability of temperature between the surface and 90 km. In turn, they should yield reasonable estimates of radiance variability when used as inputs to a radiance synthesizer program.

Aside from the expected seasonal and latitudinal variability of radiance, one would also like to estimate extreme values that might occur. For this purpose, two extreme temperature profiles have been constructed. These are based upon information on extreme temperatures between the surface and 100,000 feet that is presented in Valley (1965, Figure 2-7). Hot temperatures (those exceeded only 10 percent of time in the hottest regions) and cold temperatures (those exceeded 90 percent of the time in the coldest regions) are presented as a function of altitude. From the average range between hot and cold temperatures over this altitude span which, for a normal distribution represents

JANUARY   75°

52.5 - 90 km
Based on common temperature
of 210 °K at 90 km

30 - 52.5 km
Mean from Kantor (1966)
Cold and warm ±10 °C at 52.5 km

COLD

MEAN

WARM

0 - 30 km from
75°N Supplementary
Atmosphere

90
80
70
60
50
40
30
20
10
0

HEIGHT, km

180   190   200   210   220   230   240   250   260
TEMPERATURE T, °K
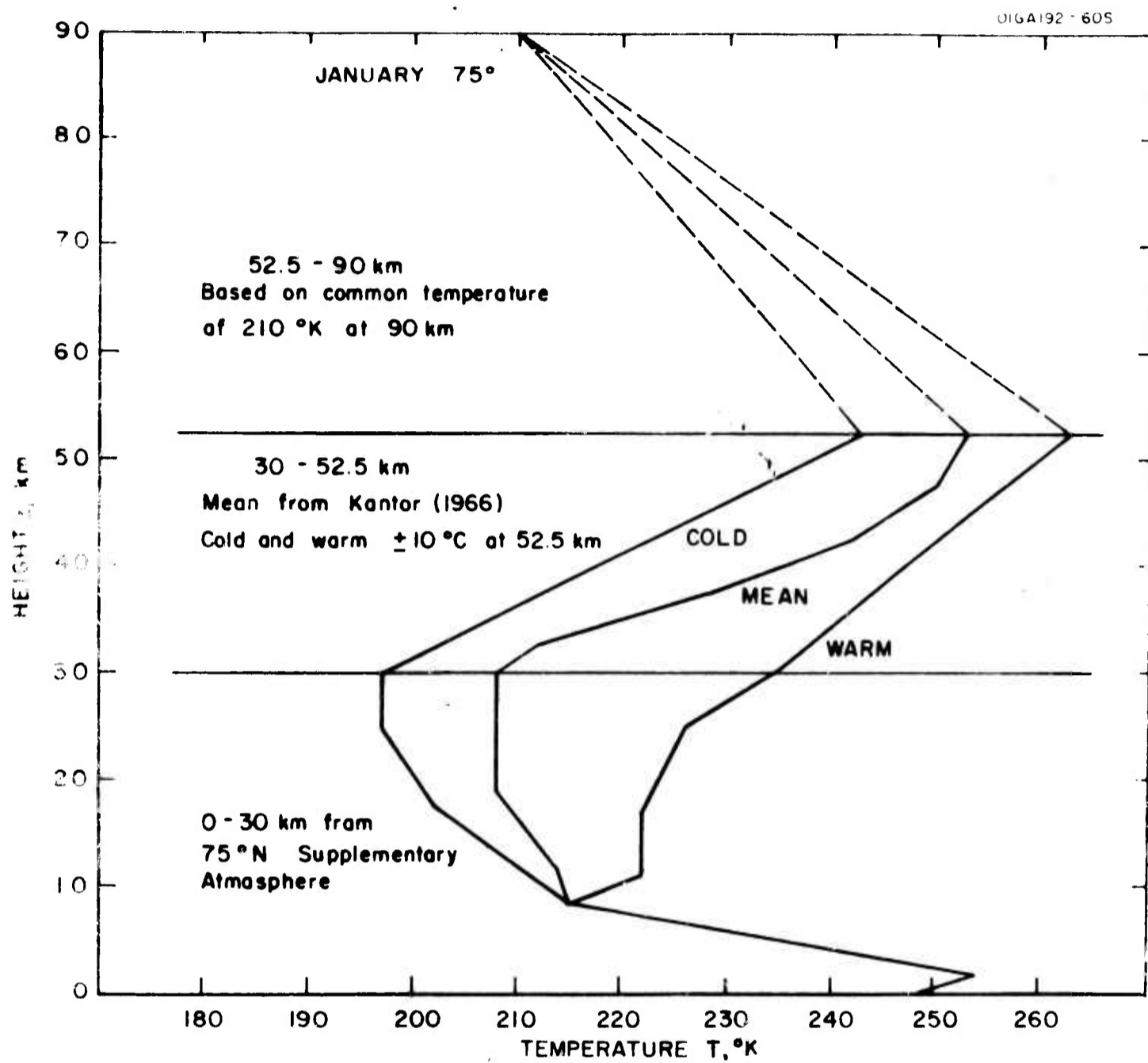
Figure 1. Adopted temperature profiles for January, 75° Latitude
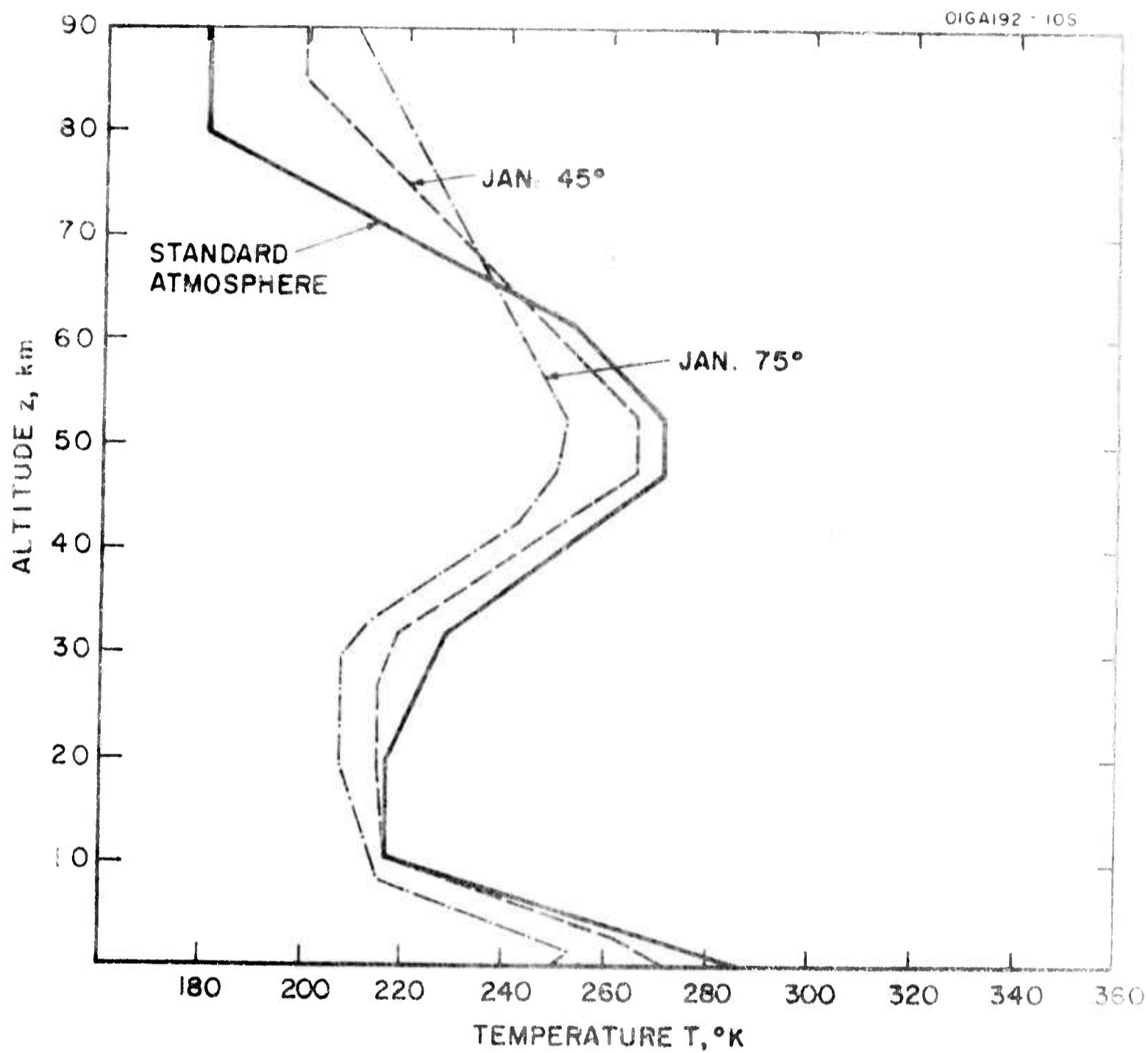
Figure 2. Standard Atmosphere, 45° January, and 75° January
(mean) Temperature Profiles
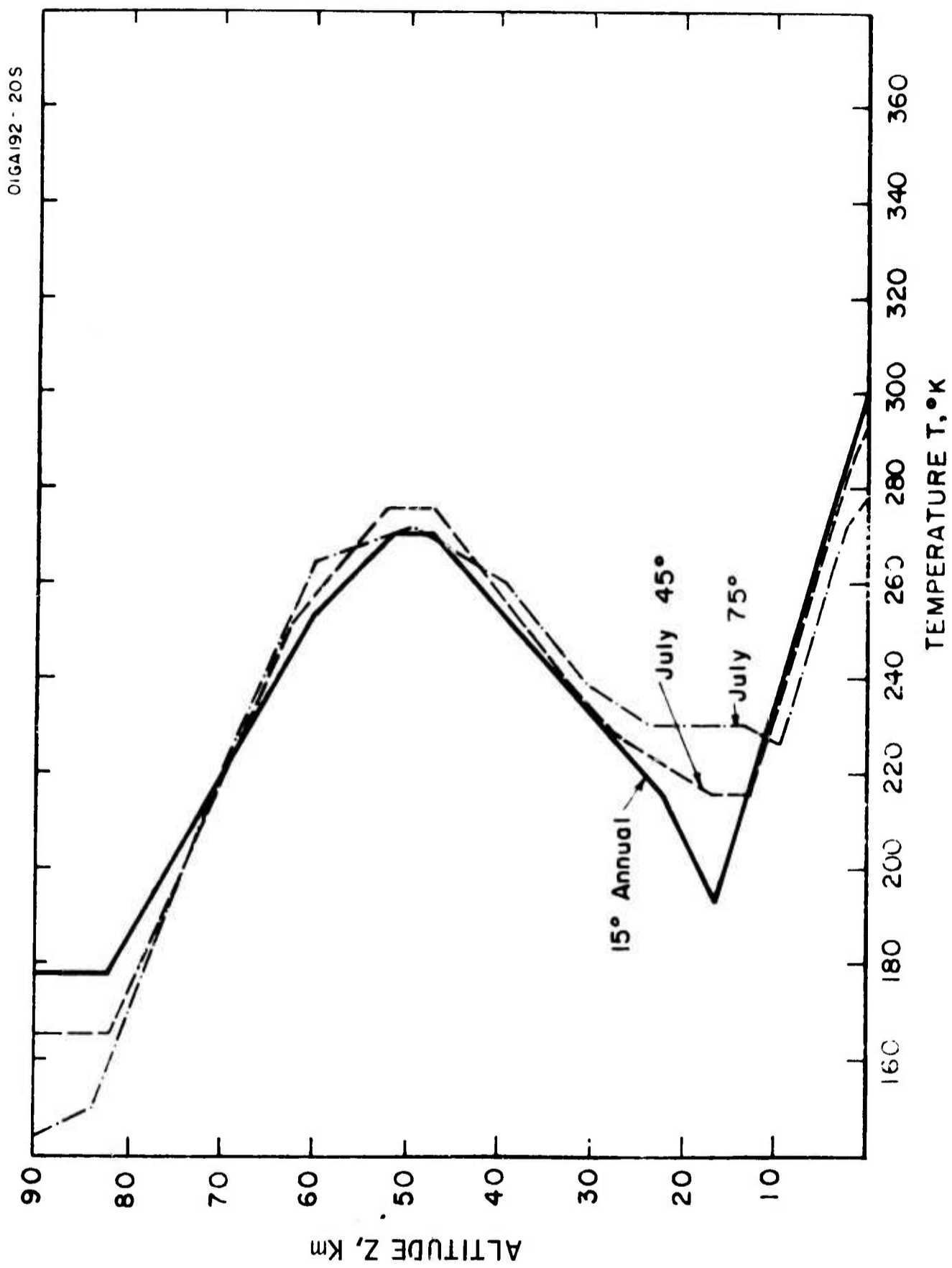
Figure 3. 15° Annual Mean, 45° July, and 75° July Temperature Profiles

11

2.6 σ, a standard deviation of 16°K is derived. For the extreme temperature profiles, a 3 σ level, or plus or minus ~50°K is adopted. By adding 50°K to the standard atmosphere temperature profile at all levels, one obtains the extreme hot profile; by subtracting 50°K, one obtains the extreme cold temperature profile. These synthetic temperature profiles should be useful for estimating extremes in infrared radiance.

Temperatures at key heights from the surface to 90 km for all the temperature profiles are tabulated in Appendix A. Linear interpolation may be used between key heights.

2. Pressure

Pressure profiles are calculated from the temperature profiles with the use of the hydrostatic equation. A surface pressure appropriate to each of the Supplemental Atmospheres is used. For the two extreme temperature profiles, a surface pressure of 1013 mbar is used. The following integrated forms of the hydrostatic equation are used in the pressure computations:

For constant lapse-rate layers:

$$P(z) = P(z_o) \left[\frac{T(z)}{T(z_o)} \right]^{g/\alpha R} \tag{1}$$

For isothermal layers:

$$P(z) = P(z_o) \exp \left[- \frac{g(z - z_o)}{R\, T(z_o)} \right] \tag{2}$$

where P is pressure, z is altitude, z_o is the altitude of the base of a layer, T is temperature, g is the gravitational acceleration, α is the temperature

lapse rate in the layer, and R is the gas constant for air. The variation of the gravitational acceleration g with altitude is included in the pressure computation.

3. Water Vapor

For purposes of constructing profiles representative of the variability of water vapor, the 0 to 90 km altitude range is divided into two regions: a lower atmospheric region extending from the surface to 15 km (troposphere), and an upper atmospheric region extending from 15 to 90 km (which, in this section, is referred to as the stratosphere). The reason for this division is the fact that there is very little information on the water vapor content of the stratosphere and quite a large amount of data on the water vapor content of the troposphere — especially the lower troposphere. Thus, H_2O profiles in the troposphere are representative of seasonal and latitudinal variabil for the stratosphere, only estimates of the mean H_2O profile and possible extremes are possible.

Mean vertical profiles of atmospheric moisture content have been prepared (Valley, 1965) from the surface to 10 km from the Supplemental Atmospheres. These data are used as the basis for the estimates of the variability within a season and latitude belt, the information provided in the Atmospheric Humidity Atlas — Northern Hemisphere (Gringorten, et al., 1966) is used. This publication contains hemispheric distribution of various percentile values of water vapor content for the surface and for the 850-, 700-, 500-, and 400-mbar levels as a function of month of the year. The analyses are based upon five years of world wide radiosonde data. From these maps, estimates of high (95 percentile) and low (5 percentile) water vapor mixing ratios for seasons and latitudes are obtained, similar to those used for the temperature profiles and mean water vapor profiles.

When the water vapor mixing ratio is plotted on a semilogarithmic graph versus altitude, it can be seen that the logarithm of the mixing ratio decreases approximately linearly with altitude. Using the data derived from the sources listed above, the high, mean and low H_2O profiles are derived as illustrated in Figure 4. The plotted points are for 45°N, July, and are from the original sources; the solid lines represent the adopted distributions; and the short horizontal bars divide the troposphere into layers in which the logarithm of the water vapor mixing ratio decreases at a constant linear rate with altitude. Profiles were constructed in a similar manner for 15° annual, 45° January, and 75° January and July conditions.

For the overall mean, or standard atmosphere, water vapor profile in the troposphere, the mixing ratio profile presented by Sissenwine, et al. (1968) is adopted which is based upon the data in Gringorten, et al. (1966).

Because of the low mixing ratios and pressures, water vapor in the stratosphere is extremely difficult to measure. Standard radiosonde sensors generally cannot measure water vapor concentrations at pressures much below 400 mbar. A recent summary of available measurements has been presented in Leovy (1969) and is quoted below.

"For observations in which serious contamination effects seem to have been avoided, both hygrometer and spectroscopic observations indicate remarkably uniform water vapor mixing ratios in the range $1-4 \times 10^{-6}$ gm/gm from just above the tropopause up to 20 or 25 km. Above 25 km, the picture is not so clear. Relatively few measurements have been made at these heights. Spectroscopic measurements are subject to ambiguity of interpretation above 20 km (Houghton, 1960; and Williamson, 1965). Some frost-point measurements have indicated continued dryness with mixing ratios of $1-4 \times 10^{-6}$ gm/gm up to 30 km (Goldsmith, 1964). In a year-long series of frost point hygrometer ascents at

14
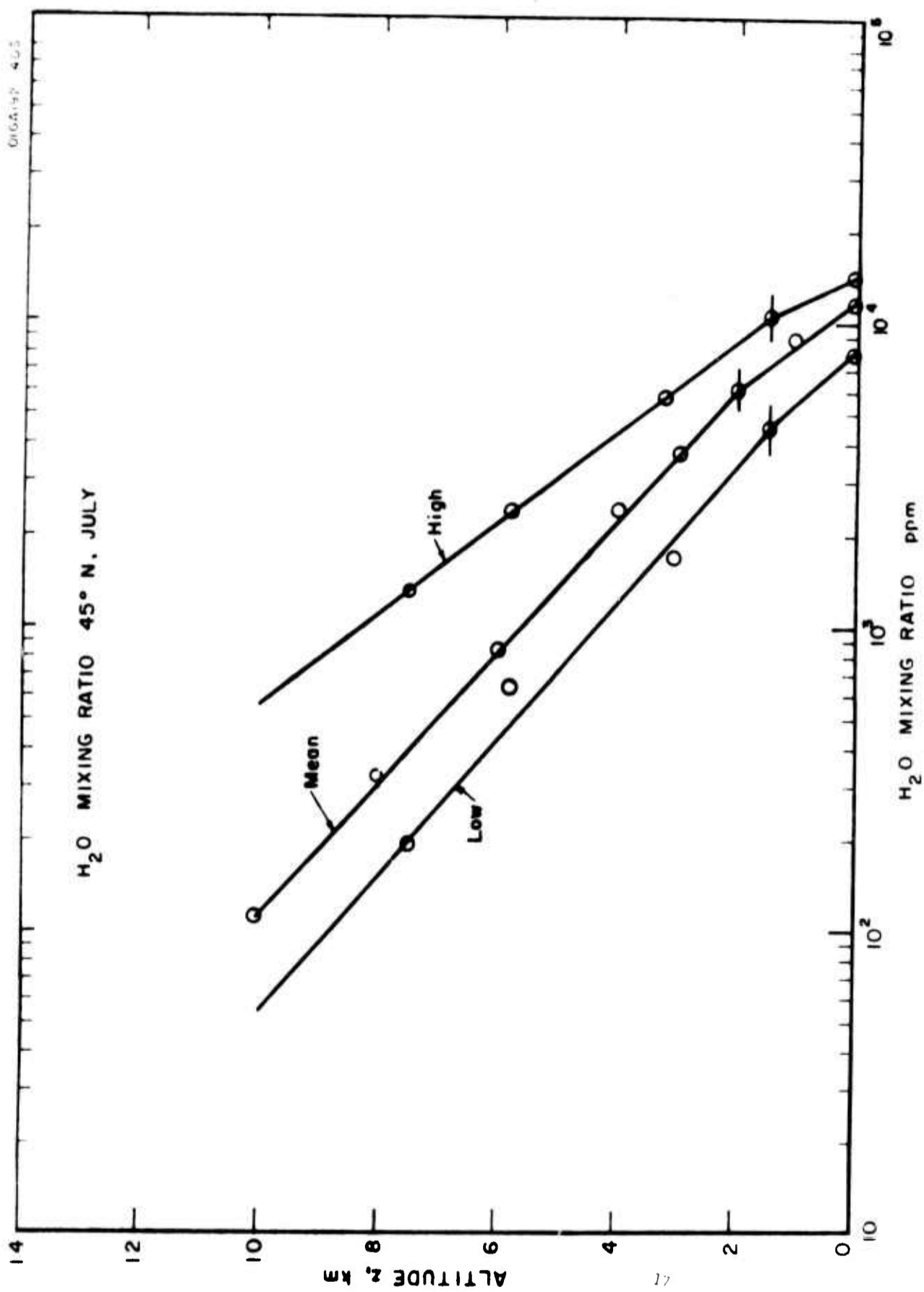
Figure 4. Illustration of Derivation of Tropospheric Water Vapor Profiles for 45° N, July. Plotted Points are Based Upon Sources Discussed in the Text. Short Horizontal Bars Divide Troposphere into Layers of Linear Decrease in Log W. Adopted Profiles Indicated by Lines.

Washington, D. C., and Trinidad, Mastenbrook (1968) has found mixing ratios predominantly in the range 1-4 x 10^{-6} gm/gm above 20 km, but with some seasonal variations, and with greater moisture concentrations at the higher levels on a few ascents. Brown, et al. (1961) flew a cooled vapor trap on a balloon between 25 and 28 km and found mixing ratios ranging from 9 to 77 x 10^{-6} gm/gm at these altitudes. They were able to rule out the possibility of contamination from the balloon by introducing a small amount of deuterium into the balloon as a tracer. The possibility remains, however, of some contamination from other parts of their system, although great care was taken to eliminate all sources of contamination. Recent frostpoint measurements by Sissenwine, et al. (1968), also indicate increasing water vapor concentration above 20 km, with mixing ratios of 20 x 10^{-6} gm/gm at 25 km. The occasional occurrence of mother-of-pearl clouds in this portion of the stratosphere has been cited as indirect evidence for mixing ratios as high as 10^{-4} gm/gm (Newell, 1963)."

As the above discussion indicates, there is, at present, no consensus as to the mean H_2O mixing ratio profile in the stratosphere nor of its variability. For the present purpose of providing inputs to radiance calculations, the three H_2O profiles for the stratosphere are adopted. These should cover the range of present uncertainty in this gas concentration as well as any natural variability.

For the mean stratospheric water vapor profile, the mid-latitude moisture profile presented by Sissenwine et al. (1968) are adopted. Up to 32 km this profile is based upon mid-latitude stratospheric frost point observations obtained by Sissenwine and his colleagues. Between 32 km and 80 km, it is based upon an extrapolation to a dewpoint of -130°C at 80 km. This dewpoint is based upon an observation of the occurrence and dissappearance of noctilucent clouds (Anonymous, 1963). The adopted profile has a maximum mixing ratio

of 19 ppm at 26 km. The mixing ratio decreases with altitude above this level to a value of 0.6 ppm at 80 km. Between 80 and 90 km, a constant mixing ratio is assumed.

Our dry stratospheric water vapor profile is based mainly upon the frost-point observations of Mastenbrook (1968). A value of 1 ppm between 15 and 30 km is assumed, a drop to 0.1 ppm at 80 km, and a constant value between 80 and 90 km.

For the wet stratosphere, a value of 50 ppm between 15 and 30 km is assumed, a drop to 5 ppm at 80 km, and a constant value between 80 and 90 km.

The adopted standard atmosphere water vapor profile for the troposphere and the dry, mean, and wet stratospheric water vapor profiles are illustrated in Figure 5. Just as the wet, mean, and dry stratospheric profiles can be placed on top of the standard atmosphere tropospheric water vapor profile, so can they be connected to any of the seasonal and latitudinal tropospheric water vapor profiles. From the top of tropospheric H_2O profiles (10 km) to the base of the stratospheric H_2O profiles (15 km) a simple linear change with altitude of the logarithm of the mixing ratio is assumed.

Water vapor mixing ratios at key altitudes between the surface and 10 km for all the tropospheric profiles, and between 15 and 90 km for the three strato-spheric profiles, are tabulated in Appendix A. Interpolation between key heights is accomplished by assuming that the logarithm of the mixing ratio is a linear function of altitude.

4. Ozone

Since 1963, a small network of North American stations has been flying chemical ozonesondes to measure the vertical distribution of atmospheric
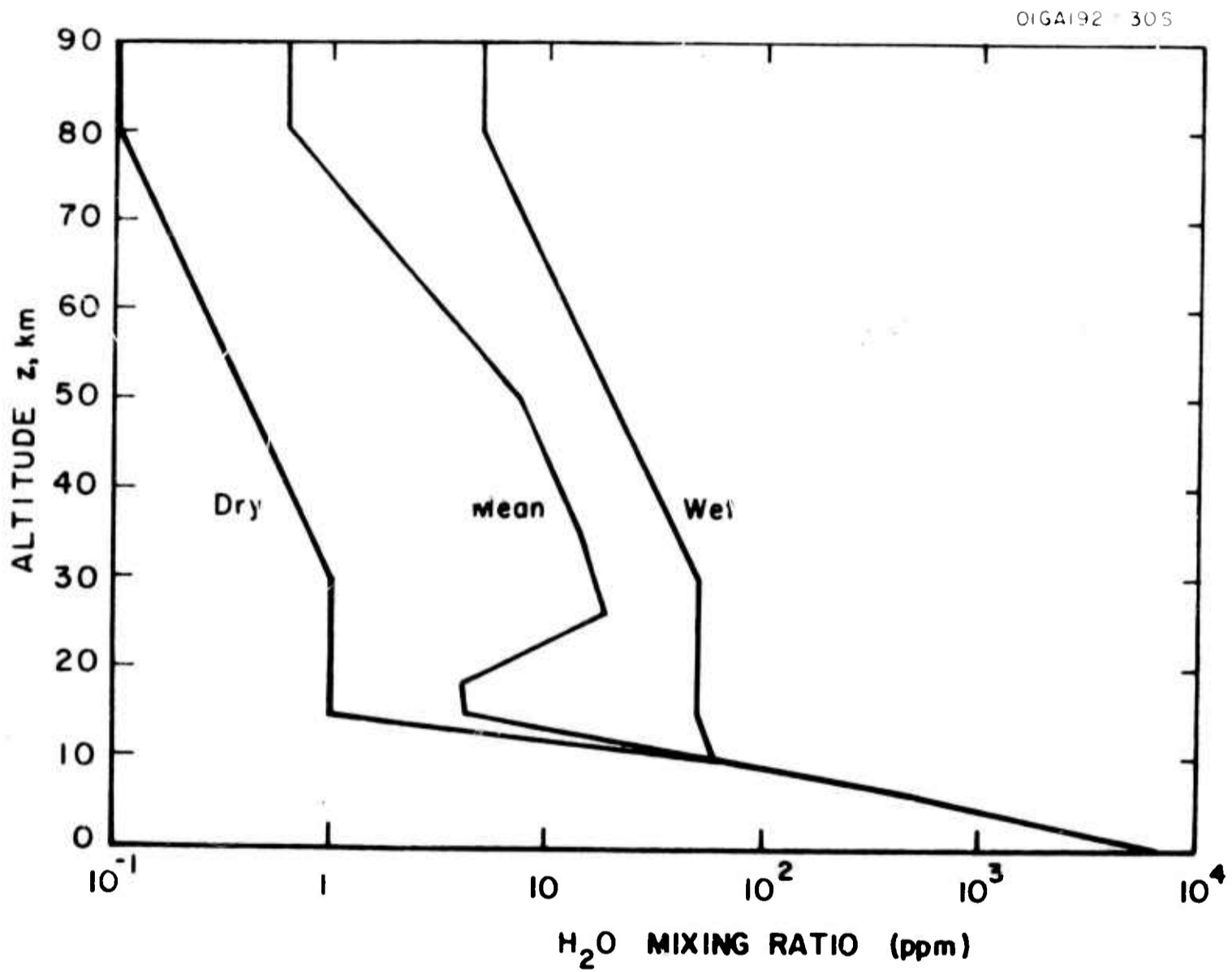
Figure 5. Adopted Standard Atmosphere Water Vapor Profile
for Troposphere and Dry, Mean, and Wet Stratospheric
Water Vapor Profiles

ozone between the surface and balloon burst altitudes (~ 30 km). An interim summary of these data, covering the years 1963 to 1964, has been published by Hering and Borden (1965). For constructing ozone profiles to 35 km in the present study, we have used unpublished ozone cross-sections recently prepared by Hering and Borden (1969) and covering all of the ozone soundings to date. Between 35 and 90 km, where ozone observations are scarce, the distributions suggested by Kuhn (1966) are used.

The Hering-Borden cross-sections extend from equator to north pole and from the surface to 10 mbar. For each season, there is one cross-section for ozone density and one for the standard deviation of the ozone density. In order to keep the number of model atmospheres within a reasonable number (47) and to be consistent with the temperature and water vapor profiles, the ozone data are grouped together into two seasons, represented as winter and summer. Based on the ozone density cross-sections, the vertical ozone profiles for 15° annual mean, 45° winter mean, 45° summer mean, 75° winter mean, and 75° summer mean are constructed. Based on the standard deviation cross-sections, the extreme profiles for each of the latitude-season zones listed above are derived. These extreme profiles are constructed by adding or subtracting a 2σ variability to or from the mean profiles for each of the latitutde-season zones. Both the mean profile and the extreme ozone were extended graphically from ~30 to 35 km. The spring and fall cross-sections given by Hering-Borden are similar and fall within the models indicated above.

For our overall mean, or standard atmosphere, ozone profile in the lowest 35 km, the standard atmosphere ozone profile presented in the U.S. Standard Atmosphere Supplements (1966) is adopted, which is based upon the results of ozonesonde flights at mid-latitude stations.

Between 35 and 90 km the shape of the ozone profile suggested by Kuhn (1966) is used. Kuhn assumes that the ozone mixing ratio is proportional to the pressure raised to a power. This may be written as:

$$O_3(z) = O_3(z_1) \left[P(z)/P(Z_1) \right]^p \qquad (3)$$

where O_3 is the ozone mixing ratio, z is altitude, z_1 is a reference altitude, and P is pressure. Between 35 and 50 km, p is based mainly on photochemical equilibrium calculations and is equal to 0.46. Between 50 and 90 km, p is based upon rocket observations, which agree with photochemical calculations, and is equal to 0.614. Photochemical theory suggests large dirunal variations in the upper layers of the ozone profile (> 50 km). These are not presently included in the ozone profiles, but can easily be programmed since the region between 35 and 90 km can be subdivided into a number of layers with different reference levels z, and values of p. Thus, as opposed to the 0 to 35 km region, where the O_3 mixing ratios are specified at key heights and the O_3 profile for any desired vertical resolution is obtained by linear interpolation, the O_3 profile above 35 km is calculated analytically by means of a group of formulas similar to equation (3).

Figure 6 illustrates the adopted standard atmosphere ozone profile. The ozone mixing ratios at key heights between the surface and 35 km for all the ozone profiles are tabulated in Appendix A. Mixing ratios between key heights are obtained by linear interpolation in altitude.

5. Nitrous Oxide

Bates and Hays (1967) have recently reviewed information on nitrous oxide and performed theoretical calculations of vertical profiles. The most probable source of atmospheric N_2O is microbiological action at the earth's surface. The N_2O produced at the earth's surface is mixed by turbulent diffusion throughout the troposphere and into the stratosphere. A mean tropospheric fractional volume abundance of 2.5×10^{-7} is suggested by the few available observations. In the stratosphere, photodissociation takes place and the N_2O abundance probably decreases with altitude.
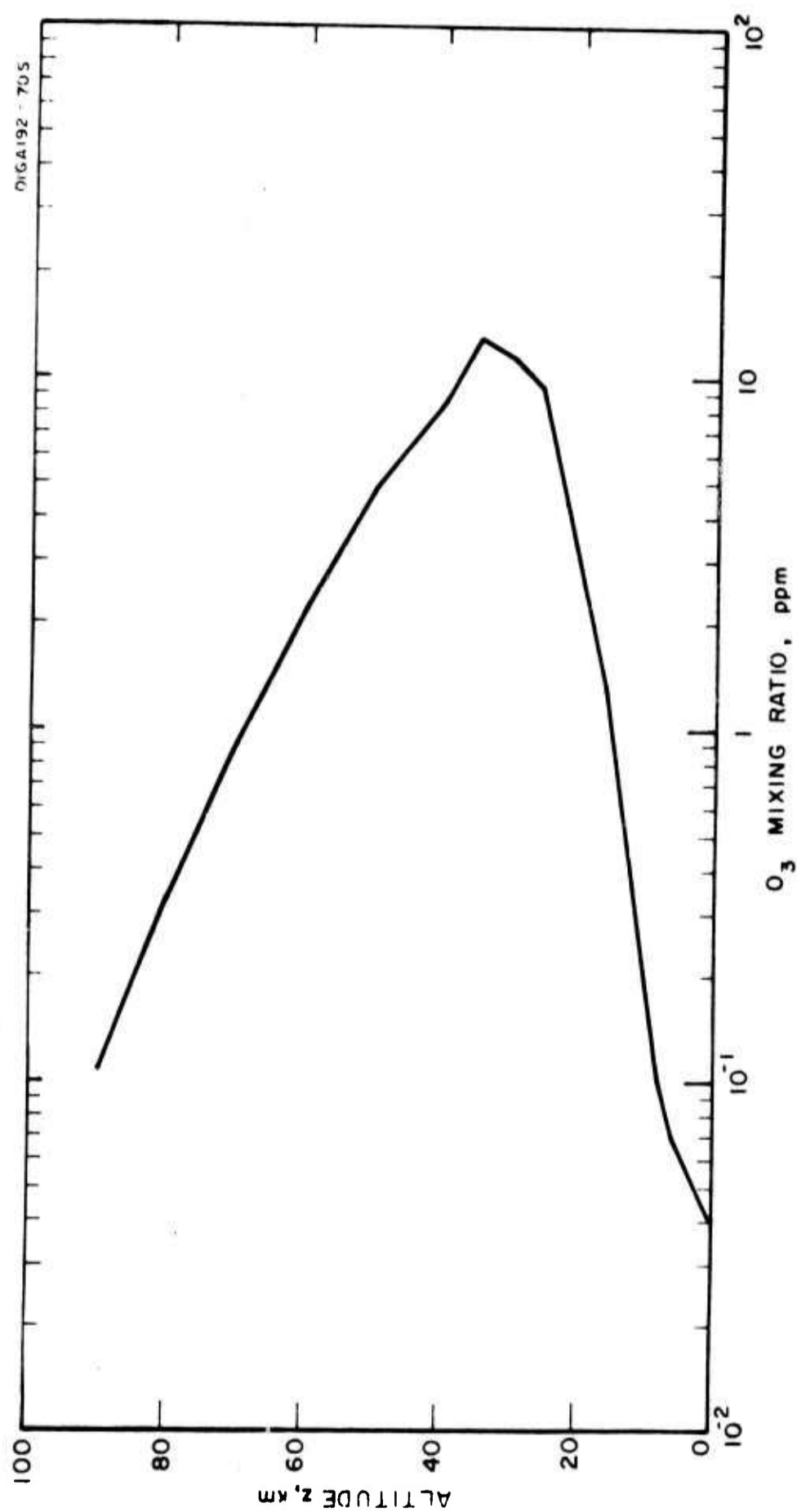
Figure 6. Adopted Standard Atmosphere Ozone Profile

21

Bates and Hays (1967) have computed vertical profiles of $f(N_2O)$, the fractional volume abundance, from the surface to 40 km, based upon a simple model in which vertical eddy diffusion, a surface source, and an atmospheric photodissociation sink are considered. The resulting profiles which are plotted in Figure 7 indicate that the stratospheric profiles are sensitive to the value of K_z, the stratospheric eddy diffusion coefficient.

These computed N_2O profiles have been extended to 90 km by noting that log $f(N_2O)$ in the range 1 or 2×10^{-7} to 10^{-8} decreases with altitude at roughly the same rate, independent of K_z. Thus, for heights above the level at which $f(N_2O) = 10^{-7}$, the following formula is used to represent the N_2O concentration:

$$f_{N_2O}(z) = f_{N_2O}(z_1) \, e^{-p(z - z_1)} \tag{4}$$

where

$$p = 0.24 \text{ km}^{-1}$$

The adopted N_2O profiles are plotted in Figure 8 for four possible values of the mean stratospheric eddy diffusion coefficient. The adopted N_2O profile for the standard atmosphere incorporates a diffusion coefficient of $K_z = 10^4 \text{ cm}^2 \text{ sec}^{-1}$. The adopted N_2O profiles, from the surface to 40 km, are tabulated in Appendix A. Above 40 km, equation (4) is used.

It should be noted again that the computer program which calculates radiances for the lower atmosphere does not include nitrous oxide in the 5 to 25 μm spectral region. However, the program does include this gas at wavelengths less than 5 μm. Therefore, N_2O profiles were derived during this study for the sake of completeness and use during future research efforts.
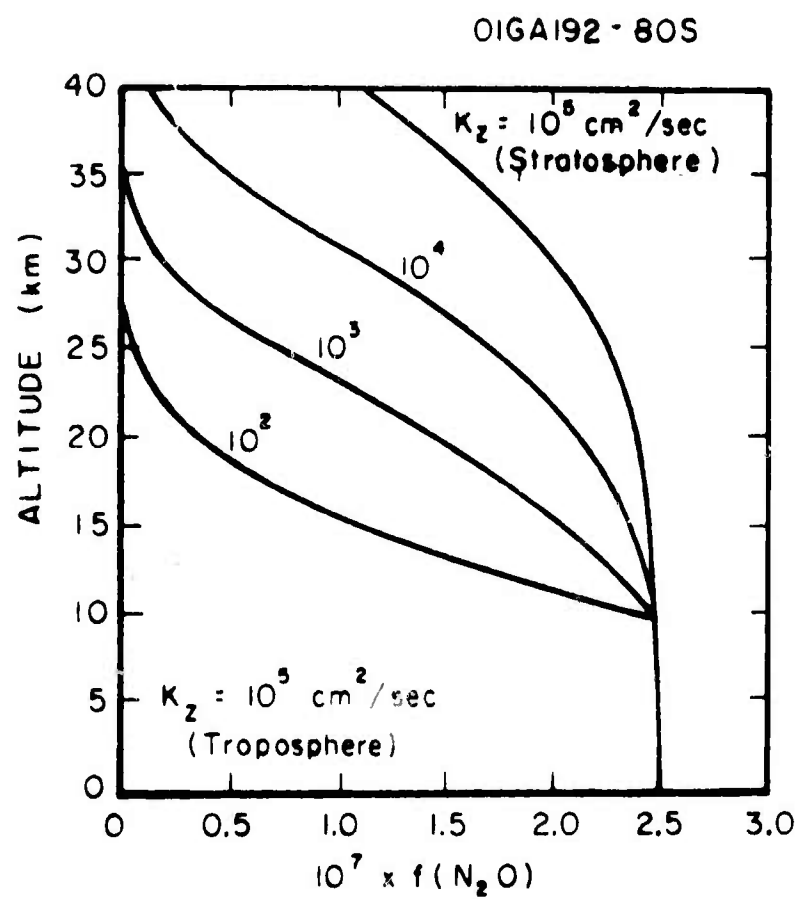
Figure 7. Fractional Volume Abundance of Atmospheric Nitrous Oxide, $f(N_2O)$, for Selected Values of the Vertical Exchange Coefficient K_z (after Bates and Hays, 1967)

23
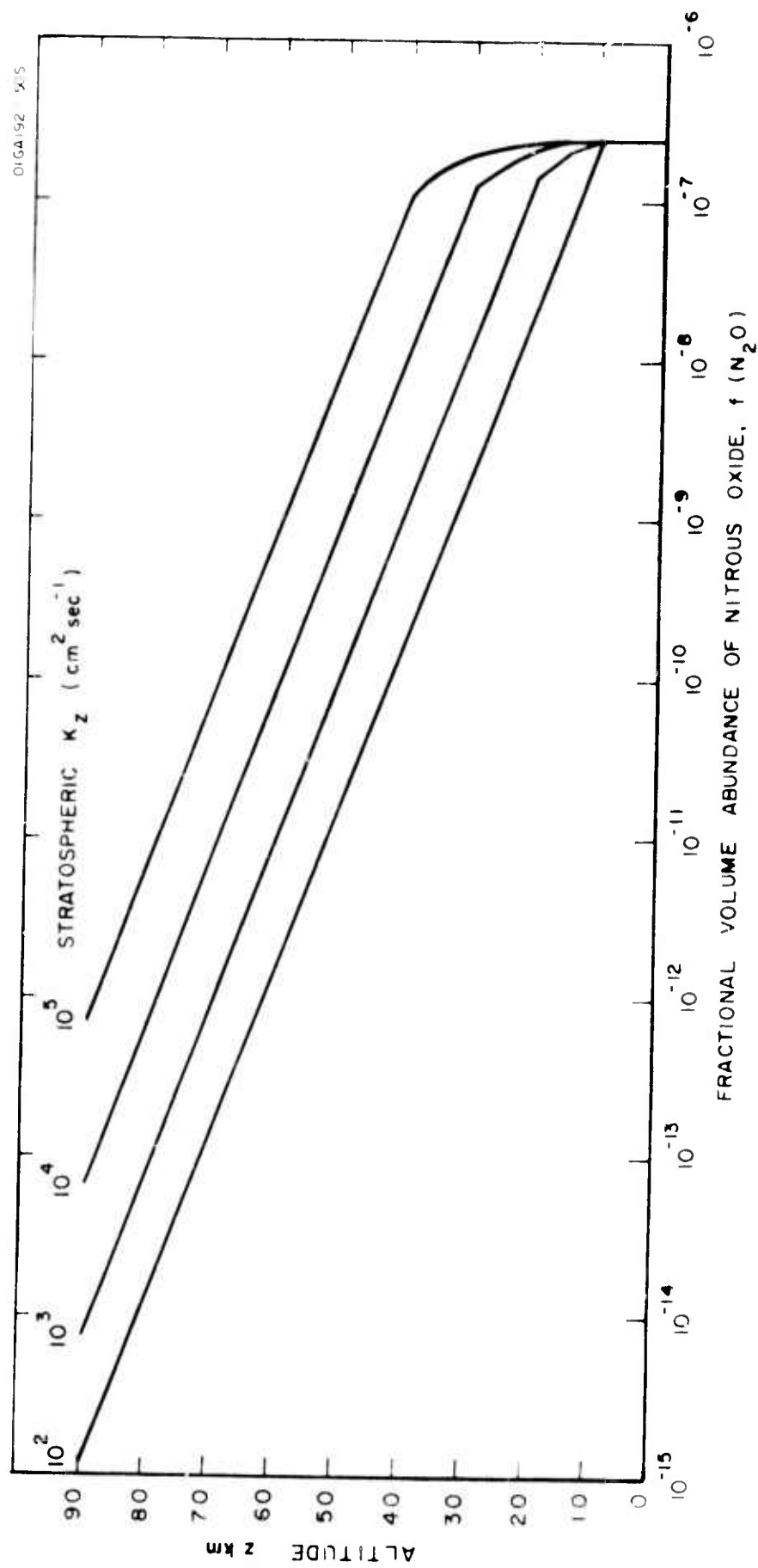
Figure 8. Adopted N_2O Profiles for Different Values of Stratospheric Eddy Diffusion Coefficient, K_z

6. Carbon Dioxide

For our present purposes, carbon dioxide may be assumed to be uniformly mixed from the surface to ~100 km. Recent aircraft observations (Georgii and Jost, 1969) suggest a decrease from the troposphere to the stratosphere of the order of 1 percent of mean mixing ratio. However, such a small variation is of little concern to the current problem. There is some uncertainty in the value of the mean atmospheric CO_2 mixing ratio. Since the beginning of the century, there has been a 10 to 15 percent increase in atmospheric CO_2 (Callendar, 1958) as a result of increased burning of fossil fuels. Recent studies (Bolin and Keeling, 1960; Keeling, 1960) suggest that this increase is continuing at a rate of the order of 1 ppm per year. A recent survey of atmospheric carbon dioxide variability (Peterson et al., 1967) suggests a mean CO_2 mixing ratio of 314 ppm by volume applicable some four to six years ago. A CO_2 mixing ratio of 320 ppm by volume is adopted in this study.

7. Nitric Acid

Nitric acid has been identified as a minor constituent in the atmosphere (Murcray, et al, 1968) with a strong absorption band near 11.2 microns. The computer program developed by Anding (1968) does not include a model for nitric acid. Calculated radiances in the window region from 10 to 12 microns have shown extremely low values; therefore, it has been necessary to synthesize a model for absorption by nitric acid. The inclusion of nitric acid represents the major change to the University of Michigan program.

Transmission by nitric acid is given by the following empirical relationship:

$$t = \exp\left[-\sqrt{0.84 \times 10^{-12} \int \left(\frac{P}{P_o}\right)^2 \left(\frac{T_o}{T}\right)^{3/2} Z^2 \, dL} \right] \tag{4a}$$

25

where

P = atmospheric pressure

P_o = pressure at normal conditions (760 mm Hg)

T = atmospheric temperature

T_o = temperature at normal conditions (288.16°K)

Z = altitude

L = path distance along line of sight

The development of the model is given in Appendix D.

SECTION III
VARIABILITY OF INFRARED LIMB RADIANCES
IN THE LOWER ATMOSPHERE

Infrared limb radiances were computed for a selected sample of model atmospheres derived in Section II. These radiances represent the mean conditions, the extreme conditions and the uncertainties in radiance magnitudes due to our knowledge of atmospheric parameters in the stratosphere and the mesophere. The results presented herein include both spectral radiances and band radiances for absorbing gases, computed as a function of tangent height. Both spatial and temporal variations of band radiances are discussed, and extreme conditions are presented as a function of tangent height. These results are useful in specifying radiometer requirements and defining data sampling requirements for tangent heights up to about 70 km.

For all calculations, carbon dioxide was assumed to be uniformly mixed throughout the atmosphere with a volumetric mixing ratio of 320 ppm. The particular meteorological profile used in a radiance calculation is represented by a four number code, the first number indicating the type of temperature profile, the second number indicating the type of trophospheric water vapor profile, the third number indicating the type of stratospheric water vapor profile, and the fourth number indicating the type of ozone profile. The codes are explained in Appendix B. For example, atmospheric profile 10-12-3-20 represents a hot extreme temperature profile, a tropospheric water vapor profile typical of an extremely moist condition at 15° latitude (this is the wettest tropospheric water vapor profile in our data set), a wet stratospheric water vapor profile, and an ozone profile typical of an extremely high ozone content at 75° latitude during the winter season (this is the ozone profile with the highest total amount in our data set).

27

Figure 9 illustrates the 5 to 25 μm spectrum of the standard atmosphere (code 1-1-1-1) for three different tangent heights: h = 50 km, 60 km, and 70 km. The major features of the spectra are the 6.3 μm H_2O band, the 9.6 μm O_3 band, the 15 μm CO_2 band, and the rotational H_2O band beyond 18 μm. These features are seen in emission since they are being viewed against the cold background of space.

The general decrease of radiance with increasing tangent height in the 50 to 70 km range is due to decreasing absorber amounts and temperatures with altitude. Highest emissions are in the middle of the 15 μm CO_2 band; lowest emissions are in the window region near 10 μm. It is noted that the range in radiance between these two regions covers almost five orders of magnitude.

Figure 10 shows how the spectrum for tangent height 60 km might vary under extreme atmospheric conditions. The topmost spectrum represents extremely hot, wet and high ozone conditions (10-12-3-20); the middle spectrum represents the standard atmosphere (1-1-1-1); and the lowest spectrum represents extremely cold, dry, and low ozone conditions (9-19-2-17).

The range between the top and bottom spectra is probably representative of the maximum range to be expected at this tangent height, and the actual magnitudes are estimates of the highest and lowest spectral radiances to be expected at this tangent height.

One of the major uncertainties in the calculations discussed above is the water vapor distribution in the stratosphere. To illustrate the effect of this uncertainty in the spectra in the 6.3μ H_2O band and rotational H_2O band, computations were performed with a standard atmosphere temperature profile with a dry and wet stratosphere. The computed spectra for the two water vapor bands for a tangent height of 60 km are plotted in Figure 11 along with the spectra for the adopted mean stratospheric H_2O profile. It can be seen that

28
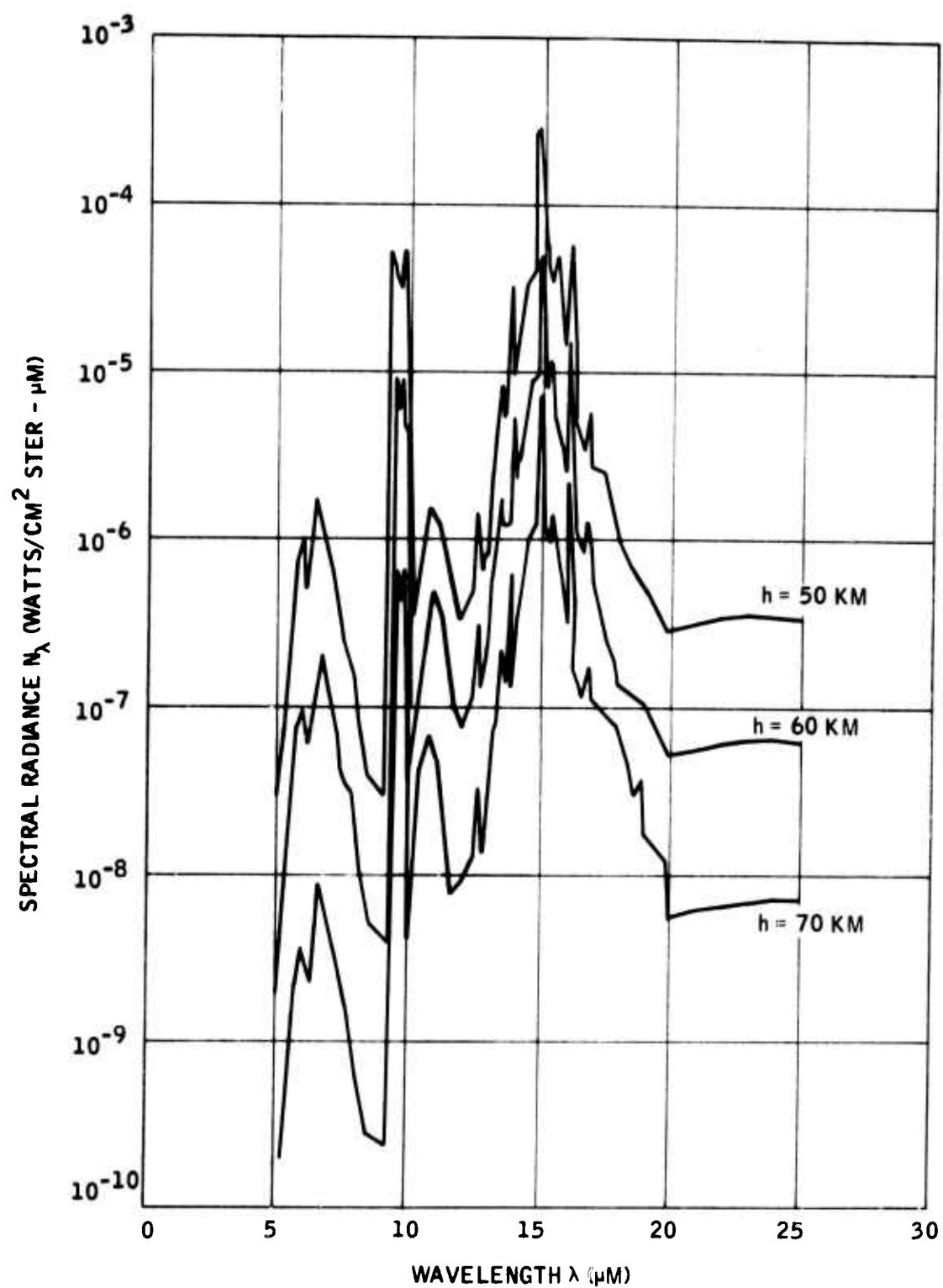
Figure 9. Infrared Spectra at Tangent Heights of 50, 60 and 70 km for Standard Atmosphere Temperature, Water Vapor, and Ozone Conditions
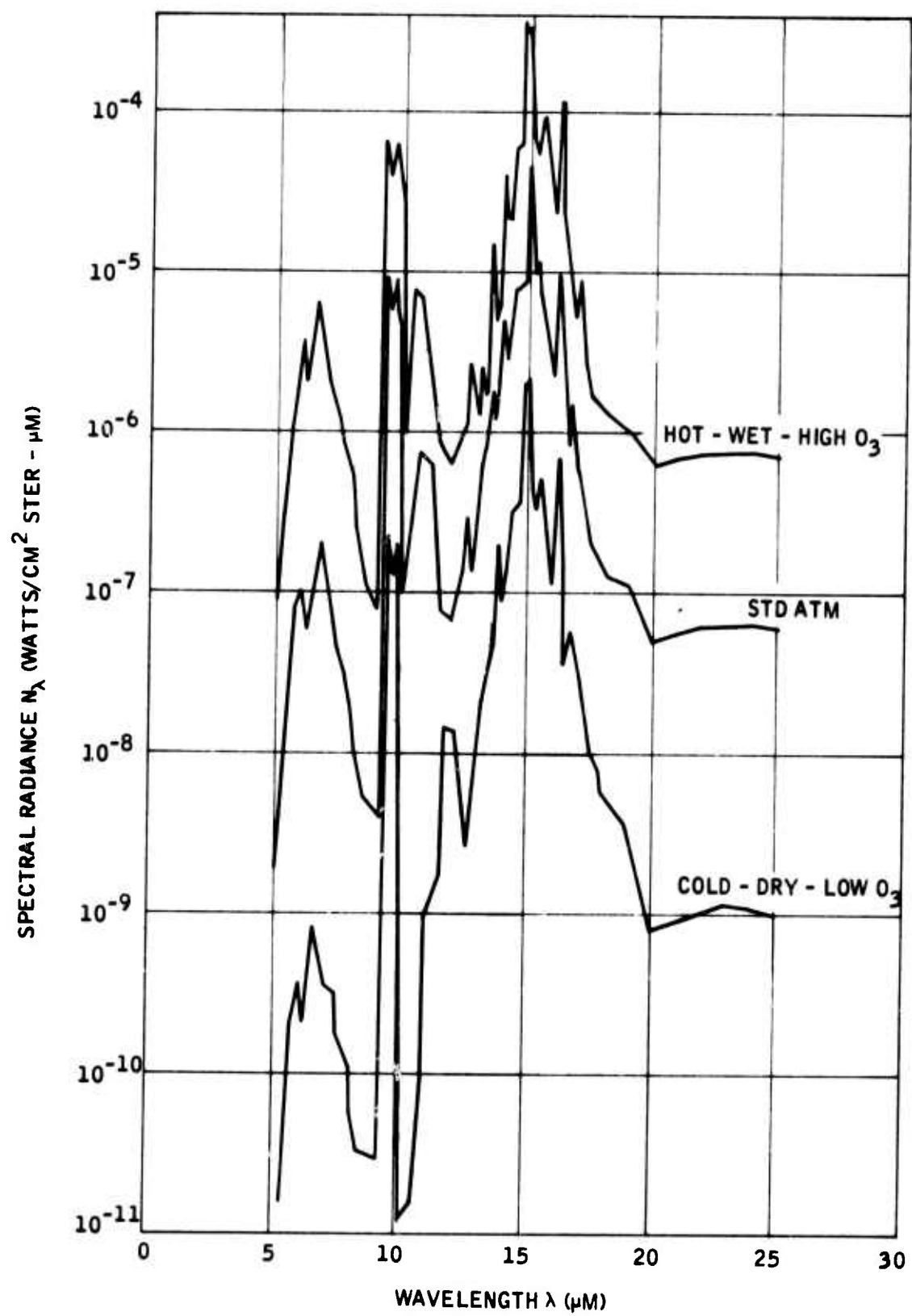
Figure 10. Infrared Spectra at a Tangent Height of 60 km for Standard Atmosphere Conditions and Extreme Conditions on Temperature, Water Vapor, and Ozone
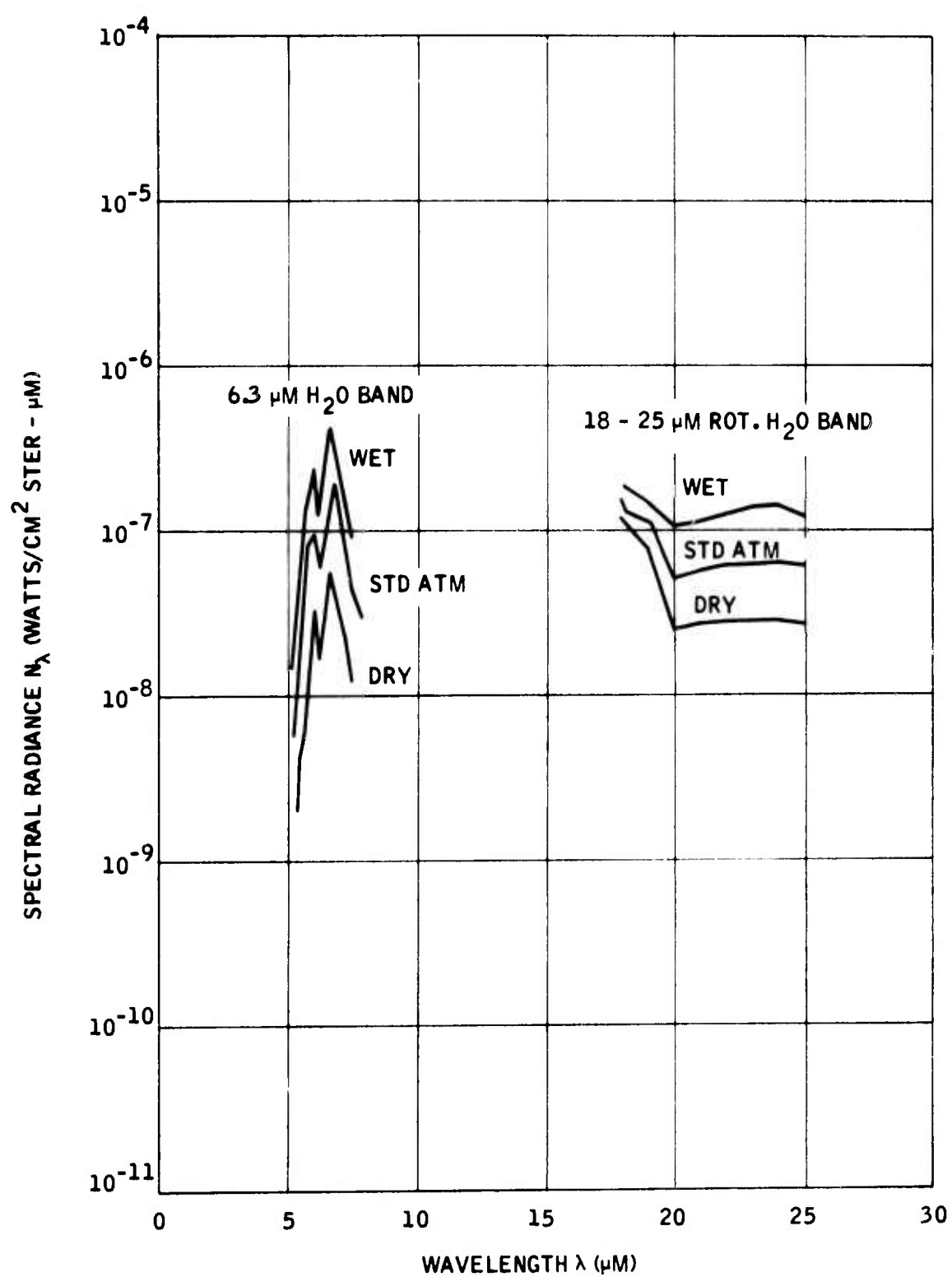
Figure 11. Infrared Spectra at a Tangent Height of 60 km
for the H_2O Bands for Different Stratospheric
H_2O Mixing Ratios

31

the range in computed spectral radiance between dry (1-19-2-20) and wet (1-12-3-20) stratospheres can be almost a full order of magnitude.

Of particular interest is the variation of radiance with tangent height (horizon radiance profile) in the absorption bands and in the windows. This is illustrated in Figures 12 through 14 for the 6.3 μm H_2O band (5.3 μm to 7.3 μm), the 9.6 μm O_3 band (9.3 μm to 10.3 μm), and the rotational band of H_2O (18.0 μm to 25 μm). Each figure contains three horizon radiance profiles. Each horizon radiance profile is computed with the standard atmosphere temperature profile but with different absorber (H_2O and O_3) amounts ranging from high (1-12-3-20) to mean (1-1-1-1) to low (1-19-2-17) absorber amounts. Thus, on one graph the differences between horizon radiance profiles are due solely to differences in absorber amount for that particular absorption band.

The general decrease of radiance with tangent height is due mainly to the general decrease of absorber concentration with altitude, and also, for some parts of the atmosphere, to a decrease of temperature with altitude. In the 9.6 μm O_3 band, there is actually a slight increase of radiance with tangent height in the vicinity of 20 km tangent height. This is due to the increase of both ozone concentration and temperature in this region of the atmosphere.

In most cases, the highest radiance at a particular tangent height is associated with the highest absorber concentration. However, at the low tangent height of the horizon radiance profiles for the water vapor bands, this situation is reversed. The highest radiances are associated with the lowest water vapor concentrations. This reversal occurs because the model with the highest H_2O concentration reaches opacity at some tangent height above the surface. For this model, any further decrease of tangent height will not result in substantial increase in radiance because only a small fraction of the emitted radiation from these lower layers escapes to space. For the model with the lowest H_2O concentration, opacity is not reached and the radiance increases with decreasing tangent height along with the temperature up to the zero tangent height (surface) level.
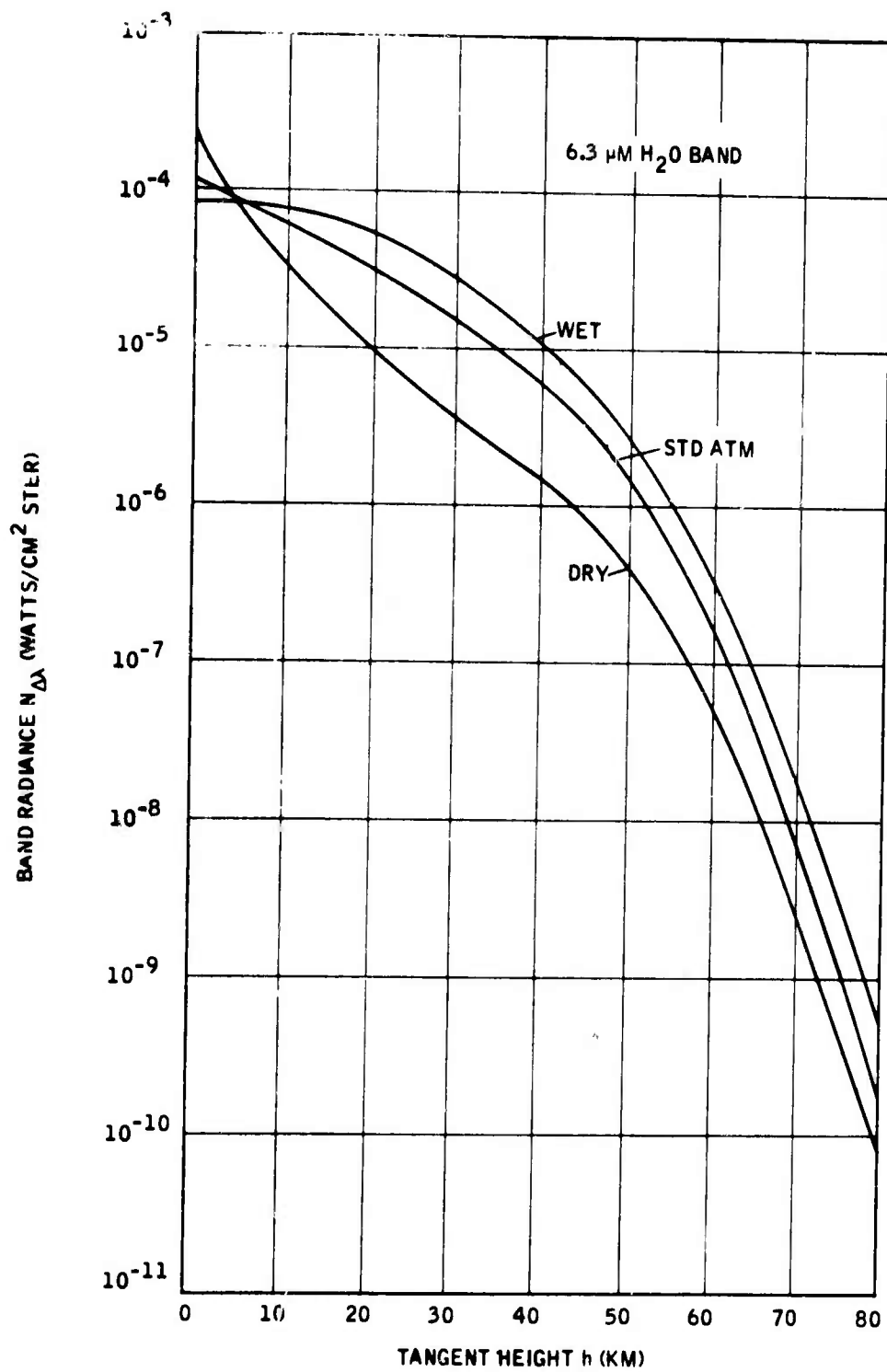
Figure 12. Horizon Radiance Profiles for the 6.3 μm H_2O Band for Standard and Extreme H_2O Profiles
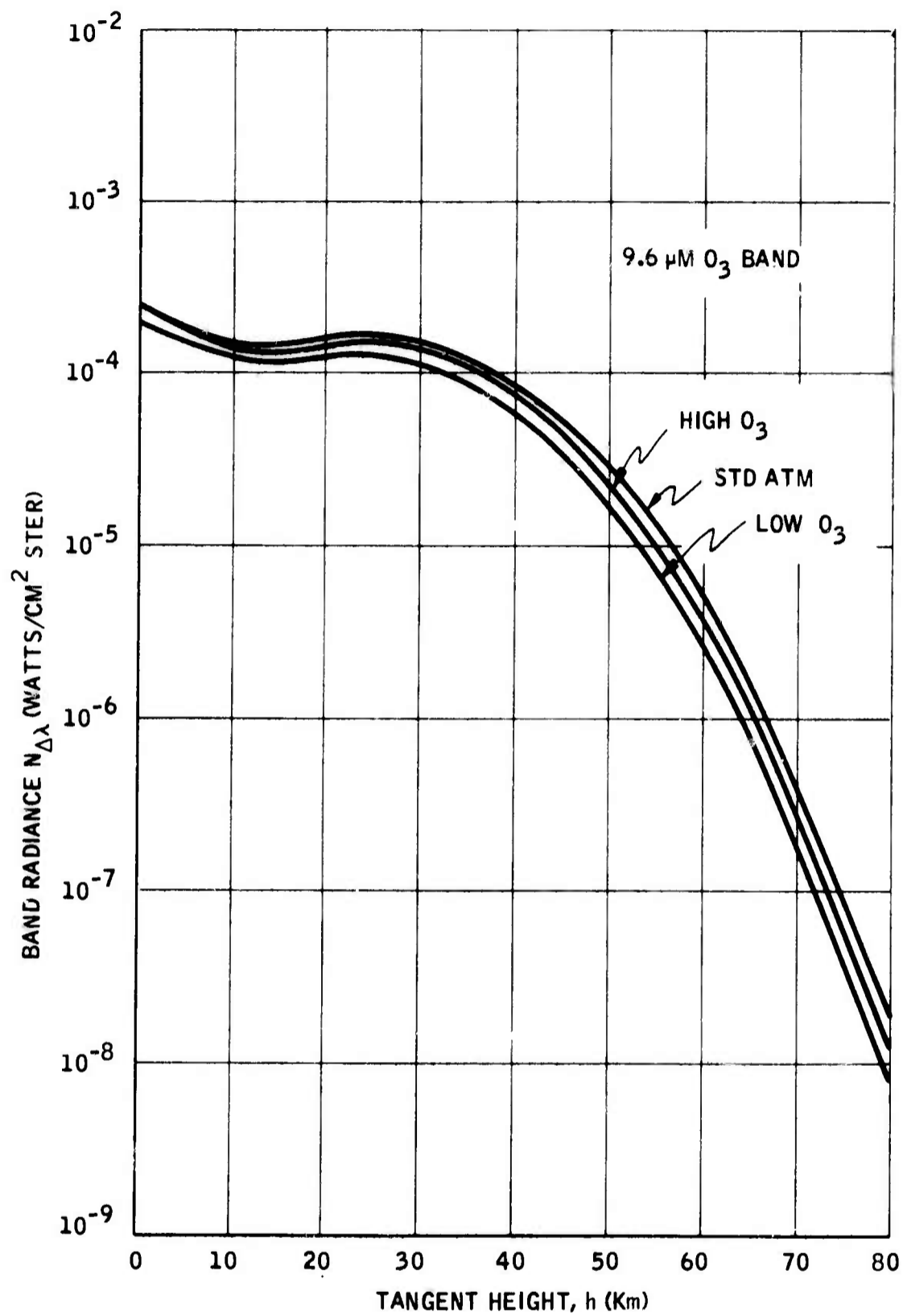
Figure 13. Horizon Radiance Profiles for the 9.6 μm O_3 Band for Standard and Extreme O_3 Profiles
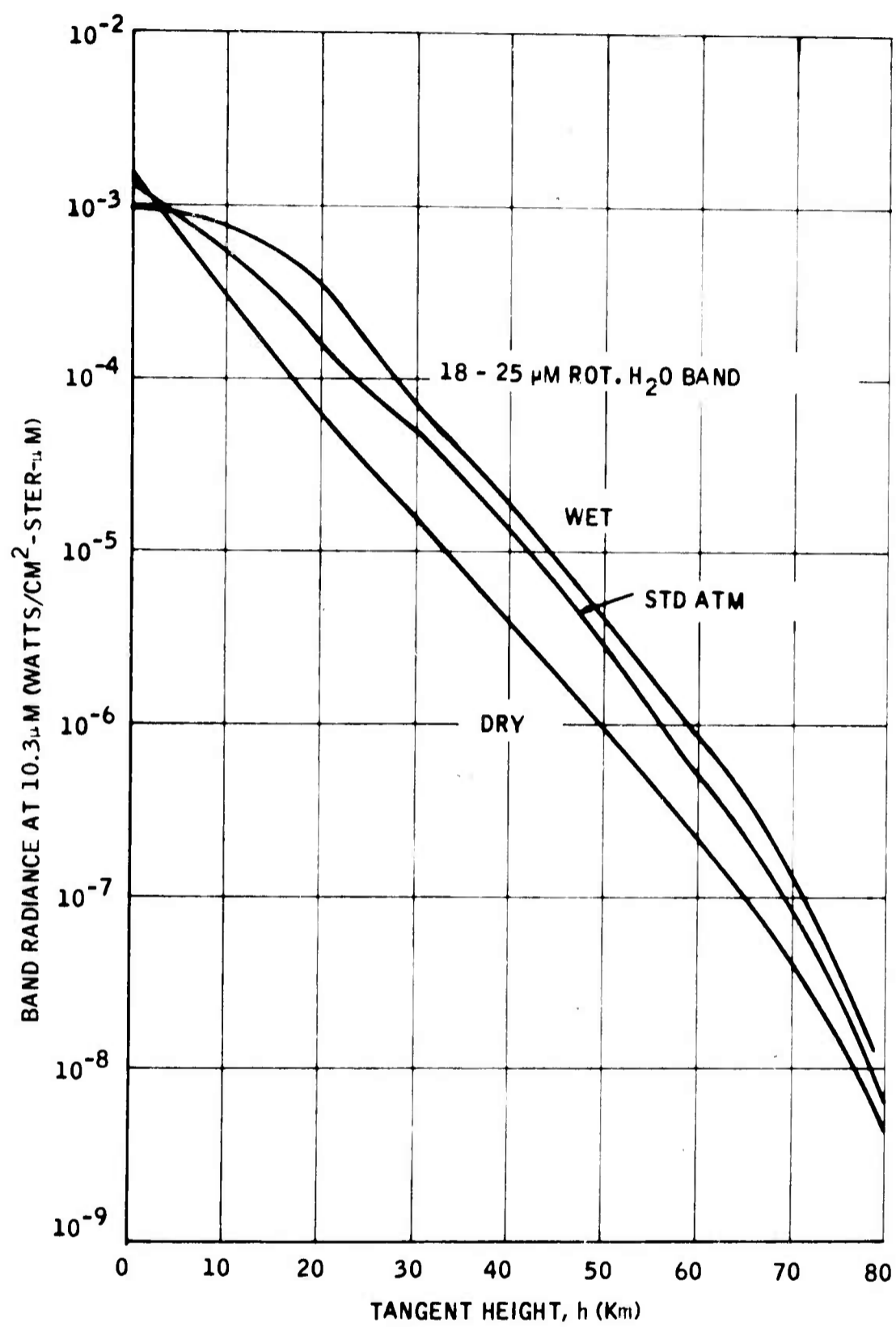
Figure 14. Horizon Radiance Profiles for the 18-25 μm Region for Standard and Extreme H_2O Profiles

Examination of the horizon radiance profiles for the 9.6 μm O_3 band reveals that above a tangent height of 10 km the radiances are highest for the standard atmosphere O_3 profile rather than for our adopted high O_3 amount profile. The reason for this is that the high O_3 abundance profile is based upon an extreme high O_3 profile that might occur at high latitudes in winter The shape of this profile is such that much of the ozone concentrated in the layer below 25 km. This shape is different from the standard atmosphere profile, which has a higher center of gravity. As a result, O_3 mixing ratios above an altitude of about 28 km are actually higher in the standard atmosphere profile rather than in the high O_3 profile, although the total amount of O_3 is highest in the high O_3 model. This difference in shape combined with the absorption characteristics of the 9.6 μm band causes the highest radiances above 10 km tangent height to be associated with the standard atmosphere O_3 distribution.

The rapid fall-off of radiance with increasing tangent height characteristic of the absorption bands at the high tangent heights is found throughout the entire horizon radiance profile in the window region at 10.3 μm (Figure 15). Over the range of tangent heights zero to 60 km, the 10.3 μm radiance drops almost seven orders of magnitude. For the window computations, besides varying the water vapor profile through its extremes, the temperature profile was simultaneously varied through its extremes. Thus, the difference between top and bottom horizon radiance profiles in Figure 15 represents the extreme range over which the 10.3 μm radiance might vary.

Figures 16 through 19 illustrate the extreme ranges of radiance to be expected in the absorption bands at tangent heights of zero, 20, 40, and 60 km. The band radiances represent integrals over the bandwidth indicated by the bar lines. The range in band radiance of the 6.3 μm H_2O band is consistently greater than the range of rotational band due to the greater sensitivity of Planckian emission to temperature, at the lower wavelengths. These are extreme ranges and should be useful in planning measurement programs.

36
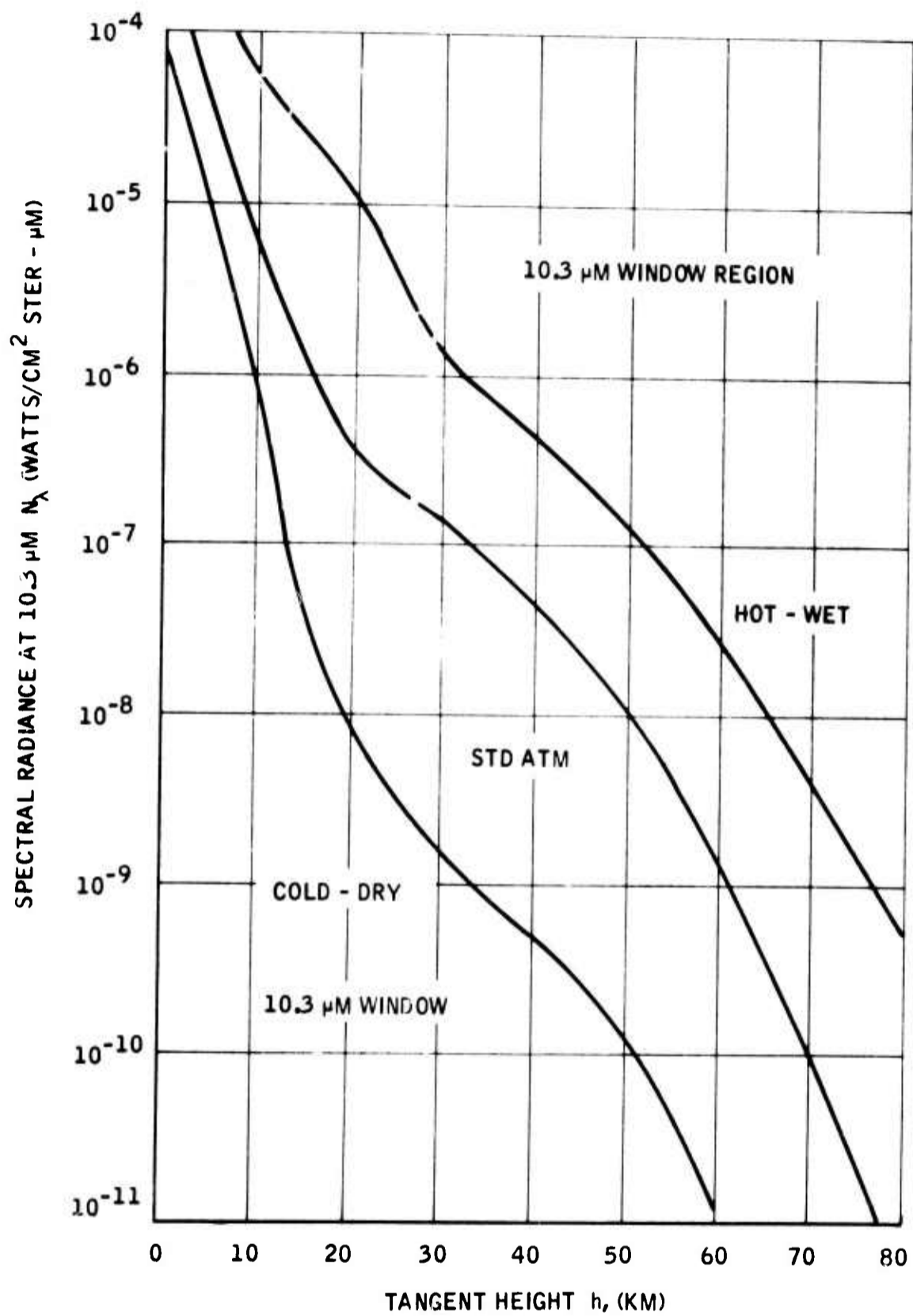
Figure 15. Horizon Radiance Profiles for the 10.3 μm window for Standard and Extreme H_2O and Temperature Profiles
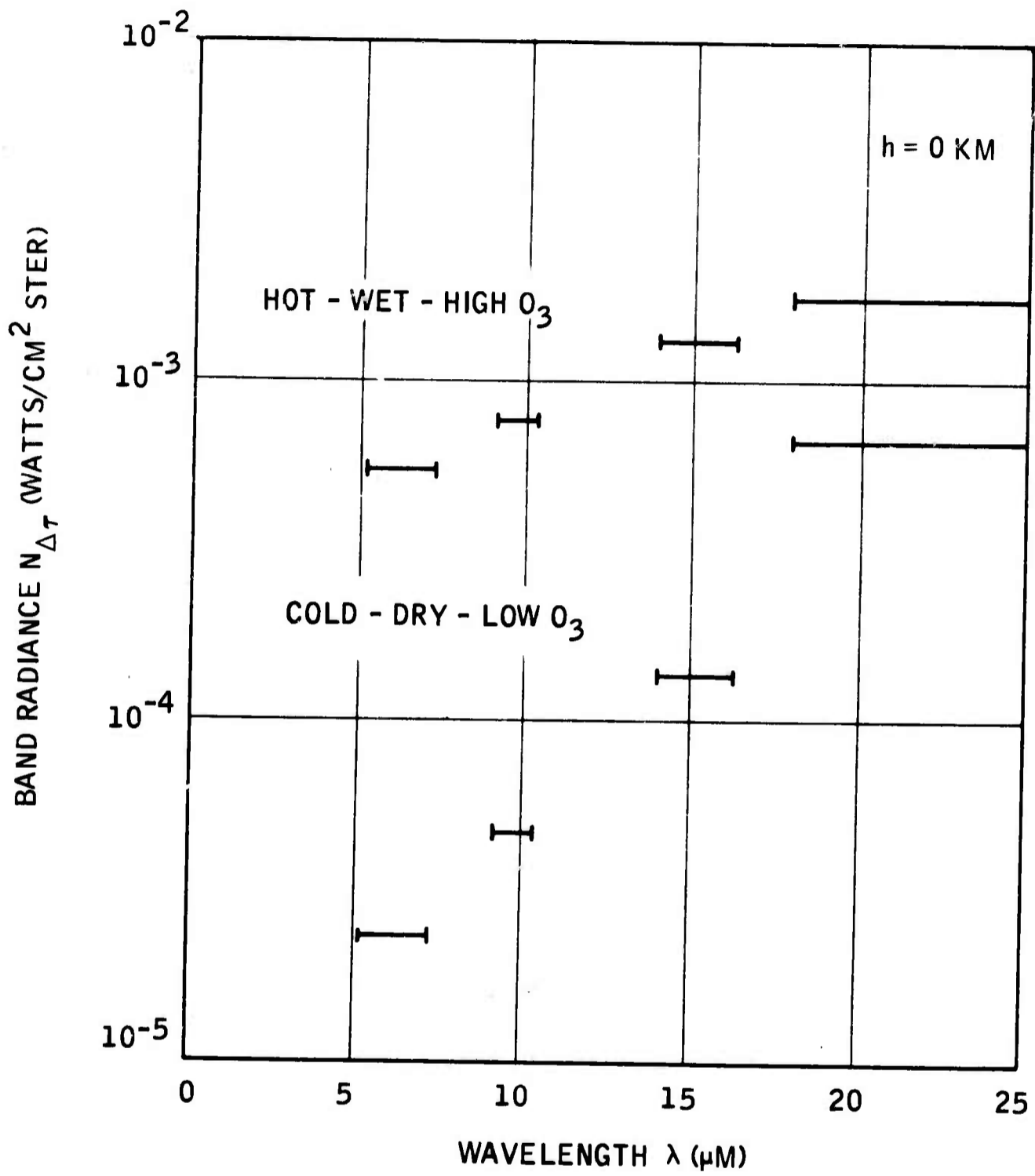
Figure 16. Extreme Ranges of Band Radiance
for Tangent Height 0 km
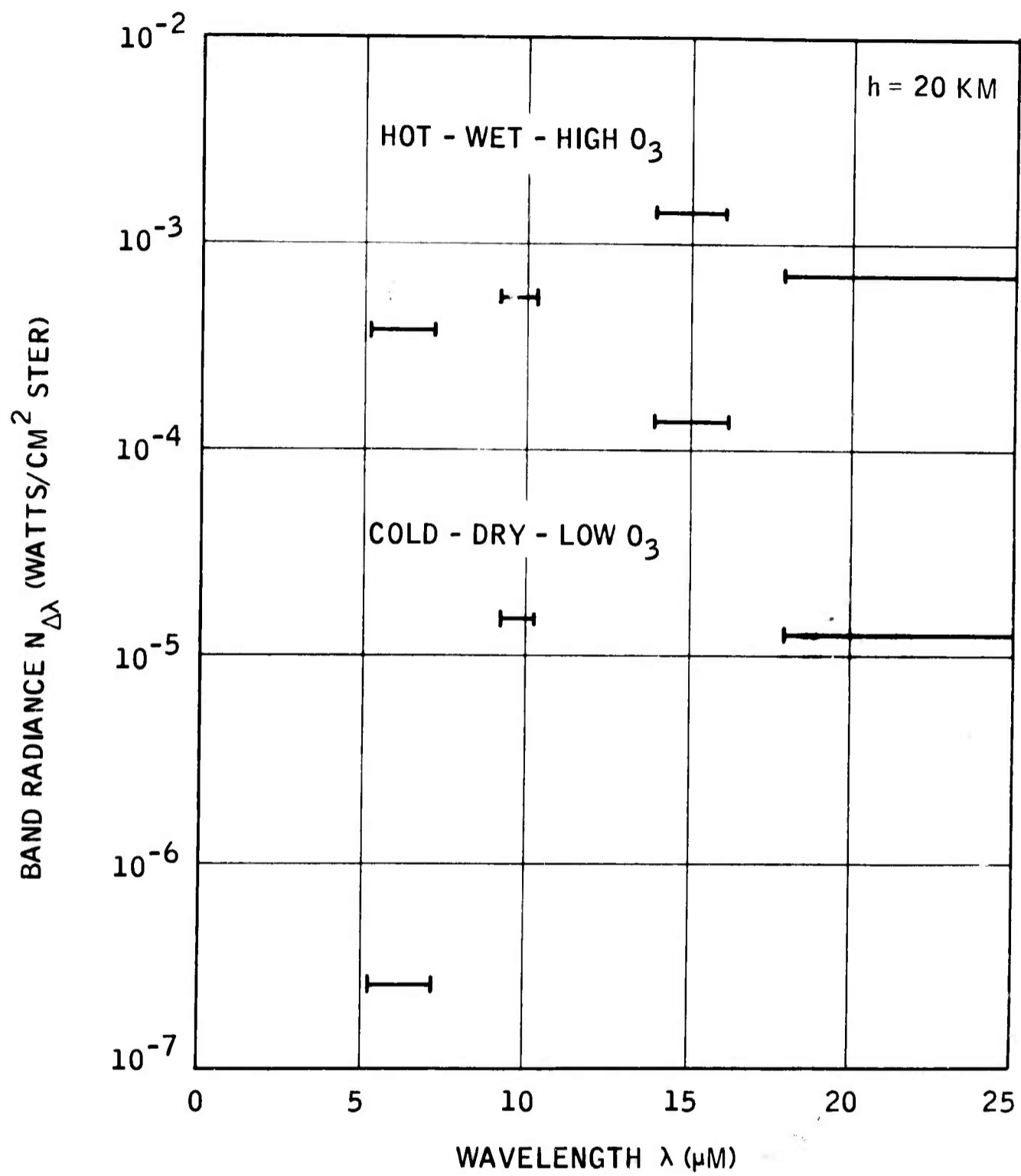
Figure 17. Extreme Ranges of Band Radiance for Tangent Height 20 km

39
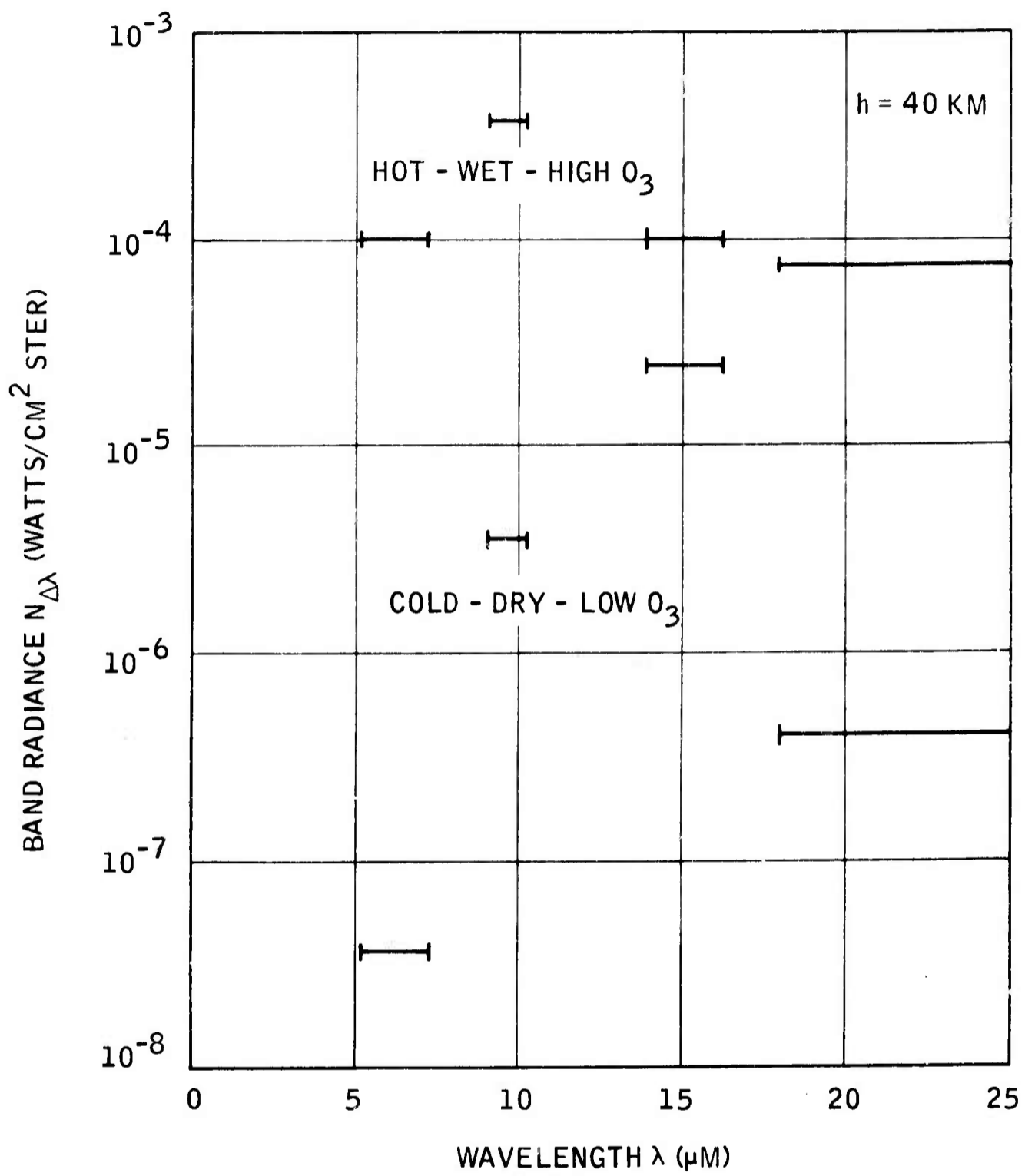
Figure 18. Extreme Ranges of Band Radiance for Tangent Height 40 km
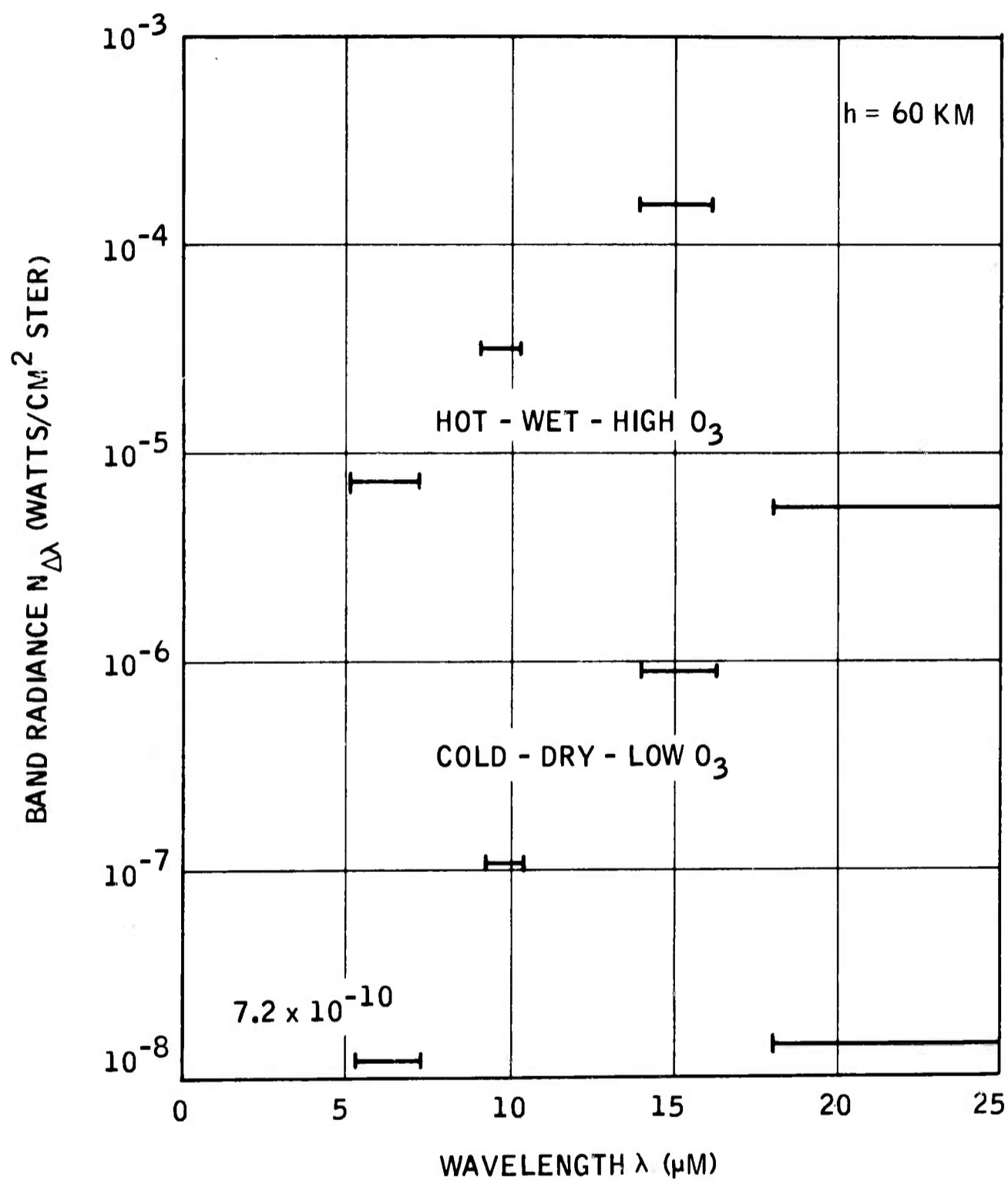
Figure 19. Extreme Ranges of Band Radiance for Tangent Height 60 km

41

Also useful in planning measurement programs is the average spatial variation of radiance over the globe. Figures 20 and 21 show the mean latitudinal variations of band radiance at 30 km tangent height for winter and summer, respectively. The decrease of radiance toward the pole during winter and the slight increase toward the pole during summer reflects mainly the upper stratospheric temperature gradient during these seasons.

Figure 22 shows the variability in band radiance at 30 km tangent height that might be experienced as a result of longitudinal temperature gradients in the arctic winter stratosphere. These temperature gradients arise as a result of the generally warm Aleutian stratosphere and cold northeastern Canada stratosphere during winter.

The sample of calculations discussed above was selected to obtain information on the mean spectra and the variability about the mean. In particular, calculations were performed with meteorological profiles representing extremes of temperature and absorber concentrations. These should provide valuable information on the high and low radiances to be expected. Calculations were also performed with meteorological profiles representative of average spatial variations. These should provide information in the normal horizontal variability of infrared limb radiance.

Spectral radiances for 47 atmospheric models are given in Appendix E in 10-kilometer steps. The model numbers and tabulated profile parameters are given in Appendix C
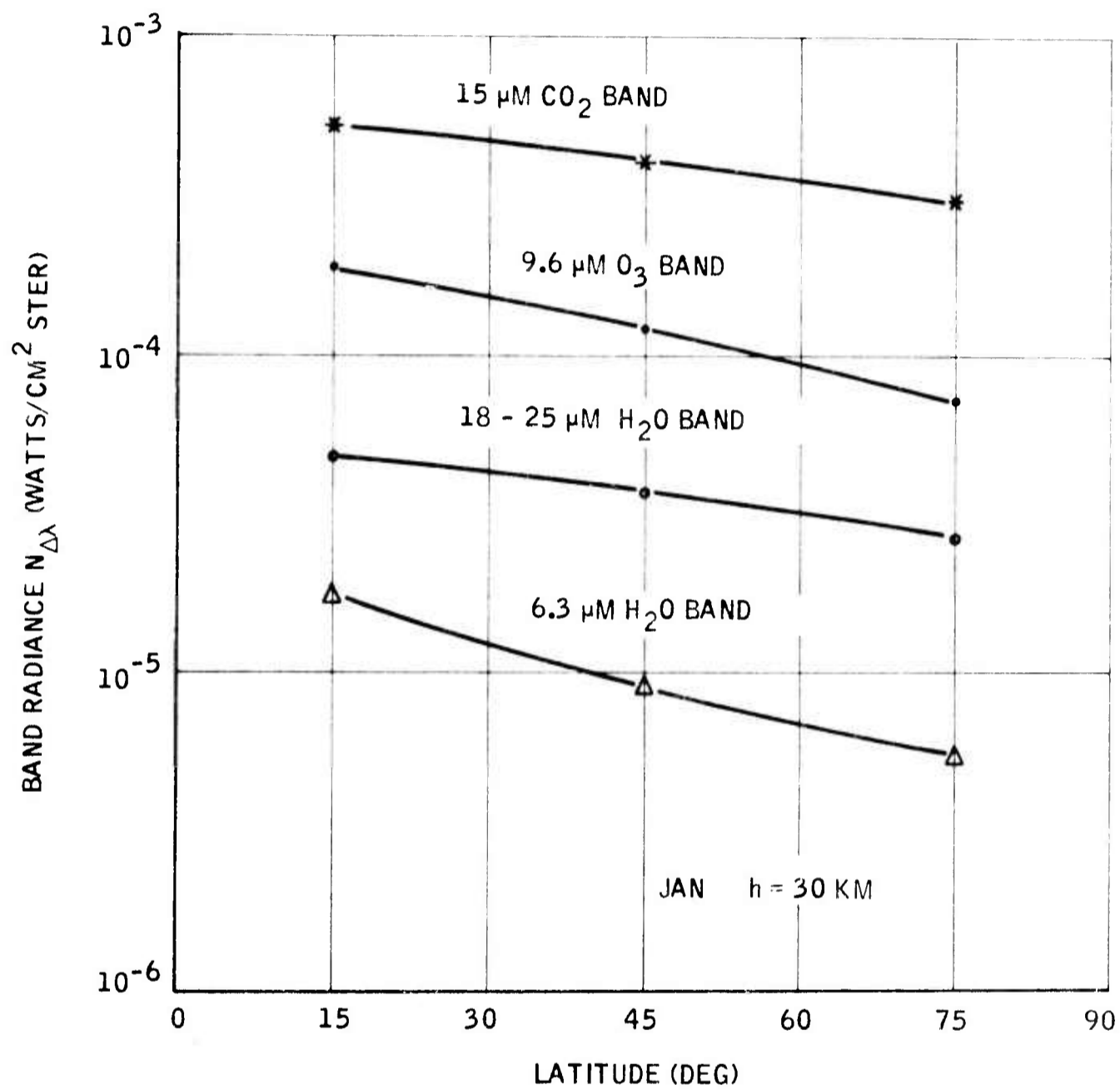
Figure 20. Mean Latitudinal Variation of Band Radiances at
h = 30 km During Winter
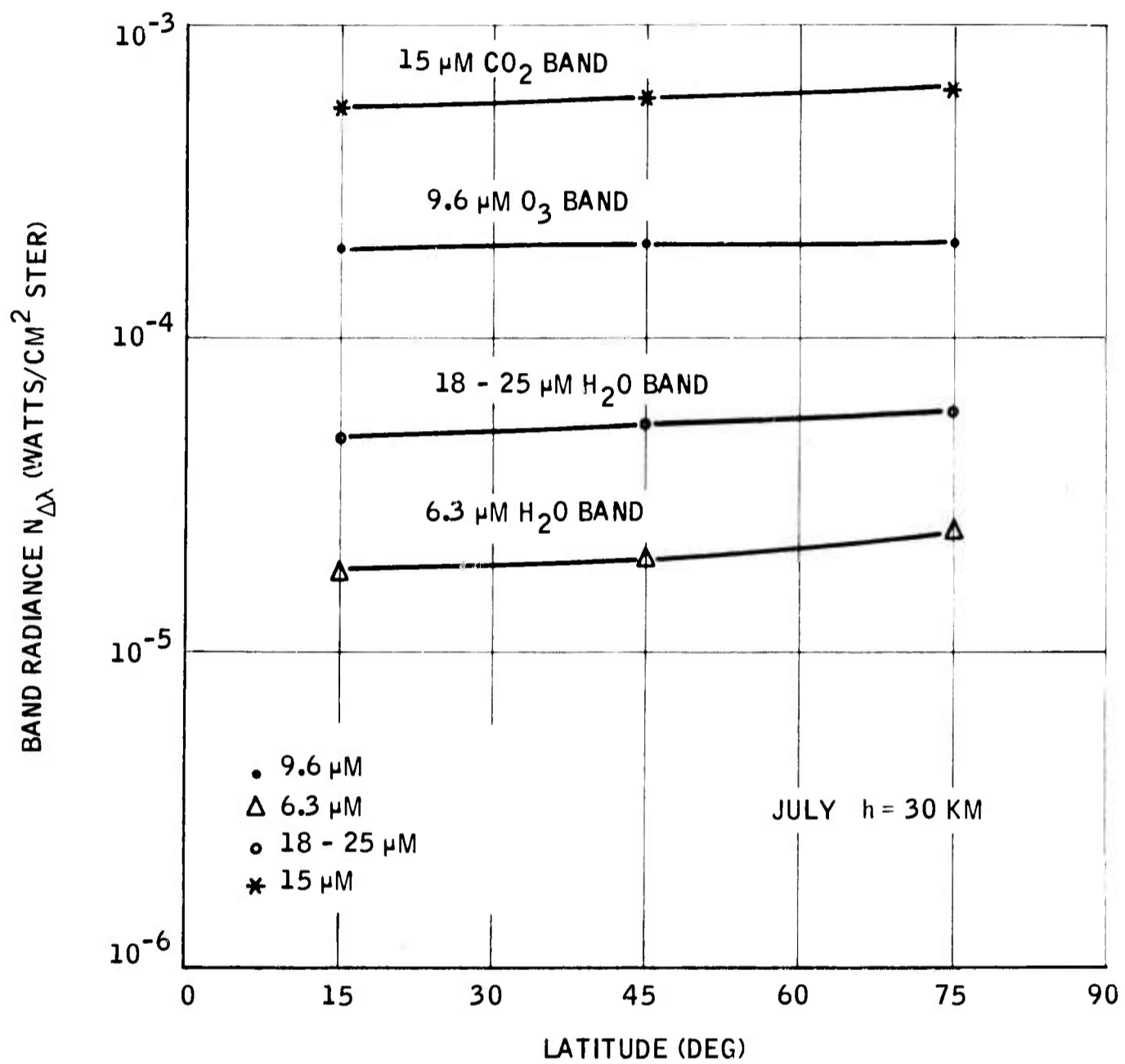
Figure 21. Mean Latitudinal Variation of Band Radiances
at h=30 km During Summer
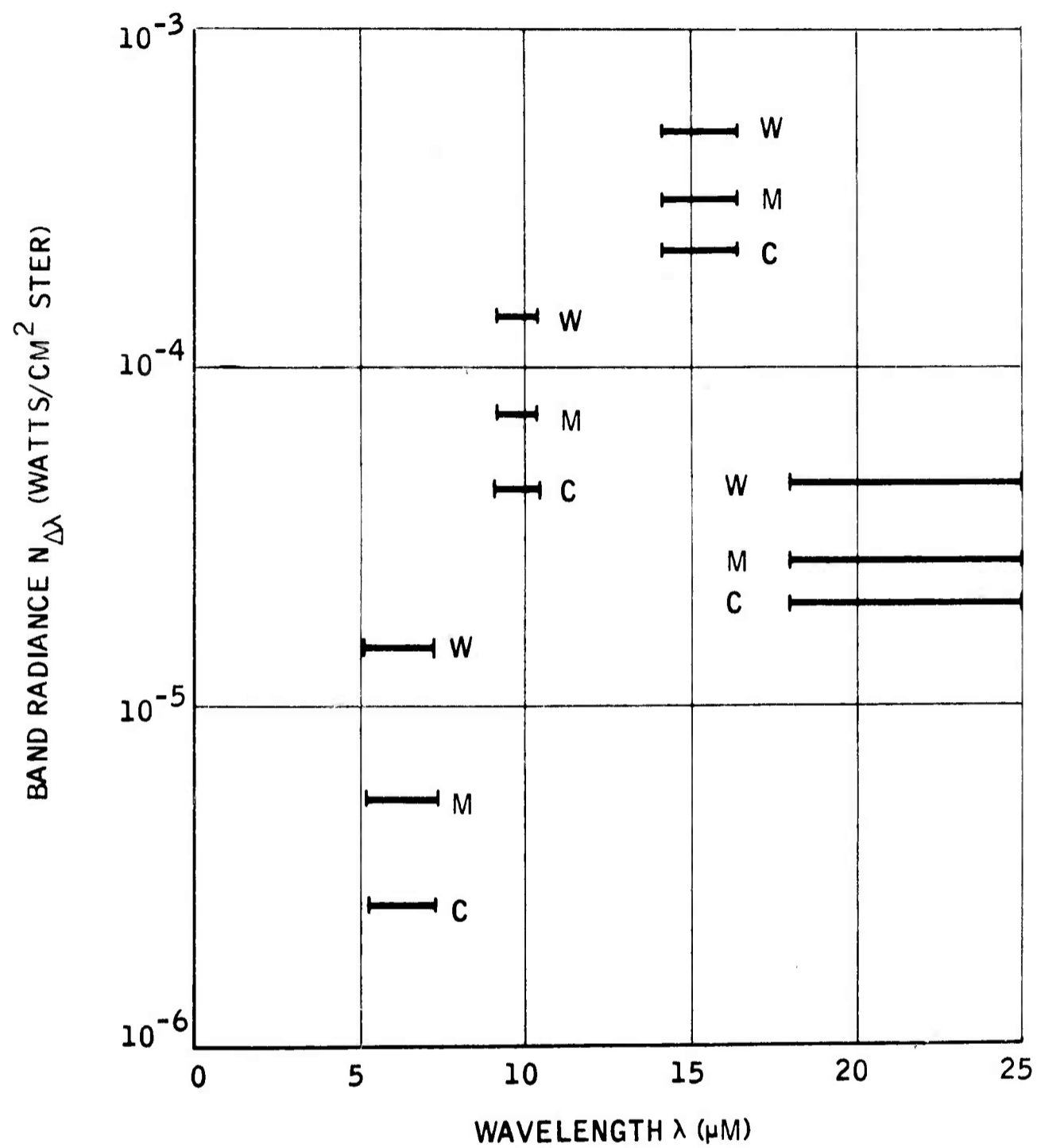
Figure 22. Band Radiances at h=30 km During Winter at 75° Latitude for Warm (W), Mean (M), and Cold (C) Stratospheric Thermal Regimes

SECTION IV

INFRARED ACTIVE GASES IN THE
UPPER ATMOSPHERE

A. GENERAL CONSIDERATIONS

Knowledge of the day and night airglow emissions in the infrared region of
the electromagnetic spectrum is of great importance to military surveillance
schemes. In addition, measurement of such radiation can provide the
scientist with information on the energy content of the atmosphere, its
chemical composition and the physical reactions which take place.

All molecules except homonuclear diatomic molecules such as N_2, O_2 and
H_2 are potential strong emitters of infrared radiation. This section dis-
cusses estimates of abundances of infrared active molecules and describes
the considerations which led to the selection of CO_2, H_2O, O_3, NO, N_2O and
CH_4 alone for inclusion in preliminary high altitude 5 to 25 μm infrared
radiance calculations. Since practically all infrared vibration-rotation
bands have strengths of the order of 100 to 1000 cm^{-2} ATM^{-1}, it was
possible to make this selection on the basis of chemical abundances and the
position of infrared vibration-rotation bands.

Most of the infrared emission of the earth's atmosphere comes from mole-
cules present as minor constituents. The energy of an infrared quantum of
radiation is such that in general it corresponds to the difference in energies
of vibrational or rotational levels within a single electronic state of a mole-
cule. In order for a transition resulting in emission of radiation to take
place between two such levels, there must be a change in the electric dipole
moment of the molecule. This is not possible in the case of homonuclear
diatomic molecules such as nitrogen or oxygen. The emission spectra of
these molecules arises from transitions between electronic states, and

46

under normal conditions their spectra does not extend to wavelengths as long as 5 μm. The electric dipole moment of heteronuclear molecules such as nitric oxide (NO) and carbon monoxide (CO) is different for different vibrational levels, and they have prominent infrared vibrational spectra. All polyatomic molecules such as carbon dioxide (CO_2) have infrared vibrational spectra. In addition, molecules with a permanent electric dipole moment such as CO, NO and water vapor (H_2O) have pure rotational spectra in the far infrared.

In the troposphere clouds, CO_2 and H_2O control the heat budget of the atmosphere through their absorption and emission of infrared radiation. Other infrared active constituents such as CH_4, NO_2, N_2O and CO are produced near the surface of the earth in trace amounts. At high altitudes, the action of solar radiation and subsequent chemical reactions produces species such as O_3, NO, NO^+, N_2O, H_2O_2, OH, and HO_2.

At low altitudes, the predominant mechanism leading to infrared emission is thermal excitation of vibrational and rotational energy levels of the ground electronic state of these minor constituents. At high altitudes, however, other activation processes must be considered.

The relative importance of each depends on the molecule involved and on the altitude. The additional mechanisms known to be of importance are chemical formation in an excited state, fluorescent emission due to excitation by visible or ultraviolet solar irradiation, resonant excitation by solar or terrestrial infrared radiation, and excitation by corpuscular radiation in the normal daytime ionosphere or during aurorae. Some of these processes continue day and night, as does thermal excitation, while others are restricted to daytime or to distrubed atmospheric conditions.

In addition to the radiation from polar molecules in excited vibrational levels of the ground electronic state, transitions between excited electronic states

of N_2, O_2 and N_2^+ provide a source of infrared emission. Figure 23 shows
the position of infrared vibration-rotation bands of selected molecular species.
The long lines indicate the position of the centers of strong bands. The short
lines show the band centers of weaker vibration-rotation bands except for NO,
where they indicate the position of transitions between highly excited electronic
states. Band positions were obtained from Herzberg (1945), Wallace (1962a,
1962b) and Wray (1969).

B. CHEMICAL ABUNDANCES

Very little experimental data is available on the distribution with altitude of
minor constituent molecular abundances. Only ozone and nitric oxide con-
centrations have been determined directly at altitudes as high as 100 km.
Hence reliance must be made on computational estimates which are only as
good as the reaction rates used. Several important rates are known only to
within an order of magnitude, while Nicolet (1965a) points out that really
meaningful computations require 20 percent accuracy.

The most complete computations of chemical abundances at high altitude are
those of Hunt (1966) and Keneshea (1967). Accurate computations must in-
clude the effects of eddy and molecular diffusion. Unfortunately, such trans-
port mechanisms have as yet not been effectively coupled with chemical
computations for minor atmospheric constituents. Computed and observed
concentrations may differ by as much as an order of magnitude as is the case
of nitric oxide between 60 and 90 km.

1. Carbon Dioxide

The most abundant minor constituent of the atmosphere is carbon dioxide.
Its abundance is well known in the lower atmosphere, and is relatively stable

48
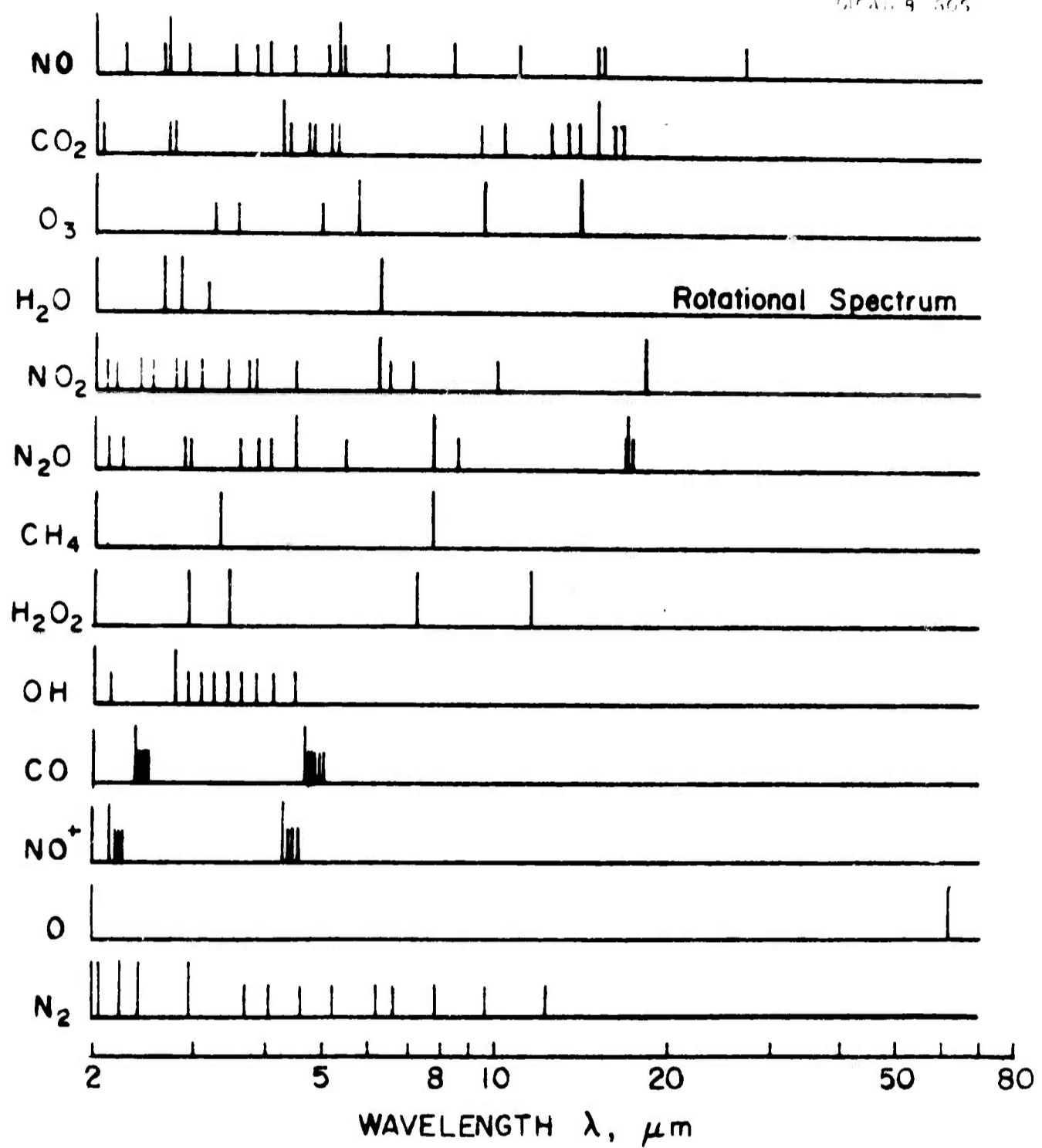
Figure 23. Band Centers of Vibration-Rotation Bands
of Selected Infrared Active Molecules

at about 320 parts per million except close to industrial areas where the burning of fuel increases its concentration locally. At altitudes above about 70 km it is dissociated by sunlight in the spectral range 1200 to 1750Å. Although Bates and Witherspoon (1952) gave a qualitative discussion of the chemistry of CO_2 at high altitude over 15 years ago, there has been no quantitative study of its abundance at high altitudes. Because of its importance as a source of infrared radiation, knowledge of its abundance at high altitudes is required.

As part of the current effort, CO_2 photochemical equilibrium concentrations above 60 km altitude have been computed using solar continuum and Lyman-Alpha fluxes from Johnson (1965). The most important reactions considered are:

$$CO_2 + h\upsilon \rightarrow CO + O \qquad\qquad (5)$$

$$CO + OH \rightarrow CO_2 + H \qquad\qquad (6)$$

$$CO + O + M \rightarrow CO_2 + M \qquad\qquad (7)$$

The reaction rate for (6) was taken from Baulch et al. (1968). Reaction (7) has been studied by many experimental groups, with widely differing results. The rate given by Barth (1964) was considered representative and was used in the calculations.

Because of the shielding of CO_2 from the continuum flux by molecular oxygen, Lyman-Alpha radiation at 1216Å accounts for most of the photodissociation of CO_2. Even so, the lifetime of CO_2 against photodissociation is on the order of a year and atmospheric diffusion will be important. On this basis the photochemical equilibrium results were used, neglecting Lyman-Alpha radiation. The results of this computation are given in Figure 24. This abundance distribution should be considered a lower limit to CO_2 abundance. Also shown as a dashed line is the CO_2 concentration profile given by
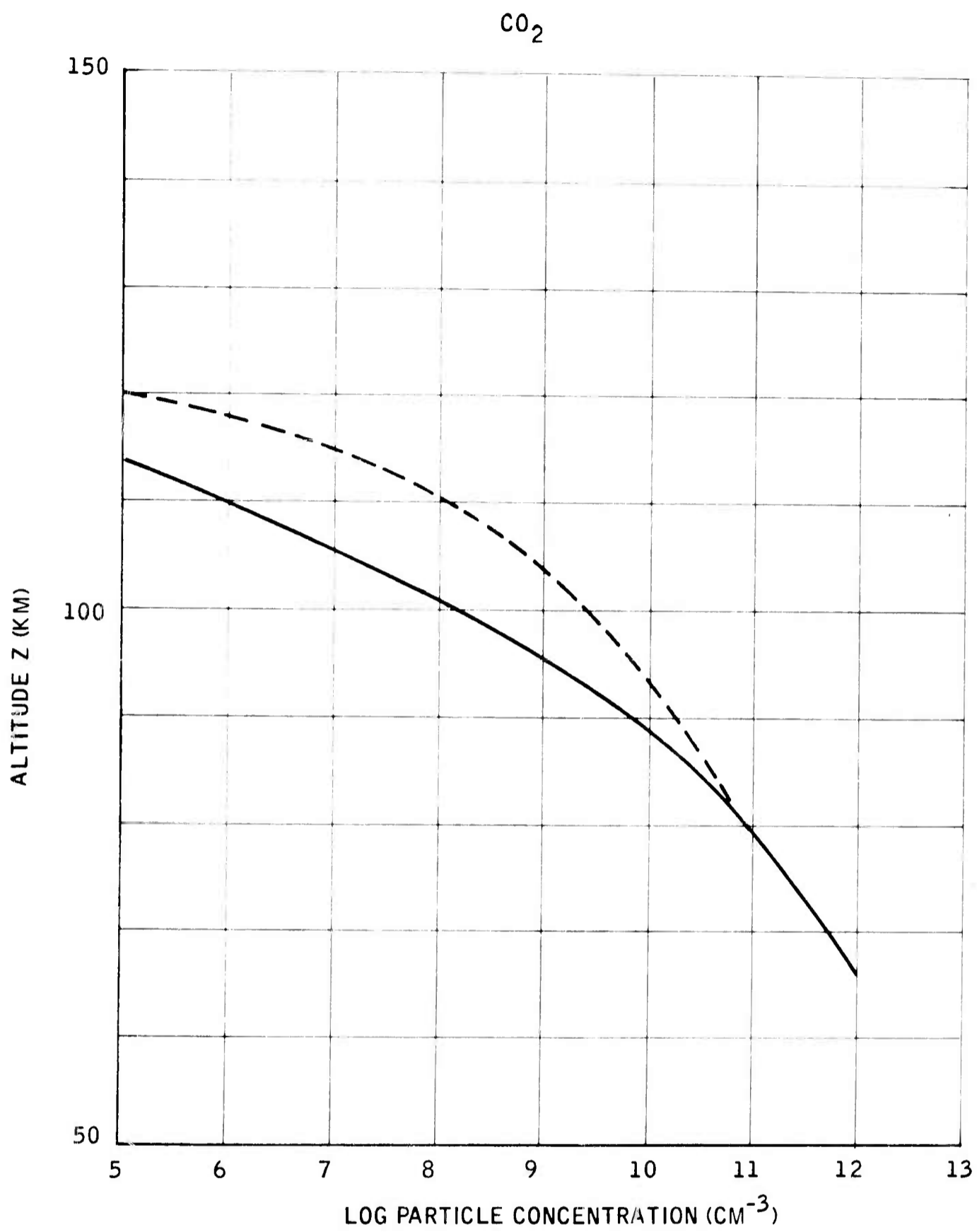
Figure 24. Carbon Dioxide Concentration Profiles

Bortner and Kummler (1968). This may be considered an upper limit to the abundance of CO_2 with altitude.

2. Water Vapor

Water vapor concentrations vary greatly near the surface of the earth. There have been no comprehensive measurements above balloon altitudes. Measurements from balloons give widely varying values, and it is probable that water vapor carried up with the balloon strongly affects measurements at the highest accessible altitudes. Recent stratospheric observations are those reported by Mastenbrook (1968). In a series of 51 flights, observed volume concentrations in the lower stratosphere were between 2 and 5 parts per million in nearly all cases, with a mean of about 3 parts per million. Extrapolation of such measurements to higher altitudes is uncertain, but there is now general agreement that this is the correct order of magnitude to use in chemical computations at altitudes up to 100 km. The results of Hunt (1966) are adopted here. He uses a similar volume mixing ratio of 5 parts per million as the initial starting point of his chemical computations. Hunt's final number densities of H_2O are shown in Figure 25.

The important reactions which produce H_2O at high altitudes are:

$$H + HO_2 \rightarrow H_2O + O \tag{8}$$

$$OH + HO_2 \rightarrow H_2O + O_2 \tag{9}$$

$$OH + OH \rightarrow H_2O + O \tag{10}$$

$$OH + H_2O_2 \rightarrow H_2O + HO_2 \tag{11}$$

$$OH + H_2 \rightarrow H_2O + H \tag{12}$$

52
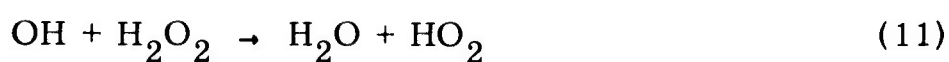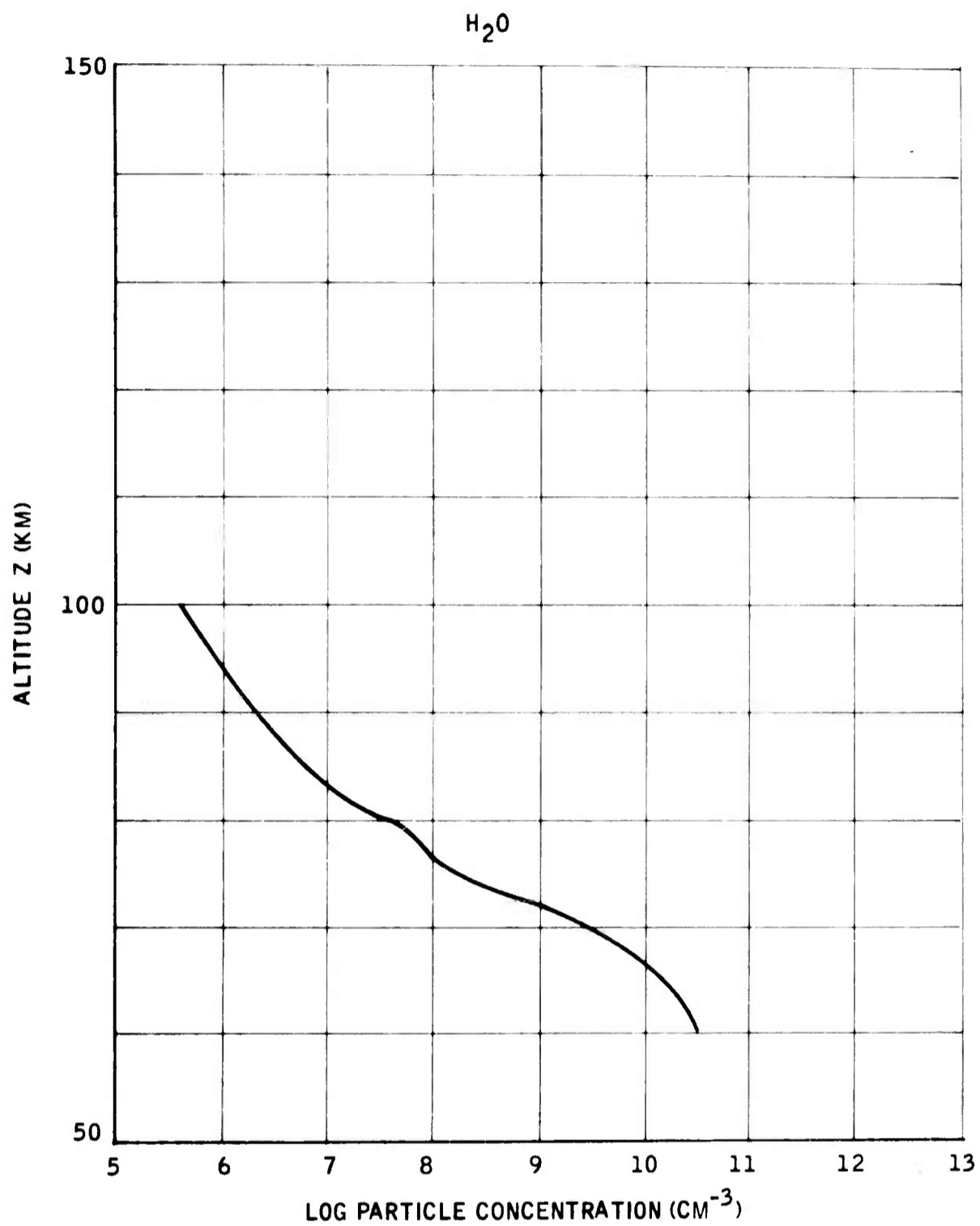
Figure 25. Mean Water Vapor Concentration Profile

A sixth reaction which produces water vapor is:

$$O + CH_4 \rightarrow H_2O + CH_2 \tag{13}$$

Bates and Nicolet (1965) have discussed this and show it to be an important source in the stratosphere, accounting for as much as half of the observed water vapor concentrations. Hunt's neglect of this reaction is not important if the H_2O produced by it is considered as part of the initial concentration.

Those reactions which destroy H_2O are:

$$H_2O + h\nu \rightarrow H + OH \tag{14}$$

$$H_2O + O(^1D) \rightarrow OH + OH \tag{15}$$

3. Ozone

The other molecules treated by Hunt which are considered as possible sources of infrared emission are O_3, H_2O_2, OH, and HO_2. Hunt's abundances for these species are shown in Figures 26 through 28. The ozone concentrations agree well with measurements below 80 km and will not be appreciably affected by the uncertainty in water vapor concentration. The concentrations of the other species must be considered as estimates only, although the OH production rates agree well with the observed altitude profiles of the OH infrared band systems.

Heestvedt (1965) has done a similar computation for several latitudes and two values of the water vapor mixing ratio. This work is useful as a guide to possible seasonal and latitudinal variation of the ozone concentration, but is limited to giving daytime photochemical equilibrium values of concentrations.
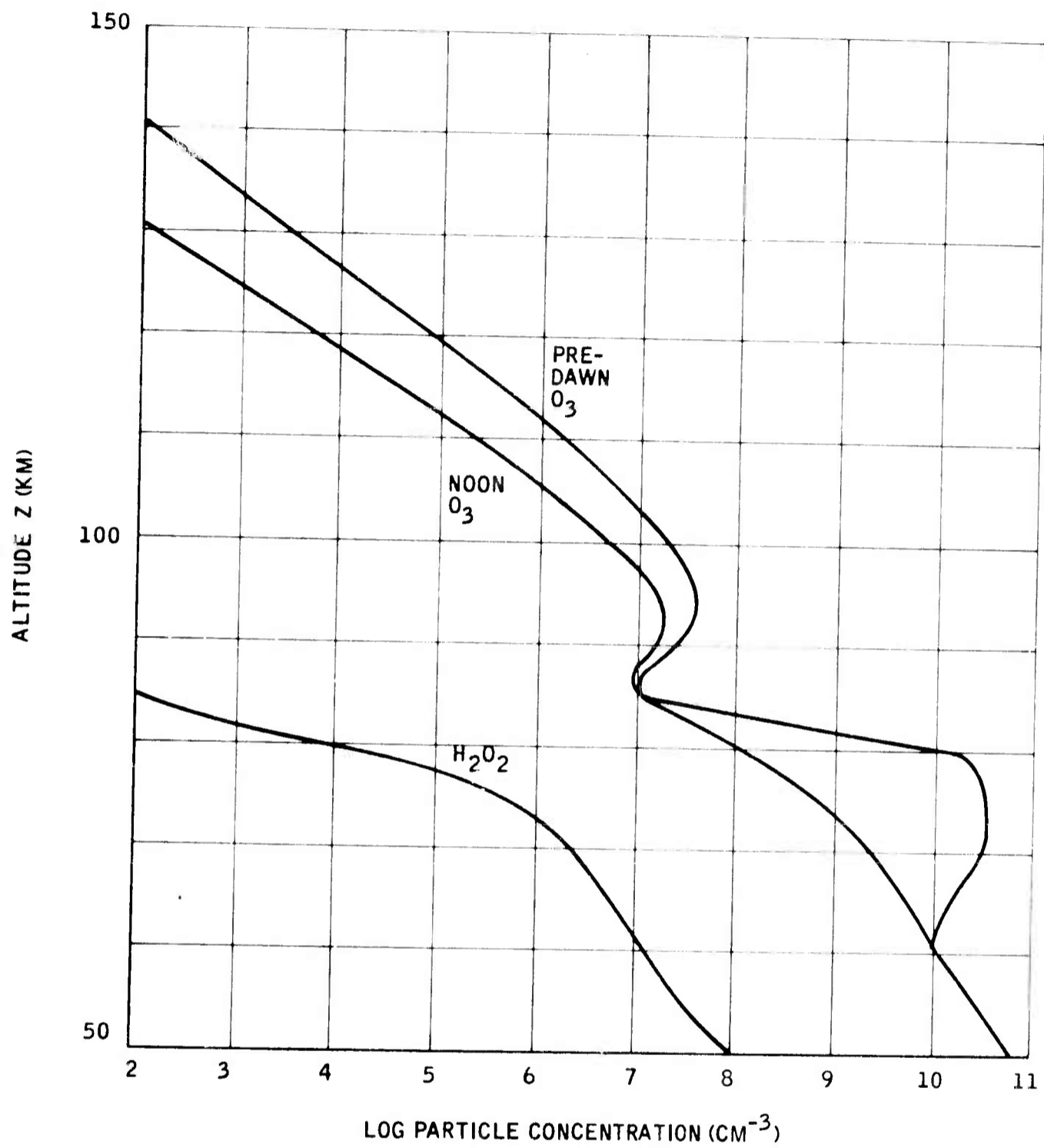
Figures 26. Ozone and Hydrogen Peroxide Concentration Profiles
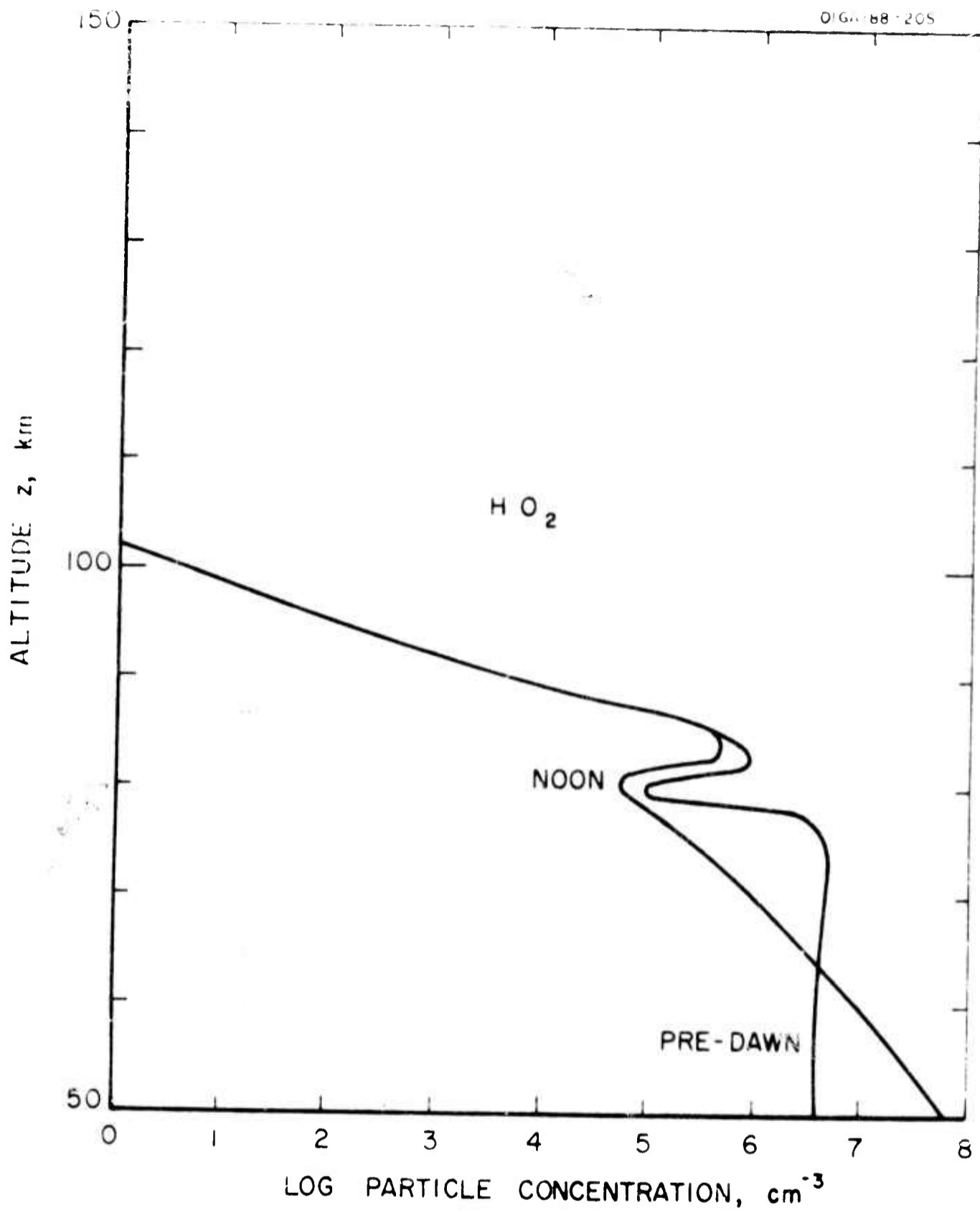
Figure 27. Perhydroxyl Concentration Profile
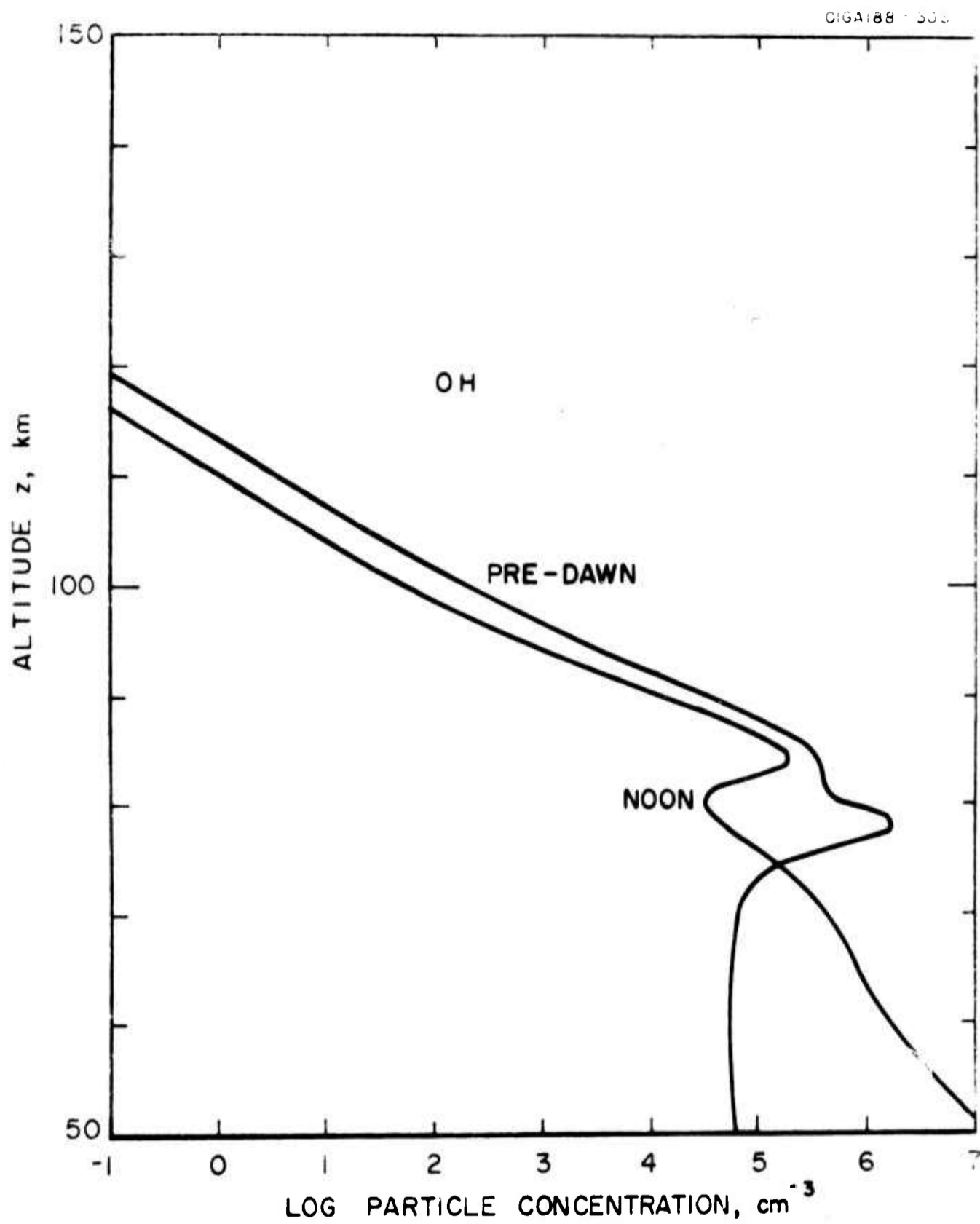
Figure 28. Hydroxyl Concentration Profile

57

The abundance of H_2O_2 is nearly three orders of magnitude less than that of O_3. The vibration-rotation bands of OH are at wavelengths shorter than 5 μm. Although HO_2 is present at 80 km in about the same abundance as O_3, there is at present insufficient data available to make meaningful calculations. These three molecules are therefore omitted from further consideration in the current study.

4. <u>Nitric Oxide</u>

The daytime concentration of nitric oxide is shown in Figure 29. This plot is the result of combining daytime observations by Barth (1966) and Pearce (1969) with computational estimates by Nicolet (1965b), Ghosh (1968) and Saxena (1968). The nighttime concentration should not be appreciably different at altitudes between 70 and 120 km (Barth, 1965a and Saxena, 1968). Below 70 km, nitric oxide is destroyed at night by reaction with ozone. Saxena (1969) has included the effects of diffusion on night abundances and obtained a lowering of concentration above 120 km. This information was obtained too late to include in the computations.

Before Barth (1964) first measured nitric oxide concentrations at high altitudes, it had been assumed that the principal reaction forming nitric oxide is

$$N(^4S) + O_2(^3\Sigma_g^-) \rightarrow NO(^2\Pi_u) + O(^3P) \qquad (16)$$
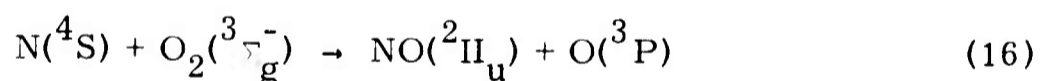
where all reactants and products are in the ground state. The measured abundances are an order of magnitude greater than those which can be generated in this way at altitudes below 90 km. Subsequently, Nicolet (1965b) proposed the reaction

$$O_2(^2\Sigma_g^+) + N_2(^1\Sigma_g^+) \rightarrow NO(^2\Pi_u) + NO^+(^1\Sigma^+) \qquad (17)$$

58
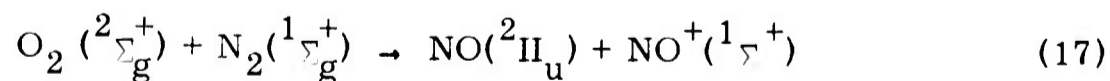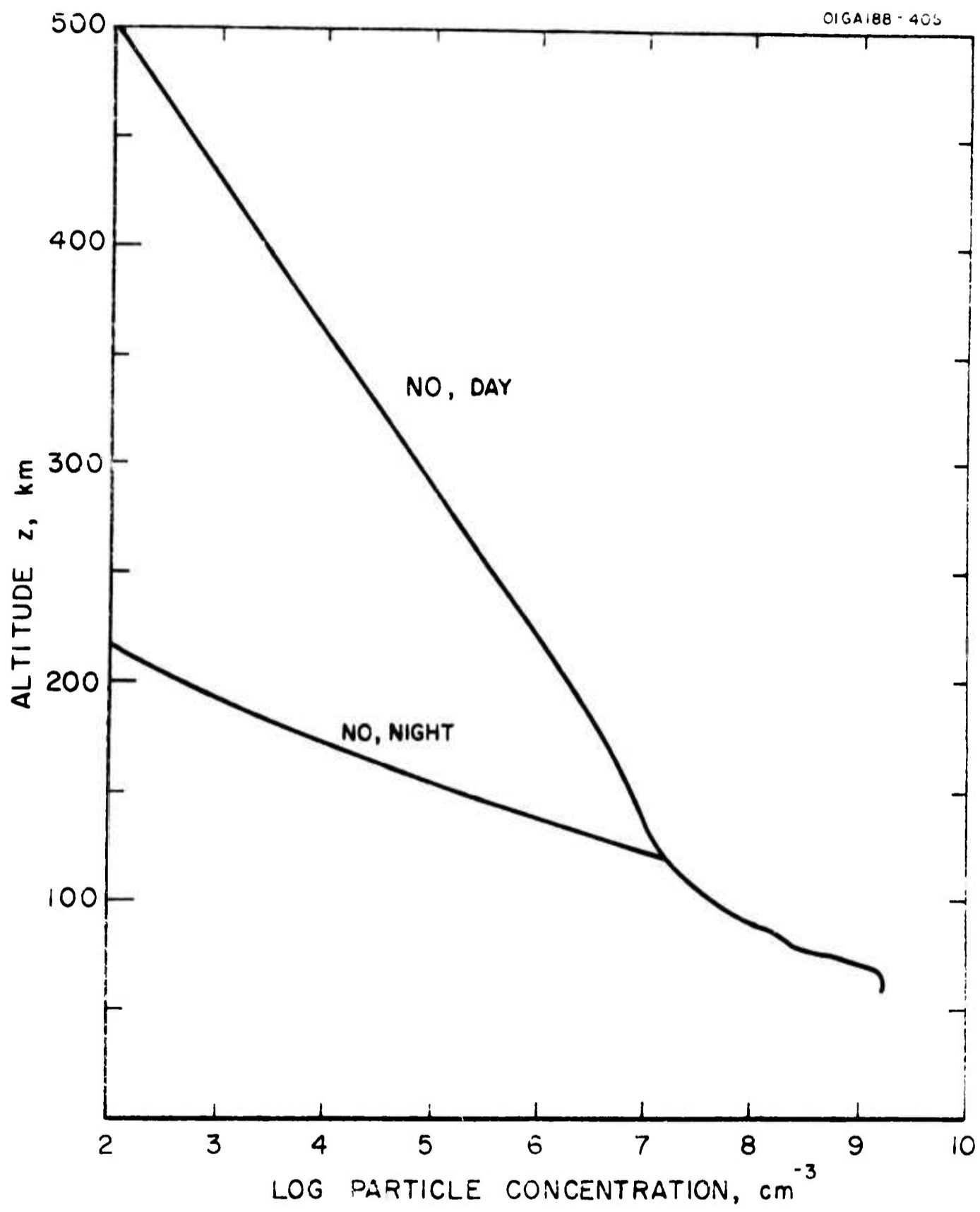
Figure 29. Nitric Oxide Concentration Profile

However, the measured upper limits to the rate make this reaction unimportant below 100 km. Hunten and McElroy (1968) have proposed the reaction

$$N(^4S) + O_2 \, (^1\Delta_g) \rightarrow NO \, (^2\Pi_u) + O(^3P) \tag{18}$$
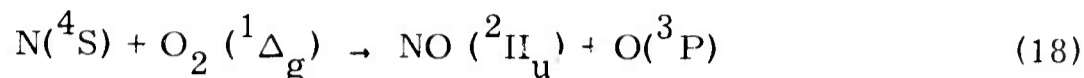
DelGreco and Kenneally (1968) have reported a lower limit for the reaction rate to be 4×10^{-14} cm^3/sec. Burt and Schiff (1969), however, find a rate constant less than 10^{-15} cm^3/sec.

The lower limit to the rate measured by DelGreco and Kenneally (1968) is about 25 times too small to produce the number densities found by Pearce (1969) below 90 km. Another possible reaction is

$$N(^2D) + O_2 \, (^3\Sigma_g^-) \rightarrow NO \, (^2\Pi_u) + O(^3P) \tag{19}$$
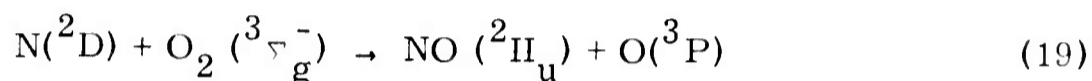
Its importance depends on the extent to which dissociative recombination of NO$^+$ forms atomic nitrogen in the ^{2}D state. At present there is no reaction known with certainty to be capable of producing observed nitric oxide concentrations below 90 km. However, Geissler and Dickenson (1968) have examined transport phenomena near the mesophere and conclude that nitric oxide produced above 85 or 90 km can be carried down rapidly enough to explain known abundances between 70 and 85 km. Observed abundances are adopted as the basis for the computations.

Nicolet (1965a) estimates daytime abundances of NO$_2$ to fall rapidly with increasing altitude. At 70 km NO$_2$ concentrations are 10^{-3} that of NO and at 100 km are 10^{-4} that of NO. NO$_2$ concentrations at night approach the NO daytime concentration below 75 km due to the reaction

$$NO + O_3 \rightarrow NO_2 + O_2 \tag{20}$$

but maintain the daytime value above 75 km.

5. Nitrous Oxide

Nitrous oxide (N_2O) concentrations have been computed by Keneshea (1967) and are shown in Figure 30. For noon near the equator, the principal reaction leading to formation of N_2O is

$$N_2 + O + M \rightarrow N_2O + M \qquad (21)$$

The principal loss reactions are

$$N_2O + h\upsilon \rightarrow N_2 + O \qquad (22)$$

$$N_2O + h\upsilon \rightarrow N + NO \qquad (23)$$

$$N_2O + O_2(^1\Delta) \rightarrow N_2 + O_3 \qquad (24)$$
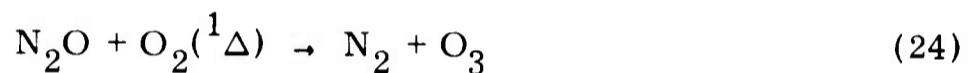
There is no significant diurnal variation.

6. Methane

Methane (CH_4) is uniformly mixed in the troposphere with a volume mixing ratio of about 1.6 parts per million. Figure 31 shows concentrations above 50 km on the assumption that the mixing ratio remains constant in the upper atmosphere. Cadle and Powers (1966) have computed the rate at which it is destroyed by reaction (19). At 60 km the lifetime may be as short as a day and is less than a month. Figure 31 is thus at best an upper limit to methane abundance.
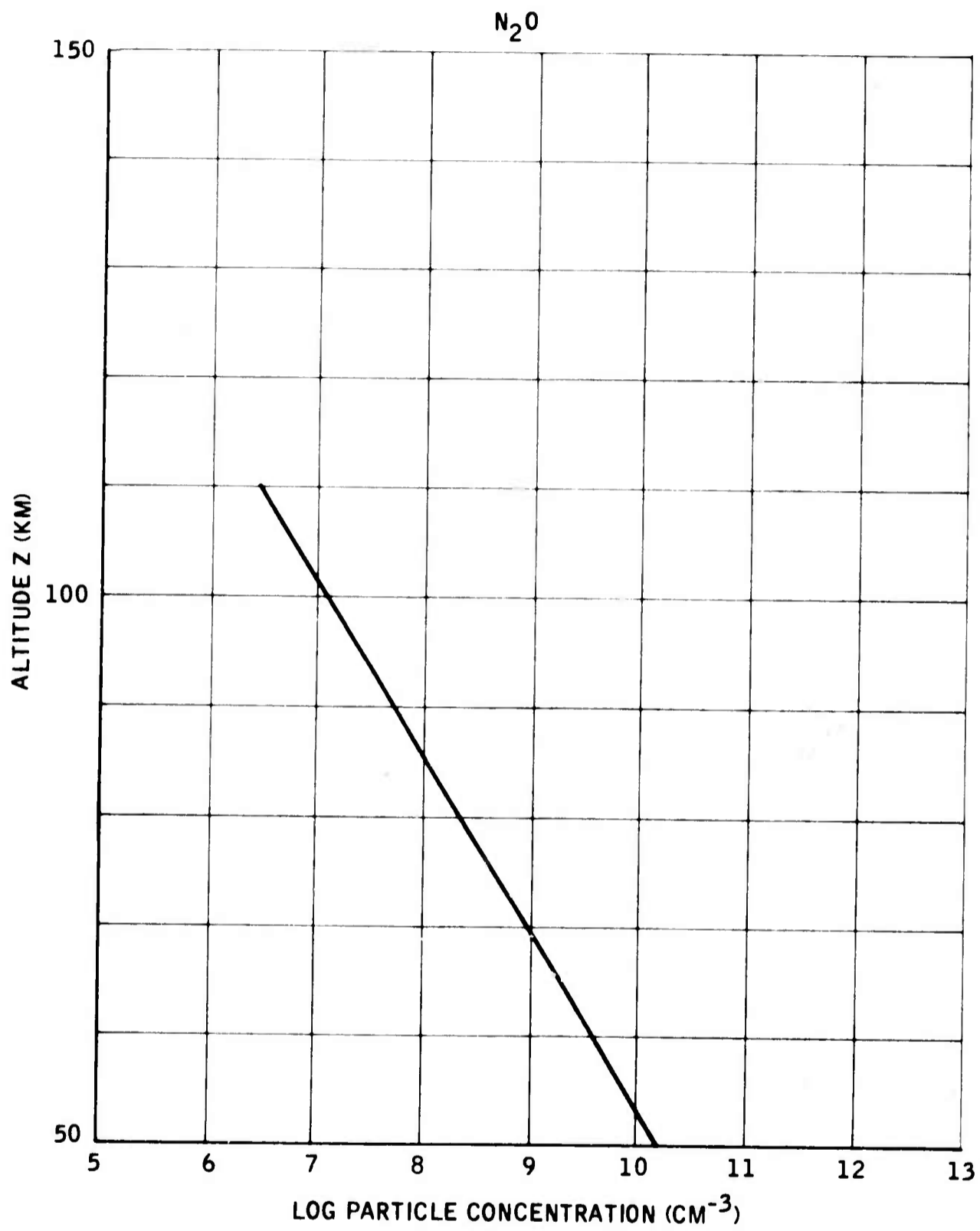
Figure 30. Nitrous Oxide Concentration Profile
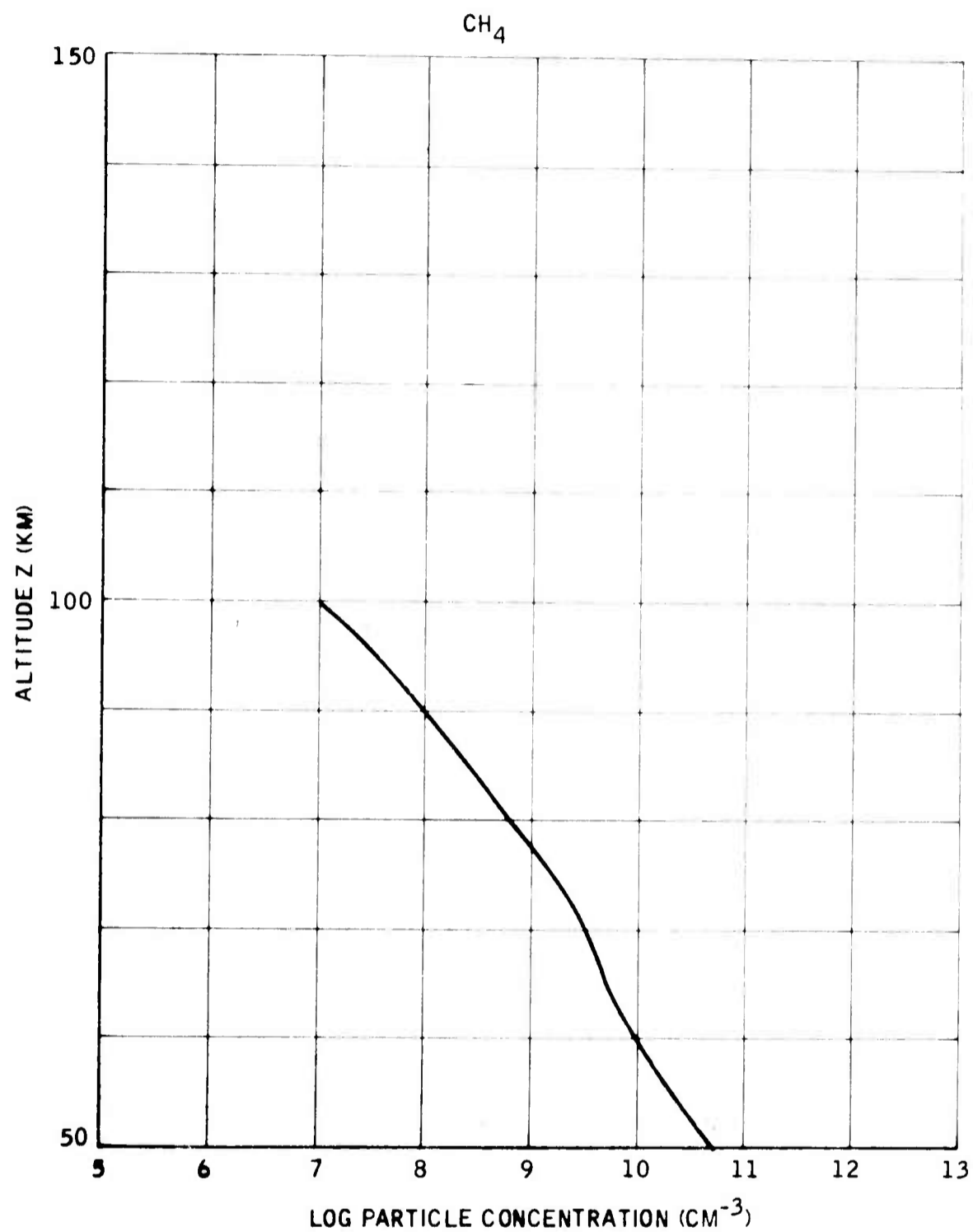
Figure 31. Methane Concentration Profile

7. Other Species

Other species which may provide a source of infrared radiation are oxides such as MgO, CaO, NaO and SiO which are deposited in the upper atmosphere by meteors. Donohue and Meier (1967) have discussed the chemistry of Na in the upper atmosphere, basing their arguments on the observed diurnal variation of the sodium dayglow. They conclude that influx rates are such that sodium in all forms is present at about 2×10^{13} molecules/cm^3 above 50 km. If mixing is uniform, the number density would be 5×10^4/cm^3 at 90 km. The abundances of other metallic oxides and SiO is expected to be of the same order of magnitude. This is three orders of magnitude below the concentrations of NO and N_2O. Therefore, these species have been omitted from further consideration in the current study.

C. SUMMARY

All molecules present in the atmosphere except N_2, O_2 and H_2 are emitters of infrared radiation. In the spectral range 5 to 25 μm, the most important at altitudes above 70 km will be CO_2, H_2O, O_3, NO, N_2O and possibly CH_4, by virtue of their abundance relative to other species.

It is not possible at present to give exact values of concentrations as a function of altitude. Observational data exists only for O_3 and NO. For other species the results of computations must be used. Such computations are only as good as the input data and physical model used. In the case of NO, computations and observations do not agree, probably because transport processes have not yet been reliably included with the chemical computation scheme.

A rough estimate of the reliability of the altitude-concentration profiles given in this section is as follows. CO_2 concentrations are bracketed by the two

curves shown in Figure 24. Water vapor concentrations may be a factor of two lower or a factor of five higher than indicated in Figure 25. Ozone is strongly controlled by the photochemistry and equatorial values are almost certainly within a factor of two of the values of Figure 26. Nitric oxide concentrations below 120 km will be within a factor of three of those shown in Figure 29 below 120 km, with expected deviation to lower and not higher values. Above 120 km, concentrations will lie between the curves for day and night. In view of the known discrepancy between computation and observation for NO, the nitrous oxide curve of Figure 30 may be in error by a factor of three. No estimate is possible for methane, which is not expected to be present in appreciable quantities above 60 km.

In view of the uncertainties in atmospheric abundances, the computational model developed in this study and described in the next section is expected to be more accurate than present knowledge of abundances and capable of determining abundances to greater accuracy when used to analyze experimental data from probes.

SECTION V
DEVELOPMENT OF COMPUTATIONAL MODEL

This section of the report presents the mathematical development of a realistic physical model for computing infrared radiances from gaseous molecules in the upper atmosphere. The abundances of important molecules as a function of altitude were discussed in Section IV, and these data will be used as input information to the computational model. A computer program was developed during the study to perform calculations as specified by the mathematics of the model. The program has the capability of performing exoatmospheric calculations of limb radiances for tangent heights from 60 to 500 km and endoatmospheric calculations as a function of zenith angle from 0° (looking up) to 90° (horizon view) and for any reference altitude within the atmosphere. The physical approximations assumed in the model generally hold for radiance calculations at altitudes above 70 km.

A. GENERAL CONSIDERATIONS

The vibrational population of molecules determines the radiation from the molecules. Several factors influence the vibrational population; collisional excitation, radiative excitation and fluorescent excitation processes, all of which are balanced by radiative de-excitation and collisional de-excitation.

In the troposphere and stratosphere collisional excitation of vibrational levels of polar molecules is sufficiently rapid to compensate for radiative de-excitation and the vibrational population levels are in thermodynamic equilibrium with translation and rotation. At altitudes above 70 or 80 km, however, radiative transitions become more effective than collisions in determining vibrational populations. Absorption of radiation becomes in

66

many cases the most important process leading to infrared radiation. At wavelengths longer than about 5 μm, the most intense source of radiation is the thermal emission from either carbon dioxide, water vapor and ozone from lower levels in the stratosphere, troposphere or the earth's surface. During the day, however, solar radiation should be included because fluorescent processes involving absorption of visible or ultraviolet radiation may lead to appreciable excitation of vibrational levels. For molecules with vibration-rotation bands at wavelengths shorter than 6 or 7 μm, solar induced excitation may be comparable to that caused by absorption of surface or atmospheric radiation.

Knowledge of vibrational populations of molecular species in the upper atmosphere is essential to the computation of band and spectral radiances. A major effort of the current study has been the development of mathematical model which treats in combination the effects of collisional excitation and de-excitation of vibrational levels and the absorption and re-emission of radiant energy. The significant new result of this study is a simple method of treating the radiative transfer problem for a single molecular vibration-rotation band with Doppler line shape. This method allows the treatment of an entire band as if it were a single line and greatly simplifies the computation of the population of vibrational states of a molecule under conditions where there is a lack of thermodynamic equilibrium.

The molecular species considered in the computational model include CO_2, H_2O, O_3, NO, N_2O and CH_4. Goody (1964) provides a good introduction to the detailed structure and infrared radiative properties of these molecules.

The following discussion of this section treats the mathematical development of the computational model, including the physical conditions of absorption and re-emission of radiant energy when absorption can be neglected, the treatment of radiative transfer in the presence of absorption, collisional excitation mechanisms, and the details of determining infrared radiation from the molecules.

67

B. BASIC RADIATIVE PROCESSES

This subsection discusses the physics of the interaction of light with an isolated atom or molecule. An understanding of the basic processes is the first step in any computation of the radiation from any gas or mixture of gases. The first paragraph introduces the problem through use of the Einstein A and B coefficients and relates these to the experimentally determined oscillator strength and band strengths. Succeeding paragraphs treat absorption from a continuum source, a spectrally varying source and fluorescent processes. Later subsections will discuss the modification necessary when a large number of molecules are present, the effects of collisions on exciting molecules to states from which radiation may occur and the combination of radiative and collisional processes in a computational model for estimating radiances from CO_2, H_2O, O_3, N_2O and CH_4 at high altitudes.

When treating a problem in which the number of photons emitted or absorbed by an atom or molecule must be considered rather than total energy emitted, it is natural and convenient to examine the physics of the interaction of radiation with matter through use of the Einstein A and B coefficients. In treating a radiative problem such as the current study of high altitude infrared radiances which involves transfer of energy between molecules through collisions, this approach is almost a necessity.

The Einstein $A_{u \rightarrow l}$ coefficient is the rate at which an atom or molecule in an excited state spontaneously emits radiation, in units of photons/sec-molecule. In an assemblage of molecules all in a state which can radiate, the average rate of radiation from each molecule is given by the Einstein $A_{u \rightarrow l}$ coefficient for the particular radiative transition from a state of higher energy (subscript u) to one of lower energy (subscript l).

In addition to spontaneous emission, two other processes occur. These are absorption, characterized by the Einstein coefficient for absorption $B_{\ell \to u}$, and induced emission, characterized by the Einstein coefficient for induced emission $B_{u \to \ell}$. In a radiation field with spectral density $\rho_{\nu_{\ell u}}$ the probability that an atom or molecule absorbs a quantum of radiation in unit time is $B_{\ell \to u} \rho_{\nu_{\ell u}}$. When the radiation density is expressed in C.G.S. units ergs-sec/cm, the coefficient $B_{\ell \to u}$ has units cm^3/ergs-sec. Similarly, an atom or molecule in a radiation field with spectral density $\rho_{\nu_{\ell u}}$ and in an excited state emits radiation at the rate $B_{u \to \ell} \rho_{\nu_{\ell u}}$ in addition to that characterized by the coefficient $A_{u \to \ell}$. The Einstein coefficients are properties of an atom or molecule. If one coefficient is known, the others may be determined by the relations

$$A_{u \to \ell} = 8\pi h \, B_{u \to \ell}/\lambda^3 \tag{25}$$

and

$$g_\ell \, B_{\ell \to u} = g_u \, B_{u \to \ell} \tag{26}$$

Thus, it is possible to treat the problem knowing only the Einstein $A_{u \to \ell}$ coefficient.

Experimental determinations of the interaction of infrared radiation with gases are usually determined by measurements of the absorption of light. Experimental results may be expressed as integrated absorption

$$S'_{\ell u} = N_\ell \, \frac{A_{u\ell} \, \lambda^2_{\ell u}}{8\pi} \, \frac{g_u}{g_\ell} \left[1 - \exp\left(\frac{bc}{\lambda_{\ell u} \, kT} \right) \right] \tag{27}$$

or band strengths

$$S_{\ell u} = S'_{\ell u}/pc \tag{28}$$

In the visible and ultraviolet regions of the spectrum, it is customary to use oscillator strengths to characterize the interaction of radiation and matter. In this case, the defining equation may be taken to be

$$S'_{\ell u} = \frac{\pi e^2}{mc} N_\ell f_{\ell \to u} \left[1 - \exp \left(- \frac{hc}{\lambda_{\ell u} kT} \right) \right] \tag{29}$$

The results of theoretical computations of the interaction of matter with radiation are frequently expressed as dipole moments. These are related to the Einstein A coefficient by

$$A_{u \to \ell} = \frac{64\pi^4}{3h\lambda^3} \frac{g_\ell}{g_u} |\mu_{u \to \ell}|^2 \tag{30}$$

The rate at which a single atom or molecule absorbs and reradiates light from a parallel beam from a continuum source at a wavelength λ_o corresponding to a resonance transition is (Mitchell and Zemansky, 1961):

$$G = 10^{-4} \frac{\pi e^2}{mc^2} I_o f_o \lambda_o^2 \quad \text{(photons/sec)} \tag{31}$$

$$= 8.852 \times 10^{-17} I_o f_o \lambda_o^2 \quad \text{(photons/sec)}$$

If the incident flux is expressed in photons/cm^2-sec-μm when the incident light intensity is expressed in watts/cm^2-μm,

$$G = 3.72 \times 10^{-24} I_o S\lambda^2 \quad \text{(watts)} \tag{32}$$

Both of these equations are necessary because, in the details of the model, photons are counted, while final results are presented as spectral power.

When the source is an extended black body surface with a spectral radiance N_λ, the G factor is obtained by integration over the solid angle subtended by the source. For radiation from a plane parallel surface of infinite extent,

$$G = 1.169 \times 10^{-23} N_\lambda S \lambda^2 \tag{33}$$

One other purely radiative mechanism is of importance in upper atmosphere radiance computations. This is fluorescence, and must be considered in treating radiation from CO_2, NO, N_2O and CH_4. A striking example occurs for the weak 10.4 μm CO_2 band. Absorption of solar radiation by the CO_2 4.3 μm band maintains the ν_3 vibration mode at a vibrational temperature of about 290°K. During the day, this leads to an enhancement of emission in the 10.42 μm band by as much as two orders of magnitude when viewed along the earth's limb from outside the atmosphere.

Fluorescence occurs when the upper state of the resonance transition can reradiate into states other than the initial one. The relative probability of a radiative transition to a lower state n from the upper state u when there are k possible lower states is:

$$P_{u \to n} = \frac{A_{u \to n}}{\displaystyle\sum_{j=1}^{k} A_{u \to j}} \tag{34}$$

where the $A_{u \to j}$ are the Einstein A coefficients for the spontaneous emission probabilities for a transition from the upper state to the jth lower state.

In the case of molecular resonance-fluorescent scattering at low temperatures, only the lowest vibrational level ($v'' = 0$) in the ground electronic state is significantly populated. Absorption of a photon excites the molecule to a vibrational

71

level v' in the same or a higher electronic state. Radiation is possible from this state to the initial level (v" = 0) or to other vibrational levels (v" ≠ 0) in the ground electronic state. The rate of resonance fluorescent scattering in a given electronic vibrational transition may be obtained by combining Equations (31) and (34) and introducing appropriate subscripts:

$$G_{v'v''} = 8.853 \times 10^{-17} \, I_{v'o} f_{v'o} \lambda_{v'o} \frac{A_{v'v''}}{\sum\limits_{v''} A_{v'v''}} \tag{35}$$

Here the subscript v'v" refers to a transition from an upper state with vibrational level v' to a lower state with vibrational level v". The subscript v'o refers to absorption of a photon by a molecule in the lowest vibrational level of the ground state, exciting the molecule to a vibrational level v' in the same or a higher electronic state.

C. RADIATIVE TRANSFER FOR LARGE OPTICAL PATHS

In developing a realistic model of the interaction of radiation with matter, it is necessary to take into account the details of absorption. Line shape must be considered because it determines the amount of radiation escaping from an optically thick layer of gas. Thus, for large optical thickness (greater than a magnitude of 10), the total emission from an isolated spectral line with Lorentz shape is proportional to the square root of the logarithm of the optical thickness. In addition, absorption of radiation emitted at one place in the gas by a molecule at another place cannot be computed without knowledge of the line shape.

At high altitudes the profile of the spectral absorption curve of an individual line in a vibration-rotation band is predominantly that due to velocity or Doppler broadening. Kuhn and London (1969) have investigated the heat budget of the atmosphere between 30 and 110 km. They report that radiative transfer calculations require the use of the Voigt profile (including both collisional and Doppler broadening) at altitudes between 20 and 70 km, but that the Doppler profile is adequate at higher altitudes, the Doppler shape being the largest contributor to line broadening above 50 km for CO_2, H_2O and O_3. The computational model therefore assumes a Doppler profile for simplicity.

In addition to the use of Doppler shape for a single line, several other assumptions are made about the radiative transfer within lines of a band. These are the following:

(1) Rotational levels within a vibrational level remain in equilibrium with the translational temperature. This is valid up to at least 150 km according to Goody (1964).

(2) There is complete redistribution of frequency within a single line following absorption of radiation.

(3) There is complete redistribution of absorbed energy among all rotational levels.

(4) The variation of line strength with rotational level is taken to be that given by the Hönl-London formulae, neglecting wavelength variation across a band.

(5) There is no overlap of adjacent lines.

(6) Temperature variations at different levels do not affect the radiative transfer. This last assumption is probably the largest source of error in computing transmission.

73

The chief result is to make computed band radiances too small when determining escape of radiation from a warm layer overlaid by a cooler layer. It will be shown in Section VI A(H_2O limb radiances) that this approximation yields an insignificant error in computed radiances for tangent heights greater than 75 km.

The above assumptions lead to the following treatment, which begins with consideration of a single line and from this develops the method used for treating radiative transfer in an entire band. The spectral absorption coefficient of a Doppler broadened line is (Mitchell and Zemansky, 1961):

$$k(\nu) = \frac{1}{\Delta \nu_D} \sqrt{\frac{\ell n 2}{\pi}} \frac{\pi e^2}{mc} N_\ell f_o \exp\left[-\left(\frac{\nu - \nu_o}{\Delta \nu_D} \sqrt{\ell n \, 2}\right)\right] \qquad (36)$$

where the Doppler half width at half maximum is

$$\Delta \nu_D = \sqrt{\frac{2 \, RT \, \ell n \, 2}{M \, c^2}} \, \nu_o \; (sec^{-1})$$

The amount of light absorbed by the line per unit frequency interval is

$$I(\nu) \, A(\nu) \, d\nu = I(\nu) \, (1 - T(\nu) \, d\nu$$
$$= I(\nu) \, (1 - e^{-k(\nu)}) \, d\nu \qquad (37)$$

and the total light absorbed is

$$\int_o^\infty I(\nu) \, A(\nu) \, d\nu = \int_o^\infty I(\nu) \, (1 - T(\nu)) \, d\nu \qquad (38)$$

$$= \int_o^\infty I(\nu) \, \left(1 - \exp\left\{-k_o \exp\left[-\left(\frac{\nu - \nu_o}{\Delta \nu_D} \sqrt{\ell n \, 2}\right)^2\right]\right\}\right) d\nu$$

74

where the integration is over all frequencies and

$$\mathcal{K}_o = \frac{1}{\Delta\nu_D} \sqrt{\frac{\ln 2}{\pi}} \ \frac{\pi e^2}{mc} \ N_\ell f_o$$

The line will absorb only near the center frequency ν_o and $I(\nu)$ may be replaced by $I(\nu_o)$. Making the substitution

$$w = \frac{\nu - \nu_o}{\Delta\nu_D} \sqrt{\ln 2}$$

$$\int_0^\infty I(\nu)\, A(\nu)\, d\nu = I(\nu_o) \frac{\Delta\nu_o}{\sqrt{\ln 2}} \int_{-\infty}^\infty (1 - e^{-\mathcal{K}_o\, e^{-w^2}})\, dw \tag{39}$$

$$= I(\nu_o) \frac{\pi e^2}{mc} N_\ell f_o \left(1 - \frac{\mathcal{K}_o}{2!\sqrt{2}} + \frac{\mathcal{K}_o}{3!\sqrt{3}} + \dots \right)$$

The corresponding expression on a wavelength basis is

$$\int_{-\infty}^\infty I(\lambda)\, A(\lambda)\, d\lambda = I(\lambda_o) \frac{\pi e^2}{mc^2} N_\ell f_o \lambda_o^2 \ 1 - \frac{\mathcal{K}_o}{2!\sqrt{2}} + \frac{\mathcal{K}_o^2}{3!\sqrt{3}} + \dots$$

$$= I(\lambda_o)\, K_o \left(1 - \frac{\mathcal{K}_o}{2!\sqrt{2}} + \frac{\mathcal{K}_o^2}{3!\sqrt{3}} + \dots \right) \tag{40}$$

$$= G\, N_\ell \left(1 - \frac{\mathcal{K}_o}{2!\sqrt{2}} + \frac{\mathcal{K}_o^2}{3!\sqrt{3}} + \dots \right)$$

The quantity in parentheses in Equation (40) is simply a factor by which the product of G and N_ℓ must be multiplied to account for the effects of total optical thickness K_0 in computing the total absorption of radiation by a column containing N_ℓ molecules/cm^2 in the lower state. This quantity is called S by Mitchell and Zemansky (1961) who present tabulations of its value. Penner (1959) gives an asymtotic expansion for large values of K_0. The astrophysical literature frequently uses the notation

$$L(K_0) = K_0 \; S(K_0) = \frac{2}{\pi} \int_0^\infty \left(1 - e^{-K_0} \; e^{-w^2} \right) \; dw \qquad (41)$$

The factor by which G must be multiplied to obtain the true rate of absorption at an optical depth K_0 may be found by differentiating Equation (41) with respect to K_0 (Ivanov and Shcherbakov, 1965):

$$M_1 \; (K_0) = \frac{d \; L(K_0)}{d \; K_0}$$

$$= \frac{2}{\pi} \int_0^\infty e^{-w^2} - K_0 \; e^{-w^2} \; dw \qquad (42)$$

The factor by which G must be multiplied to obtain the actual absorption from a black body source is (Ivanov and Shcherbakov, 1965)

$$N_1(K_0) = \int_0^{2\pi} d\varphi \int_0^{\pi/2} \cos\theta \, \sin\theta \; M_1 \; \frac{K_0}{\cos\theta} \; d\theta \qquad (43)$$

When the source of radiation is a Doppler profile exactly that of the absorbing line, the differential absorption at optical thickness K_0 is given by

$$M_2(\varkappa_o) = \frac{2}{\pi} \int_o^\infty e^{-2w^2} - \varkappa_o e^{-w^2} \, dw \tag{44}$$

and G must be multiplied by this factor. Also, if the source is an infinite plane layer (not a surface) radiating with a Doppler profile, G must be multiplied by

$$N_2(\varkappa_o) = \int_o^{2\pi} d\varphi \int_o^{\pi/2} M_2\left(\frac{\varkappa_o}{\cos\theta}\right) \sin\theta \, d\theta \tag{45}$$

The functions of Equations (41) through (45) were evaluated by numerical integration and polynomial approximations obtained for the entire range of variation of $\varkappa_o$ from zero to infinity, using the known asymtotic forms as a guide at large values.

If the line strengths for each line of a vibration-rotation band of a linear molecule such as CO_2, NO, and N_2O are determined, and the optical thickness of the strongest line in the band is taken as a parameter, functions analagous to those in Equations (41) to (45) may be computed numerically. It is noted that temperature affects the Doppler width in the calculations. However, results indicate that a temperature variation of up to a factor of 50 results in less than a 10 percent variation in the values of these functions. Therefore, only two sets of computations are required for linear molecules, one for perpendicular bands and one for parallel bands. These two sets are adequate even in cases where nuclear spin effects cause alternation of intensities of rotational lines.

The method of extending these functions to an entire band is illustrated for the function $M_1(\varkappa_o)$ of Equation (42) for a parallel $^1\Sigma - ^1\Sigma$ transition.

The rotational energy levels of a linear molecule in a $^1\Sigma$ state are given to a first approximation by

$$E(J) = J(J + 1)\ B_v\ hc \tag{46}$$

The relative population of a single rotational level is $(2J + 1)$ $\exp(-E(J)/kt)/Q_R$ where Q_R is the rotational partition function

$$Q_R = \sum_{J=0}^{\infty} (2J + 1)\ \exp(-E(J)/kt) \tag{47}$$

The band for a $^1\Sigma$ - $^1\Sigma$ transition contains two sets of lines or branches, one corresponding to a change in J between the upper and lower state by +1 (R branch), the other to a change in J of -1 (P branch). The relative strength of each line is

$$S_J^R = (J'' + 1) \tag{48}$$

$$S_J^P = J'' \tag{49}$$

At a given temperature the (fictitious) J value of the strongest line is computed by setting the derivative with respect to J of $(J'' + 1)\ \exp(-E(J)/kt)$ equal to zero

$$J''_{max} = \sqrt{\frac{kT}{B_{v''}\ hc}} - 1 \tag{50}$$

An optical thickness K_o is assigned to the strongest line and the optical thicknesses for all lines in the band are computed. The product $K\ M_1\ (K)$ is computed for each line and summed for all lines for which the product is more than 10^{-14} that of the strongest line. This sum is divided by the sum of

optical thicknesses to obtain the band function

$$M_1{}^B(\kappa_o) = \frac{\sum\limits_{J}\sum\limits_{I=P,R} x_{J,I}\, M_1\,(K_{J,I})}{\sum\limits_{J}\sum\limits_{I=P,R} K_{J,I}}$$

(51)

Similar band functions corresponding to Equations (41), (43) to (45) are indicated by using a superscript B with the symbol for the basic function. Polynomial approximations have been obtained for all the functions and are used in the numerical calculations.

Time has not permitted a similar treatment of the more complex bands of H_2O, O_3 and CH_4. A proper treatment will require the use of a complete set of line strengths such as that being developed by Dr. McClatchey at AFCRL. In treating these non-linear molecules for the current investigation, a fictitious value of B_v has been estimated which leads to the effective use of about 500 lines per band instead of the thousands actually present.

D. INCLUSION OF COLLISIONAL EXCITATION IN THE MODEL

In computing radiances at high altitudes, it must be recognized that vibrational levels are not populated at thermal equilibrium values. Radiation depopulates vibrational states rapidly and collisional excitation is not efficient enough to maintain a Boltzmann distribution of vibrational states. Collisional excitation and de-excitation rates are required to compute the balance of opposing mechanisms which determine actual vibrational populations. This subsection discusses the addition of collisional mechanisms to the radiative processes described previously and illustrates the use of the model for water vapor radiance computations.

Three collisional processes are considered which affect the vibrational state of a molecules. These are: (1) translational-vibrational (T-V) interactions in which translational energy is transformed into vibrational energy or vice-versa during a collision, (2) intermolecular vibrational exchange (V-V) in which a molecule of one species exchanges a quantum of vibrational energy with a molecule of another species and (3) intramolecular vibrational exchange in polyatomic molecules in which a collision transfers the energy in one mode of vibration into another mode within the same molecule.

When a molecule in the ground state collides with another molecule there is a finite probability P_{VT} that a part of the relative translational energy will be transformed to vibrational energy if the translational energy is equal to or exceeds the vibrational energy. Similarly, if the molecule is in an excited vibrational state, there is a finite probability P_{TV} that the vibrational energy will be converted to relative translational energy during the collision. For a Boltzmann distribution of translational energies at a given temperature,

$$P_{TV} = P_{VT} \frac{g_u}{g_\ell} \exp \left[- \frac{hc}{\lambda_0 kT} \right] \tag{52}$$

Similar expressions hold for intermolecular and intramolecular V-V transfer.

The rate at which a vibrational level is excited (k_{TV}) or de-excited (k_{VT}) is given by the product of the collision frequency Z and the transition probability. Experimental determinations of collisional excitation rates may be reported as probabilities, excitation rates or relaxation times. The latter are related to excitation and de-excitation rates by (Herzfeld and Litovitz, 1959)

80

$$\frac{1}{\tau} = k_{VT} + k_{TV} \tag{53}$$

Excitation rates depend on temperature and number density through the strong temperature variation of the transition probability and the square root temperature and linear density variation of the collision frequency.

All parts of the model are now ready for use. The computational method may be illustrated by application to a system in which only one excited vibrational level is considered, say water vapor. This level is assumed to be excited and de-excited by both radiative and collisional processes.

At a given altitude, there will be N_ℓ molecules/cm^3 in the ground state and N_u molecules/cm^3 of nitrogen and oxygen which are the dominant collision partners in collisional excitation and de-excitation processes.

In unit volume, molecules in the ground state are excited to the upper state by

(1) Collisional T-V excitation at a rate $N_\ell k_{TV}$

(2) Collisional V-V excitation at a rate $N_\ell k_{MV}$

(3) Absorption of solar flux at a rate $N_\ell I_o G' M_1{}^B (\varkappa_s)$

(4) Absorption of lower atmosphere radiance at a rate
$N_\ell N_{\lambda, T} G' N_1{}^B (\varkappa_T)$

(5) Absorption of radiance emitted at other levels of the atmosphere at a rate $N_\ell \int N_{\lambda, D} G' N_2{}^B (\varkappa_D)\ dZ$

81

Molecules in the upper state are de-excited by

(1) Collisional V-T de-excitation at a rate $N_u k_{VT}$

(2) Collisional V-V de-excitation at a rate $N_u k_{VM}$

(3) Spontaneous radiative de-excitation at a rate $N_u A_{u \rightarrow \ell}$

For each level, there is a differential equation

$$\frac{dN_u}{dt} = N_\ell (k_{TV} + k_{MV} + I_o G' M_1{}^B (\varkappa_s) + N_{\lambda, T} G' N_1{}^B (\varkappa_T)$$

$$+ \int N_{\lambda, D} G' N_2{}^B (\varkappa_D) dZ) - N_\ell (k_{VT} + k_{VM} + A_{u \rightarrow \ell}) = 0 \qquad (54)$$

The equations are solved iteratively, with starting conditions being those appropriate to thermodynamic equilibrium. For molecules in which more than one vibrational level is considered, an equation must be added at each altitude level.

After the vibrational populations have been determined at each level, both exospheric and endospheric radiances are computed, taking into account the necessary geometry.

A brief comment on treatment of nitrogen vibrational temperatures is in order at this point. At altitudes above 100 km, it is possible for the nitrogen vibrational levels to be populated above the thermal equilibrium condition, either by electron impact or as a result of collisional quenching of atomic oxygen in the excited ^1D electronic state. Walker (1968) has discussed the excitation of N_2 resulting from the quenching of $O(^1D)$. His analysis of Langmuir probe measurements of E-region electron temperatures concludes

that at 110 km and above, the vibrational temperature of N_2 is of the order of 3000°K or more during the daytime. When the program was set up to include such high vibrational temperatures, it was found that the nitrogen transferred more energy to the lower density CO_2 concentration model near 110 km than could be produced by quenching of $O(^1D)$. This suggests that CO_2 may play an important role in relaxing the N_2 vibrational temperature at altitudes up to 120 km.

The program contains the option of using either ambient translational temperature or an arbitrary temperature profile for the N_2 vibrational temperature.

The following subsection describes the molecular data used for each of the species CO_2, H_2O, O_3, NO, N_2O and CH_4.

E. APPLICATION OF MODEL TO INDIVIDUAL MOLECULAR SPECIES

This subsection discusses briefly the data which were used in the band radiance computations reported in Section VI. Table 1 summarizes values of band strengths and Table 2 summarizes collisional excitation rates. It must be recognized that the latter are not as well known as the former. In some cases the exact path through which vibrational energy is transferred is not known. The vibrational energy level scheme used for each molecule is treated below.

1. Carbon Dioxide

Figure 32 shows the vibrational energy levels that have been included in the computations, together with the first excited vibrational energy level of molecular nitrogen. Seven levels in addition to the ground state have been considered, and nine radiative transitions, eight of which lie between 10 and 17 μm. The scheme is a good first approximation to the real physical processes. Levels formed by combinations of vibrational modes have been neglected but are considered of less importance. Dashed lines indicate radiative transitions and solid lines indicate paths by which collisions transfer vibrational energy or transform translational to vibrational energy. The high band strength for CO_2 at 4.3 microns shown in Table 1 is expected because the frequency is high and the vibration is a fundamental.

Collisional excitation rates are taken from Bitterman (1969). The V-T rates for the transition between the ground state and level 2 were applied to the other transitions in the ν_2 vibrational series, making the necessary modifications due to the differing statistical weights of the levels. Band strengths for the seven bands near 15.0 μm were taken from Drayson and Young (1966). Those for the 10.4 μm and 4.3 μm bands were taken from Burch et al. (1962).

Table 1. Band Strengths of Infrared Vibration-Rotation Bands

Molecule	Band Center wavelength, μm	Band Strength $(ATM\text{-}cm^2)^{-1}$	Temperature	References
CO_2	4.3	2500	299	Burch et al. (1962)
	10.4	**0.023**	299	Burch et al. (1962)
	13.9	5.0	300	Drayson and Young (1967)
	15.0	194	300	Drayson and Young (1967)
	15.0	15.0	300	Drayson and Young (1967)
	15.0	0.85	300	Drayson and Young (1967)
	15.4	1.0	300	Drayson and Young (1967)
	16.2	4.27	300	Drayson and Young (1967)
	16.7	0.14	300	Drayson and Young (1967)
H_2O	6.3	300	273	Ludwig et al. (1965)
O_3	9.1	10.6	273	Clough and Kneizys (1967)
	9.6	455	273	
NO	5.3	122	273	
N_2O	4.5	1850	303	Burch and Williams (1962)
	7.8	12	303	Burch and Williams (1962)
	17.0	33	303	Burch and Williams (1962)
CH_4	3.3	320	273	Burch and Williams (1962)
	5.8	0.01	300	Estimate
	6.6	2.5	273	Burch and Williams (1962)
	7.7	185	273	Burch and Williams (1962)

NOTE: Nitric acid has absorption bands at 7.5 and 11.2 microns; however, band strengths were not available at the writing of this report.

Table 2. Collisional Excitation Rates

A. Vibrational-Translational Energy Exchange Probabilities

Molecule	P_{VT}	Temperature	Reference
CO_2	3.6×10^{-6}	300	Taylor and Bitterman (1969)
H_2O	1×10^{-5}	300	Taylor and Bitterman (1969)
O_3	1×10^{-4}	300	Estimate
NO	4×10^{-8}	292	Estimate
N_2O	7×10^{-6}	297	Yardley (1968)
CH_4	9×10^{-4}	296	Yardley and Moore (1968)

B. Vibrational-Vibrational Energy Exchange Probabilities

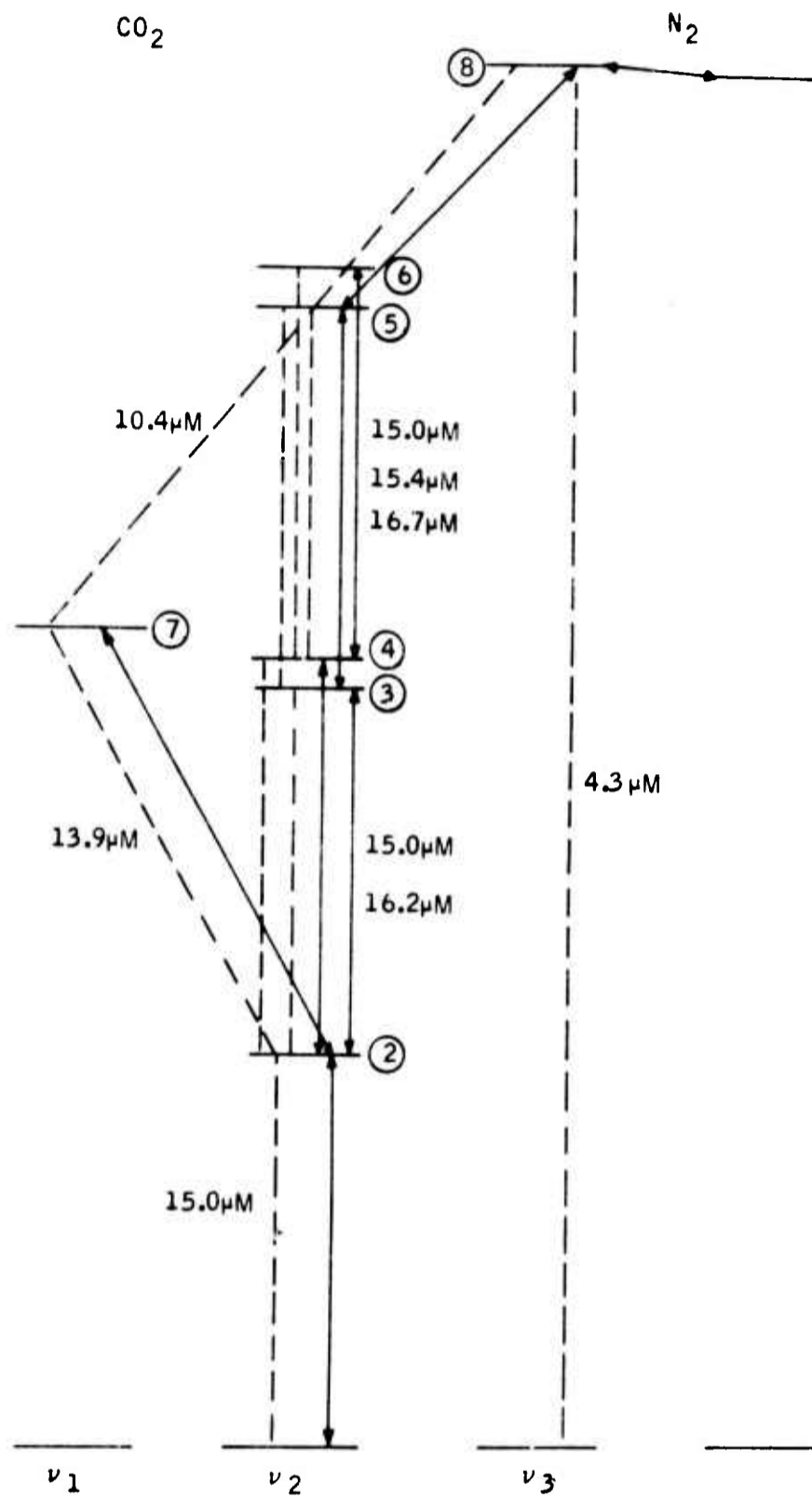| Molecule	P_{mv}	Temperature	Reference
CO_2	2.3×10^{-3}	300	Taylor and Bitterman (1969)
H_2O	1×10^{-5}	300	Taylor and Bitterman (1969)
O_3	5×10^{-4}	300	Estimate
NO	4×10^{-7}	292	Basco et al. (1961)
N_2O	8.7×10^{-4}	297	Yardley (1968)
CH_4	2.3×10^{-3}	296	Yardley and Moore (1968)

Figure 32. Carbon Dioxide Vibrational Levels and Collisional and Radiative Transitions Included in Infrared Radiance Model

87

2. Water Vapor

Because the water vapor molecule is extremely efficient in relaxing its vibrational excitation, vibrational states other than that which gives rise to the 6.3 μm band have been neglected. As for CO_2, vibrational relaxation and exchange data were taken from the curves of Taylor and Bitterman (1969). The band strength used was taken from Ludwig et al. (1965).

3. Ozone

No experimental data on vibrational energy transfer in ozone were found. Values for vibrational-translational and vibrational-vibrational transfer intermediate between those for methane and water vapor have been used. The two bands at 9.1 μm and 9.6 μm were treated as a single band, using the total strengths given by Clough and Kneizys (1967).

4. Nitric Oxide

The vibrational-translational energy exchange rate for nitric oxide in nitrogen has not been determined accurately because the rate for vibrational-vibrational exchange is much faster. The experimental determination of the latter by Basco et al. (1961, 1962) has been used and the former taken to be one-tenth that value. The band strength for the fundamental was taken from Abels and Shaw (1966) and that for the first overtone from Schruin and Ellis (1966).

Fluorescent excitation following absorption of ultraviolet solar radiation by the gamma band system at wavelengths below 2270Å has been included as follows. Neglecting variation of solar flux and transition probability with wavelength, the Einstein A coefficients are proportional to the Franck-Condon

88

factors $q_{v'v''}$. The relative population of each vibrational level v' of the upper electronic state is given by the Franck-Condon factor $q_{v'0}$ (assuming absorption only from the lowest vibrational level $v'' = 0$ of the ground electronic state). For each value of v', the sum $\sum_{v''} v'' q_{v'v''}$ gives the mean vibrational excitation of the molecule after emission of visible or ultraviolet radiation. The double sum $\sum_{v'} q_{v'0} (\sum_{v'} v'' q_{v'v''})$ gives the mean vibrational level of the molecule following all short wavelength excitations. Using Franck-Condon factors from Nicholls (1964), the mean vibrational level of NO after excitation is 3.85.

The gamma band absorption was approximated by a single gand with an oscillator strength the average of that of the $v' = 0$ to $v' = 4$ bands.

Chemiluminescence from the reaction

$$N + O_2 \rightarrow NO + O$$
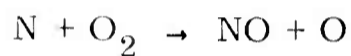
with both reactants in the ground state was included using the production rate curve of Ghosh (1968). The average vibrational level during formation is assumed to be $v'' = 4$, as suggested by Dalgarno (1963).

5. Nitrous Oxide

Figure 33 shows the energy level scheme adopted for N_2O. As for CO_2, vibrational excitation processes are shown by solid lines and radiative processes by dotted lines. The upper multiplets in the ν_2 were treated as single levels. Einstein A coefficients were assigned according to the statistical weights of the upper levels (Equation 34), and all radiations assumed to be at the fundamental wavelength. Collisional excitation rates were obtained from Yardley (1968), who states that the experimental data do not permit a good determination of the rate of population of the ν_1 vibrational level. Level 6
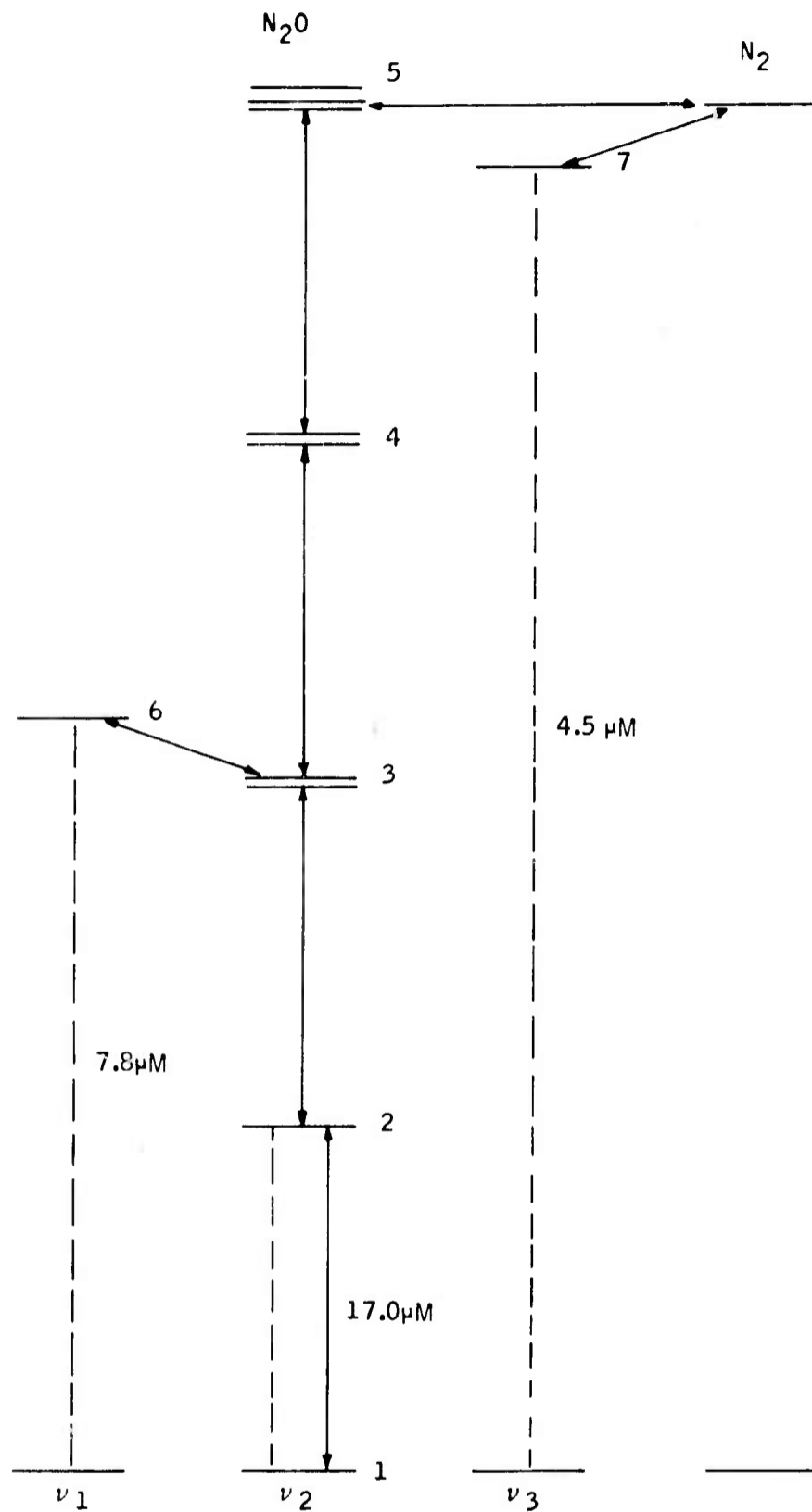
Figure 33. Nitrous Oxide Vibrational Levels and Collisional
and Radiative Transitions Included in Infrared
Radiance Model

has been coupled to level 3 by an interaction with the same strength as that for exchange of vibrational energy between nitrogen and levels 5 and 7.

6. Methane

Figure 34 illustrates the energy level scheme considered for methane. Again, experiment does not give a complete picture of vibrational exchange rates. Interactions with the infrared inactive υ_1 fundamental have been neglected. The collisional excitation data used were obtained from Yardley and Moore (1968) and band strengths from Burch and Williams (1962).

F. SUMMARY

This section of the report has described the development of a mathematical model which can be used to calculate infrared band radiances in the upper atmosphere for the molecules CO_2, H_2O, O_3, NO, N_2O and CH_4. The physical assumptions and the expected accuracy of the computational model are commensurate with uncertainties in the knowledge of physical properties of the upper atmosphere.

The model incorporates both collisional and radiative excitation mechanisms and collisional and radiative de-excitation mechanisms when computing the populations of vibrational states. Collisional mechanisms are considered in as great a detail as available experimental results permit. In addition, fluorescent and chemiluminescent mechanisms are included as processes which populate the vibrational states. For those altitude regions of the atmosphere where radiative transfer can be important (about 70 to 100 km), the model utilizes a Doppler line shape when calculating the transmission properties of the atmosphere. The assumption that rotational lines in a band do not overlap makes it possible to treat the radiative transfer problem
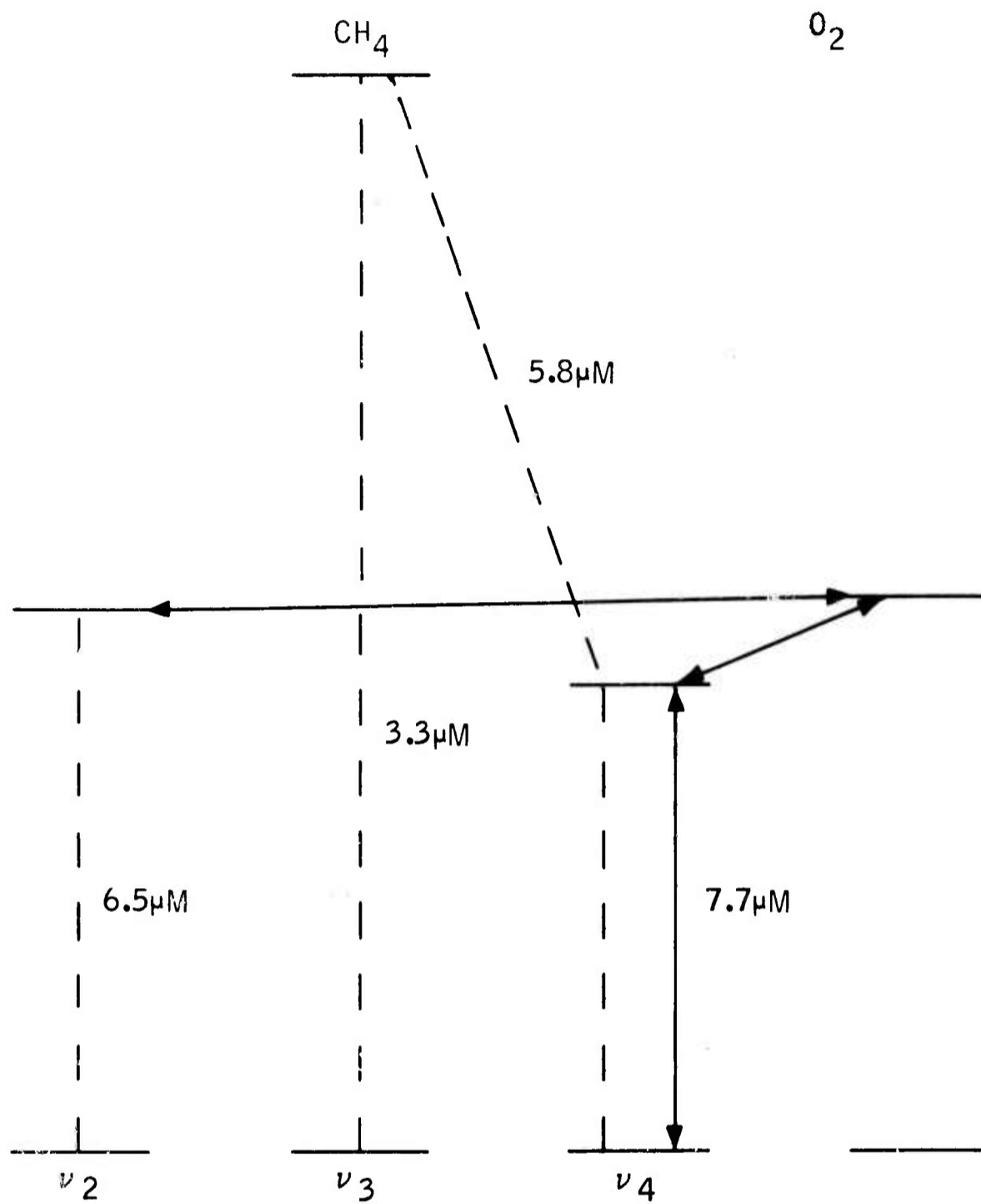
91

Figure 34. Methane Vibrational Levels and Collisional and Radiative Transitions Included in Model

for an entire band of a linear molecule as simply as if it were a single line. Finally, the detailed computational scheme for each molecule is outlined for future reference.

This section of the report presents the results of computations of high altitude infrared radiances using the model described in the previous section. The calculations are based on the six species CO_2, H_2O, O_3, NO, N_2O and CH_4 which are expected to contribute most significantly to high-altitude radiation in the 5 to 25 μm spectral region. The best estimate abundance profiles of Section IV have been used with temperature and pressure profiles from the U.S. Standard Atmosphere, 1962. Upwelling terrestrial and lower atmosphere intensities at the 60 km level were obtained from the low altitude radiance program described in Section II. Solar flux values were obtained from Johnson (1964).

Band radiance values for noon and night are presented for all six species for exoatmospheric viewing, and endoatmospheric calculations are illustrated by band radiances for the nitric oxide 5.3 μm band. Spectral radiances from the water vapor rotational band are given for exoatmospheric viewing. It is emphasized that these results are estimates based on uncertain chemical abundances. Certainly further investigations, including radiance measurements by probes and/or satellites will be required to determine temporal and spatial variations of radiances and information concerning chemical abundances of atmospheric species.

A. LIMB RADIANCES

1. Carbon Dioxide

At present the computer program calculates the vibrational populations of the seven vibrational levels of CO_2 shown in Figure 32 and calculates band radiances for nine bands, seven of which lie near 15 μm.

94

It is of interest to examine the effects of each of the exciting mechanisms which contribute to maintaining the populations of the various levels and hence, the resulting radiation field. The results in Figure 35 illustrate these effects and show the sum of the limb radiances of the seven bands near 15 μm for the highest expected CO_2 concentration. Curves are drawn for four conditions; local thermodynamic equilibrium (LTE), collisional excitation only (but including radiative transport of radiation arising from collisional excitation), nighttime illumination from the lower atmosphere, and equatorial noon illumination. The CO_2 ν_2 fundamental vibration mode which radiates at 15.0 μm is populated efficiently by collisions, and the first excited vibrational level remains populated within a factor of two of the thermal equilibrium value up to about 70 km. This is not apparent from the curves in Figure 35 when comparing LTE and the collisional excitation curve because the optical depth is large along a limb view path and much of the radiation arises from altitudes above the tangent height. A large fraction of the radiation from lower altitudes is absorbed by CO_2 at high altitudes before escaping to space. When the radiation from the earth and lower atmosphere is added, there is only a small increase in band radiance, noticeable on the scale of the drawing only at tangent heights between 85 and 105 km. The noon curve shows a larger increase because some of the solar energy absorbed by the strong ν_3 fundamental mode at 4.3 μm is converted to excitation of vibrational levels which radiate in the 15 μm spectral region.

Figure 36 shows the same data for the band at 10.4 μm. The large increase in radiance (one to three orders of magnitude) above 70 km at noon is due to fluorescent emission following absorption of solar energy at 4.3 μm.

Figures 37 and 38 give LTE, noon and night radiances for the lower limit to CO_2 abundance (see Figure 24). For the 15 μm band complex and the 10.42 band, respectively, there is little difference in radiances for tangent heights below 90 km. The radiance magnitudes associated with the low abundances are one to two orders of magnitude less than those shown for the high abundances profiles (Figures 35 and 36) for tangent heights greater than 100 km.
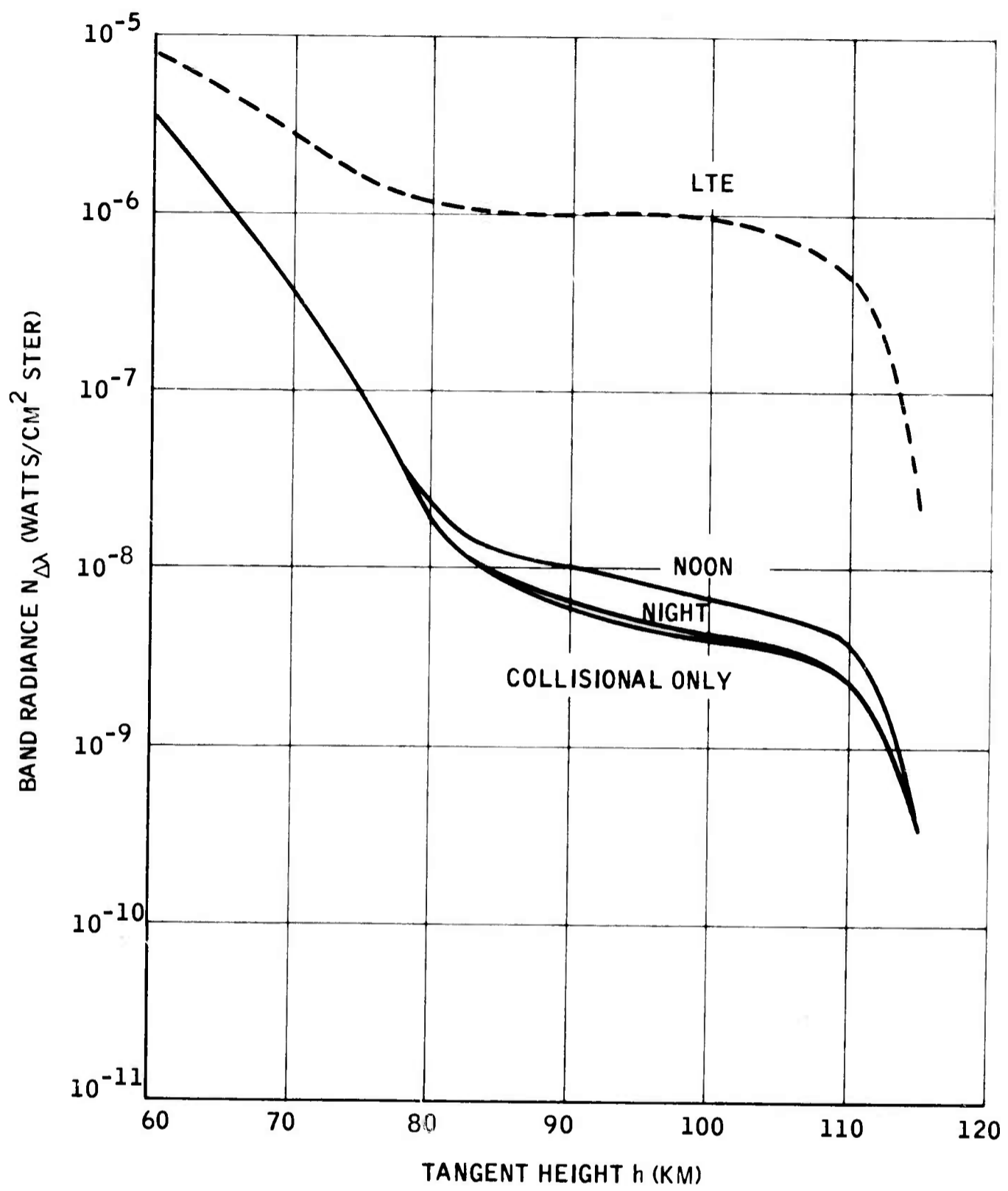
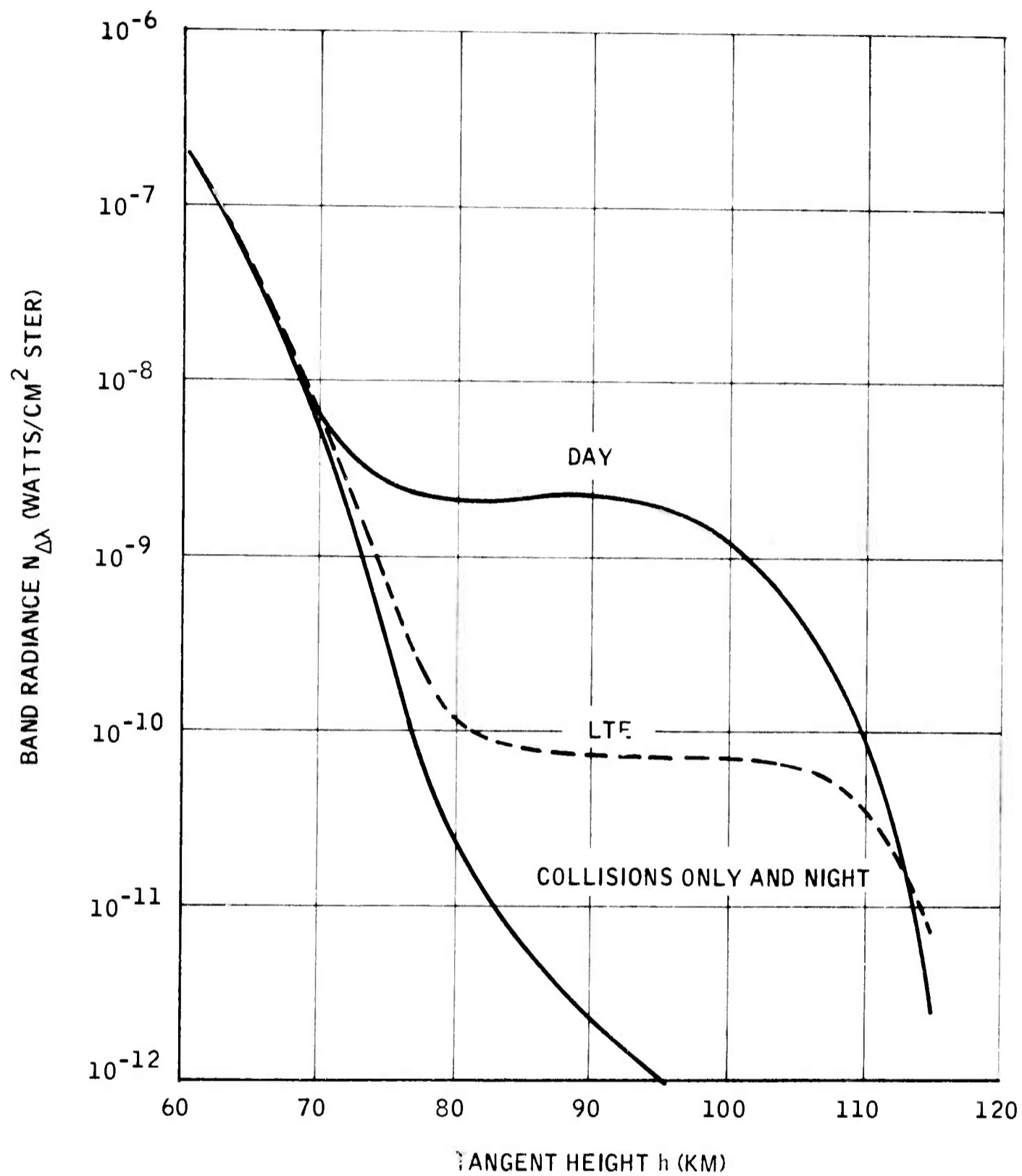Figure 35. Limb Radiance of Carbon Dioxide 15 μm Bands, Upper Limit Concentration Profile

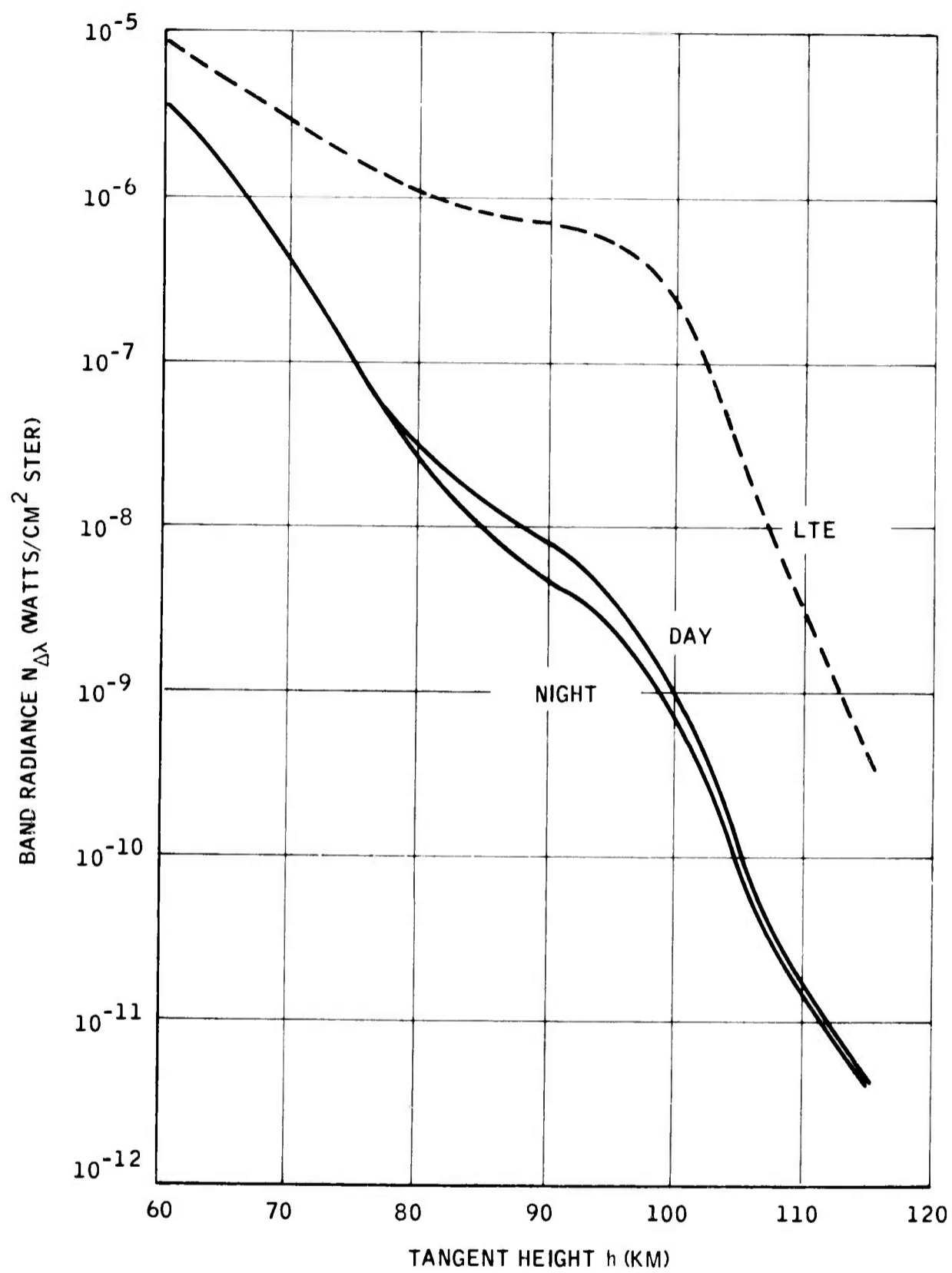Figure 36. Limb Radiance of Carbon Dioxide 10.4 μm Band, Upper Limit Concentration Profile

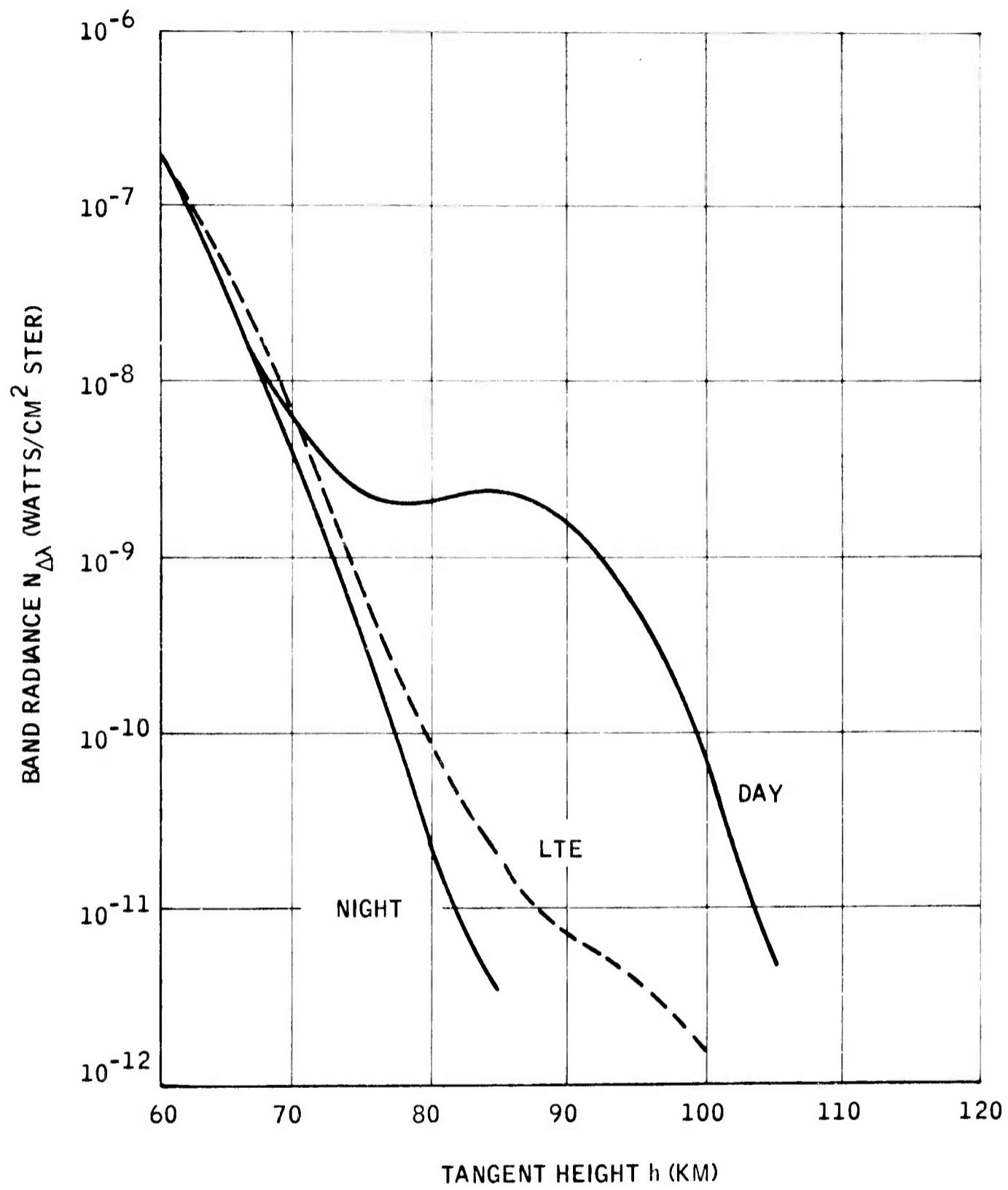Figure 37. Limb Radiance of Carbon Dioxide 15 μm Bands, Lower Limit Concentration Profiles

Figure 38. Limb Radiance of Carbon Dioxide 10.4 μm Band,
Lower Limit Concentration Profiles

2. Water Vapor

Figure 39 shows a comparison of the 6.3μ H_2O limb view radiances computed for LTE, noon and night conditions. Below 75 km, collisional processes maintain the vibrational population of the ν_2 mode first vibrational level near equilibrium. Between 75 and 95 km, the absorption of radiation from lower levels of the atmosphere maintains the vibrational population above that which holds at LTE, even at night. At noon, absorption of solar radiation increases the radiance by about a factor of two over that of night at all altitudes above 75 km.

It is noted that the computational model used to calculate band radiances from non-linear molecules represents a first approximation to the absorption problem because the number of lines is underestimated (see Section V). The lower dashed line at the left of the illustration is for LTE conditions with an extremely large over-estimation of the effects due to absorption. As can be seen, the radiance magnitudes are depressed by an order of magnitude for tangent heights of 60 to 65 km. However, there is little difference between the two LTE curves for tangent heights greater than 75 km. It is concluded from this comparison that the treatment of absorption by non-linear molecules in the computational model will result in significant errors only at the lower tangent heights where the physical approach is marginal anyway. At tangent heights greater than 70 km, the treatment of absorption is reasonably accurate and the errors introduced into the calculations are of little significance to the overall magnitudes.

3. Ozone

Figure 40 presents band radiances for the 9.6 μm O_3 band for noon and pre-dawn conditions. The results indicate that there is less than an order of magnitude difference in radiance magnitudes at all heights due to diurnal
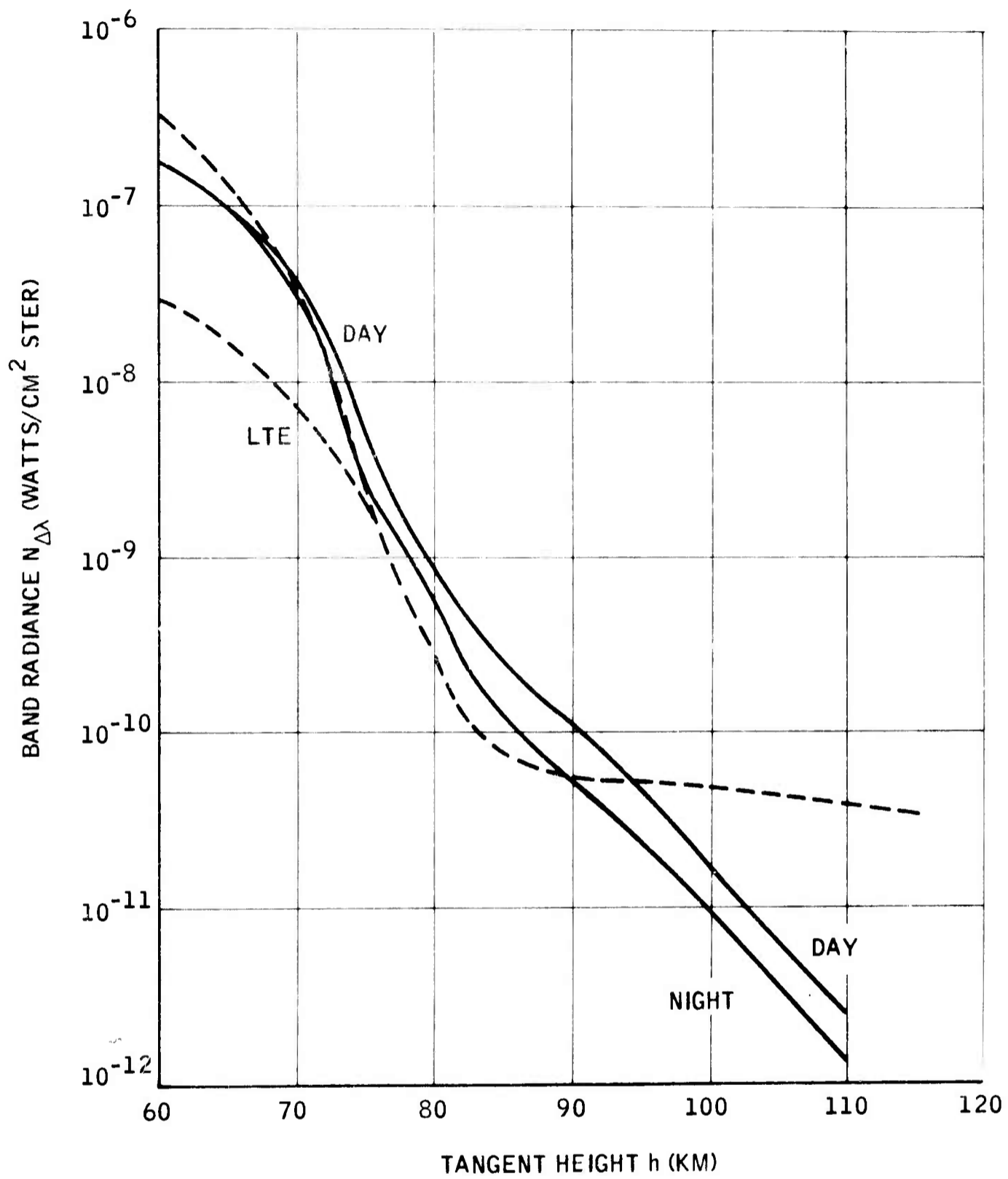
100

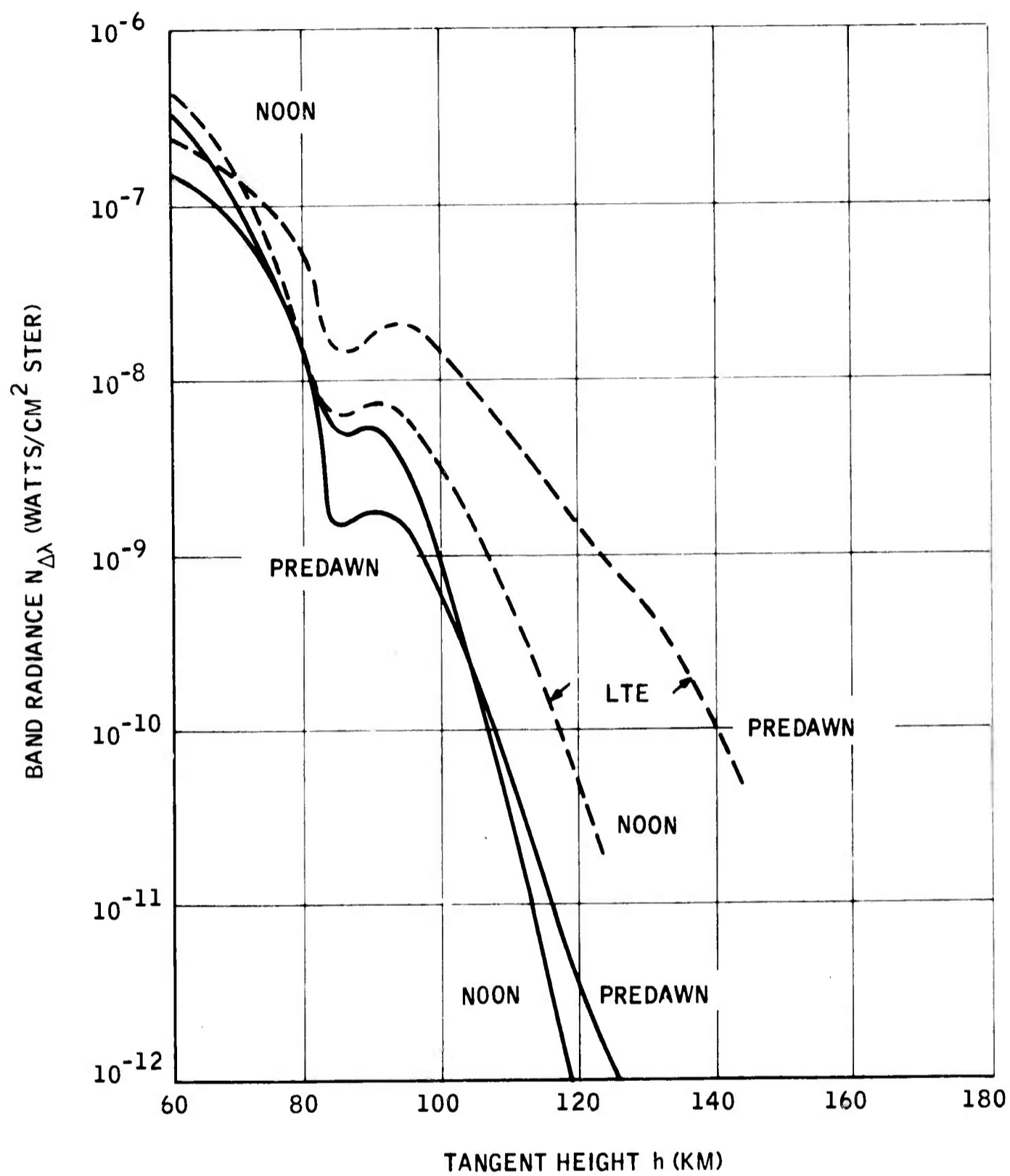Figure 39. Limb Radiance of Water Vapor 6.3 μm Band

101

Figure 40. Limb Radiance of Ozone 9.6μ m Band

variations. Ozone reaches its maximum concentration just before dawn and it might be expected that solar illumination would suddenly enhance the radiance field. However, the nighttime ozone distribution has appreciable optical thickness and radiative transfer from the lower atmosphere and within the ozone distribution are important. Therefore, solar illumination of the pre-dawn ozone maxima with noon flux values increases limb radiances by no more than about 50 percent at any one altitude. It can be predicted on this basis that the effect of photodissociation as the sun rises will be such that limb radiance values will relax toward the noon values with a time scale on the order of minutes during sunrise.

4. Nitric Oxide

During the day, and at altitudes above 90 km, nitric oxide is expected to radiate more strongly in the 5 to 25 μm region than any of the other molecules studied. The chief source of this radiant energy is chemiluminescence. The results of limb radiance computations for the NO 5.3 μm fundamental band are shown in Figure 41. The contribution from each excitation mechanism is shown as was done in the case for CO_2 (see Figure 35). The solid curves give computed radiances based on the assumption that the nitrogen vibrational temperature is equal to the translational temperature. As a comparison, the dashed curves show radiances computed using the translational temperatures up to 100 km, a linear temperature variation between 100 and 110 km and a 3000°K temperature above 110 km. The effects due to vibrationally excited nitrogen are apparent between 80 and 120 km. The results show that the radiation field is the strongest mechanism populating the vibrational levels during the night and partial noon at other heights. However, during full day, chemiluminescence is the major source of radiation, and the uncertainty in the estimate of the temperature of vibrationally excited nitrogen becomes irrelevant.
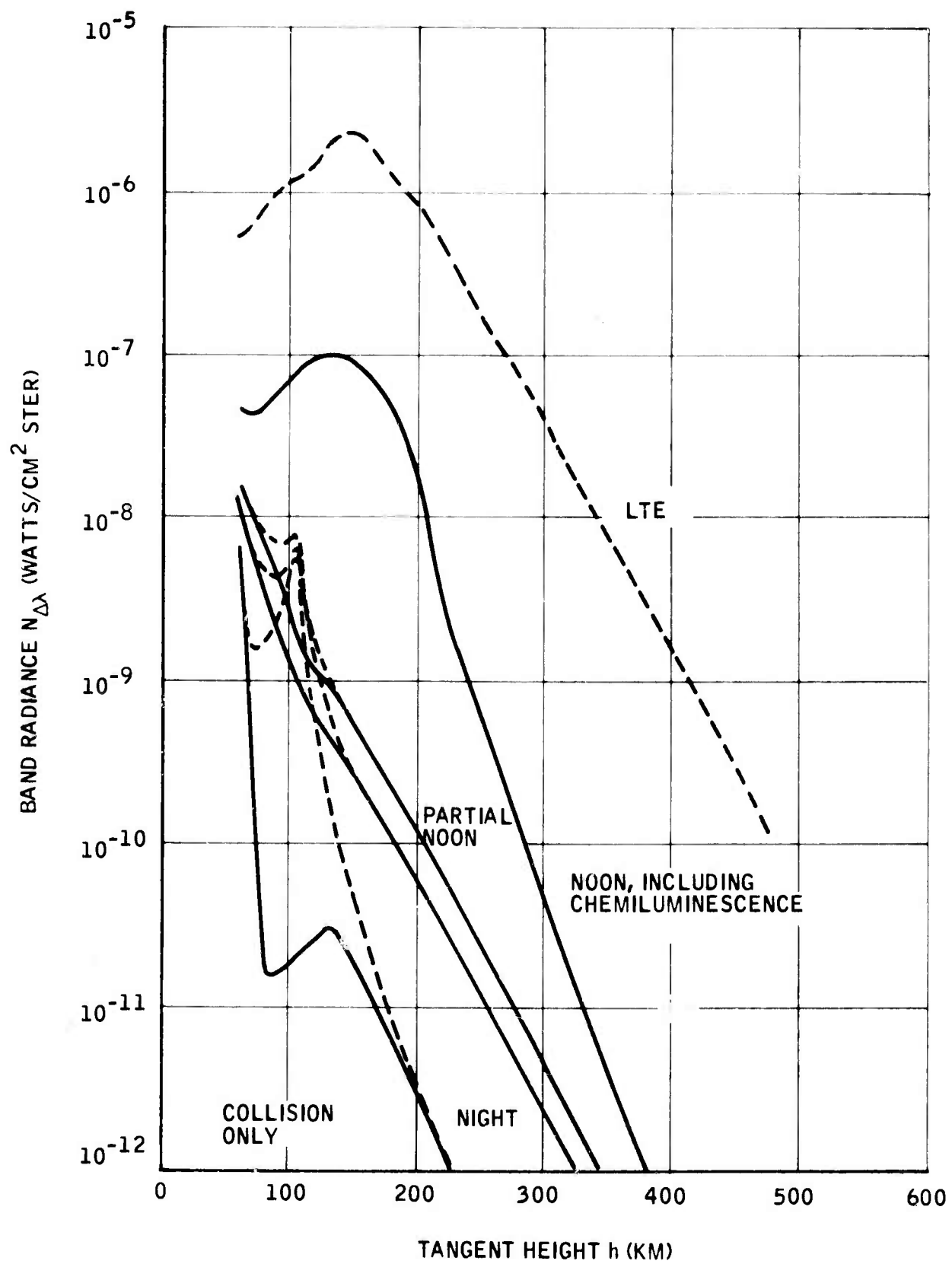
Figure 41. Limb Radiance of Nitric Oxide 5.3 μm Band

104

It is emphasized that nitric oxide radiances vary more between day and night than do those of any other species considered in this study.

5. Nitrous Oxide

Computed limb radiance profiles for the N_2O 7.8 and 17.0 μm bands are shown in Figures 42 and 43. Radiation from the lower atmosphere is the dominant source of excitation for the 7.8 μm band at all altitudes and is the most important exciting mechanism for the 17.0 μm band above 80 km. There is practically no day-night variation in radiances.

6. Methane

Although methane is not expected to be present in appreciable amounts above the stratosphere because of the rapid reaction with atomic oxygen, limb radiance computations have been performed using the tropospheric mixing ratio as an upper limit estimate. Figures 44, 45 and 46 present the results of limb radiance calculations for the CH_4 5.8 μm, 6.5 μm and 7.7 μm bands. Absorption of radiation is the chief excitation mechanism for all of these bands, and collisional excitation plays a negligible role.

B. ENDOATMOSPHERIC RADIANCES

The computational model developed in this study has the capability of performing radiance calculations as a function of zenith angle from an assumed reference platform within the atmosphere. Endoatmospheric calculations are useful in simulating radiances that would be measured by rocket borne radiometers during ascent and descent portions of flight programs. Endoatmospheric radiances were calculated for all the bands discussed in
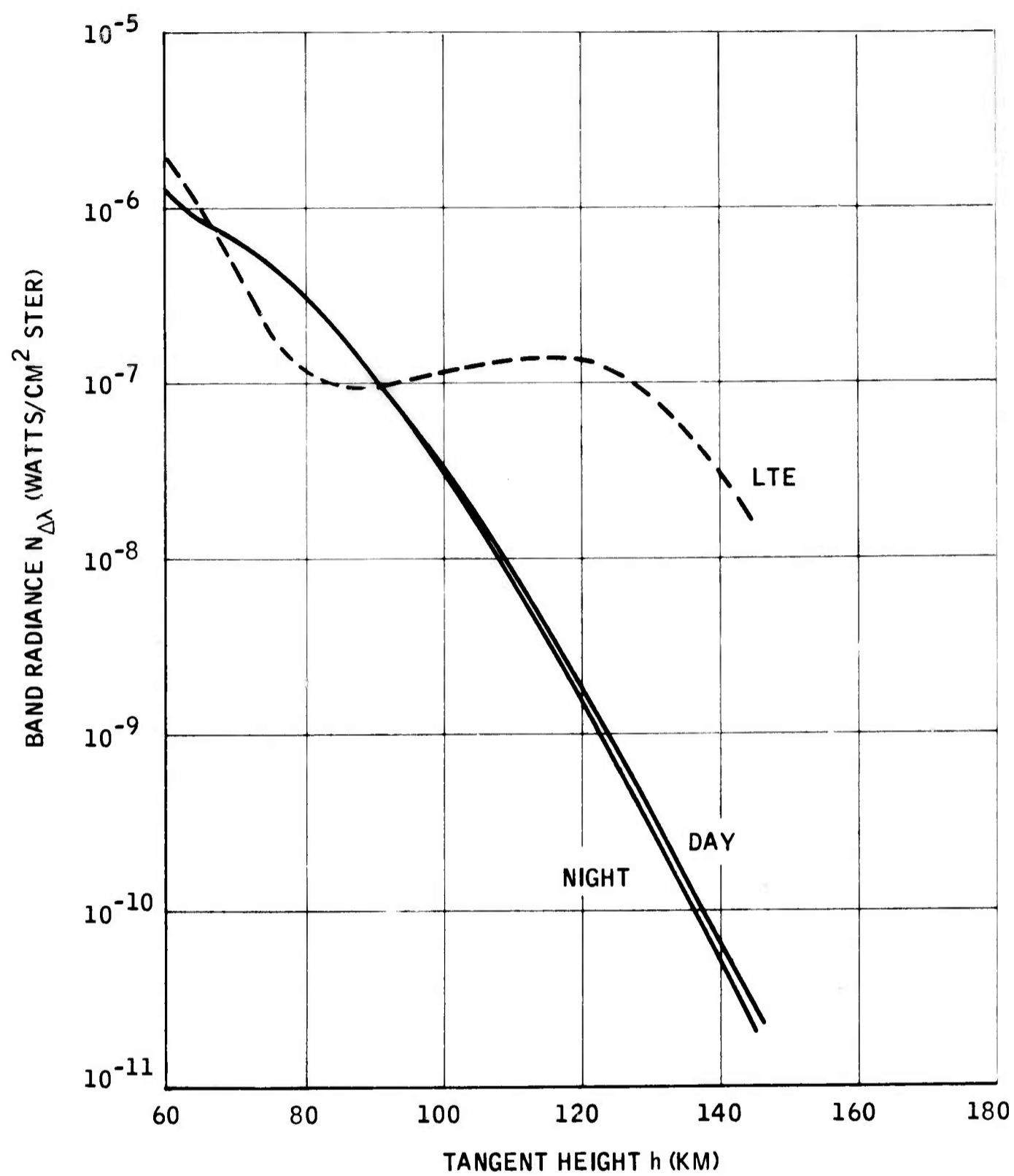
105

Figure 42. Limb Radiance of Nitrous Oxide 7.8 μm Band
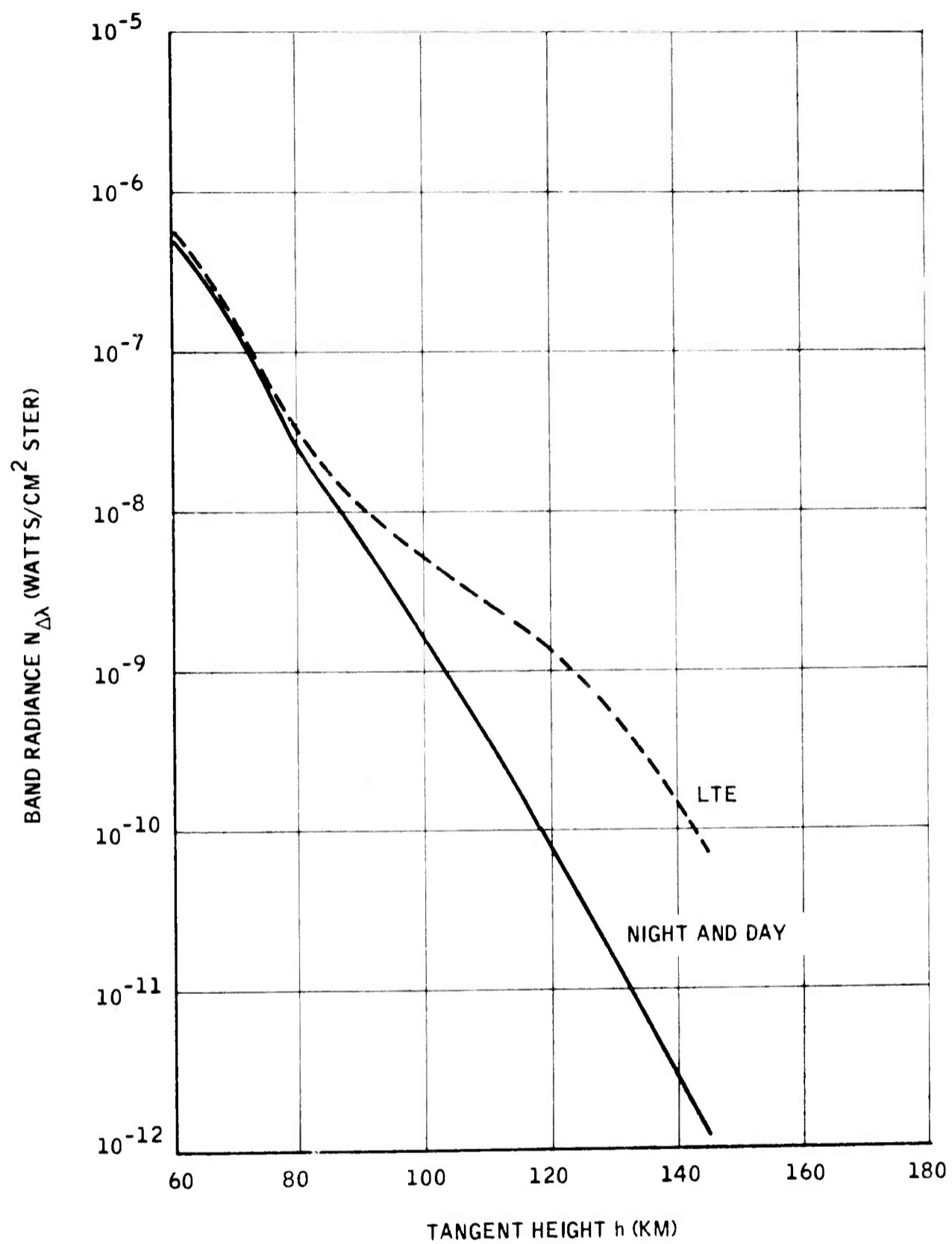
106

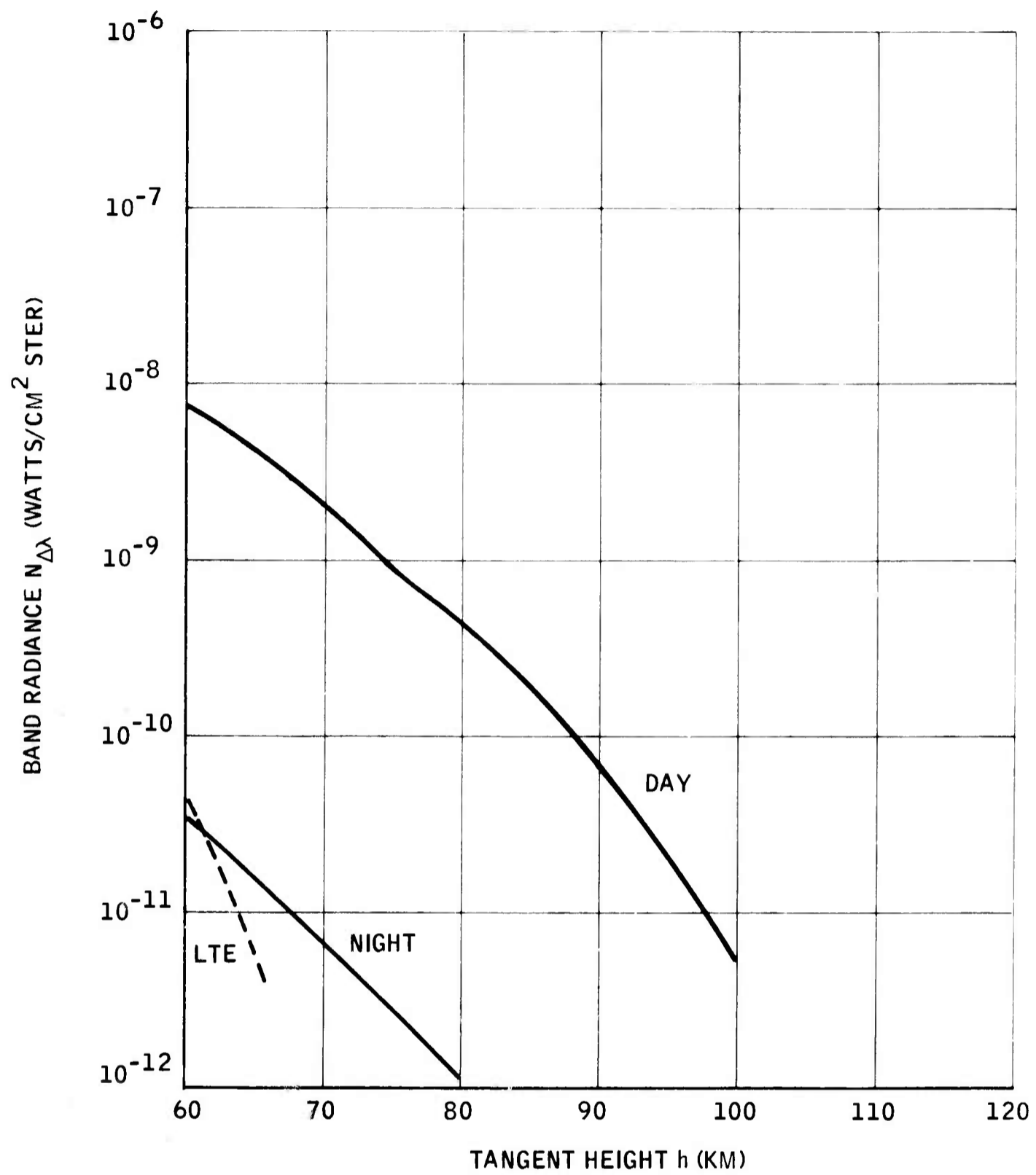Figure 43. Limb Radiance of Nitrous Oxide 17.0 μm Band
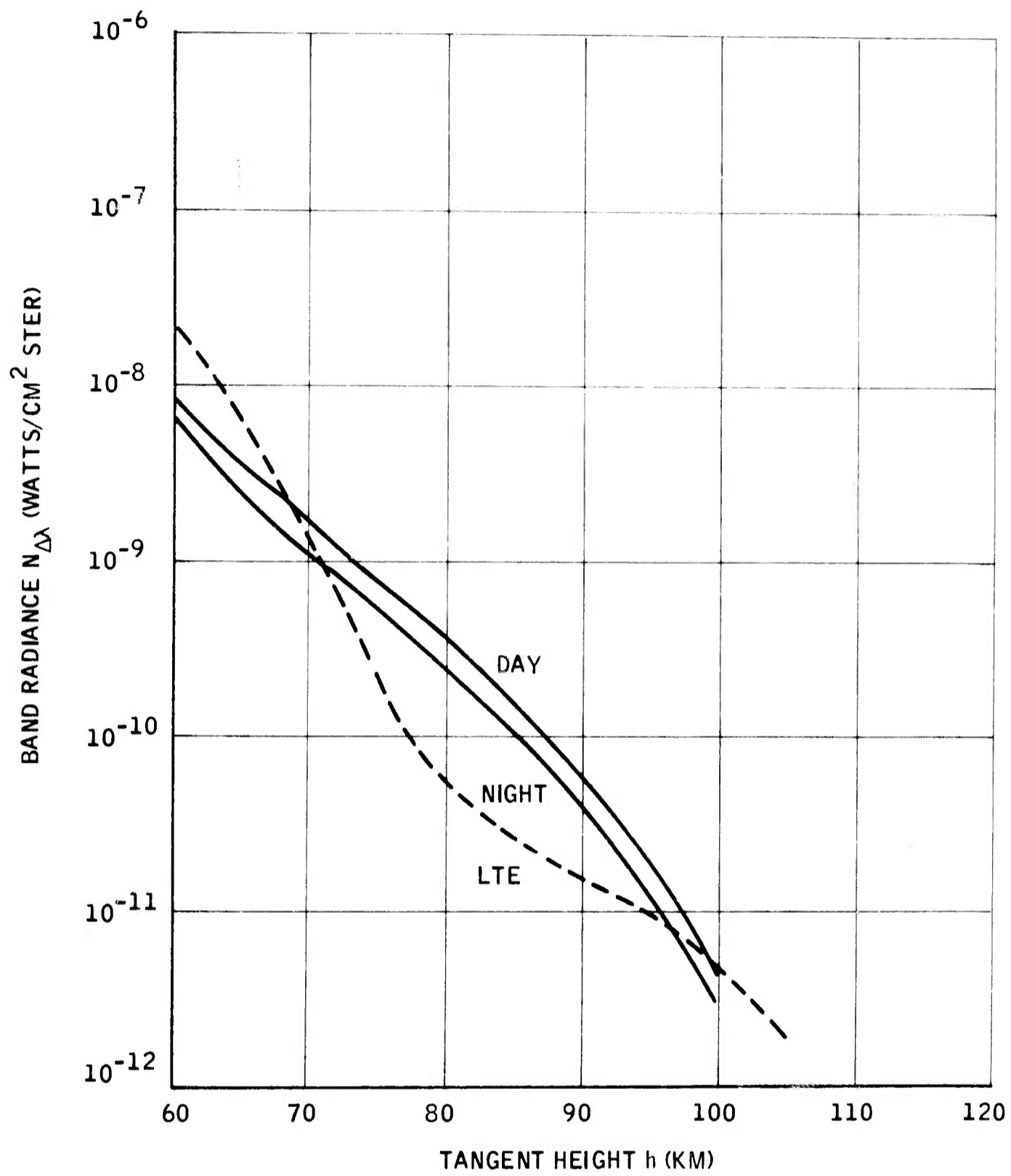
107

Figure 44. Limb Radiance of Methane 5.8 μm Band

108

Figure 45. Limb Radiance of Methane 6.5 μm Band
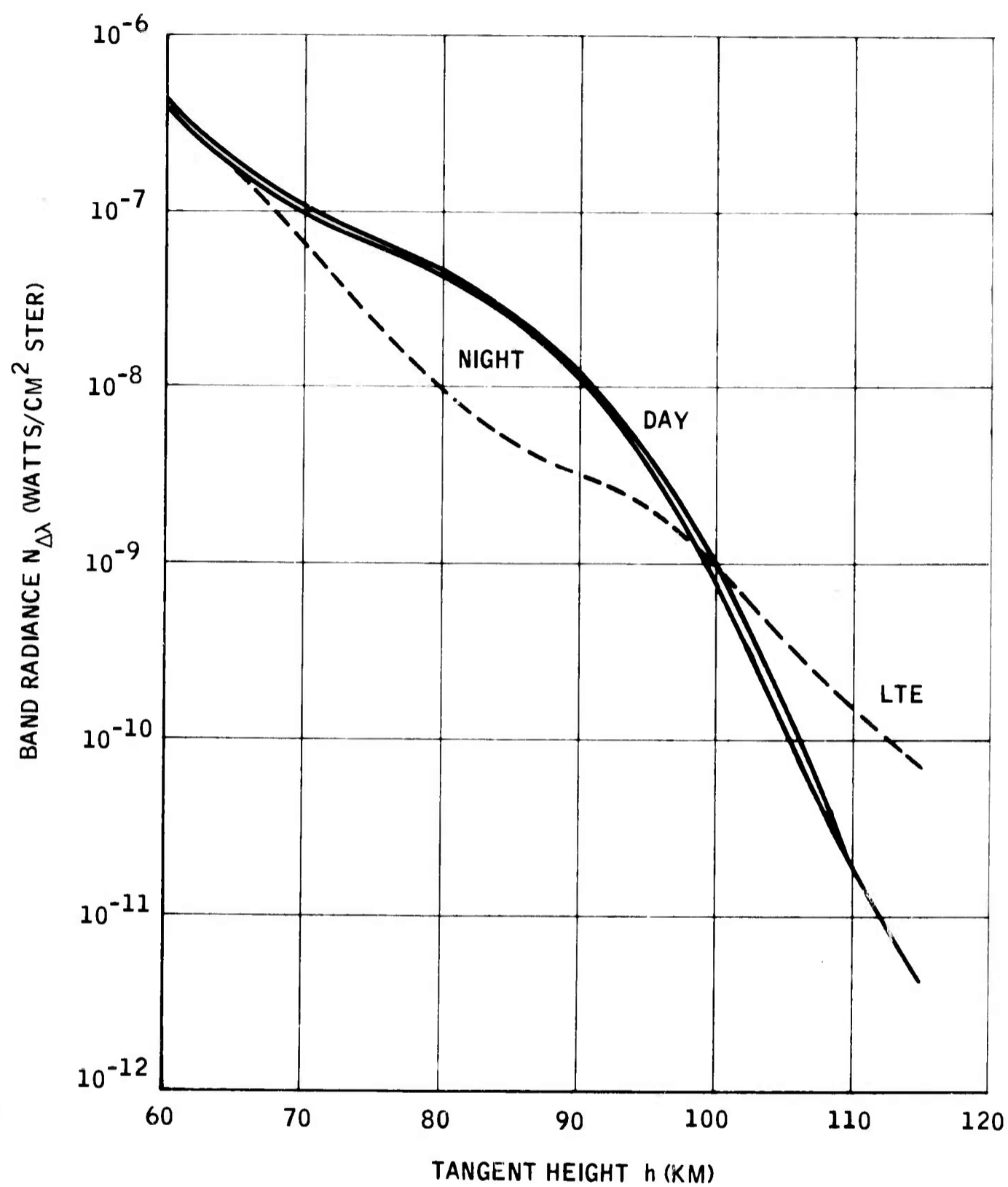
Figure 46. Limb Radiance of Methane 7.7 μm Band

110

Section A above. Only one example is included in the current report since this study has emphasized limb radiances that would be measured from exo-atmospheric platforms.

Figure 47 illustrates the variation in NO band radiances as a function of zenith angle and reference altitudes of 100 km, 200 km and 300 km. The effect of increased optical paths with increasing zenith angle is apparent in the increased radiance magnitudes at all altitudes. The curvature of the radiance variations at 100 km is less than those indicated at 200 and 300 km. This is due to the fact that the transmission properties for the horizon view at 100 km are becoming optically thick, and absorption is significant and radiative transfer is becoming important. The calculations for the higher altitudes are optically thin. Thus, the radiance variations with zenith angle are similar at 200 and 300 km, a function principally of the geometry of view.

C. SPECTRAL RADIANCES

The final goal of this study of upper atmospheric infrared radiance is the prediction of spectral radiance values at wavelengths between 5 and 25 μm for all species and for both exoatmospheric and endoatmospheric viewing. As an example, Figure 48 shows spectral limb radiances for the water vapor rotational band at wavelengths between 10 and 25 μm for tangent heights of 60 km, 80 km and 100 km. These radiances were computed by a program which is included as a subroutine in the final radiance model computer program. The basic assumption used in the computation is that rotational levels are in thermodynamic equilibrium and that emission and absorption may be computed using Equations 42 and 44. The necessary dipole moments were obtained from the dipole matrix element values tabulated by Gates et al. (1964) for wavelengths longer than 12 μm and from values of absorption coefficients supplied by Dr. R. McClatchey of AFCRL for shorter wavelengths. About 250 of the strongest lines in this spectral region are included in the computational results. The spectral radiance for all species is given in Appendix F.

111

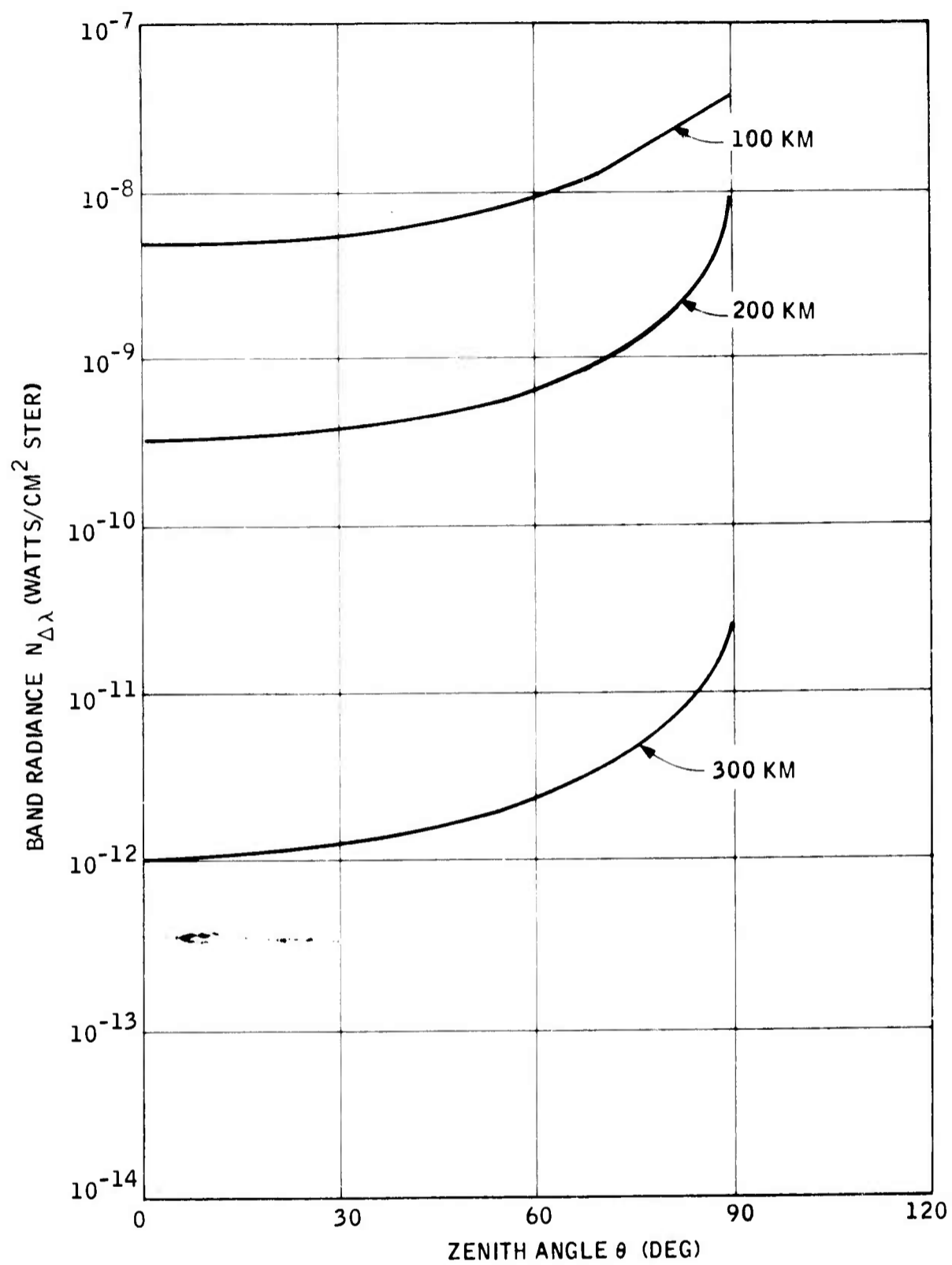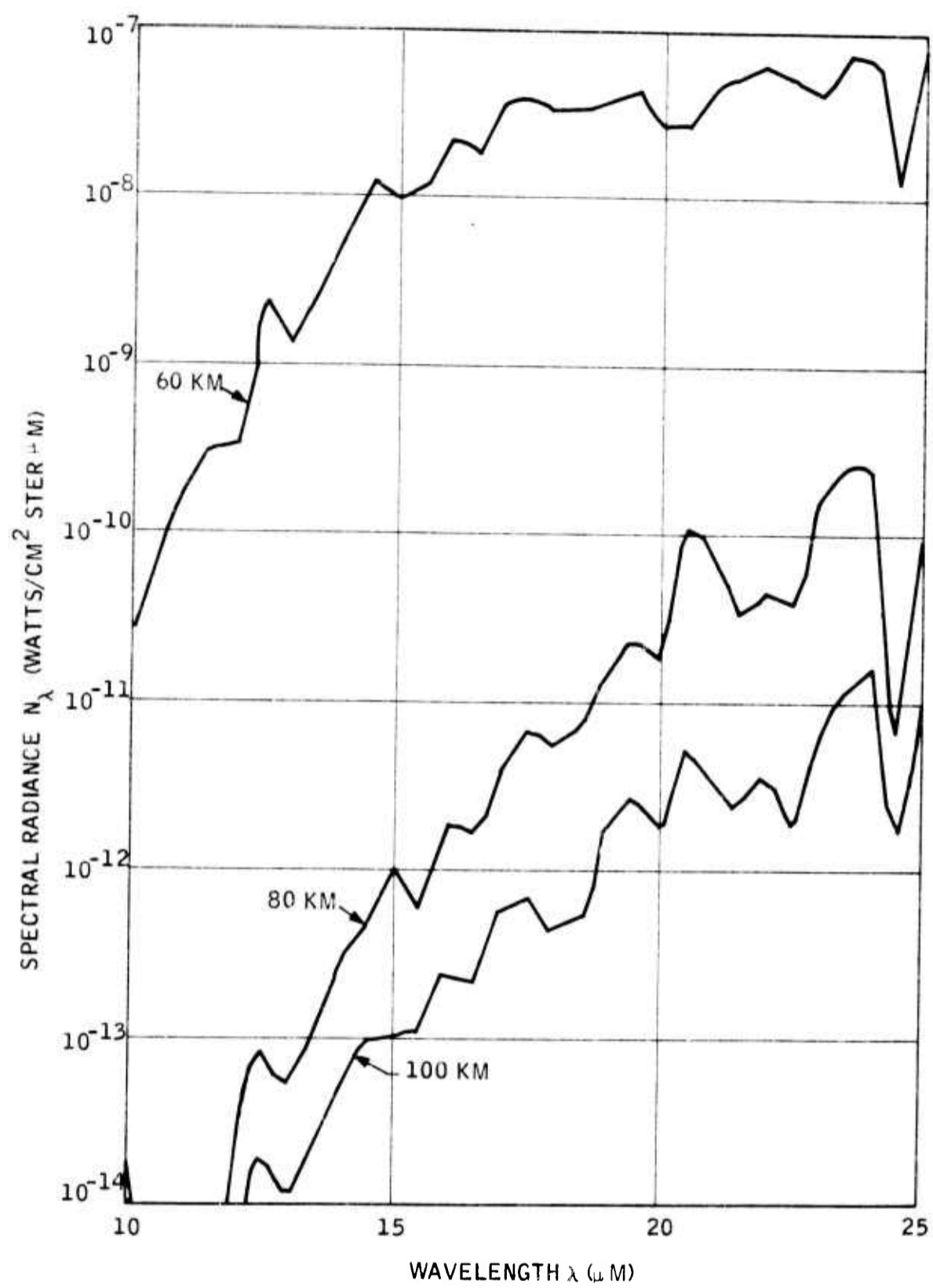Figure 47. Endoatmospheric Radiances of Nitric Oxide 5.3 μ m Band

Figure 48. Spectral Limb Radiance of Water Vapor Rotational Lines

D. SUMMARY OF RESULTS AND COMPARISON WITH OBSERVATIONS

A summary comparison of limb radiance profiles, presented in Section A, is shown in Figure 49 for equatorial noon conditions and for important molecular bands considered in this study. The results presented here allow a comparison of the relative magnitudes of different bands for tangent heights from 60 to about 120 km. It is noted again that the physical assumptions made in the computational model are valid above the 70 km tangent height.

By far the dominant source of radiance at all altitudes is the 5.3 μm NO band. The 15 μm CO_2 complex, representing the total contribution of seven bands between 13.9 and 16.7 μm appears to be the second largest radiance source at heights between 70 and 75 km, and at heights above 90 km up to where the molecule is dissociated. CH_4, O_3 and N_2O have about the same order of magnitude in the 70 to 100 km altitude range. Above 100 km, N_2O is about an order of magnitude larger than the radiances from CH_4 and O_3, as well as that from the 10.4 μm CO_2 band. The results indicate that radiances from the 6.3 μm CO_2 are the smallest of all the molecules considered for heights above about 75 km. Furthermore, the radiance magnitudes from the H_2O rotational spectra in Figure 48 indicate the same order of magnitude as those for the 6.3 μm band. Therefore, H_2O radiances for the abundances assumed in the upper atmosphere are least important of all species considered.

The most extensive experimental observations which correspond to the exo-atmospheric limb radiances presented above are those of Markov (1969). This paper, which summarizes several articles which have appeared in the Russian literature, reports radiances in the 3 to 8 μm spectral region which far exceed any estimates from the computational model of the current study. Even at LTE (Figure 41), nitric oxide cannot explain Markov's radiances, which vary from 10^{-4} to 7×10^{-2} watts/cm^2 (about 10^{-5} to 4×10^{-3} watts/cm^2-ster) in layered structure at altitudes between about 150 and 500 km.

114
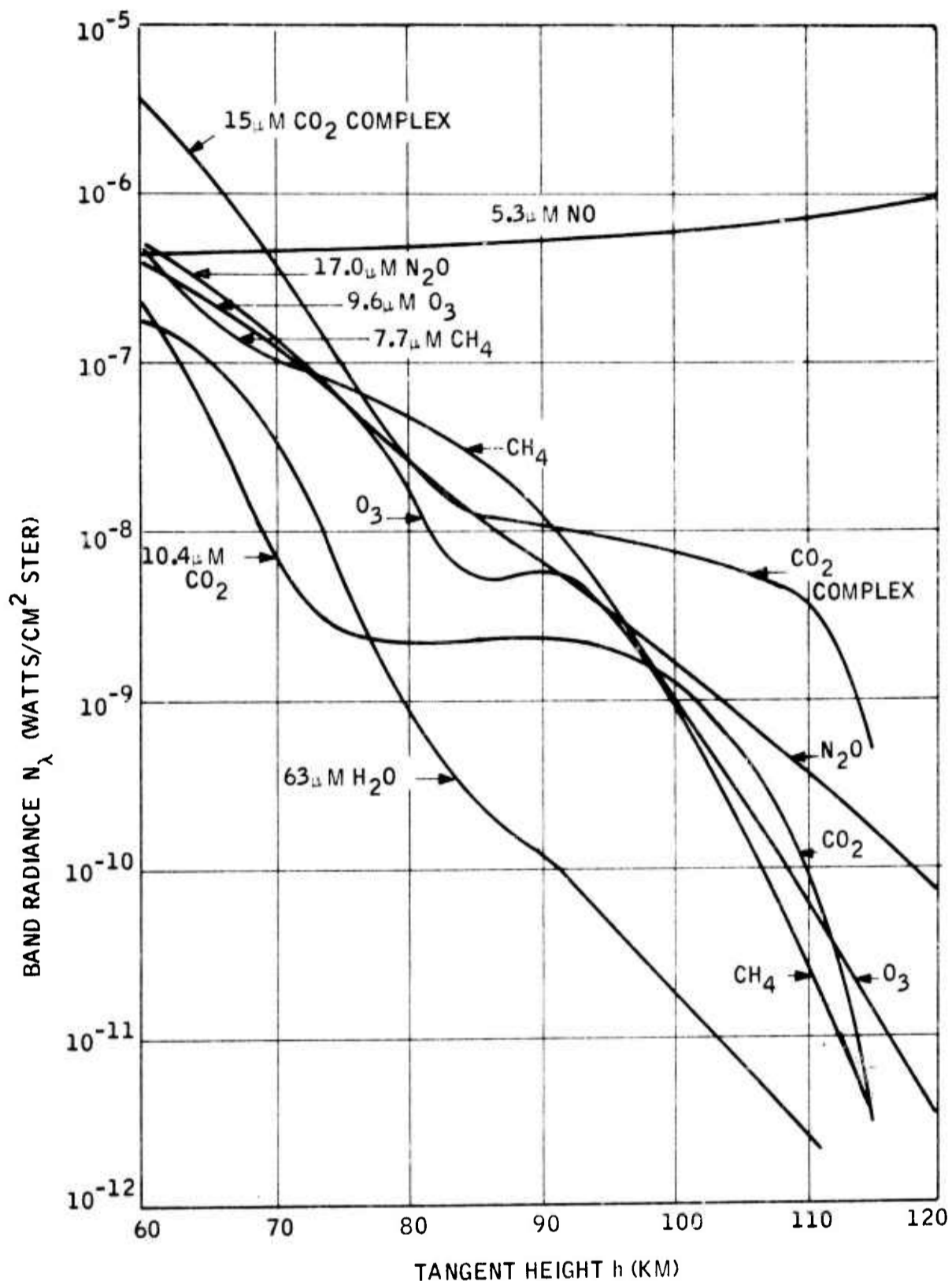
Figure 49. Summary Comparison of Limb Radiance Profiles for Noon Conditions and Important Molecular Bands Considered in This Study

115

The most plausible partial explanation of Markov's results invokes collisional transfer of nitrogen vibrational excitation to carbon monoxide formed by photo-dissociation of CO_2 at high altitudes. Excitation of CO in the 4.7 μm band is about 200 times as efficient as excitation of NO by collision (Walker, 1968; Vasco et al., 1961). Further, there may be up to 10 times as much CO as NO at 120 km. This could result in limb band radiances from CO on the order of 10^{-5} watts/cm^2-ster at altitudes near 120 km which is about equal to the lower values of Markov's observations. CO band radiances, however, cannot explain layered structure at altitudes above 120 km. Balloon observations of spectral radiances performed by Hampson and discussed by Houghton (1964) further substantiate the hypothesis that CO is an important radiance source in the upper atmosphere.

It is certainly worthwhile in the future to examine CO in greater detail and to estimate its contribution to the infrared radiant background of the earth. Other molecules such as N_2O and OH may also be significant radiance sources at wavelengths below 5 μm.

116

SECTION VII
INFRARED RADIATION FROM PARTICULATE MATERIAL

The results presented in Section VI indicate the order of magnitude and variability of limb radiances from gaseous sources in the upper atmosphere. Limb radiances can vary by five orders of magnitude for different wavelengths in the 5 to 25 μm spectral region. It is important in the overall problem of determining the natural infrared radiant background of the earth to estimate the spectral radiances arising from non-gaseous sources such as particulate material. These may include naturally observed phenomena such as clouds and dust layers as well as infrared radiation from dust in interplanetary space. A comparison of radiances from gaseous sources with those from particulate sources will give answers to questions such as (1) which source is dominant?, (2) over what regions of the spectrum is each source important?, and (3) at what altitudes is a given source important? Answers to these questions will help to complete the overall picture of the earth's infrared radiant background.

It is important in the following discussion to keep in mind the general order of magnitude of limb radiances from gaseous sources in the 80 km to 100 km tangent height range. Summarizing the magnitudes presented in Section VI, the 5.3 μm NO band has a magnitude of about 10^{-7} watts/cm^2-ster. The orders of magnitude from other bands in units of watts/cm^2-ster and increasing wavelengths are: 6.3 μm H_2O band – 10^7; 6.55 μm CH_4 band – 6 x 10^{-7} to 5 x 10^{-12}; 7.66 μm CH_4 band – 10^{-8} to 10^{-10}; 7.8 μm N_2) band – 3 x 10^{-8} to 3 x 10^{-9}; 9.6 μm O_3 band – 2 x 10^{-8} to 10^{-9}; 10.4 μm CO_2 band – 2 x 10^{-9} to 2 x 10^{-10}; 10-12 μm H_2O rotational band – 10^{-13}; 14-16 μm CO_2 band – 3 x 10^{-8} to 5 x 10^{-9}; 17 μm N_2O band – 3 x 10^{-8} to 2 x 10^{-9}; and the 20-25 μm H_2O rotational band – 5 x 10^{-10} to 5 x 10^{-11}. It is noted that regions of the spectrum having low spectral radiances are those in the

atmospheric window at 11 μm ($\sim$ 10^{-13} watts/cm^2-ster-μm) and the rotational water vapor band from about 18 μm to 25 μm ($\sim$ 10^{-10} watts/cm^2-ster-μm). These spectral regions should be kept in mind when considering the radiances from particulate material sources.

A. GENERAL CONSIDERATIONS

The infrared background radiation between 5 and 25 μm, as observed at or near the earth's limb from particulate material, can be produced by three mechanisms:

(a) Rayleigh scattering of infrared radiation (particles < 1 μm)

(b) Mie scattering of infrared radiation (particles > 1 μm)

(c) Thermal emissions from particles.

Infrared radiation from interplanetary space is considered in the same context as radiation from clouds and dust layers since its origin is from particulate material and may be of significance in the absence of sources imbedded in the earth's atmosphere.

The two contributions due to scattering above require an outside source of energy. The important sources of irradiation are the earth-atmosphere system and the sun. The magnitude of irradiance from the earth is dominant in the upper atmosphere for wavelengths greater than about 6 μm. On the other hand, solar irradiance is dominant in interplanetary space at distances more than about 200,000 km from the earth.

The magnitude of infrared radiation from particulate material depends on the wavelength of light, the number of particules, the size distribution of particles, their physical characteristics and composition, and, in the case

118

of thermal emission, the temperature of the particles. The first step in modeling the radiation from particulate material in the upper atmosphere and interplanetary space has been to review the present state of knowledge of particle number concentration, size distribution and composition (if available), as functions of altitude above the surface of the earth from about 20 km on upwards. Sixteen references were reviewed which include: Blandari et al. (1968); Hodge and Wright (1968); Farlow (1968); Rossler and deBary (1966); Kiaser (1968); Friend (1966); Newkirk and Eddy (1964); Beard (1959); Divar (1959); Cadle (1966); Junge (1961); Rosen (1964); Wright and Hodge (1968); and COSPAR (1968). This literature search is condensed in graphical form of Figure 50 (as far as particle concentration is concerned) which depicts the particle number concentration per cm^3 as a function of altitude. Particle sizes covered in this survey range from about 0.1 μm to about 10 μm in diameter, with a predominance of particles of the order of 1 μm in diameter. The horizontal lines represent concentration ranges either measured or estimated by particular authors; vertical lines represent such determinations over a given range of altitudes; and the data points represent specific measurements or estimates at a given altitude. Arrows indicate a possible continuation of the particular line.

Figure 50 illustrates the enormous range of uncertainties and discrepancies of the available information in this field, even at altitudes accessible by research balloons. If any significant conclusion can be reached at this juncture, it is that above about 50 km, or even lower, the dust particle concentration falls off very rapidly as a function of altitude from typical levels of 0.1 to 1 cm^{-3} at 30 km to less than 10^{-6} cm^{-3}, at about 100 km. Beyond this altitude the concentration continues to decrease to a level about which there is at best only a fair agreement, ranging from a maximum of 10^{-8} cm^{-3} to a minimum of 10^{-11} cm^{-3} (one estimate indicating a concentration of 10^{-16} cm^{-3} appears unreasonably low) with a most probable value around 10^{-9} cm^{-3}. If the presently preferred model of a heliocentric zodiacal dust cloud is correct, its contribution to the infrared background radiation can be significant. Even

119
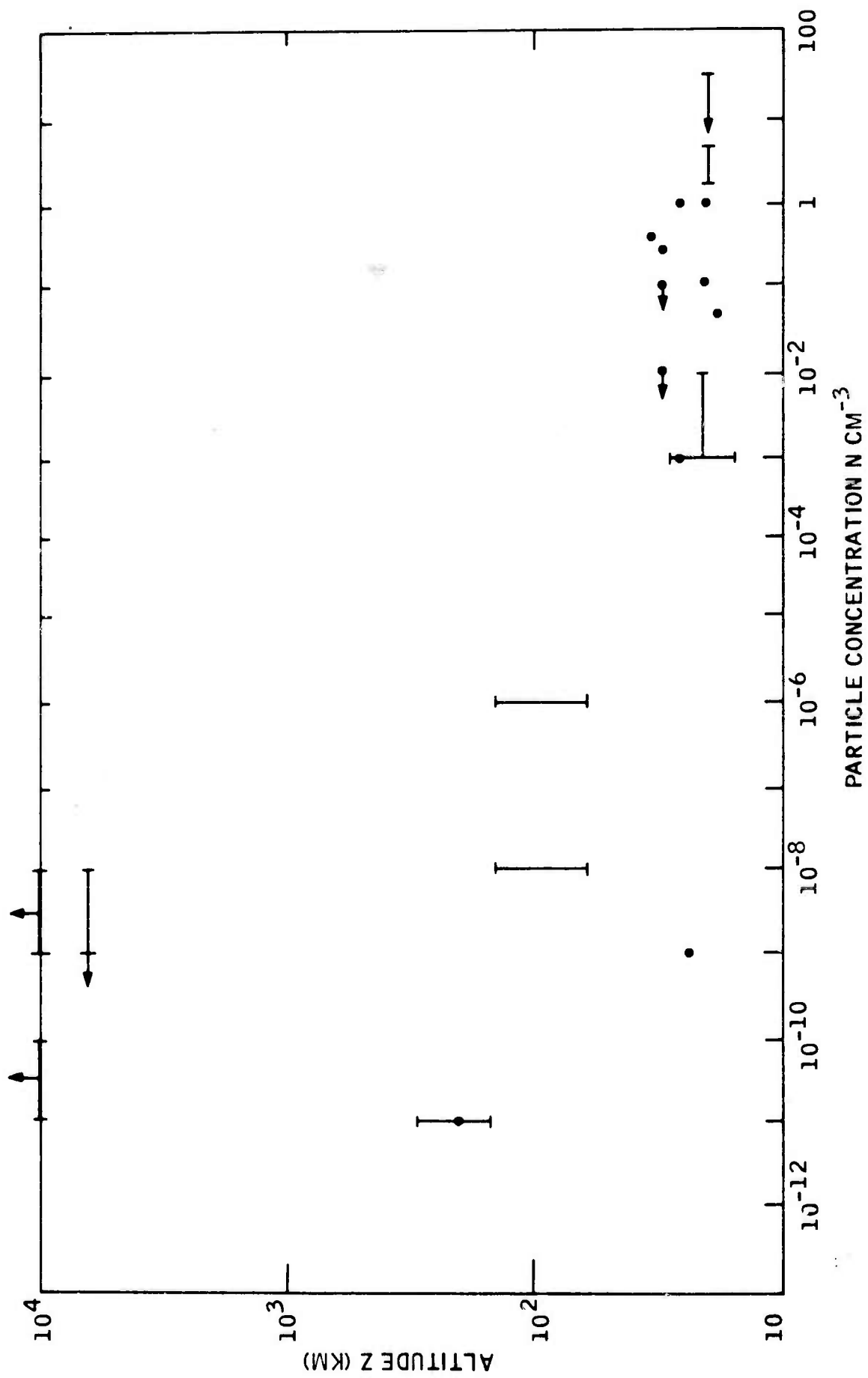
Figure 50. Dust Particle Concentration as a Function of Altitude

though the above-mentioned number concentration of particles is very low in interplanetary space at one astronomical unit from the sun, the path lengths involved, especially along the ecliptic plane, are considerable; and thus, the integrated contribution of radiation can be significant.

In addition to the relatively invariant or stable dust concentrations near the earth and in interplanetary space, there exist transient and localized particulate concentrations such as nacreous clouds, noctilucent clouds, "leuchtstreifen" and artificial injections mainly due to the combustion of solid rocket fuel propellants.

Nacreous clouds typically appear at altitudes below 30 km and will not be considered for the present study since their effect is overshadowed by gaseous emission of CO_2, O_3 and H_2O in the lower atmosphere. Insufficient quantitative information precludes the inclusion of either the leuchtstreifen (luminous bands at about 120 to 130 km) or of artifically produced noctilucent clouds. Naturally occurring noctilucent clouds will be treated in detail with respect to their contribution to the natural infrared radiant background of the earth.

B. RADIATION FROM THE STABLE DUST CONTENT IN THE EARTH'S ATMOSPHERE

As pointed out above (see Figure 50) particle number concentration appears to drop off very rapidly above 30 or 40 km such that no significant contribution of infrared radiation can be expected from the stable dust content above those altitudes. Since only a few reliable measurements have been performed in the altitude region between the balloon ceiling and low orbit levels, it is fair to assume that stable particle concentrations in that region should be of the order of 10^{-5} to 10^{-3} cm^{-3}, several orders of magnitude below the stratospheric values. Preliminary calculations using the above concentrations and typical associated path lengths show levels of infrared

radiance well below those obtained from other radiating mechanisms and sources even in 10.3 μm "window" discussed in Section III of this report (see subsequent section on noctilucent clouds).

C. RADIATION FROM INTERPLANETARY DUST

The presence of dust particles outside the earth's atmosphere has long been surmised on the basis of the observation of Zodiacal light. The characteristics of this phenomenon has led investigators to attribute it to the presence of the so-called Solar F corona or dust corona. The particles associated with the dust corona appear to form a very large lenticularly shaped cloud around the plane of the ecliptic. It true extent is unknown but its outer limits may extend as far as the orbit of Jupiter. The main area of uncertainty is associated with the actual number density of the particles within this distributed cloud. Estimates have ranged from 10^{-16} cm^{-3} to 10^{-8} cm^{-3} at 1 AU from the sun, depending on whether a geocentric or a heliocentric zodiacal dust model was preferred. The prevailing trend is to accept the latter of these two models with typical particle number concentrations of 10^{-9} to 10^{-8} cm^{-3} at 1 AU. Measurements of infrared radiation from zodiacal dust have been restricted to solar elongations (angle of observation with respect to the direction of the sun) of a few degrees, and at wavelengths shorter than the band of interest of 5 to 25 μm, e.g., 2.2 μm (Peterson, 1967; MacQueen, 1968). Several authors have developed models of infrared emission from interplanetary dust clouds, among them are Peterson (1963) and Kiaser (1968). Kaiser's model incorporates the latest experimental observations at 2.2 μm in his emission model using a more rigorous treatment than Peterson. Kaiser utilizes a composite "dirty quartz" particle model and extends his calculations to 13 μm. Again, only small solar elongation angles were considered (up to 2.5°).

Figure 51 shows the calculated spectral infrared radiance from the inter-planetary dust replotted from Kaiser's work (solid lines). These curves
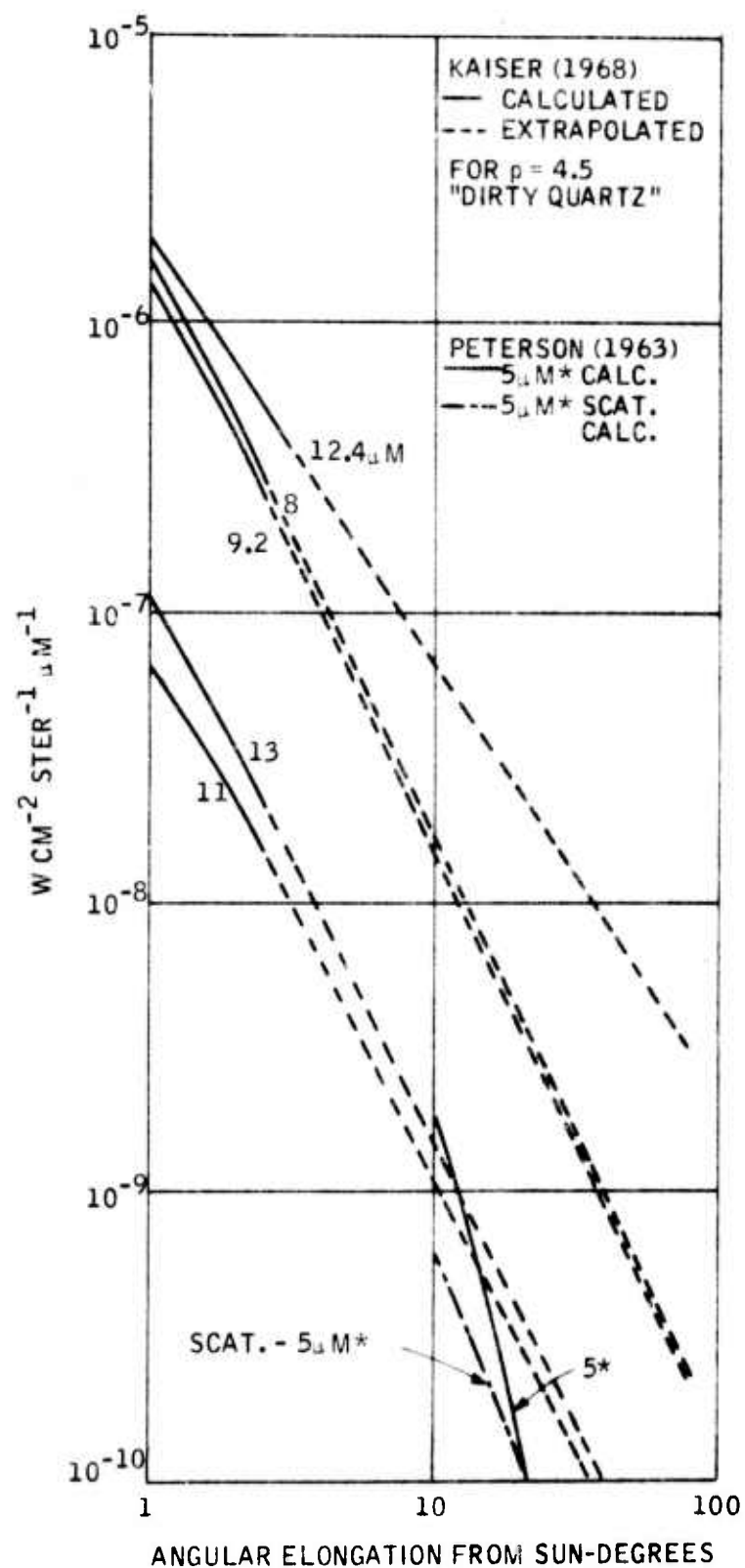
Figure 51. Spectral Radiance from Interplanetary Dust for Different Elongation Angles from the Sun

have been extrapolated (dashed lines) on the basis of the general trends of Kaiser's calculations. These extrapolated curves most probably furnish an upper limit of the expected infrared radiance from interplanetary dust if the assumptions of particle number concentration and size distribution, as well as composition are all valid. Figure 51 also depicts the results of prior calculations performed by Peterson (1963), for 5 μm emission and scattering. The scattering contribution falls off vary rapidly for wavelengths longer than 5 μm and can thus be neglected as compared with the expected emission levels. A more rigorous treatment of the emission from interplanetary dust in the infrared for elongations beyond 2.5° was not attempted at this point in view of practical time constraints and based on the confidence which the overall trends of the emission characteristic provide to a simple extrapolation as shown in Figure 51. The validity of the particular model of the spectral characteristic of this emission is predicated on a possible experimental confirmation of this band structure associated with the optical characteristics of the material assumed to predominate in the form of interplanetary dust particles (Kaiser, 1968).

The results in Figure 51 indicate that the magnitude of radiance from interplanetary dust decreases with increasing angle to the sun and depends on the composition and reststrahlen bands of the dust material. Spectral radiance magnitudes on the order of 10^{-9} to 10^{-10} watts/cm^2-ster-μm appear to be possible for viewing angles of about 50 degress to the sun. A probable magnitude for angles greater than 90 degrees is between 10^{-10} and 10^{-11} watts/cm^2-ster-μm. These results are in general agreement with recent calculations made by Walker (1969); however, they do not agree with calculations reported by Mikirob (1966).

It is noted that these magnitudes are greater than limb radiance magnitudes at 11 μm mentioned earlier, and are of the same order or larger than the magnitudes in the 18 to 25 μm H_2O rotational band.

124

D. RADIATION FROM NOCTILUCENT CLOUDS

1. General Characteristics of Noctilucent Clouds

Notcilucent clouds have been observed scientifically since the late 19th century, and their characteristics have slowly been elucidated as more advanced probing methods and a larger number of observing sites have been utilized during the past decade. However, many unanswered questions remain such as the exact composition and origin of the particles in these clouds, the reasons for their relatively large number density, and their actual frequency, duration and geographical extent. The prevalent technique of visual sighting only provides a partial source of information about the actual permanence of noctilucent clouds since the conditions for their visual observation are restricted to a relatively narrow period of time and geographical location (Fogle and Haurwitz, 1966).

The present state of knowledge of noctilucent clouds, as related to the problem of infrared brightness with which we are concerned, can be described as follows (Fogle and Haurwitz, 1966; Fiocco and Graws, 1969):

    (a) Average height: about 82 km (observed range 72 to 92 km)

    (b) Average thickness: about 2 km (probable range 0.5 to 5 km)

    (c) Latitude of observations: 45° to 80° N and S, most frequent at about 60°)

    (d) Seasonal characteristic: sharp summer maximum

    (e) Spatial extent: 10^4 to more than 4×10^6 cm^2.

    (f) Duration of visual observation: several minutes to several hours.

(g) Particle size distribution equation: $N = Kd^{-p}$ (55)

(Fogle and Haurwitz, 1966; Hemenway et al.)

where: N is the number density of particles larger
than d (typically $N = 200 \text{ cm}^{-3}$ for $d > 0.05 \ \mu m$)

d is particle diameter,

p varies between 3 and 4.

(h) Particle size range: 0.05 μm to about 0.5 μm diameter.

(i) Estimated particle composition: probably meteoric for
particles smaller than about 0.2 or 0.3 μm, and mostly
ice for larger particles (by nucleation).

(j) Temperature range of mesosphere between 72 and 92 km:
135°K to more than 200°K. Probably temperature in the
presence of NLC: 135 to 160°K.

(k) Longitudinal variations. Not clearly established, although
there is some evidence of regions of preferential sightings
such as Scandinavia and north-western U.S.S.R.

The relatively high particle number concentration (see above and Figure 52)
and the possibility of sighting with long slant paths (limb view) from outside
the atmosphere indicates a possible source of significant infrared radiation
from these noctilucent clouds.

2. Rayleigh Scattering

For the range of particle sizes cited above, only the Rayleigh type scattering
has to be considered. The Rayleigh scattering equation as related to the
geometry of this problem is:

126
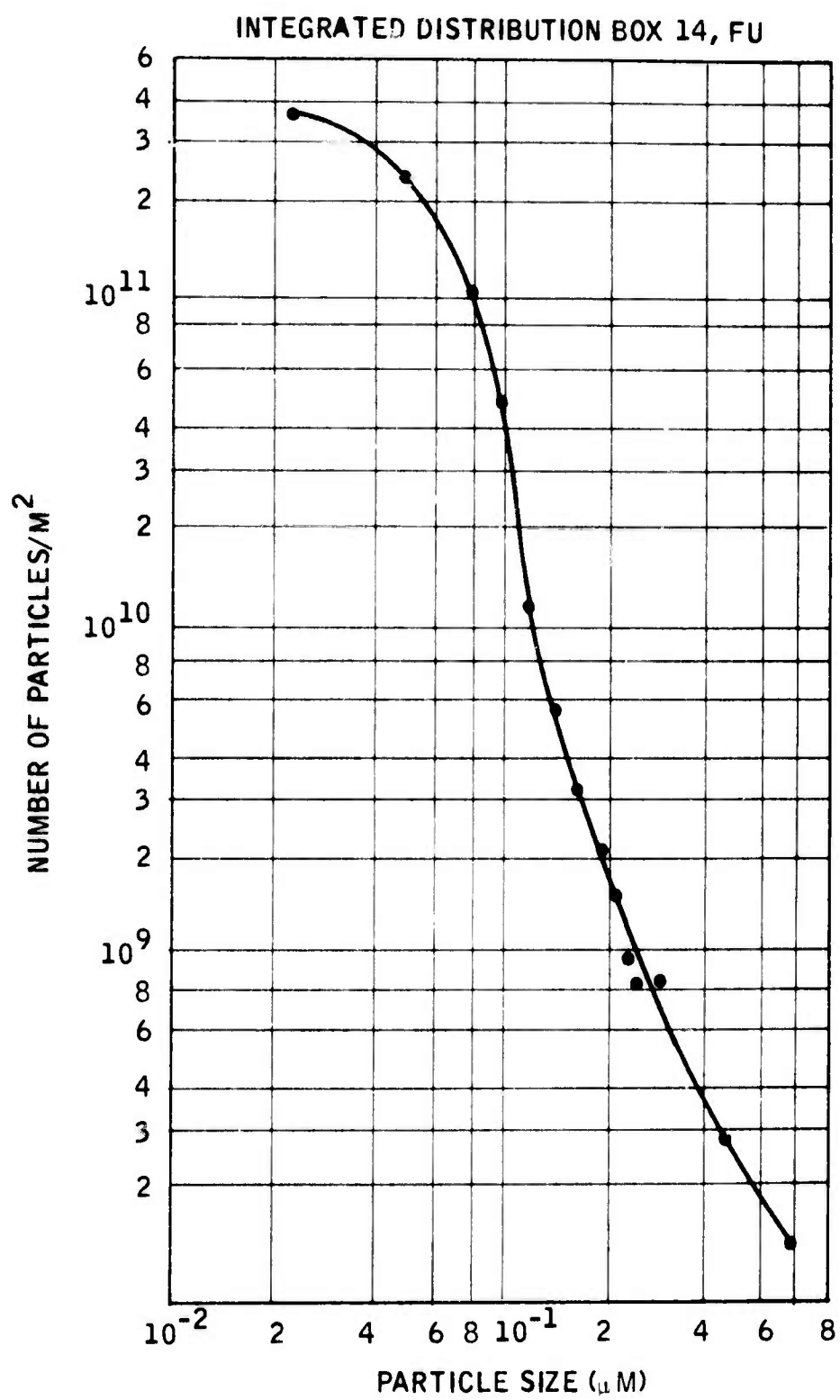
Figure 52. Integrated Size Distribution of Noctilucent
Cloud Particles

127

$$N_\lambda = N_{\lambda_o} \frac{9\pi^2 V_p^2}{2\lambda^4} \, nL \left(\frac{m^2 - 1}{m^2 + 1} \right)^2 (1 + \cos^2 \theta) \tag{56}$$

where:

N_λ = scattered intensity

N_{λ_o} = incident radiation intensity

n = particle number concentration

V_p = particle volume

λ = wavelength

m = index of refraction of particle

θ = scattering angle

L = path length

The integral size distribution of Figure 52 shows the number of particles larger than a given diameter d (Blandari et al., 1968; Farlow, 1968).

If a vertical path length of 1 km is assumed and a lower cutoff diameter of 0.05 μm is used, $N \cong 200$ for $d > 0.05$ μm ($d_{max} \cong 0.5$ μm).

Starting from equation (55) and assuming the worst case condition of $p = 3$, one obtains:

$$K = Nd^p = 200 (5 \times 10^{-6})^3 = 2.5 \times 10^{-14} \tag{57}$$

Since $i \propto V_p^2 n$ and $V_p = \frac{\pi d^3}{6}$

128

$$\frac{di}{dd} = \frac{\pi^2 d^6}{36} \frac{dn}{dd} = \frac{\pi^2 d^6}{36} (-pKd^{-p-1}) = -2.06 \times 10^{-14} d^2$$

$$V_p^2 n = -\int_{5 \times 10^{-5}}^{5 \times 10^{-6}} 2.06 \times 10^{-14} d^2 dd = 8.5 \times 10^{-28} cm^3$$

Replacing this value of $V_p^2 n$ in equation (56) one obtains:

$$N_\lambda = 3.78 \times 10^{-26} N_{\lambda o} \frac{L}{\lambda^4} \left(\frac{m^2 - 1}{m^2 + 1}\right)^2 (1 + \cos^2 \theta) \qquad (58)$$

The maximum Rayleigh scattering contribution would be obtained at $\lambda = 5~\mu m$, within the spectrum of interest. A worst case calculation is based on the following values:

$\lambda \quad = \quad 5~\mu m = 5 \times 10^{-4}~cm$

$m \quad = \quad 1.247$ for ice (Irvine and Pollock, 1968)

$\theta \quad = \quad 0°$ or $180°$ (maxima)

$L \quad = \quad 320~km = 3.2 \times 10^7~cm$ (worst case assuming a 2 km thickness viewed tangentially from outside the earth's atmosphere).

$N_{\lambda o}$ is determined by the additive contributions from the solar and terrestrial irradiances at $5~\mu m$, estimated from theoretical computations in Section III.

$$N_{\lambda o} = 7 \times 10^{-4} + 4 \times 10^{-4}~watts/cm^2 - \mu m^1 = 1.1 \times 10^{-3}~watts/cm^2 - \mu m$$

Replacing these values in equation (58) one obtains:

$$N_\lambda = 3.78 \times 10^{-26} \times 1.1 \times 10^{-3} \times \frac{3.2 \times 10^7}{5^4 \times 10^{-16}} \left(\frac{1.247^2 - 1}{1.247^2 + 1}\right)^2 (1+1)$$

$$= 1.98 \times 10^{-9}~watts/cm^2 - \mu m$$

129

For one steradian:

$$N_\lambda = 1.57 \times 10^{-10} \text{ watts/cm}^2\text{-ster-}\mu\text{m}$$

The value of N_λ for the parameters chosen above would vary as shown in Table 3 as a function of wavelength, on the basis of a composite Sun-earth irradiance at about 140 km above the earth's surface, assuming extreme magnitudes of irradiance from the earth-atmosphere system.

Table 3.   Infrared Scattering from Noctilucent Clouds
Path Length 320 km - Limb View

λ, μm	N_λ, watts/cm^2-ster-μm
3	7.8×10^{-9}
4	8.75×10^{-10}
5	1.57×10^{-10}
8	1.52×10^{-11}
10	6.8×10^{-11}
15	2.5×10^{-12}

It thus appears that for wavelengths shorter than 5 μm the scattered intensity grows very rapidly, almost one order of magnitude for every micrometer of decreasing wavelength.

The magnitudes of radiance at wavelengths greater than 5 μm are on the order of 10^{-10} to 10^{-12} watts/cm^2-ster-μm, respectively. These magnitudes are considerably lower than those expected from gaseous emission processes from about 5 μm to 10 μm, and are lower in magnitude than thermal emission from interplanetary dust. Therefore, infrared scattering from noctilucent clouds can be neglected.

3. Thermal Emission from Noctilucent Clouds

The problem of determining the thermal emission from noctilucent clouds is uncertain since the actual particle temperature and composition are unknown. The calculation of this temperature is complicated by the fact that Rayleigh particles are cooler than the black body temperature since their absorption cross section is less than their emission cross section, the actual mean ratio of these cross sections being dependent on the composition of the particles. Even if it is assumed that these are ice particles, the problem is not entirely resolved since at an altitude of about 80 km thermal conduction by air molecules still plays a role (probably in the direction of cooling the particles). In any case, if the particles are indeed ice spheres, their temperature will most probably be lower than 200°K. Most authors expect their temperature to be as low as 130 to 150°K (Fogle and Haurwitz, 1966).

The thermal emission from noctilucent clouds can be calculated from the following integral (Kaiser's (1968) nomenclature is being utilized in this equation):

$$N_\lambda = \int_{a_o}^{a_1} n(a)\, C_\lambda(a)\, B_\lambda(T) L\, da \tag{59}$$

where:

a_o and a_1 are the minimum and maximum particle radii of the integral particle size distribution (see equation (55)).

$n(a)\, da = -K_{pa}^{-p-1}$ as defined before (scattering analysis)

$C_\lambda(a) = 4/3\, \pi a^3\, \delta_\lambda$ = absorption or emission cross section, where δ_λ is the Rayleigh coefficient defined as follows:

131

$$\delta_\lambda = \frac{18\pi}{\lambda} \frac{\eta}{(\varepsilon+2)^2 + \eta^2}$$

where $\varepsilon = \bar{n}^2 - \bar{n}'$ and $\eta = 2\,\bar{n}\,\bar{n}'$, where ε is the dielectric constant, η is the resistivity, $\bar{n}$ and $\bar{n}'$ are the real and the imaginary parts of the particle index of refraction at wavelength λ. $B_\lambda(T)$ is the Planck function (at wavelength λ and temperature T). L is the path length within the emitting cloud.

Performing the above replacements we obtain:

$$N_\lambda = 4/3\pi \; \delta_\lambda \; B_\lambda(T) \; L \; K_\rho \int_{a_1}^{a_o} a^{-p+2} \, da \tag{60}$$

Equation (60) was incorporated in a computer program to calculate N_λ as a function of λ for various dust size distribution and composition models, as well as a function of the particle temperature T. Calculations were performed for two sets of cloud characteristics. A "worst case" path length of 320 km was assumed which represents a 2 km thick cloud viewed tangentially (limb view) from outside the earth's atmosphere. Particle concentrations and size distribution were assumed to be the same, 200 part./cm^3 and $a_o = 0.025\mu$ to $a_1 = 0.250\ \mu m$, respectively. Temperatures of 135°K and 160°K and size distribution powers of 3.5 and 3.0 (Fogle and Haurwitz, 1966) were assumed as being representative and upper limit cases, respectively. Three models of particle composition were used: (1) an all dust cloud composed of dirty quartz, (2) an all ice sphere cloud, and (3) a composite ice-dust model where the small particles below 0.05 μm were dust and the larger particles $\geq$ 0.05 μm were ice spheres on the basis of Hemenway's determinations.

Substitution of the above physical parameters into Equation (60) lead to the spectra presented in Figures 53, 54 and 55. Figure 53 depicts the spectra for the upper limit (1) and typical (2) cases of a noctilucent cloud composed exclusively of dust. The results in Figure 54 are based on a cloud composed

132

Figure 53. Variation in Spectral Radiance for a Noctilucent Cloud Composed Exclusively of "Dirty Quartz". Curve 1 Represents an Upper Limit and Curve 2 Represents the Typical Case

133
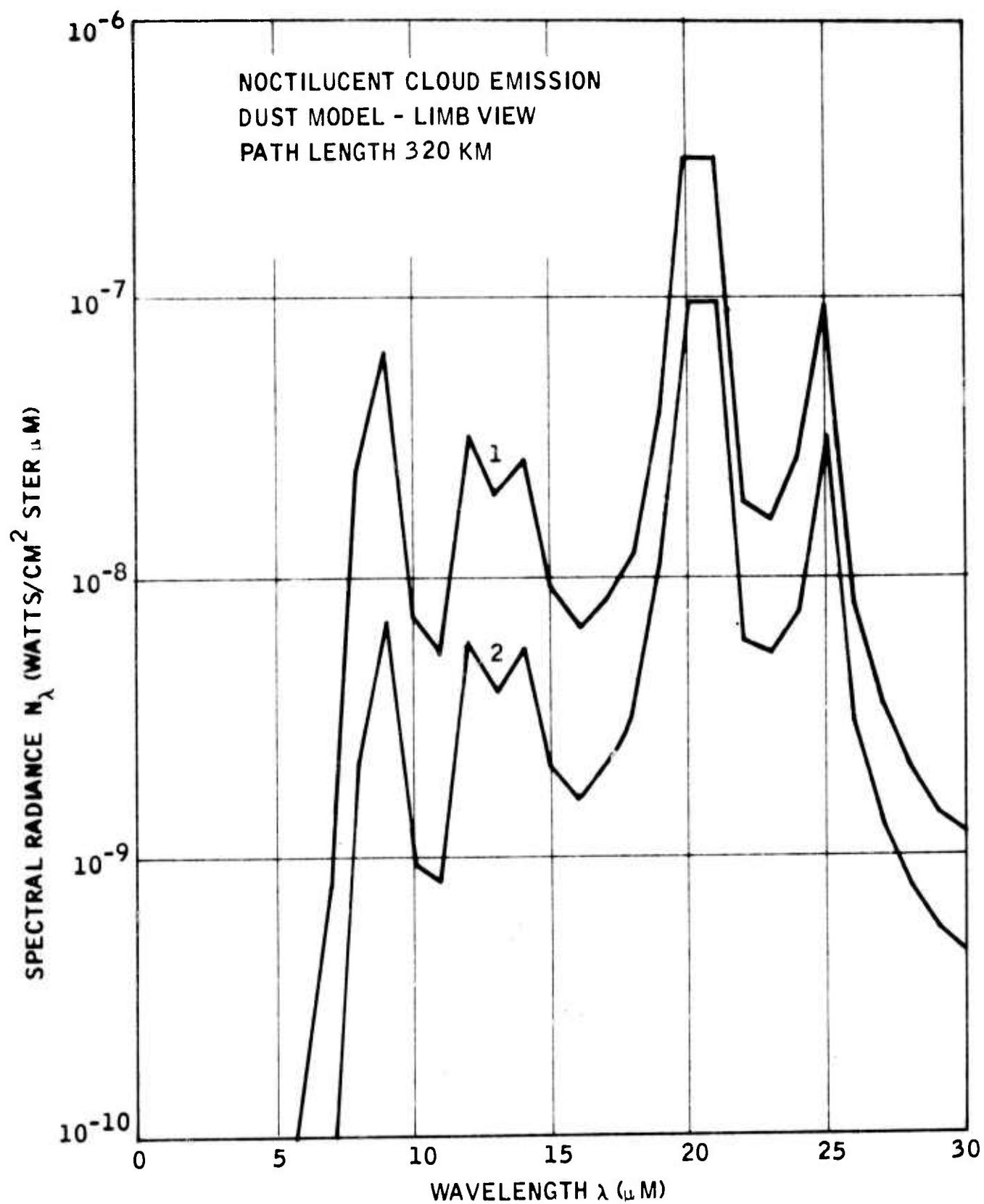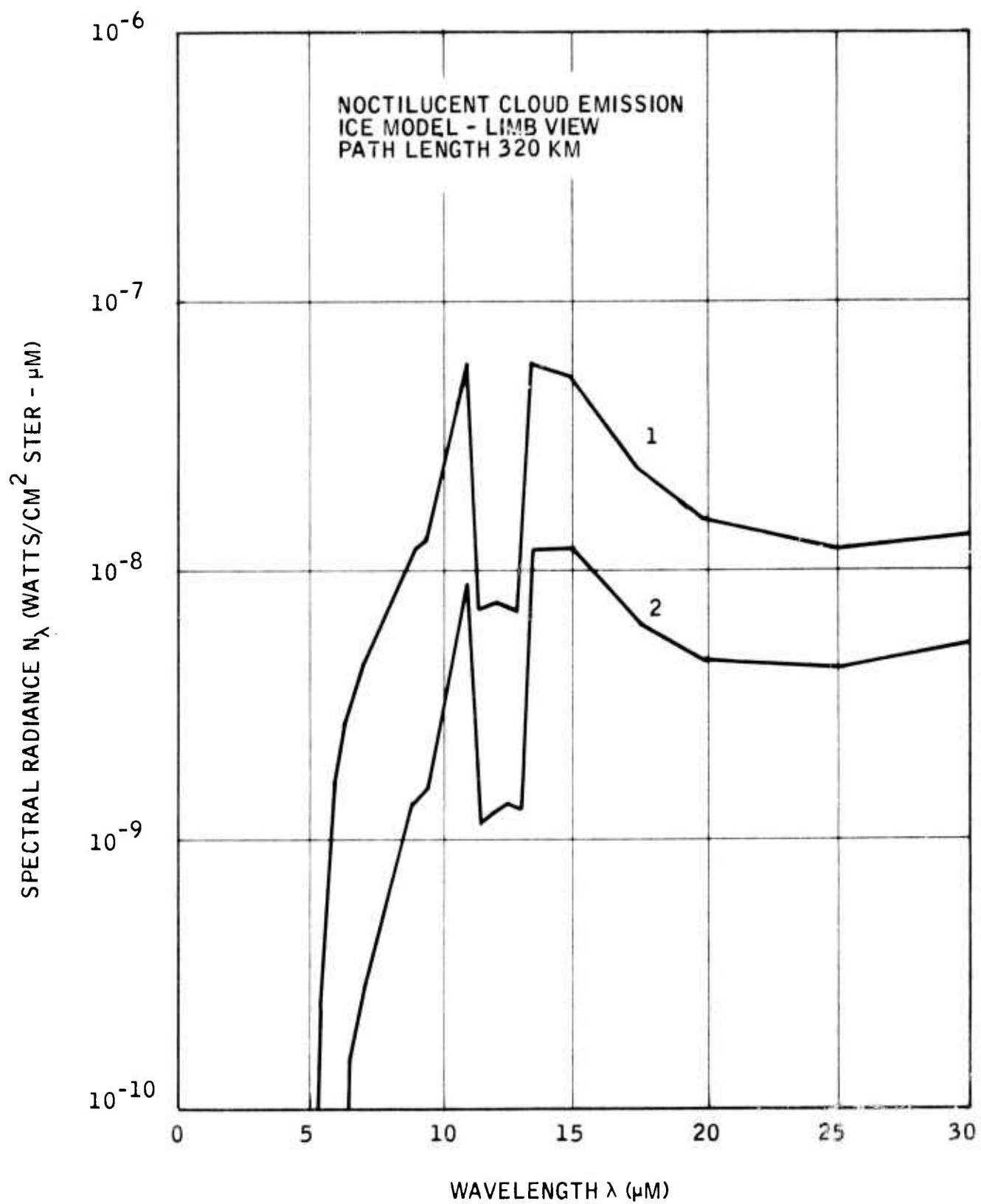
Figure 54. Variation in Spectral Radiance for a Noctilucent Cloud Composed Exclusively of Ice Particles. Curve 1 Represents an Upper limit and Curve 2 Represents the Typical Case
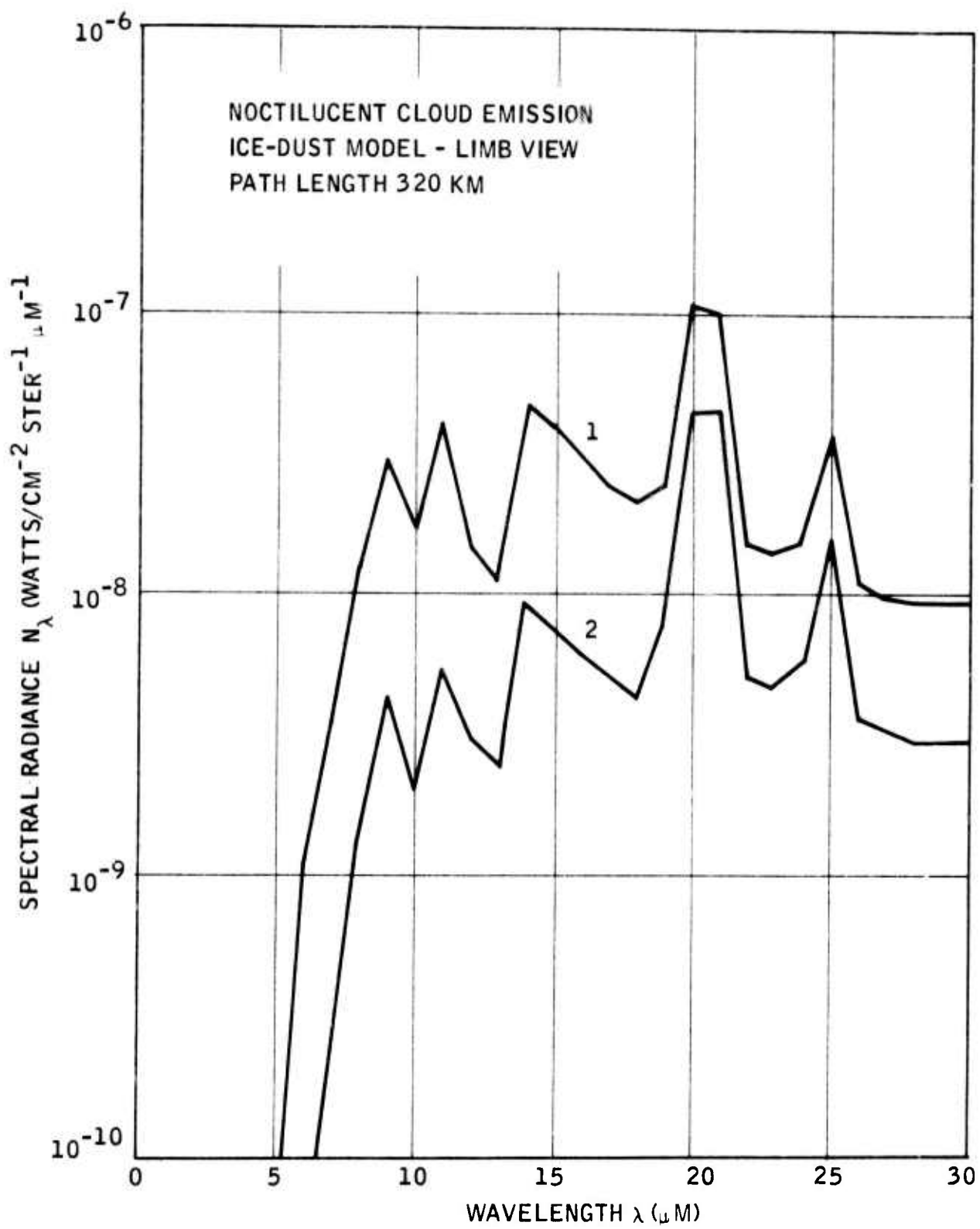
134

Figure 55. Variation in Spectral Radiance for a Noctilucent Cloud Composed of Both Ice and Dust Particles, a Best Estimate Curve 1 Represents an Upper Limit and Curve 2 Represents the Typical Case

135

exclusively of ice particles, and Figure 55 shows the spectra for the ice-dust model cloud, a best estimate. The variations in the magnitudes of the spectra with wavelength are due to strong reststrahlen bands of the materials assumed.

The ice-dust model represents the most probable magnitudes of thermal emission to be expected from noctilucent clouds. In general, a magnitude of about 10^{-8} watts/cm^2-ster-μ would be a reasonable spectral radiance. It is emphasized again that this represents the worst case of viewing a cloud, edge-on with the entire field-of-view of a radiometer filled by the cloud. Had the direction of view been in the vertical sense, the path length would be about 3 km instead of 320 km for the limb view. Under these conditions, the radiance magnitudes would be reduced by two orders of magnitude, to about 10^{-10} watts/cm^2-ster-μm.

In summary, thermal emission from noctilucent clouds is of considerable importance when considering the natural infrared radiant background in the 70 to 90 km altitude region. The estimate of 10^{-8} watts/cm^2-ster-μm is definitely a competing magnitude of radiance as compared to the magnitudes expected from gaseous sources at these altitudes. Limb radiances from noctilucent clouds would definitely be the dominant source at 11 μm and in the 16 to 25 μm spectral range. The transient and unpredictable nature of noctilucent clouds makes this source extremely important when considering variations in natural background sources.

BIBLIOGRAPHY

Abels, L.L., and Shaw, J.H., 1966: Widths and strengths of vibration-rotation lines in the fundamental band of nitric oxide, J. Mol. Spectrosc. 20, 11-28.

Anding, D., 1968: Calculations of atmospheric spectral radiance for slant paths from several altitudes. Report No. 8416-20-F(IV), Vol. IV. Willow Run Laboratories of the Institute of Science and Technology, The University of Michigan, Ann Arbor.

Anon., 1963: Lowest measured temperature in the earth's atmosphere recorded in U.S. — Sweeden experiments. Bull. Am. Met. Soc., 44, 806.

Bandeen, W.R., Conrath, B.J., and Hanel, R.A., 1963: Experimental confirmation from the TIROS VII Meteorological Satellite of the theoretically calculated radiance of the earth within the 15-micron band of carbon dioxide. J. Atmos. Sci. 20, 609-614.

Barth, C.A., 1964a: Three-body reactions. Ann. Geophys. 20, 182-196.

_____, 1964b: Rocket measurement of the nitric oxide dayglow. J. Geophys. Res. 69, 3301-3303.

_____, 1966: Nitric oxide in the upper atmosphere. Ann. Geophys. 22, 198-207.

Basco, N., Callear, A.B., and Norrish, R.G.W., 1961: Fluorescence and vibrational relaxation of nitric oxide studied by kinetic spectroscopy. Proc. Roy. Soc. A260, 459-474.

_____, 1962: Vibrational relaxation of nitric oxide and carbon monoxide studied by kinetic spectroscopy. Proc. Roy. Soc. A269, 180-187.

Bates, D., and Hays., P., 1967: Atmospheric nitrous oxide. Planet. Space Sci., 15, 189-197.

Bates D.R., and Nicolet, M., 1965: Atmospheric hydrogen. Planet. Space Sci., 13, 905-909.

Bates, D.R., and Witherspoon, A.E., 1952: The photo-chemistry of some minor constituents of the earth's atmosphere. Mon. Not. Roy. Astr. Soc. 112, 101-124.

Baulch, D.L., Drysdale, D.D., and Lloyd, A.C., 1968: Critical evaluation of rate data for homogeneous, gas-phase reactions of interest in high-temperature systems. High Temperature Reaction Rate Data, The University Leeds, England.

Beard, D. B., 1959: Interplanetary dust distribution. Astrophys. J., 129, p. 496.

Blandari, N., et al., 1968: Cosmic dust in the stratosphere. J. Geophys. Res., 73, (5), 1837.

Bolin, B., and Keeling, C., 1963: Large-scale atmospheric mixing as deduced from the seasonal and meridional variations of carbon dioxide. J. Geophys. Res., 68, 3899-3920.

Bortner, M., and Kummler, R., 1968: The chemical kinetics and the composition of the earth's atmosphere. GE-9500-ECS-SR-1.

Brown, F., Goldsmith, P., Green, H., Holt, A., and Parham, A., 1961: Measurements of the water vapor, tritium and carbon-14 content of the middle stratosphere over southern England, Tellus, 13, 407-416.

Burch, D. E., Gryvnak, D. A., and Williams, D., 1962: Total absorptance of carbon dioxide in the infrared. Appl. Opt. 6, 759-765.

Burch, D. E., and Williams, D., 1962: Total Absorptance of carbon monoxide and methane in the infrared. Appl. Opt. 1, 587-594.

Burt, J. A., and Schiff, H. I., 1969: The reaction of N atoms with $O_2(^1\Delta_g)$ molecules. Paper presented at the DASA Symposium on Physics and Chemistry of the Upper Atmosphere, S. R. I., Menlo Park, Calif., 24-25 June.

Cadle, R. D., 1966: Particles in the Atmosphere and Space. Reinhold Pub. Corp.

Cadle, R. D., and Powers, J. W., 1966: Some aspects of atmospheric chemical reactions of atomic oxygen. Tellus 18, 176-186.

Callendar, G., 1958: On the amount of carbon dioxide in the atmosphere. Tellus 10, 243-248.

Clough, S. A., and Kneizys, F. X., 1965: Ozone absorption in the 9.0-micron region. AFCRL Phys. Sci. Papers No. 170, AFCRL 65-862.

COSPAR, 1968: Space Research Vol. VIII, Part 6, various authors, North-Holland Publishing Co.

Dalgarno, A., 1963: Vibrationally excited molecules in atmospheric reactions. Planet. Space Sci. 10, 19-28.

DelGreco, F. P., and Kennealy, J. P., 1968: The reactions of N atoms with O_2 $(a^1\Delta)$ and $O_2(b^1\Sigma)$, Paper presented at the DASA Symposium on Physics and Chemistry of the Upper Atmosphere. Waltham, Mass.

Griggs, M., 1969: Measured and calculated earth-atmosphere radiance in the 8-14μ window as a function of altitude. Appl. Opt. 8, 171-177.

Gringorten, I., Salmela, H., Solomon, I., and Sharp, J., 1966: Atmospheric humidity atlas - Northern Hemisphere. Air Force Surveys in Geophysics No. 186, 142 pp.

Hanel, R.A., Bandeen, W.R., and Conrath, B.J., 1963: The infrared horizon of the planet earth. J. Atmos. Sci. 20, 73-86.

Hemenway, C.L. et al., p. 84; soberman, R.K. et al., p. 89, Hemenway, C.L. et al.

Hering, W., and Borden, T., 1965: Mean distributions of ozone density over North America 1963-1964. Office of Aerospace Research, Environmental Research Papers No. 162, 19 pp.

————, 1969: Personal communication.

Herzberg, G., 1945: Molecular Spectra and Molecular Structure II. Infrared and Raman Spectra of Polyatomic Molecules. D. van Nostrand Co., Inc. New York.

Herzfeld, K.F., and Litovitz, T.A., 1959: Absorption and Dispersion of Ultrasonic Waves. Academic Press, New York.

Hesstvedt, E., 1965: On the spatial distribution of some hydrogen components in the mesosphere and lower thermosphere. Tellus 17, 341-349.

Hodge, P.W., and Wright, F.W., 1968: Studies of particles for extra-terrestrial origin. J. Geophys. Res. 73, (24), p. 7589.

Houghton, J., 1963: Absorption in the stratosphere by some water vapor lines in the ν_2 band. Quart. J. Roy. Met. Soc., 86, 332-338.

————, 1969: Absorption and emission by carbon dioxide in the mesosphere. Quart. J. Roy. Met. Soc., 95, 1-20.

Hunt, B.G., 1965: A non-equilibrium investigation into the diurnal photo-chemical atomic oxygen and ozone variations in the mesosphere. J. Atmos. Terr. Phys. 27, 133-144.

————, 1966: Photochemistry of ozone in a moist atmosphere. J. Geophys. Res., 71, 1385-1398.

Hunten, D.M., and McElroy, M.B., 1968: Metastable O_2 $(^1\Delta)$ as a major source of ions in the D region. J. Geophys. Res. 73, 2421-2428.

139

Divari, N. B., 1959: Light scattered by the earth's dust cloud. Astrophys. J., 129.

Donohue, T. M., and Meier, R. R., 1967: Distribution of sodium in the daytime upper atmosphere as measured by a rocket experiment. J. Geophys. Res. 72, 2803-2829.

Drayson, S. R., and Young, C., 1966: Theoretical investigations of carbon dioxide radiative transfer. Univ. of Mich., Final Report ORA Project 07349.

Farlow, N. H., 1968: Electron microscope studies of particles on sampling surfaces recovered from space with sounding rockets. J. Geophys. Res. 73, 4363.

Fedynskii, A., Perov, S., and Chizhov, A., 1967: An attempt to measure directly the concentration of water vapor and atomic oxygen in the mesosphere. AGU Transl. 3(5), 315-317.

Feinberg, R. M., and Camac, M., 1967: Band intensity of NO fundamental. J. Quant. Spectrosc. Radiat. Transfer 7, 581-590.

Fiocco, G., and Grams, G., 1969: Optical radar observations of mesospheric aerosols in Norway during the summer of 1966. J. Geophys. Res. 74 2453.

Fogle, B., and Hauriwitz, B., 1966: Noctilucent clouds. Space Sci. Rev. 6 No. 3.

Friend, J. P., 1966: Properties of stratospheric aerosol. Tellus 18, No. 2, 465.

Geissler, J. E., and Dickinson, R. E., 1968: Vertical motions and nitric oxide in the upper mesosphere. J. Atmos. Terr. Phys. 30, 1505-1521.

Georgii, H., and Jost, D., 1969: Concentration of CO_2 in the upper troposphere and lower stratosphere. Nature 2?1, 1040.

Ghosh, S. N., 1968: Distributions and lifetimes of N and NO between 100 and 280 kilometers. J. Geophys. Res. 73, 309-318.

Goldsmith, P., 1964: Measurements of humidity up to 30 km using a new hygrometer. Proc. Ozone Symp. Albuquerque (H. Dütsch, ed.), WMO Geneva.

Goody, R. M., 1964: Atmospheric Radiation, I, Theoretical Basis. Oxford University.

Irvine, W. H., and Pollack, J. B., 1968: Infrared optical properties of water and ice spheres. Icarus 8, p. 324.

140

Ivanov, V. V., and Sacherbakov, V. T., 1965: Tables of functions encountered in the theory of resonance radiation transfer. Astrophys. 1, 10-12.

Johnson, F.S., 1965: Solar radiation, Chapter 4, in F.S. Johnson, ed. Satellite Environment Handbook, Stanford University Press, Stanford.

Junge, C.E., et al., 1961: Stratospheric aerosols. J. Met. 18, p. 81.

Kaiser, C.B., 1968: The thermal emission of interplanetary dust cloud models. NCAR Cooperative Thesis No. 10, Univ. of Colorado and High Altitude Observatory, NCAR.

Kantor, A., 1966: Speculative mean monthly temperatures in the Arctic (75°N) stratosphere, 25 to 55 kilometers. J. Geophys. Res. 71, 2445-2450.

Keeling, C., 1960: The concentration and isotopic abundance of carbon dioxide in the atmosphere. Tellus, 12, 200-203.

Keneshea, T.J., 1967: A technique for solving the reaction rate equations in the atmosphere. Environmental Research Papers No. 263, AFCRL-67-0221.

Kuhn, W.R., and London, J., 1969: Infrared radiative cooling in the middle atmosphere. J. Atmos. Sci., 26, 189-204.

Leovy, C., 1969: Energetics of the middle atmosphere. Advances in Geophysics, 13, 191-221.

Loysen, P. 1964: Particle size distribution of stratospheric aerosols at 110,000 feet. AEC Symposium on Radioactive Fallout from Nuclear Weapons Tests.

Ludwig, C.B., Ferriso, C.C., and Abeyta, C.N., 1965: Spectral emissivities and integrated intensities of the 6.3μ fundamental band of H_2O. J. Quant. Spectrosc. Radiat. Transfer, 5, 281-290.

MacQueen, R., 1968: Infrared observations of the outer solar corona. Astrophys. J., 154, p. 1059.

Maeda, K., 1968: The auroral O_2-dissociation and the infrared OH-emission. Ann. Geophys., 24, 173-184.

Markov, M.N., 1969: Molecular radiation of the upper atmosphere in the 3-8 μm spectral region. Appl. Opt. 8, 887-891.

Mastenbrook, H., 1968: Water vapor in the stratosphere and high troposphere. J. Atmos. Sci., 25, 294-311.

Mitchell, A.C.G., and Zemansky, M.W., 1961: Resonance Radiation and Excited Atoms. Cambridge Univ. Press, Cambridge.

Mikirob, 1966: Aeronomy and Geophysics.

Murcray, D.G., Kyle, T.G., Murcray, F.H., and Williams, W.G., 1958: Nitric Acid and Nitric Oxide in the Lower Stratosphere. Nature 218, 78.

Newell, R., 1963: Transfer through the tropopause and within the stratosphere. Quart. J. Roy, Met. Soc. 89, 167-204.

Newkirk, G., and Eddy, J.A., 1964: Light scattering by particles in the upper atmosphere. J. Atmos. Sci. 21, p. 35.

Nicholls, R.W., 1964: Franck-Condon factors to high vibrational quantum number IV: NO band systems. J. Res. NBS 68A, 535-540.

Nicolet, M., 1965a: Nitrogen oxides in the chemosphere. J. Geophys. Res. 70, 679-689.

_____, 1965b: Ionospheric processes and nitric oxide. J. Geophys. Res. 70, 691-701.

Oppenheim, U.P., Yair Aviv, and Aharon Goldman, 1967: Integrated intensity of NO fundamental. Appl. Opt. 8, 1305-1307.

Pearce, J.B., 1969: Rocket measurement of nitric oxide between 60 and 96 kilometers. J. Geophys. Res. 74, 853-861.

Penner, S.S., 1959: Quantitative Molecular Spectroscopy and Gas Emissivities. Addison-Wesley Pub. Co., Reading, Mass.

Peterson, A.W., 1963: Thermal radiation from interplanetary dust. Astrophys. J., 138, p. 1218.

_____, 1967: Experimental detection of thermal radiation from interplanetary dust. Astrophys. J., 1a8, p. 137.

Peterson, R., Scheutz, J., Shenk, W., and Tang, W., 1967: Derivation of a meteorological body of data. NASA Contractor Report NASA CR-723, 171 pp.

Pivovonsky, M., and Nagel, M.R., 1961: Tables of Blackbody Radiation Functions. The MacMillan Co., New York.

Rosen, J.M., 1964: The vertical distribution of dust to 30 kilometers. J. Geophys. Res., 69, (21), p 4673.

Rossler, F., and deBary, E., 1966: Size distributions of atmospheric aerosols derived from scattered radiation measurements aloft. J. Geophys. Res., 71(4), p. 1011.

Roxen, J., 1968: Simultaneous dust and ozone soundings over North and Central America. J. Geophys. Res. 73(2), p. 479.

Ryan, K.R., 1968: The production of nitric oxide around 100 km. J. Atmos. Terr. Phys. 30, 1331-1340.

Saxena, P.P., 1968: Atomic nitrogen and nitric oxide in the upper atmosphere during daytime. Ann. Geophys. 24, 1023-1030.

_____, 1969: Atomic nitrogen and nitric oxide in the upper atmosphere during night time. Ann. Geophys. 25, 147-152.

Schurin, B. and Ellis, R.E., 1966: First- and second-overtone intensity measurements for CO and NO, J. Chem. Phys. 45, 2528-2532.

Sissenwine, N, Grantham, D., Salmela, H., 1968: Humidity up to the mesopause. Air Force Surveys in Geophysics No. 206, AFCRL-68-0550, 49 pp.

Taylor, R.L., and Bitterman, S., 1969: Survey of vibrational relaxation data for processes important in the CO_2-N_2 laser system. Rev. Mod. Phys. 41, 26-47.

Theon, J., 1968: Short term temperature variations in the atmosphere below 120 km. Proc. Third Nat. Conf. on Aerospace Meteorology, Amer. Met. Soc., 449-456.

Theon, J., Nordberg, W., Katchen, L., and Horvath, J., 1967: Some observations of the thermal behavior of the mesophase. J. Atmos. Sci., 24, 428-438.

U.S. Standard Atmosphere, 1962: 278 pp.

U.S. Standard Atmosphere Supplements, 1966: 289 pp.

Valley, S., 1965: Handbook of Geophysics and Space Environments. McGraw-Hill, New York.

Varanasi, P., and Penner, S.S., 1967: Absolute infrared intensity measurements on the fundamental of NO. J. Quant. Spectrosc. Radiat. Transfer, 7, 279-282.

Walker, J.C.G., 1968: Electron and nitrogen vibrational temperatures in the E-region of the ionosphere. Planet. Space Sci. 16, 321-327.

Walker, R.G., 1969: Private communications, Air Force Cambridge Research Laboratory, Hanscom Field, Bedford, Mass.

Wallace, L., 1962a: A collection of the band-head wavelengths of N_2 and N_2^+. Astrophys. J. Supple. 6, 445-480.

_____, 1962b: Band-head wavelengths of C_2 CH, CN, CO, NH, NO, O_2, OH, and their ions. Astrophys. J. Supple. 7, 1965-290.

Wark, D.Q., Yamamoto, G., and Lienesch, J.H., 1962: Methods of estimating infrared flux and surface temperatures from meteorological satellites. J. Atmos. Sci. 19, 369-384.

Williamson, E., and Houghton, H., 1965: Radiometric measurements of emission from stratospheric water vapor. Quart. J. Roy. Met. Soc., 91, 330-338.

Wray, K.L., 1969: Oscillator strengths of transitions between Rydberg states of nitric oxide in the near IR. J. Quant. Spectrosc. Radiat. Transfer, 9, 255-276.

Wright, F.W., and Hodge, P.W., 1962: Space density and dust in the stratosphere. Nature 195, p. 269.

Yardley, J.T., 1968: Vibration-to-vibration energy transfer in gas mixtures containing nitrous oxide. J. Chem. Phys. 49, 2816-2821.

Yardley, J.T., and Moore, C.B., 1968: Vibration-vibration and vibration-translation energy transfer in methane-oxygen mixtures. J. Chem. Phys., 48, 14-17.

OTHER SOURCES (BIBLIOGRAPHY) RELATED
TO DUST EMISSION

Alvarez, J. M., 1967: Satellite measurements of particles causing zodiacal light. Symposium on the Zodiacal light and the interplanetary medium, Hawaii (NASA SP-150).

Belton, M. J. S., 1966: Dynamics of interplanetary dust. Science 151, p. 35.

Berg, O. E., and Secretan, L., 1967: Evidence of dust concentration in the mesosphere. Symposium on the Zodiacal light and the interplanetary medium, Hawaii (NASA SP-150).

Colin, L., and Dufours, S. W., 1968: Charged particle temperatures and concentrations in the earth's exosphere. J. Geophys. Res. 73, (9), p. 2967.

Conel, J. E., 1969: Infrared emissivities of silicates: Experimental results and a cloudy atmosphere model of spectral emissions from condensed particulate mediums. J. Geophys. Res. 74(6).

Davies, C., ed. 1966: Aerosol Science, Academic Press.

Elterman, L., and Campbell, A. B., 1964: Atmospheric aerosol observations with searchlight probing. J. Atmos. Sci., 21(4), p. 457.

Fiocco, G., and Grams, G., 1966: Observations of the upper atmosphere by optical radar in Alaska and Sweden during the summer of 1964. Tellus 18(1), 34.

Gasiev, Y. I., et al., 1966: The size distribution of radioactive particles from nuclear weapon tests and their transport in the atmosphere. Tellus 18(1), p. 474.

Griggs, M., 1968: Emissivities of natural surfaces in the 8 to 14 micron spectral region. J. Geophys. Res. 73, p. 7545.

Handbook of Geophysics and Space Environments, 1965: AFCRL.

Handbook of Military Infrared Technology, 1965: ed. W. L. Wolfe, Office of Naval Research Department of the Navy, Washington, D. C.

Harwit, M., 1964: I. R. Appearance of Different Zodiacal Cloud Models. Internat. Astro-Physics Symposium (12) Mem. Royal Soc. Sci., Liege Vol. 9, p. 605.

Harwit, M., et al., 1966: Results of the first infrared astronomical rocket flight. Astron. J. 71(10), 1026.

MacQueen, R. M., 1968: A note of the stratospheric infrared sky radiance. J. Atmos. Sci., 25(2).

Martell, E. A., 1966: The size distribution and interaction of radioactive and natural aerosols in the stratosphere. Tellus 18(2), p. 486.

Peale, S. J., 1968: Evidence against a geocentric contribution to the zodiacal light. J. Geophys. Res. 73(9), p. 3025.

Penndorf, R. B., 1963: Research on Aerosol Scattering in the Infrared. Avco Corp. Tech. Rep. RAD-TR-26, AFCRL-63-668.

Pilipowskyj, S., et al, 1968: Investigations of the stratospheric aerosol by infrared and lidar techniques. J. Geophys. Res. 73, p. 7553.

Powell, R. S., et al. 1967a: Optical scattering from non-spherical, randomly aligned, polydisperse particles. Planet. Space Sci., 15, p. 1641.

_____, 1967b: Analysis of all available zodiacal-light observations. Symp. on the Zodiacal Light and the Interplanetary Medium, Hawaii (NASA SP-150).

Shedlovsky, J. P., and Paisley, S., 1966: On the meteoritic component of stratospheric aerosols. Tellus 18(2), p. 499.

Shifrin, K. S., and Perelman, A. Y., 1966: Determination of particle spectrum of atmosphere aerosol by light scattering. Tellus, 18(2), p. 566.

Singer, S. F., and Bandermann, L. W., 1967: Nature and origin of zodiacal dust. Symp. on the Zodiacal Light and Interplanetary Medium, Hawaii, (NASA SP-150).

Telegadas, K., and List, F. J., 1969: Are particulate radioactive tracers indicative of stratospheric motions. J. Geophys. Res. 74(6), p. 1339.

Tousey, R., and Koomen, J. J., 1967: Particles of unknown origin photographed at rocket altitudes. Symp. on the Zodiacal Light and the Interplanetary Medium, Hawaii, (NASA SP-150).

Van De Hulst, H. C., 1962: Light Scattering by Small Particles. John Wiley & Sons.

Witt, G., 1968: Optical characteristics of mesospheric aerosol distributions in relation to noctilucent clouds. Tellus 20(1).

146

APPENDIX A
TABULATED DATA FOR ADOPTED
ATMOSPHERIC PROFILES

As noted in Section II, this appendix contains tables of the adopted temperature, water vapor, ozone, and nitrous oxide profiles. Data are tabulated only at key heights which represent break points in the particular profile. Ozone values above 35 km and nitrous oxide values above 40 km may be obtained from analytic formulas given in the text. Each parameter profile has a number code associated with it. A summary of these number codes is contained in Appendix B.

147

Table A-1. Data for Adopted Temperature Profiles
(Heights in km, Temperatures in °K)

Code: 1 Standard Atmosphere		2 15° Annual		3 45° Jan.		4 45° July	
Ht.	T	Ht.	T	Ht.	T	Ht.	T
0	288	0	300	0	272	0	294
11.0	217	2.3	286	3.0	272	2.0	285
20.1	217	2.5	287	10.0	220	6.0	261
32.2	229	16.6	193	19.1	215	13.0	216
47.4	271	22.1	215	27.1	215	17.1	216
52.4	271	47.5	270	32.2	219	27.1	228
61.6	253	51.5	270	47.4	266	32.2	238
80.0	181	59.7	254	52.4	266	47.4	276
90.0	181	82.2	177	64.7	242	52.4	276
		90.0	177	85.1	200	62.6	165
				90.0	200	82.0	165
						90.0	165

148

Table A-1. Data for Adopted Temperature Profiles (Continued)
(Heights in km, Temperatures in °K)

Code: 5		6		7		8	
75°		75°		75°		75°	
Jan. (warm)		Jan. (cold)		Jan. (mean)		July	
Ht.	T	Ht.	T	Ht.	T	Ht.	T
0	249	0	249	0	249	0	278
1.5	254	1.5	254	1.5	254	2.5	272
8.5	215	8.5	215	8.5	215	9.5	226
11.0	222	17.6	202	11.5	214	13.5	230
17.1	222	25.1	197	19.0	208	23.6	230
25.1	226	30.2	197	30.1	208	30.2	238
30.2	234	52.5	243	37.5	212	40.0	260
52.5	263	90.0	210	37.5	228	50.0	270
90.0	210			42.5	242	60.0	265
				47.5	250	70.0	220
				52.5	253	80.0	170
				90.0	210	85.0	150
						90.0	145

Table A-1. Data for Adopted Temperature Profiles (Continued)
(Heights in km, Temperatures in °K)

Code:	9		10	
	Cold Extreme		Hot Extreme	
	Ht.	T	Ht.	T
	0	238	0	338
	11.0	166	11.0	266
	20.1	178	32.2	278
	32.2	178	32.2	278
	47.4	220	47.4	320
	52.4	220	52.4	320
	61.6	203	21.6	303
	80.0	130	80.0	230
	90.0	130	90.0	230

150

Table A-2. Data for Adopted Water Vapor Mixing Ratio Profiles
(Heights in km; Mixing Ratios in ppm)

A. Tropospheric Profiles

Code:	1		2		3		4	
	Standard Atmosphere		15°, Annual (mean)		45°, Jan. (mean)		45°, July (mean)	
	Ht.	H_2O	Ht.	H_2O	Ht.	H_2O	Ht.	H_2O
	0	6.24×10^3	0	1.63×10^4	0	2.9×10^3	0	1.14×10^4
	6.0	4.95×10^2	2.25	9.0×10^3	3.0	1.2×10^3	2.0	6.0×10^3
	10.0	6.0×10	2.5	4.6×10^3	10.0	2.0×10	10.0	1.1×10^2
			6.0	1.2×10^3				
			10.0	8.7×10				

Code:	5		6		7		8	
	75°, Jan. (mean)		75°, July (mean)		15°, Annual (low)		15°, Annual (high)	
	Ht.	H_2O	Ht.	H_2O	Ht.	H_2O	Ht.	H_2O
	0	3.3×10^2	0	4.5×10^3	0	8.2×10^3	0	2.4×10^4
	1.5	5.0×10^2	2	3.1×10^3	6	6.0×10^2	6	4.5×10^3
	10	6.1	6	4.5×10^2	10	3.5×10	10	5.2×10^2
			10	3.0×10				

151

Table A-2. Data for Adopted Water Vapor Mixing Ratio Profiles (Continued)
(Heights in km; Mixing Ratios in ppm)

Code: 13		14		15		16	
45°, July (low)		45°, July (high)		45°, Jan. (low)		45°, Jan. (high)	
Ht.	H_2O	Ht.	H_2O	Ht.	H_2O	Ht.	H_2O
0	8.0×10^3	0	1.4×10^4	0	1.5×10^3	0	6.0×10^3
1.5	4.5×10^3	1.5	1.06×10^3	2.9	5.0×10^2	2.9	3.8×10^3
10.0	5.4×10	10.0	5.6×10^2	10.0	1.1×10	10.0	1.05×10^2

17		18		19		20	
75°, July (low)		75°, July (high)		75°, Jan. (low)		75°, Jan. (high)	
Ht.	H_2O	Ht.	H_2O	Ht.	H_2O	Ht.	H_2O
0	2.9×10^3	0	8.0×10^3	0	1.4×10^2	0	4.0×10^3
1.4	2.1×10^3	1.4	6.5×10^3	1.5	2.3×10^2	10.0	2.4×10
6.0	2.6×10^2	6.0	1.2×10^3	10.0	3.5		
10.0	1.7×10	10.0	1.9×10^2				

Table A-2. Data for Adopted Water Vapor Mixing Ratio Profiles (Continued)
(Heights in km; Mixing Ratios in ppm)

B. Stratospheric Profiles

| Code: | 1 | | 2 | | 3 | |
| | Mean | | Low (dry) | | High (wet) | |
Ht.	H$_2$O	Ht.	H$_2$O	Ht.	H$_2$O
15	4.3	15	1.0	15	5.0 x 10
18	4.1	30	1.0	30	4.0 x 10
26	1.86 x 10	80	1.0 x 10^{-1}	80	5.0
35	1.54 x 10	90	1.0 x 10^{-1}	90	5.0
50	7.6				
80	6.33 x 10^{-1}				
90	6.33 x 10^{-1}				

Table A-3. Data for Adopted Ozone Profiles
(Heights in km; Ozone Values in ppm by Weight)

Code:	1		2		3		4	
	Standard Atmosphere		15°, Annual (mean)		45°, Winter (mean)		45°, Summer (mean)	
	Ht.	O_3	Ht.	O_3	Ht.	O_3	Ht.	O_3
	0	4.0×10^{-2}	0	3.2×10^{-2}	0	4.3×10^{-2}	0	5.1×10^{-2}
	6	7.0×10^{-2}	10	5.7×10^{-2}	6	7.4×10^{-2}	6	7.8×10^{-2}
	8	1.0×10^{-1}	14	1.0×10^{-1}	8	1.13×10^{-1}	8	1.0×10^{-1}
	16	1.3	18	6.0×10^{-1}	14	1.0	14	6.0×10^{-1}
	26	9.5	20	1.9	18	3.1	18	2.1
	30	1.14×10	28	1.29×10	23	8.4	28	1.04×10
	35	1.3×10	30	1.38×10	30	1.06×10	30	1.08×10
			35	1.45×10	35	1.15×10	35	1.1×10

154

Table A-3. Data for Adopted Ozone Profiles (Continued)
(Heights in km; Ozone Values in ppm by Weight)

Code:	5		6		7		8	
	75°, Winter (mean)		75°, Summer (mean)		15°, Annual (low)		15°, Annual (high)	
	Ht.	O_3	Ht.	O_3	Ht.	O_3	Ht.	O_3
	0	3.8×10^{-2}	0	3.0×10^{-2}	0	1.2×10^{-2}	0	5.2×10^{-2}
	6	7.5×10^{-2}	6	7.0×10^{-2}	10	2.0×10^{-2}	10	9.4×10^{-2}
	8	2.0×10^{-1}	8	1.44×10^{-1}	14	1.6×10^{-2}	14	1.84×10^{-1}
	12	1.4	12	7.5×10^{-1}	18	2.8×10^{-1}	18	9.22×10^{-1}
	20	6.8	22	6.0	20	1.23	20	2.57
	22	7.6	30	7.8	28	1.18×10	28	1.4×10
	28	8.4	35	8.0	30	1.24×10	30	1.52×10
	35	7.3			35	1.31×10	35	1.59×10

155

Table A-3. Data for Adopted Ozone Profiles (Continued)
(Heights in km; Ozone Values in ppm by Weight)

| Code: 13 | | 14 | | 15 | | 16 | |
| 45°, Summer (low) | | 45°, Summer (high) | | 45°, Winter (low) | | 45°, Winter (high) | |
Ht.	O_3	Ht.	O_3	Ht.	O_3	Ht.	O_3
0	1.7×10^{-2}	0	8.5×10^{-2}	0	2.3×10^{-2}	0	6.3×10^{-2}
6	3.6×10^{-2}	6	1.2×10^{-1}	6	2.8×10^{-2}	6	1.2×10^{-1}
8	1.0×10^{-2}	8	1.9×10^{-1}	8	1.0×10^{-2}	8	2.49×10^{-1}
14	2.0×10^{-2}	14	1.2	14	4.0×10^{-2}	14	1.96
18	1.3	18	2.9	18	1.5	18	4.7
28	9.2	28	1.16×10	23	6.9	23	9.9
30	9.5	30	1.21×10	30	8.14	30	1.31×10
35	9.7	35	1.23×10	35	8.84	35	1.42×10

156

Table A-3. Data for Adopted Ozone Profiles (Continued)
(Heights in km; Ozone Values in ppm by Weight)

Code:	17		18		19		20	
	75°, Summer (low)		75°, Summer (high)		75°, Winter (low)		75°, Winter (high)	
Ht.	O_3	Ht.	O_3	Ht.	O_3	Ht.	O_3	
0	1.3×10^{-2}	0	4.7×10^{-2}	0	1.8×10^{-2}	0	5.8×10^{-2}	
6	1.3×10^{-2}	6	1.3×10^{-1}	6	1.7×10^{-2}	6	1.3×10^{-1}	
8	1.0×10^{-2}	8	2.9×10^{-1}	8	3.0×10^{-2}	8	3.7×10^{-1}	
12	8.0×10^{-2}	12	1.4	12	7.0×10^{-1}	12	2.1	
22	4.9	22	7.1	20	5.6	20	8.0	
30	5.1	30	1.05×10	22	6.4	22	8.8	
35	5.2	35	1.06×10	28	6.3	28	1.05×10	
				35	5.3	35	9.3	

157

Table A-4. Data for Adopted Nitrous Oxide Profiles
(Heights in km; N_2O Values are Fractional
Volume Abundances)

Code:	1	2	3	4
K_z Strat. $(cm^2 sec^{-1})$	10^4	10^2	10^3	10^5
Ht.	N_2O	N_2O	N_2O	N_2O
0	2.5×10^{-7}	2.5×10^{-7}	2.5×10^{-7}	2.5×10^{-7}
10	2.5×10^{-7}	2.5×10^{-7}	2.5×10^{-7}	2.5×10^{-7}
15	2.4×10^{-7}	7.5×10^{-8}	2.0×10^{-7}	2.5×10^{-7}
20	2.1×10^{-7}	2.3×10^{-8}	1.5×10^{-7}	2.4×10^{-7}
25	1.75×10^{-7}	6.8×10^{-9}	4.5×10^{-8}	2.25×10^{-7}
30	1.25×10^{-7}	2.1×10^{-9}	1.4×10^{-8}	2.0×10^{-7}
35	3.8×10^{-8}	6.1×10^{-10}	4.1×10^{-9}	1.6×10^{-7}
40	1.1×10^{-8}	1.9×10^{-10}	1.2×10^{-9}	1.15×10^{-7}

APPENDIX B
CODES FOR ATMOSPHERIC PROFILES

This appendix contains a summary of the identification of codes associated
with the tabulated data for adopted atmospheric profiles in Appendix A.

Table B-1. Codes

	T	H$_2$O (Lower Atm)	O$_3$	CO$_2$	N$_2$O	H$_2$O (Upper Atm)
Standard Atmosphere	1	1	1	1	1	1
Annual Average 15°	2	2	2			
January 45°	3	3	3			
July 45°	4	4	4			
Winter (mean) 75°	5	5	5			
July 75°	6	6	6			

Table B-1. (Cont.)

H$_2$O (Lower Atm.) and O$_3$			
			Code
Annual	15°	Low	11
Annual	15°	High	12
Summer	45°	Low	13
Summer	45°	High	14
Winter	45°	Low	15
Winter	45°	High	16
Summer	75°	Low	17
Summer	75°	High	18
Winter	75°	Low	19
Winter	75°	High	20

NOTE: (1) H$_2$O Low and High based upon 5% and 95%
              percentile values. O$_3$ Low and High based
              upon ±2σ values, or 2.5%, 97.5% percentile.

Table B-1. (Cont.)

T		
		Code
Winter (cold strat.)	75°	7
Winter (warm strat.)	75°	8
Cold extreme		9
Hot extreme		10

H_2O (Upper Atmos.)	
	Code
Mean	1
Dry	2
Wet	3

N_2O	
$K_z(cm^2 sec^{-1})$	Code
10^4	1
10^2	2
10^3	3
10^5	4

NOTE: K_z refers to vertical exchange coefficient
in stratosphere.

APPENDIX C
SELECTION OF MODEL ATMOSPHERES FOR RADIANCE CALCULATIONS

This appendix contains a selection of 47 models for radiance calculations in the lower atmosphere. These model atmospheres are representative of the spatial and temporal variations, means and extremes of atmospheric conditions that are likely to be encountered about the earth.

The identification of these codes is presented in Appendix B, and these codes are used as input values to the computer program which compiles the model atmospheres.

It is noted that any combination of codes presented in Appendix B can be used to develop a wide variety of model atmospheres. The 47 models selected here are only a small but representative fraction of the total number of possibilities.

Table C-1. Selection of Models for Radiance Calculations in the Lower Atmosphere

Number of Profile	T	H_2O (trop)	H_2O (strat)	O_3
CLIMATOLOGICAL MEANS				
1	1	1	1	1
2	2	2	1	1
3	3	3	1	3
4	4	4	1	4
5	5	5	1	5
6	6	6	1	6
7	7	5	1	5
8	8	5	1	5
EXTREME TEMPERATURE PROFILES				
9	9	1	1	1
10	10	1	1	1
H_2O (trop.) AND O_3 VARIABILITY				
11	2	11	1	11
12	2	12	1	12
13	4	13	1	13
14	4	14	1	14
15	3	15	1	15
16	3	16	1	16
17	6	17	1	17

Table C-1. (Cont.)

Number of Profile	T	H₂O (trop.)	H₂O (strat)	O₃
H_2O (trop.) AND O_3 VARIABILITY (Cont.)				
18	6	18	1	18
19	5	19	1	19
20	5	20	1	20
EXTREME CONDITIONS, ALL PARAMETERS				
21	10	12	3	20
22	10	12	3	12
23	9	19	2	17
CLIMATOLOGICAL MEANS WITH MOIST STRATOSPHERE				
24	1	1	3	1
25	2	2	3	2
26	3	3	3	3
27	4	4	3	4
28	5	5	3	5
29	6	6	3	6
30	7	5	3	5
31	8	5	3	5

Table C-1. (Cont.)

Number of Profile	T	H₂O (trop.)	H₂O (strat)	O₃
CLIMATOLOGICAL MEAN WITH DRY STRATOSPHERE				
32	1	1	2	1
33	2	2	2	2
34	3	3	2	3
35	4	4	2	4
36	5	5	2	5
37	6	6	2	6
38	7	5	2	5
39	8	5	2	5
STANDARD ATMOSPHERE TEMPERATURE PROFILE EXTREMES OF H₂O AND O₃				
40	1	12	3	12
41	1	12	3	20
42	1	19	2	17
43	1	1	1	12
44	1	1	1	20
45	1	1	1	17
46	1	19	2	1
47	1	12	3	1

The column headers in the table above read: Number of Profile, T, H_2O (trop.), H_2O (strat), O_3.

CLIMATOLOGICAL MEAN WITH DRY STRATOSPHERE, and STANDARD ATMOSPHERE TEMPERATURE PROFILE EXTREMES OF H_2O AND O_3.

APPENDIX D
ATMOSPHERIC MODEL FOR NITRIC ACID

A. JUSTIFICATION FOR THE MODEL

Recent measurements made during balloon flights flown by the University of Denver have shown the existence of nitric acid in the earth's atmosphere (Murcray, et al, 1968). Identification of nitric acid was made using a balloon-borne spectrograph at an altitude of 30 km to observe the solar spectrum at zenith angles near 90°. Identification was made by the absorption anomaly at 7.5 microns.

Nitric acid also has a strong absorption band near 11.2 microns, which is important to the present atmospheric studies. The present investigation has been to assess the radiation from the limb from 5 to 25 microns with emphasis on the window regions where the horizon background is low for enhancement of detection of cold objects in space. The previously used atmospheric models have consistently shown a transparent atmospheric window in the spectral region from 10 to 12 microns. This discrepancy between the previously existing models and recent measurements has made it necessary for the inclusion of a preliminary model for nitric acid absorption; even a crude model to give first-order effects is sufficient for the design of a space experiment and should be more accurate than its omission from the limb calculations.

A subsequent balloon flight was made by the University of Denver with a spectral-radiometer system capable of measuring the absolute radiance of the earth and its atmosphere in the wavelength region from 5 to 20 microns at selected elevation angles. Nine spectra have been reported for the spectral interval from 10 to 13 microns for three different altitudes and for three different elevation angles near the horizon (Murcray 1969). An analysis of the nine spectra was made to give a first-order approximation for the limb radiance calculations.

167

B. DETERMINATION OF THE MODEL

Polyatomic molecules in the gaseous phase, such as atmospheric water vapor, ozone and methane exhibit vibration-rotation spectra at infrared frequencies. It has been shown that for pressures and temperatures encountered in the lower atmosphere, a good approximation to the absorption can be obtained from the statistical absorption model (Goody, 1952), given by:

$$t = \exp\left[\frac{-\beta x}{\sqrt{1 + 2x}}\right] \qquad (D1)$$

where

t = transmission

$$\beta = \frac{2\pi \Delta\nu L}{v} \qquad (D2)$$

$$x = \frac{S w}{2\pi \Delta\nu_L} \qquad (D3)$$

S = average strength of the absorption lines

v = average frequency spacing between lines

w = optical path of absorber reduced to standard conditions

$\Delta\nu_L$ = average width of absorption lines, measured as half-width at half peak intensity. The half-width has been shown to be directly proportional to pressure and inversely proportional to the square root of temperature. For the atmospheric paths involved in the Denver measurements, the temperature variation was small, therefore the temperature contribution to half-width can be neglected.

For long slant paths through the atmosphere, where the line width is very small compared to the line strength, then absorption by an increase in

168

optical path will predominently result from the wings of the rotational lines, and the statistical model can be approximated by the following equation:

$$t = \exp\left[-(1/2\ \beta^2\ x)^{1/2}\right] \tag{D4}$$

The optical slant path through the atmosphere can be approximated by a Curtis-Godson slant path integration (Curtis, 1952). For a uniformly distributed molecule, the optical path should be proportional to the density times pressure, integrated over the path, and transmission should be approximately given by:

$$t = \exp\left[-K\sqrt{\int \rho\ p\ d\ L}\right] \tag{D5}$$

where ρ is the atmospheric density

For the altitudes represented by the Denver measurements, the atmosphere is nearly in local thermodynamic equilibrium and the net radiation received at the detector is given by:

$$N_\lambda = \int B_\lambda\ d\ t \tag{D6}$$

where

N_λ is the net atmospheric radiance

B_λ is the Planck radiation function at the temperature of the atmosphere and wavelength measured

Atmospheric transmission was estimated at peak absorption wavelength of 11.2 microns for each of the nine University of Denver measurements by dividing measured radiance by the Planck function calculated for the average temperature in the line of sight.

Figure D1 shows a plot of the quantity

$$\frac{- \log_e t}{\sqrt{\int w \, p \, d L}}$$

vs the effective altitude of the observation.

The effective altitude was taken as 2.8 km above the minimum altitude of the ray path. If nitric acid were uniformly distributed over the altitudes for the measured data then the above parameter would be a constant, independent of altitude. However, Figure D1 indicates that the mixing ratio is increasing with altitude. The figure shows a nearly linear increase in the parameter which requires that mixing ratio be proportional to the square of the altitude. An iterative inversion technique was attempted to fit the following expression:

$$t = \exp \left[-\left\{ K \int \left(\frac{p}{P_o}\right) \left(\frac{T_o}{T}\right)^{3/2} Z^2 \, d L \right\}^{1/2} \right] \tag{D7}$$

where P_o and T_o are taken as normal temperature and pressure and Z is the altitude above the earth.

The result of this inversion gave a value of $K = 0.84 \times 10^{-12}$, which is interpreted as a product of the nitric acid absorption parameter times a mixing ratio parameter.

C. CONCLUSIONS AND LIMITATIONS OF THE MODEL

The radiance values calculated from the model were compared with the measured values at 11.2 microns. Figure D2 shows the comparison for each of the nine measurements, and shows fair agreement except for one value. This one extreme value was obtained for the lowest measurement with the instrument looking down into the atmosphere at the zenith angle of 93.5°. This measurement represents a minimum ray path altitude of

approximately 6.4 km. This extreme value leads to the conclusion that the nitric acid mixing ratio falls of much more rapidly than that given by the model for altitudes below 10 km.

If the atmospheric absorption and emission does sensibly behave like the model assumed above and if the line strength is reasonbly independent of pressure, then the relative density of nitric acid in the atmosphere will be given as:

$$\rho_{HNO_3} = K' \, Z^2 \, \rho_{Air} \tag{D8}$$

where

ρ_{HNO_3} = relative distribution of nitric acid

ρ_{Air} = density of the air

Z = altitude

K' = normalization constant chosen to give a relative distribution of one at the altitude of peak nitric acid density.

Figure D3 shows the relative distribution for the nitric acid model. The peak density occurs at an altitude of approximately 12 km.

Dr. Williams of the University of Kansas has considered the results of this inversion and has suggested the following explanation (Williams, 1969).

Nitric acid may be formed from ozone in the atmosphere. The peak of the ozone distribution has been observed at altitudes of approximately 20 to 30 kilometers. Being a heavy molecule, nitric acid could diffuse to lower altitudes until it came into contact with liquid water, whose propensity for adsorption of nitric acid is high. Water droplets are not likely to be encountered above the tropopause. The atmospheric tropopause at mid-latitudes is at about 10 to 12 kilometers.

171

The above explanation indicates that the model determined for nitric acid may be realistic and appears to be adequate for a first-order approximation for the design of an experiment. However, it must be realized that the model was synthesized from a minimum of experimental evidence and that the assumption of a different absorption model may give an entirely different distribution; also, the model has been extrapolated to high altitudes and rapidly loses validity above 30 to 35 km.
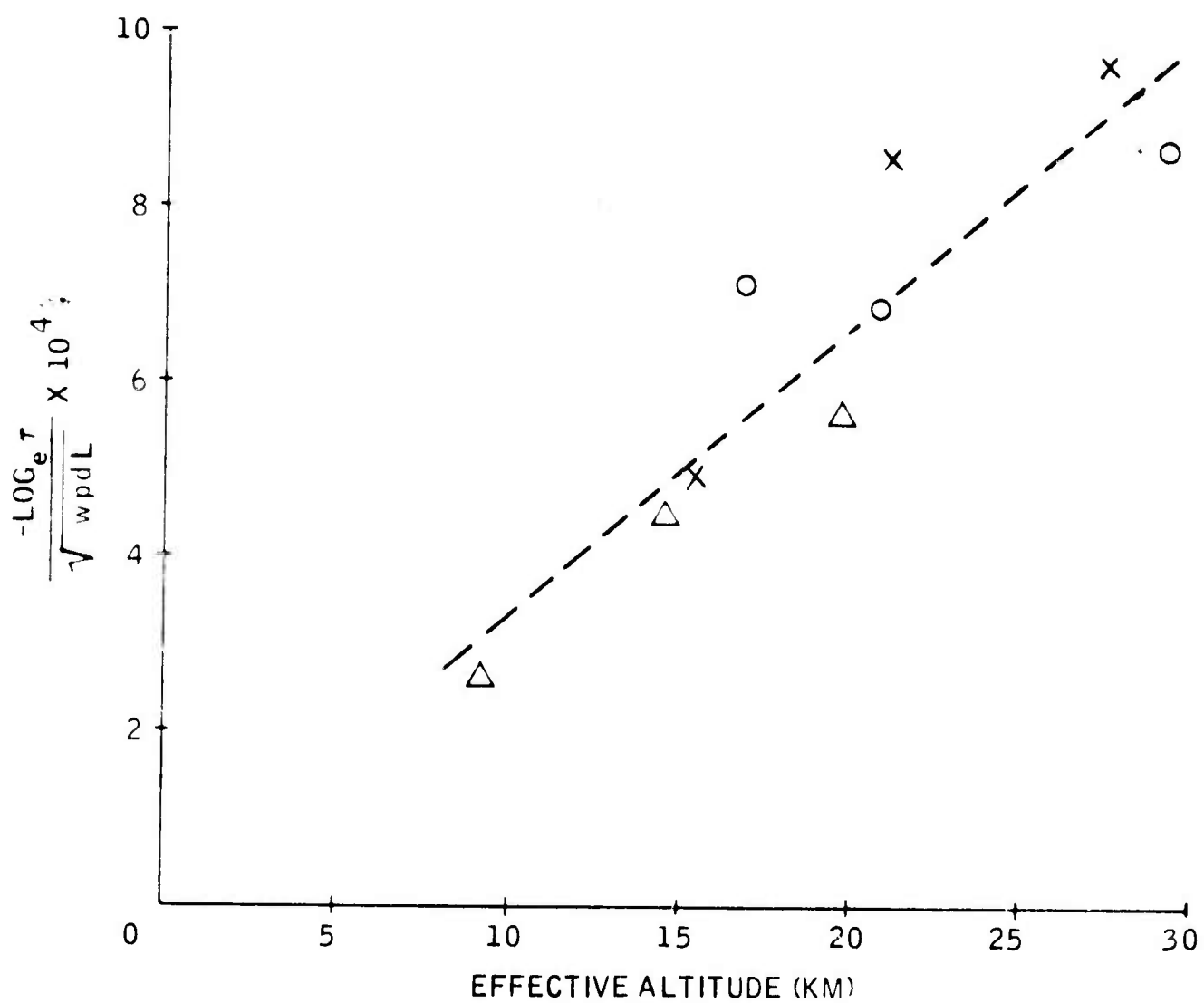
Figure D1. Test of Hypothesis of Uniform
Distribution of HNO_3

173
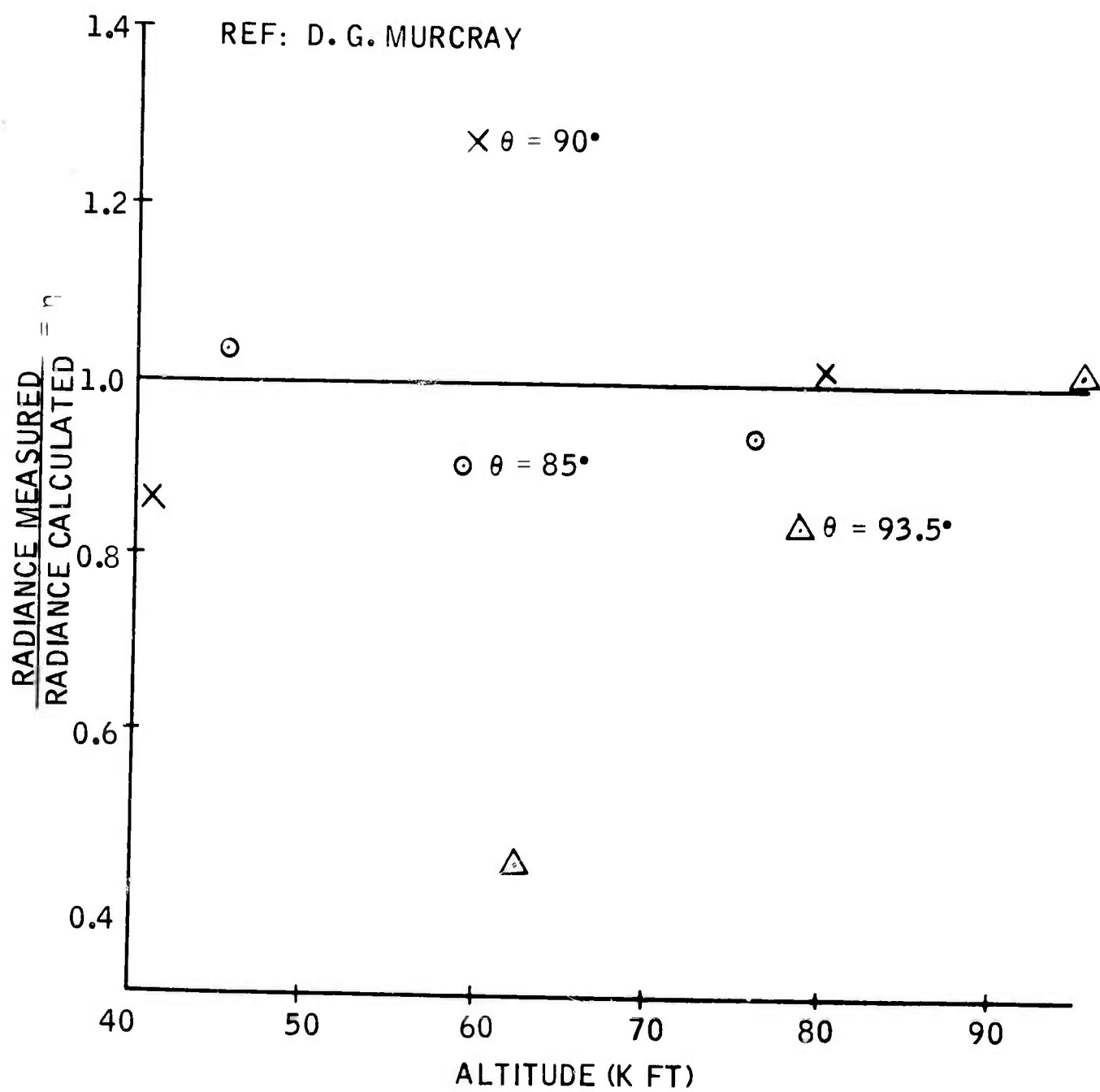
Figure D2. Comparison between Measurements
and Model At 11.2 Microns

174
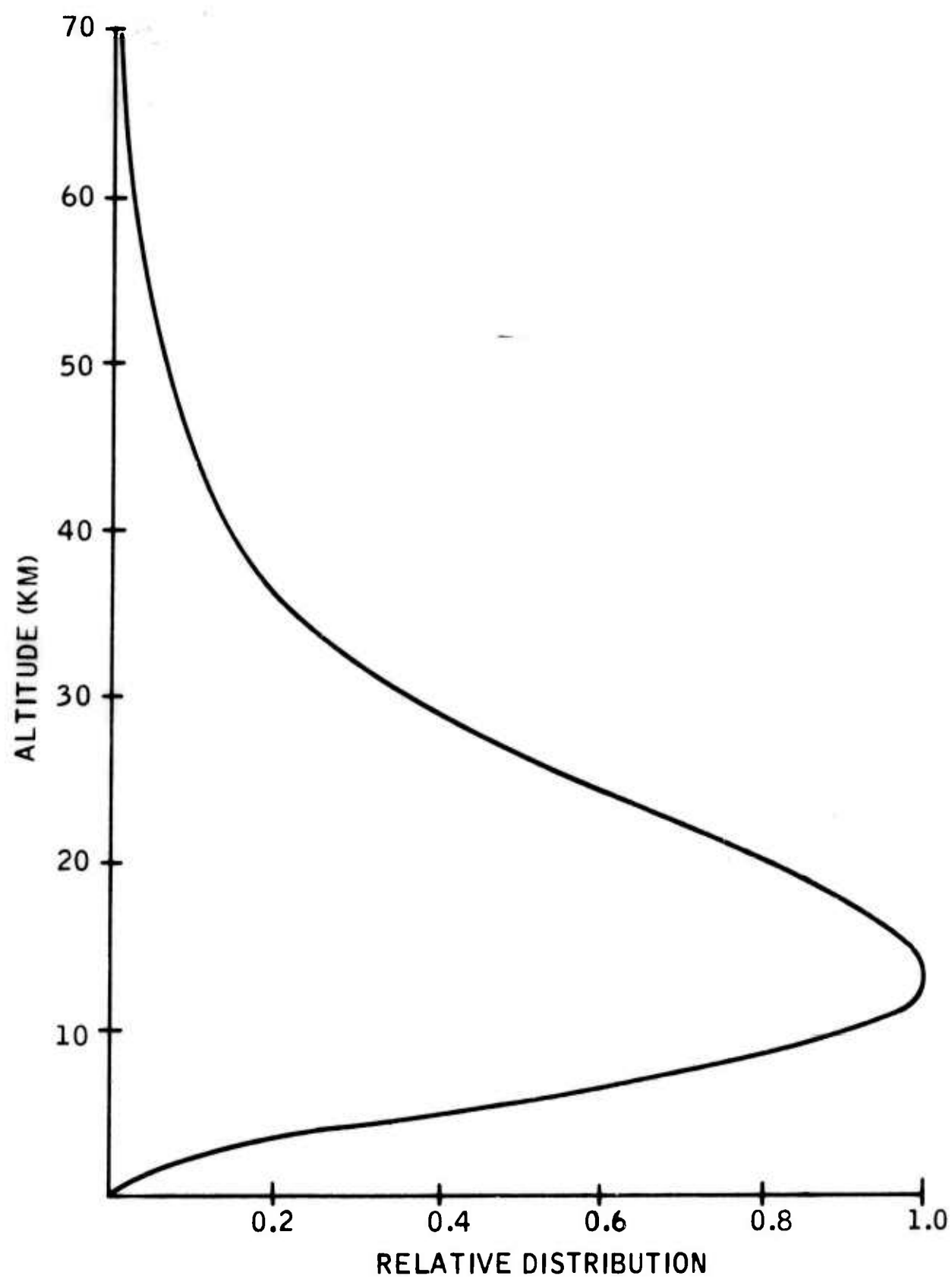
Figure D3. Atmospheric Distribution of Nitric Acid

175

APPENDIX E
SPECTRAL RADIANCE FOR 47 SELECTED
LOWER ATMOSPHERIC MODELS

This appendix contains spectra calculated for the 47 atmospheric profiles tabulated in Appendix C, Table C-1. For each profile, the profile number is given together with the profile code explained in Appendix C. For each profile, spectra are given for scale heights from 10 to 80 kilometers, in increments of 10 kilometers. The scale height for each spectrum is labeled. The abscissa is given as spectral wavelength in microns and the ordinate is given as spectral radiance in watts cm^{-2} steradian^{-1} micron^{-1} and is plotted on seven cycle semilogarithmic paper.

Figures E11 to E39 do not give radiance beyond 10.5 microns because the same information is contained in other spectra. For each model, reference is made to the appropriate model for longer wavelengths.
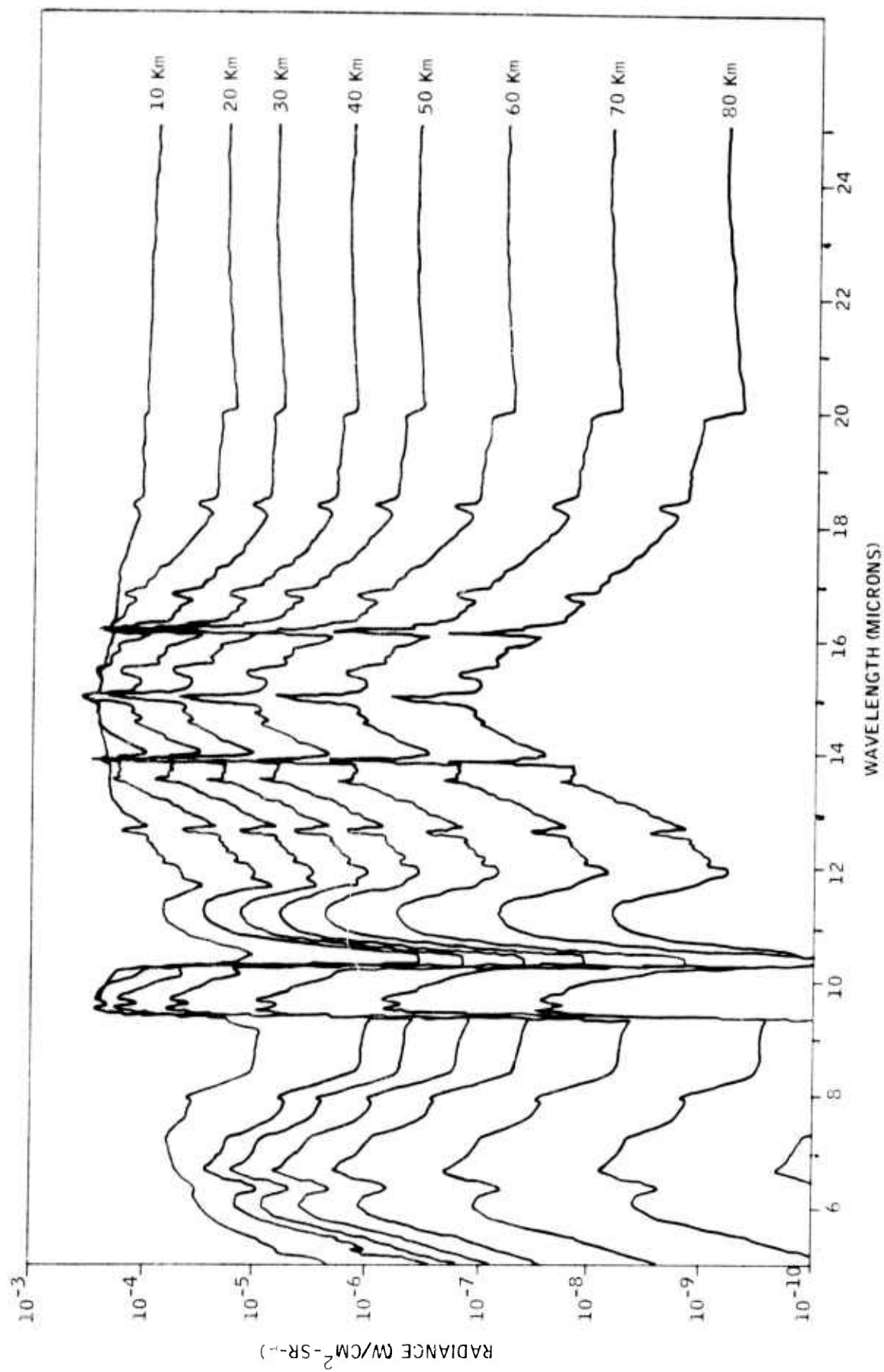
Figure E1

Profile No. 1 (1-1-1-1)
Horizon Spectral Radiance
U. S. Standard Atmosphere
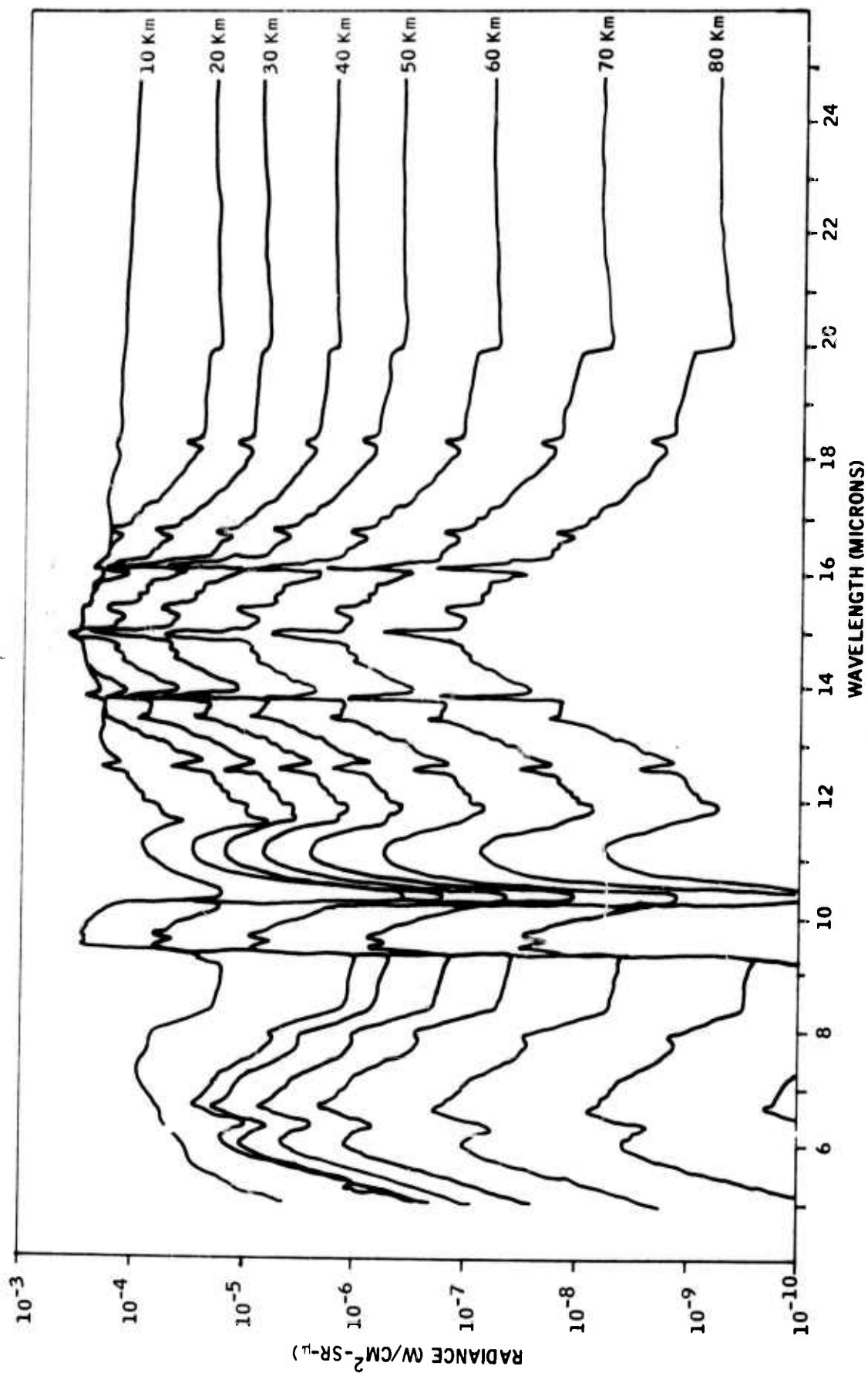
Figure E2

Profile No. 2 (2-2-1-2)
Horizon Spectral Radiance
Tropical Atmosphere

178
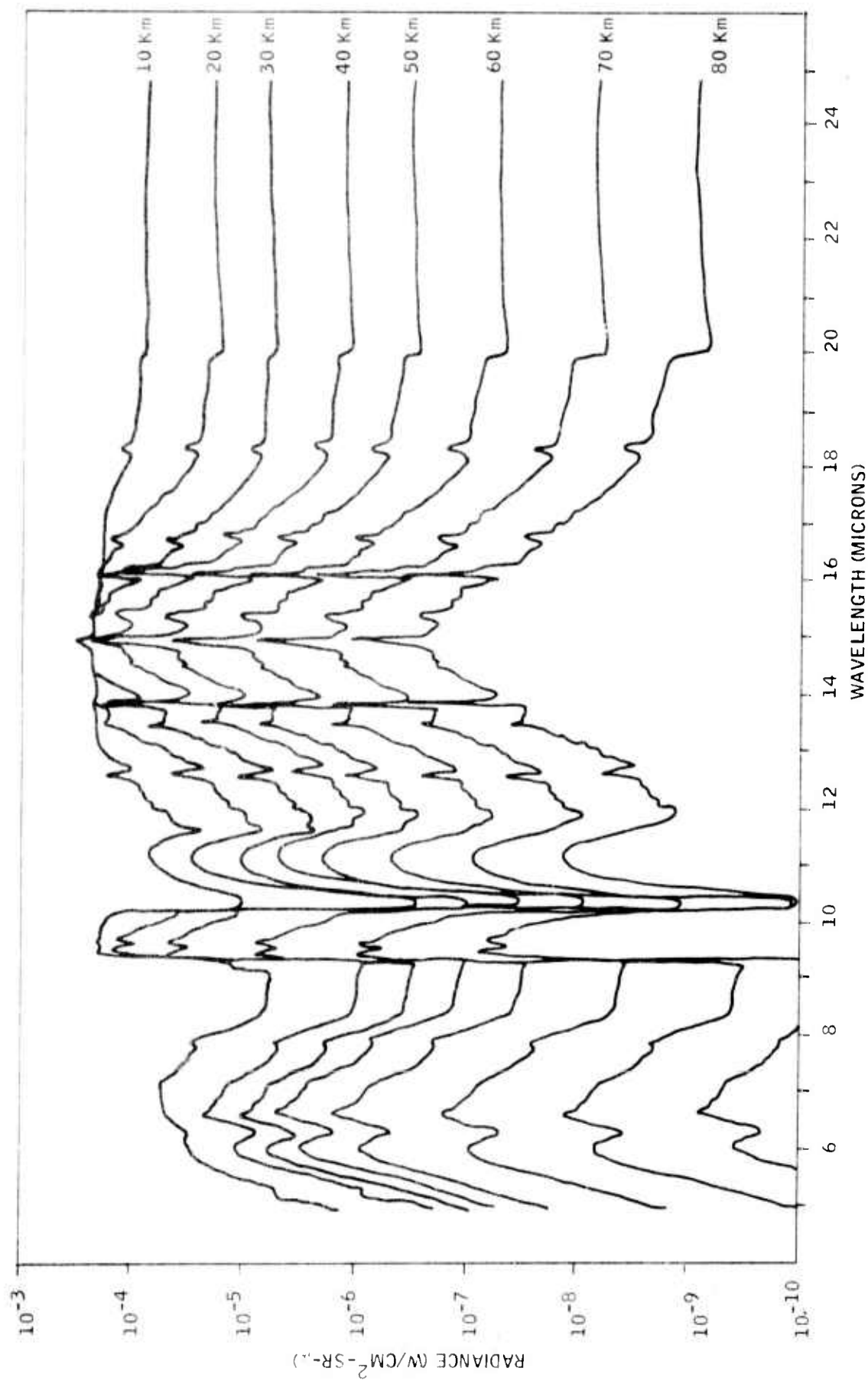
Figure E3

Profile No. 3 (3-3-1-3)
Horizon Spectral Radiance
Mid-latitude Winter Atmosphere

179
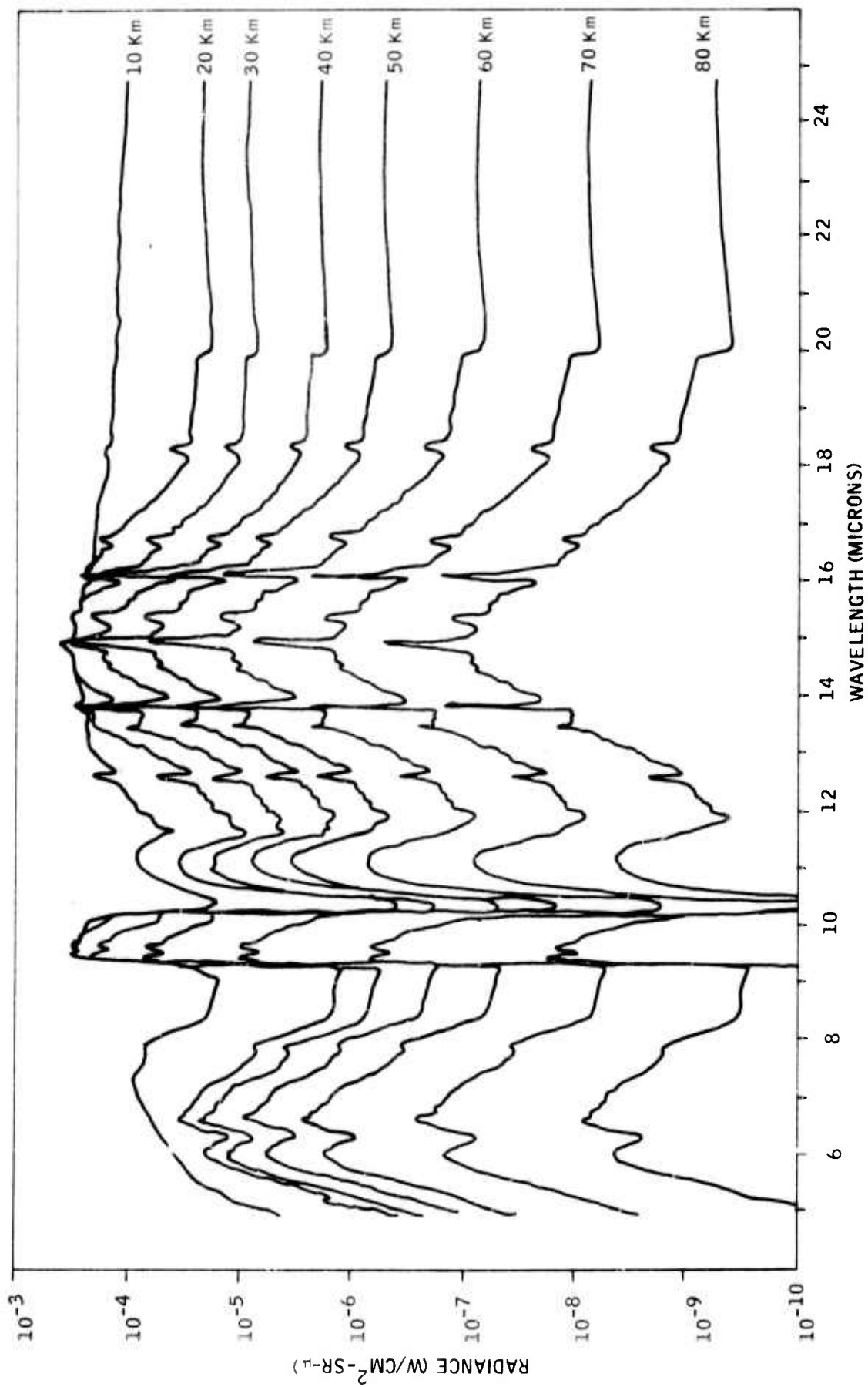
Figure E4
Profile No. 4 (4-4-1-4)
Horizon Spectral Radiance
Mid-latitude Summer Atmosphere
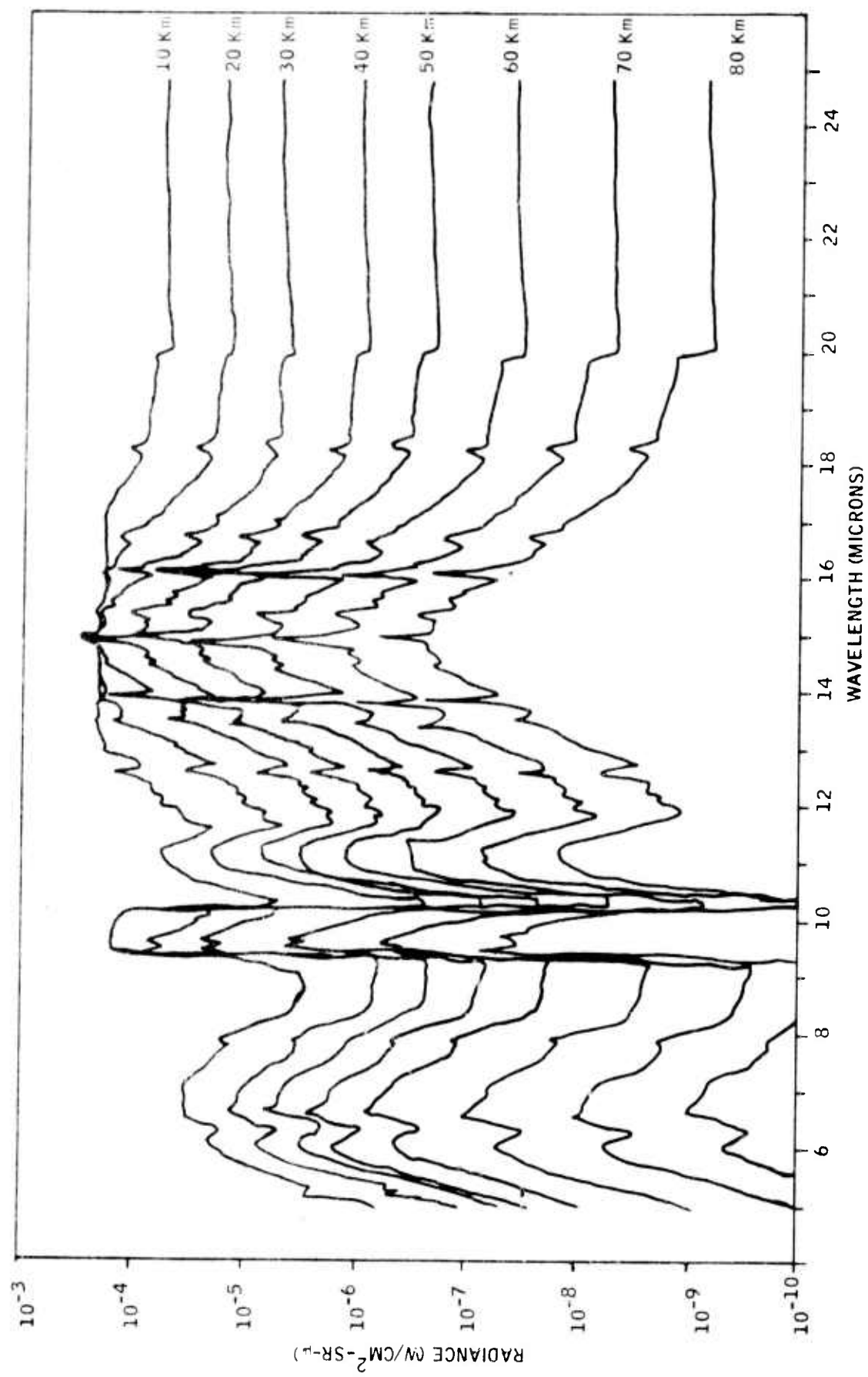
Figure E5
Profile No. 5 (5-5-1-5)
Horizon Spectral Radiance
Artic Winter Atmosphere
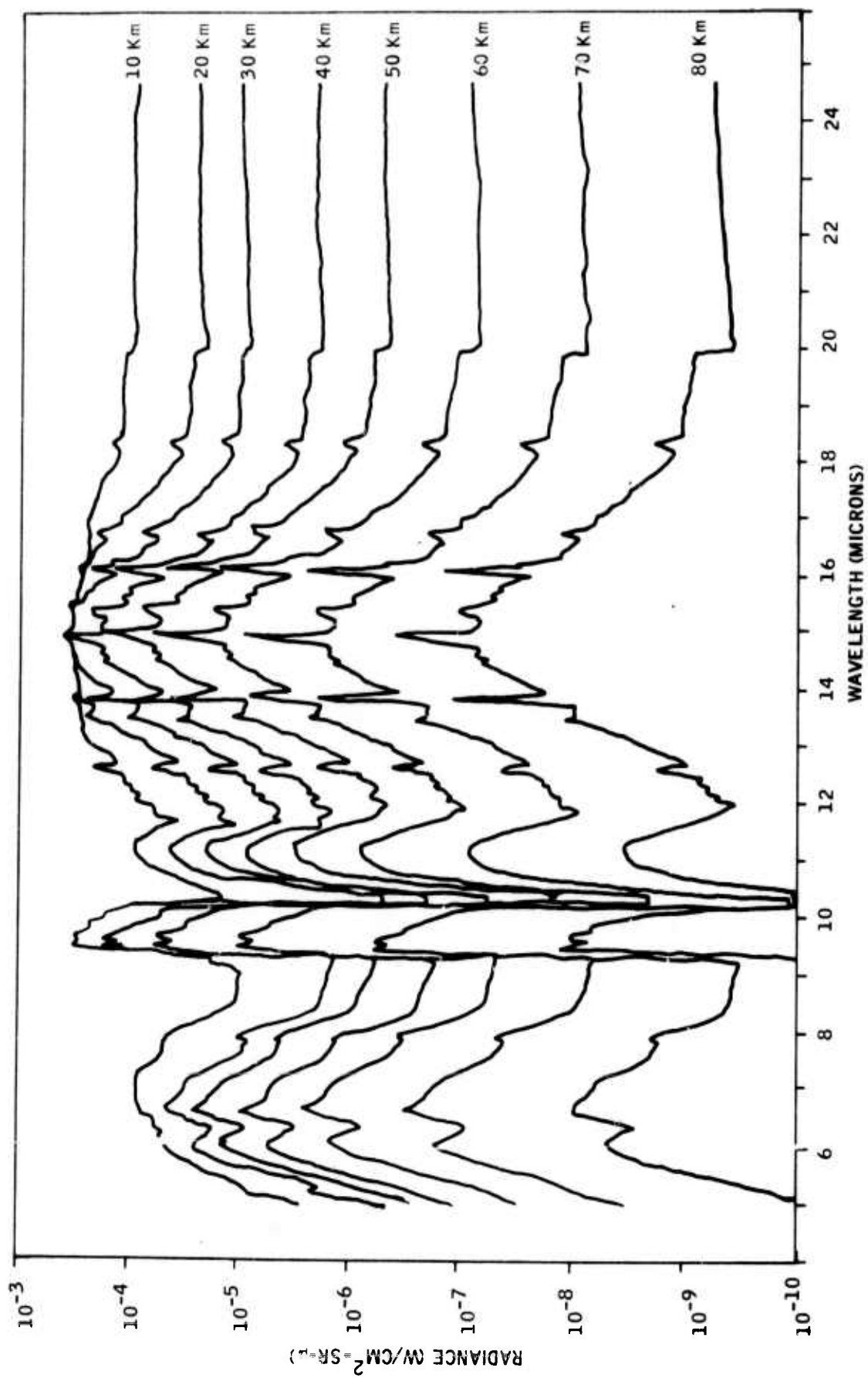
Figure E6

Profile No. 6 (6-6-1-6)
Horizon Spectral Radiance
Arctic Summer Atmosphere
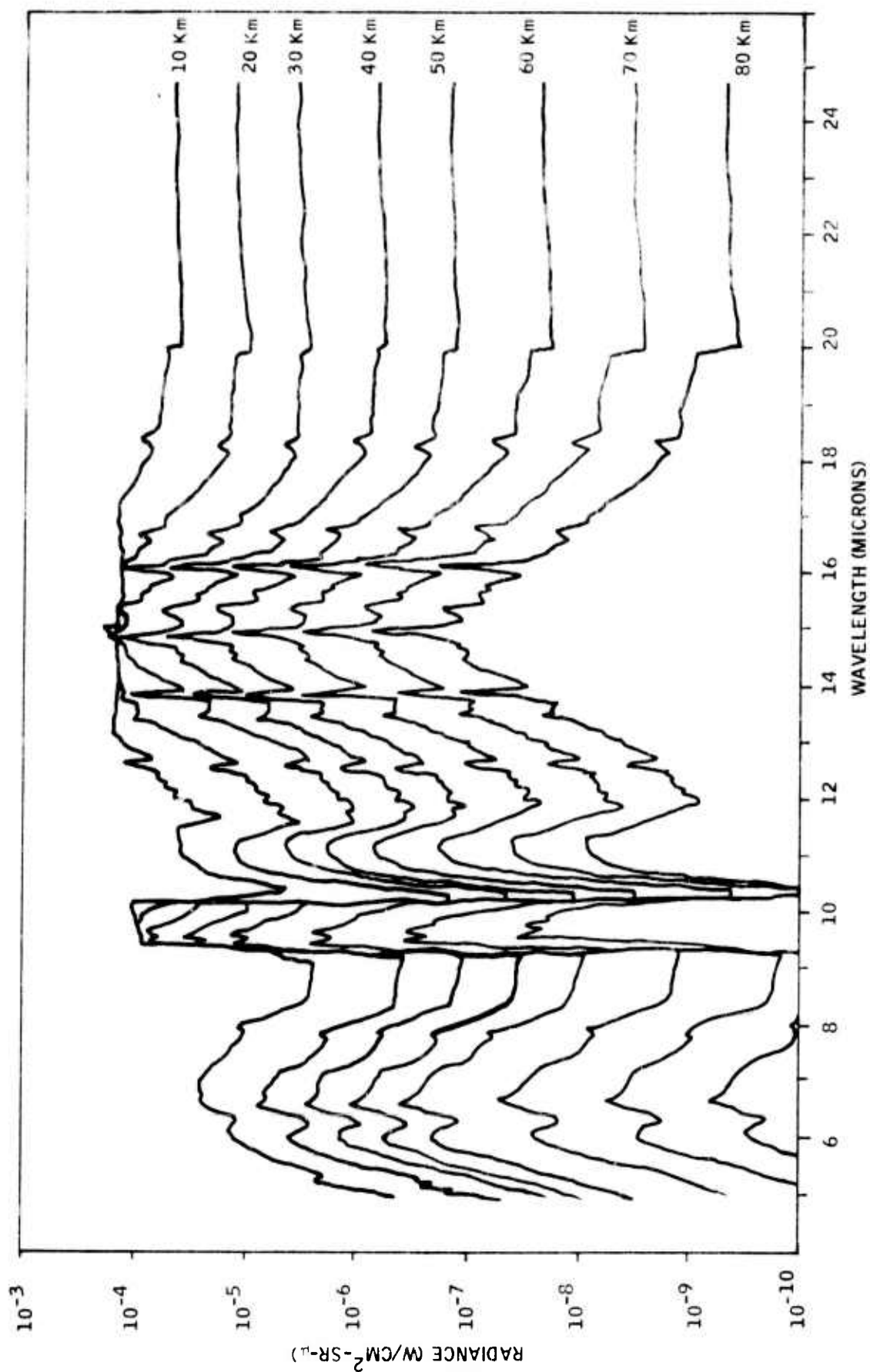
Figure E7

Profile No. 7 (7-5-1-5)
Horizon Spectral Radiance
Arctic Atmosphere - Cold Stratosphere

183
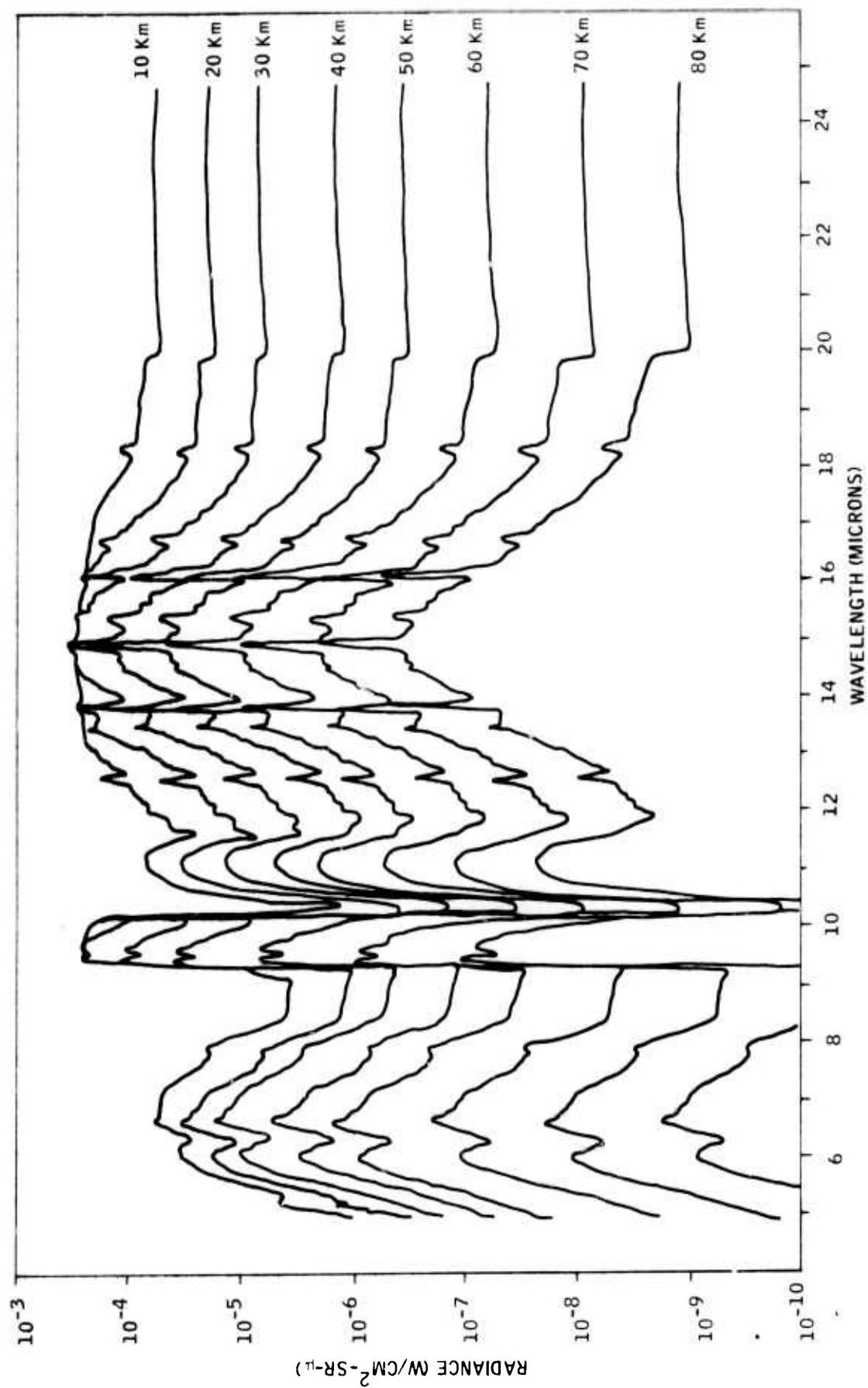
Figure E8

Profile No. 8 (8-5-1-5)
Horizon Spectral Radiance
Arctic Atmosphere – Warm Stratosphere

184
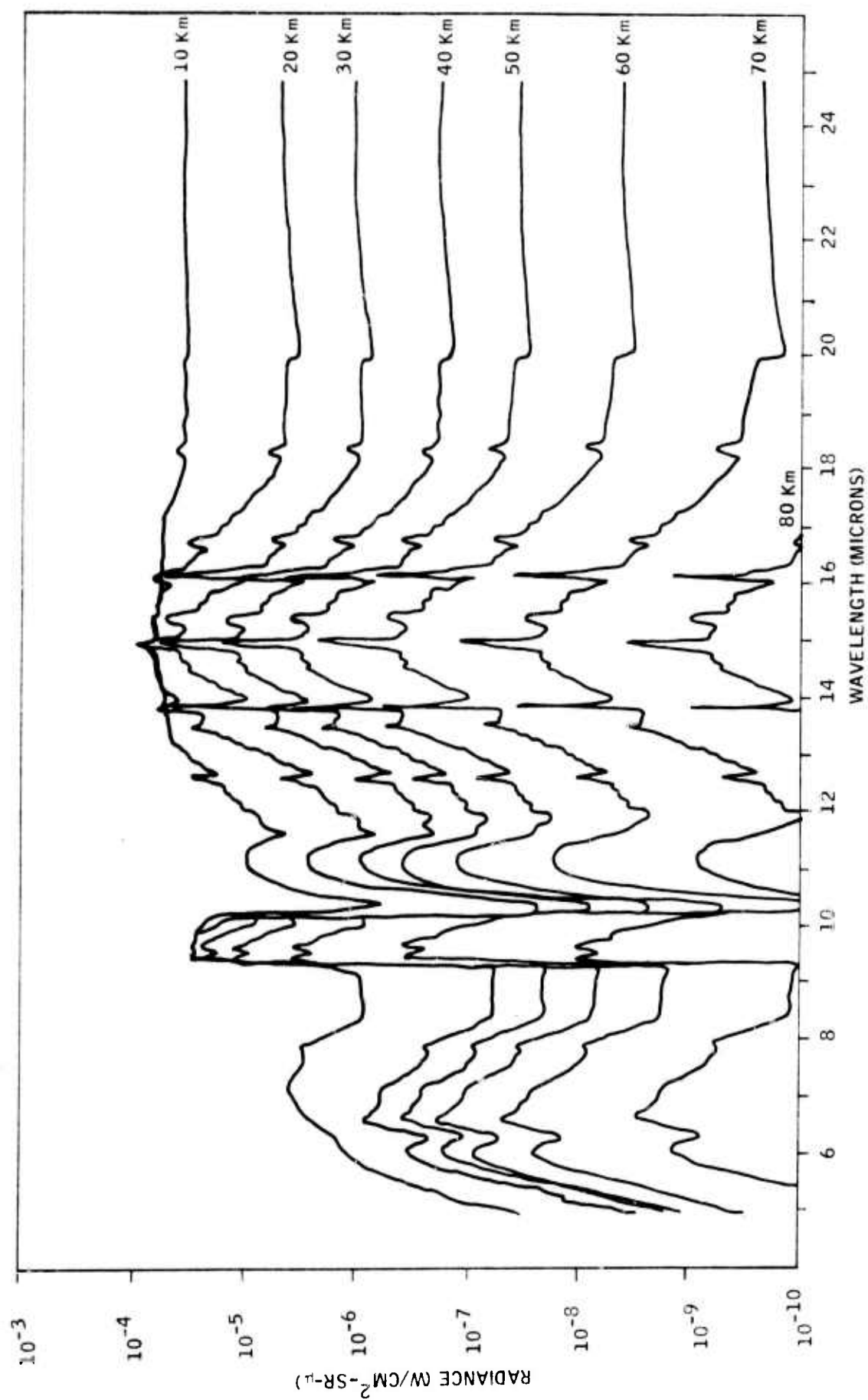
Figure E9

Profile No. 9 (9-1-1-1)
Horizon Spectral Radiance
Extreme Cold Atmosphere

185
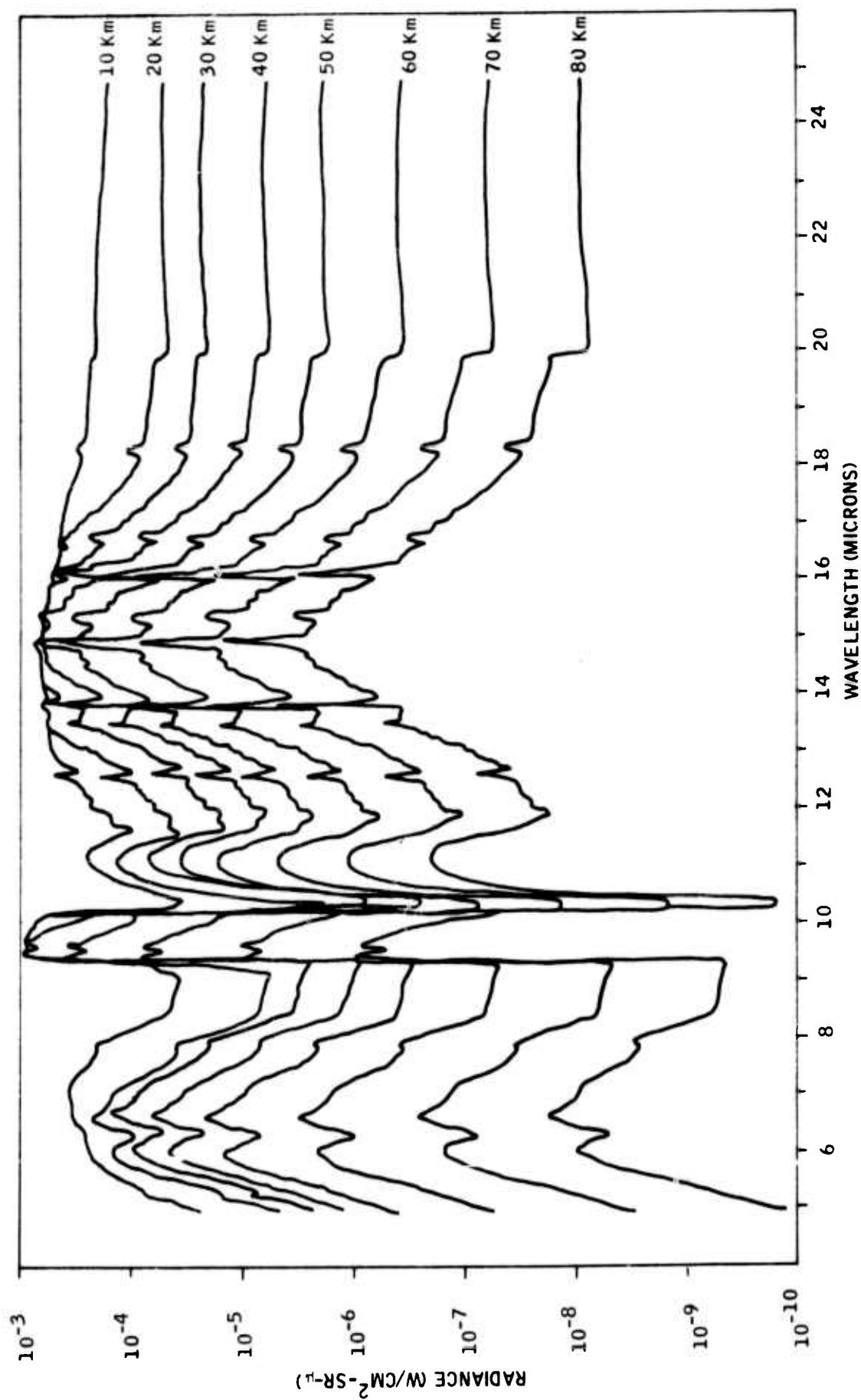
Figure E10

Profile No. 10 (10-1-1-1)
Horizon Spectral Radiance
Extreme Hot Atmosphere

186
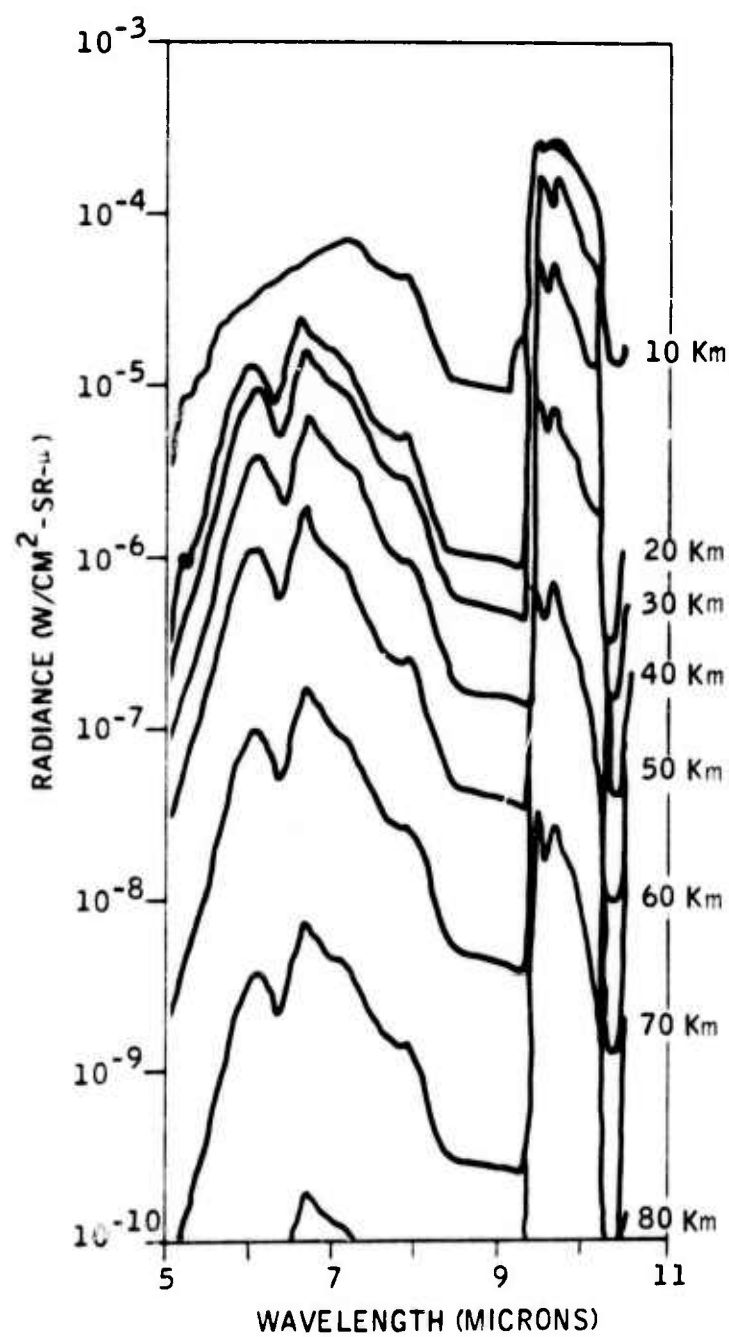
Figure E11

Atmospheric Model No. 11 (2-11-2-11)
Horizon Spectral Radiance
Tropical-Dry Troposphere
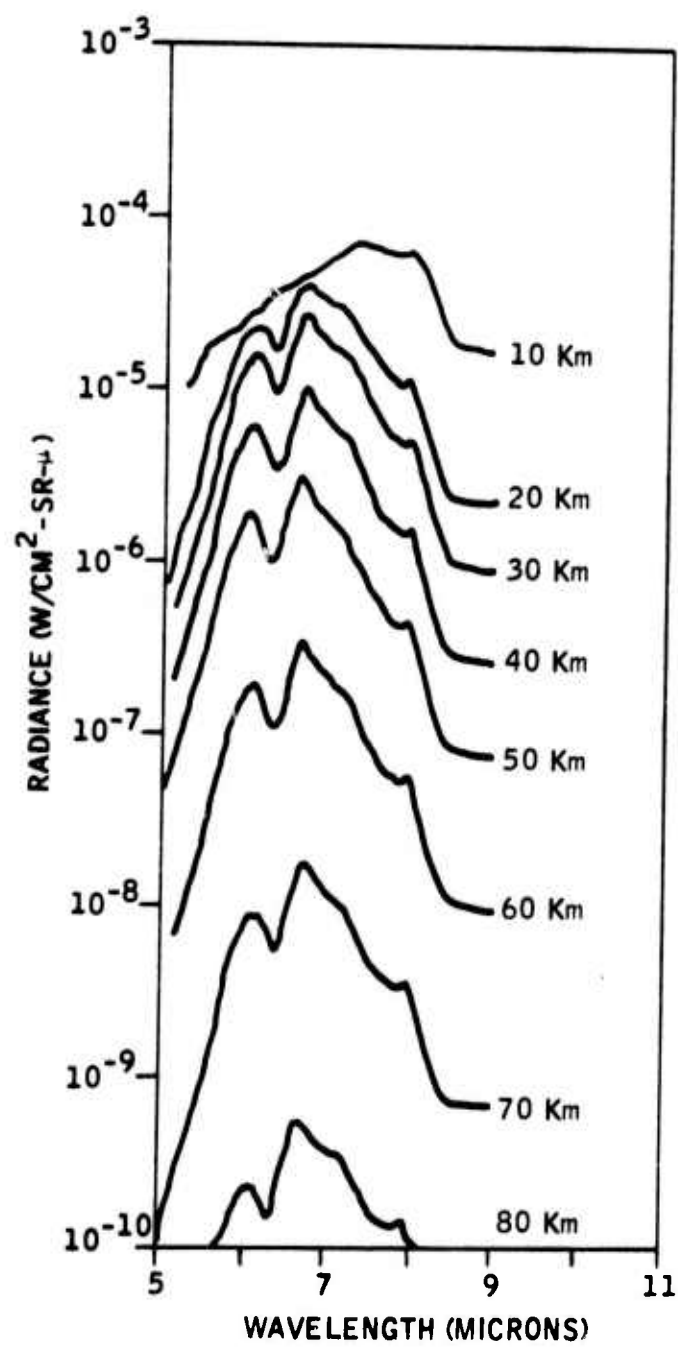
(From 10.5 to 25 microns, see Model No. 2)

187
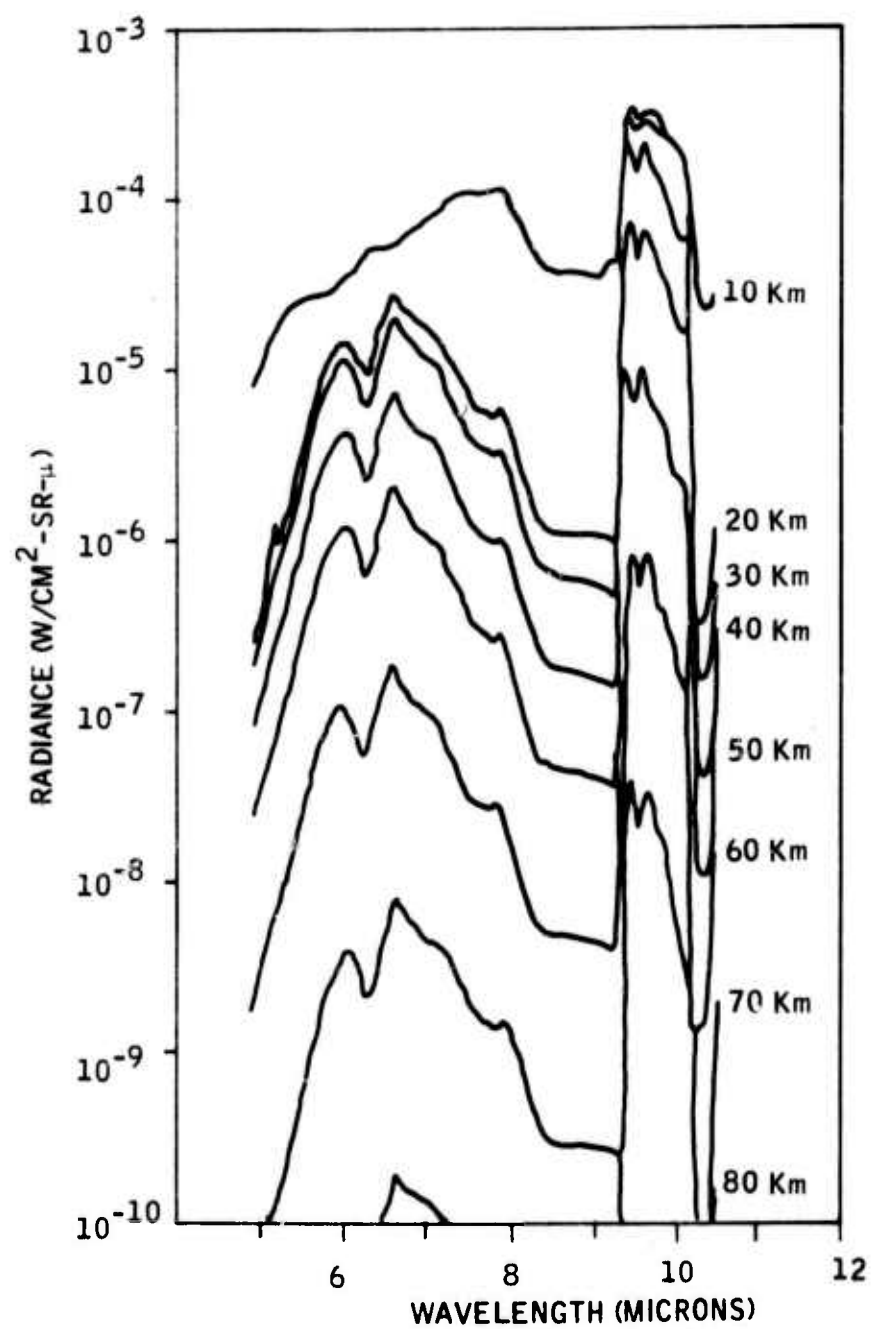
Figure E12

Atmospheric Model No. 12 (2-12-1-12)
Horizon Spectral Radiance
Tropical-Moist Troposphere

(From 10.5 to 25 microns, see Model No. 2)

188
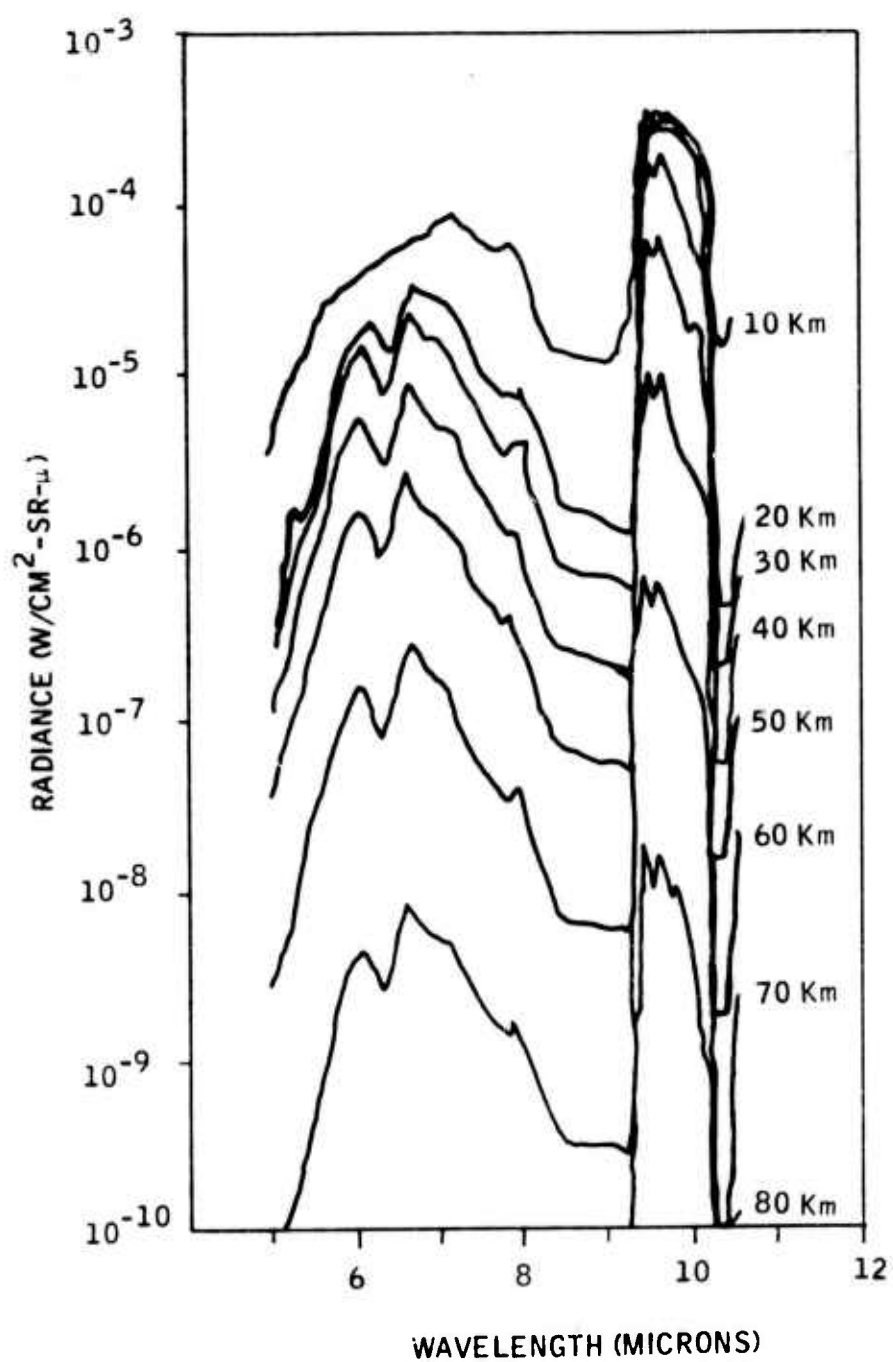
Figure E13

Atmospheric Model No. 13 (4-13-1-13)
Horizon Spectral Radiance
Mid-latitude, Summer, Dry Troposphere

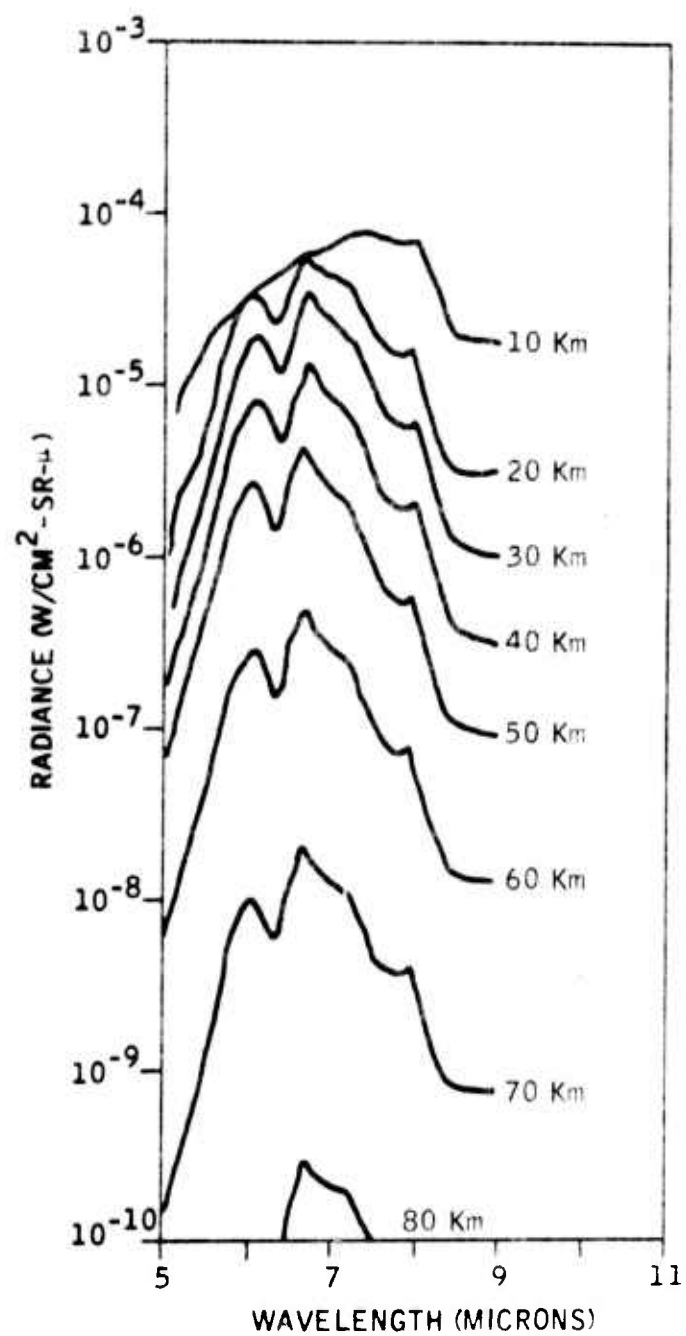(From 10.5 to 25 microns, see Model No. 4)

189
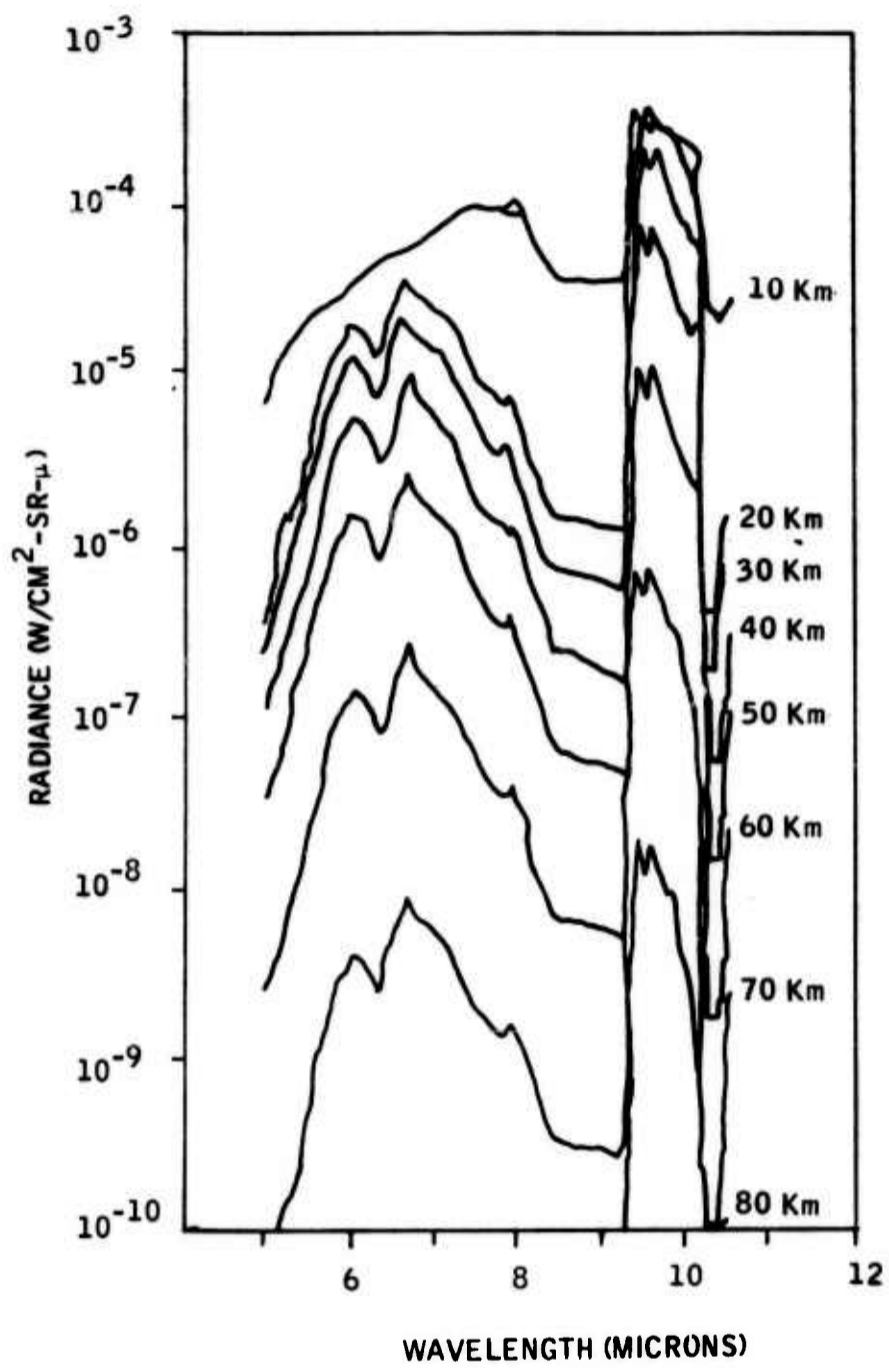
Figure E14

Atmospheric Model No. 14   (4-14-1-14)
Horizon Spectral Radiance
Mid-latitude, Summer, Moist Troposphere
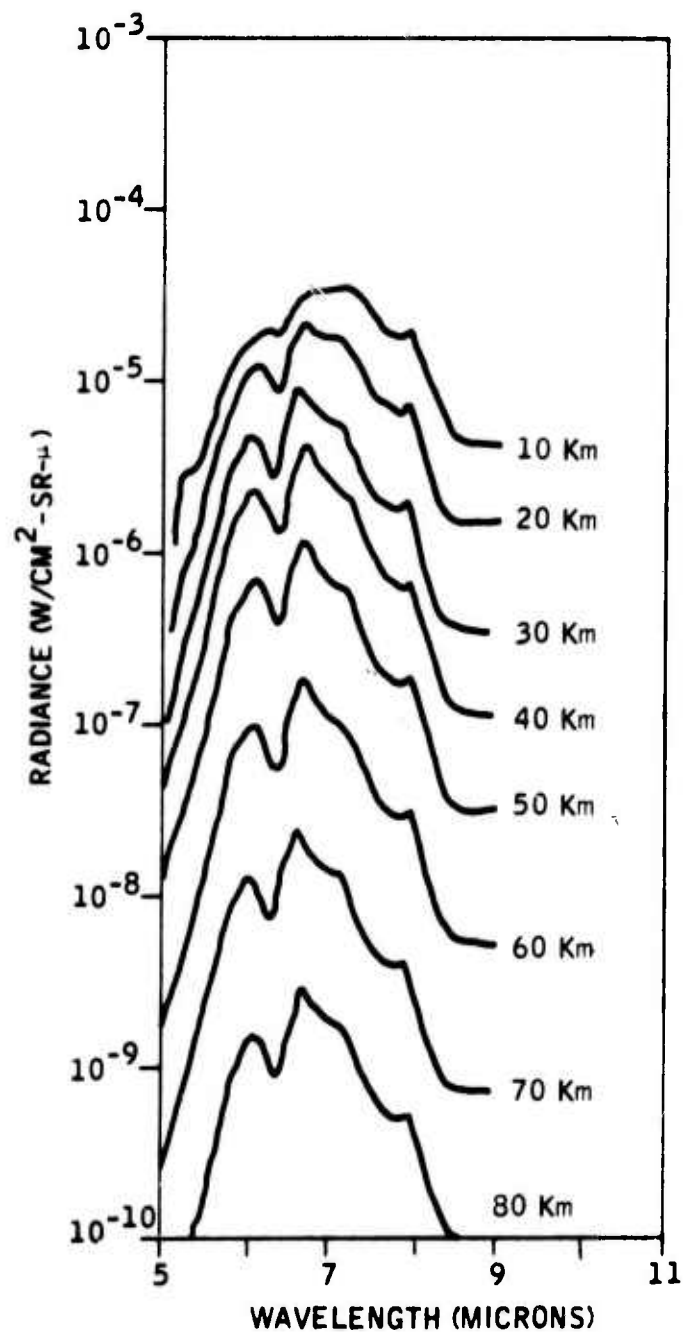
(From 10.5 to 25 microns, see Model No. 4)

190
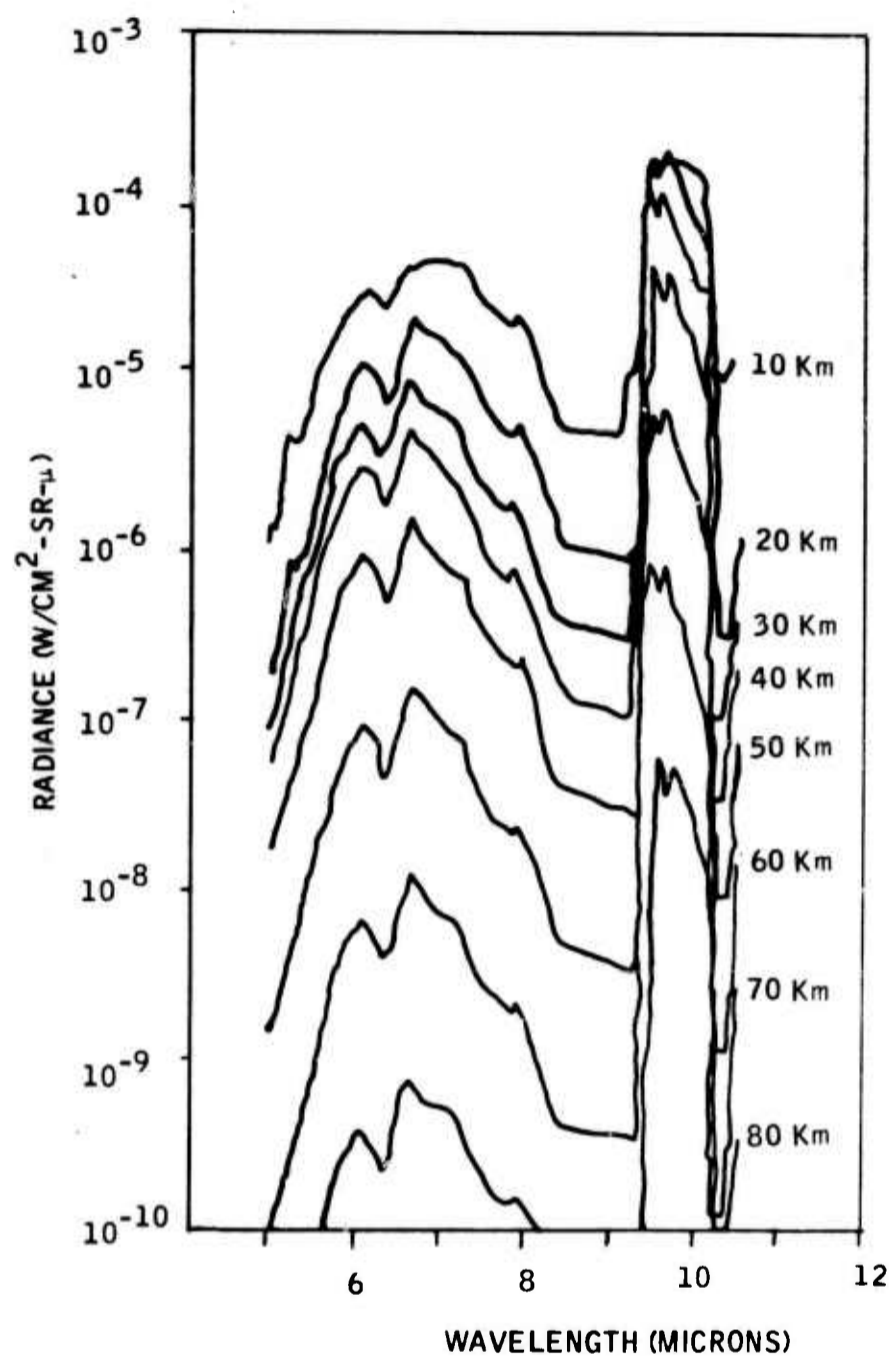
Figure E15

Atmospheric Model No. 15 (3-15-1-15)
Horizon Spectral Radiance
Mid-latitude, Winter, Dry Troposphere

(From 10.5 to 25 microns, see Model No. 3)

191
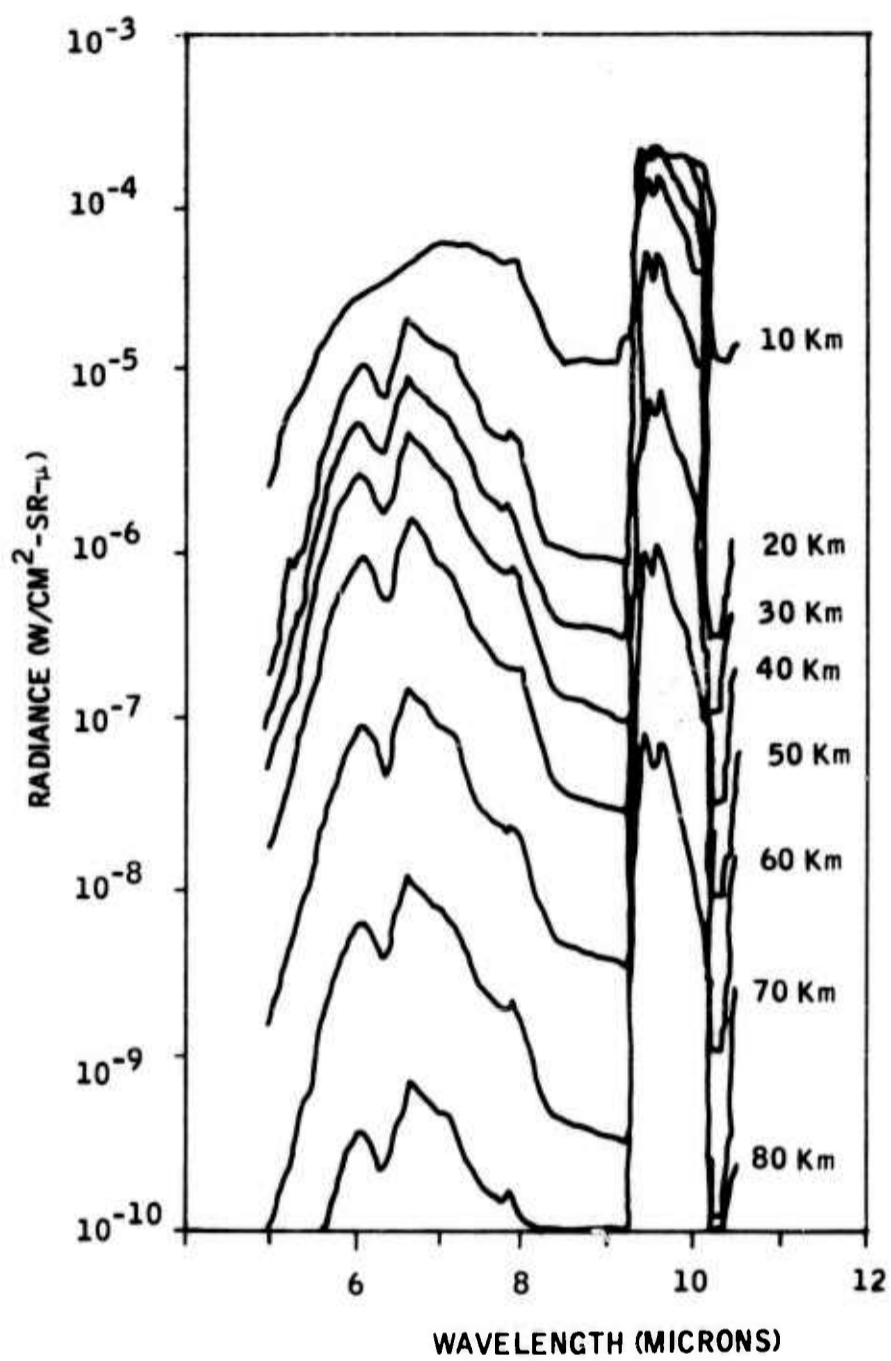
Figure E16

Atmospheric Model No. 16 (3-16-1-16)
Horizon Spectral Radiance
Mid-latitude, Winter, Moist Troposphere

(From 10.5 to 25 microns, see Model No. 3)

192
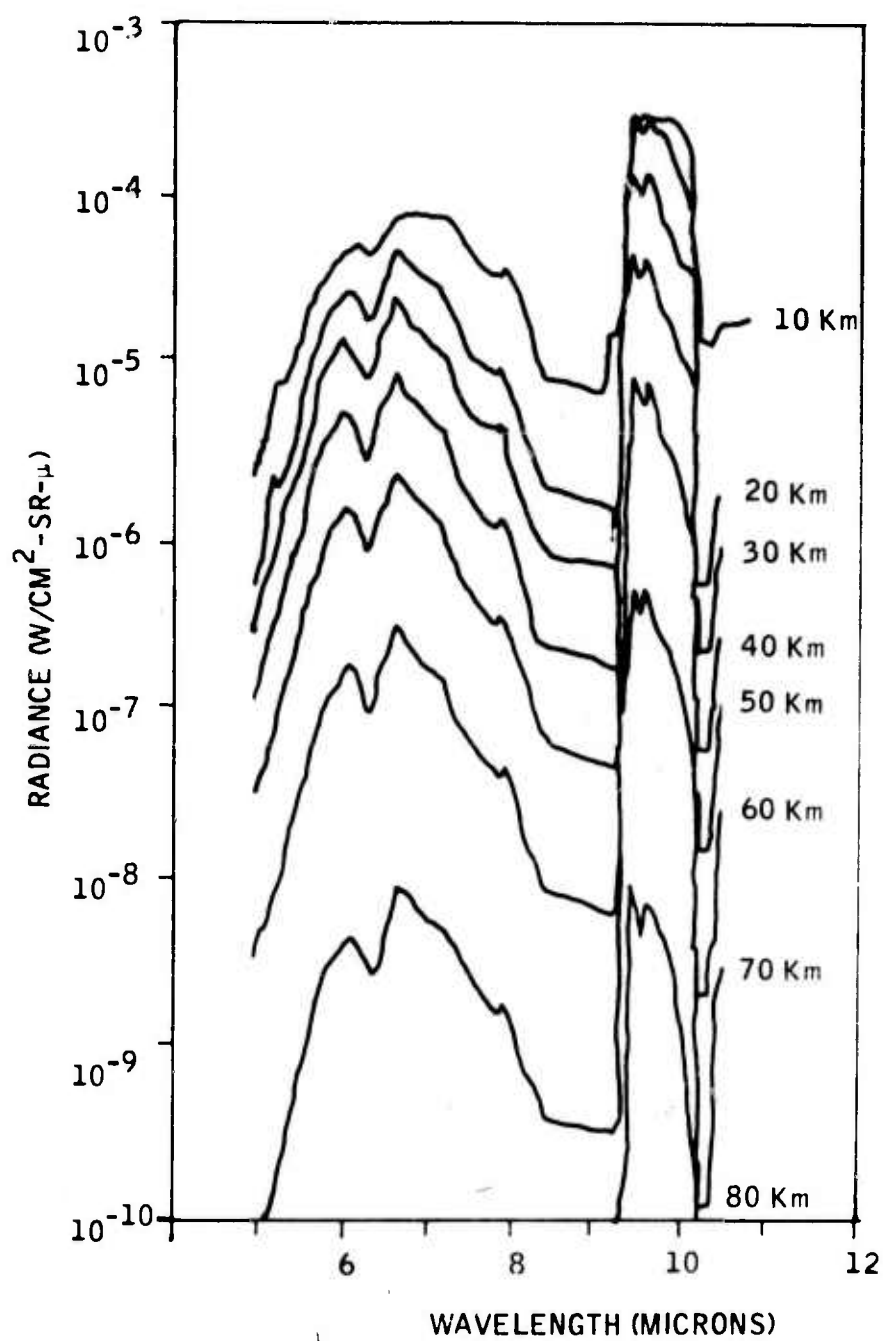
Figure E17

Atmospheric Model No. 17 (6-17-1-17)
Horizon Spectral Radiance
Arctic Summer, Dry Troposphere

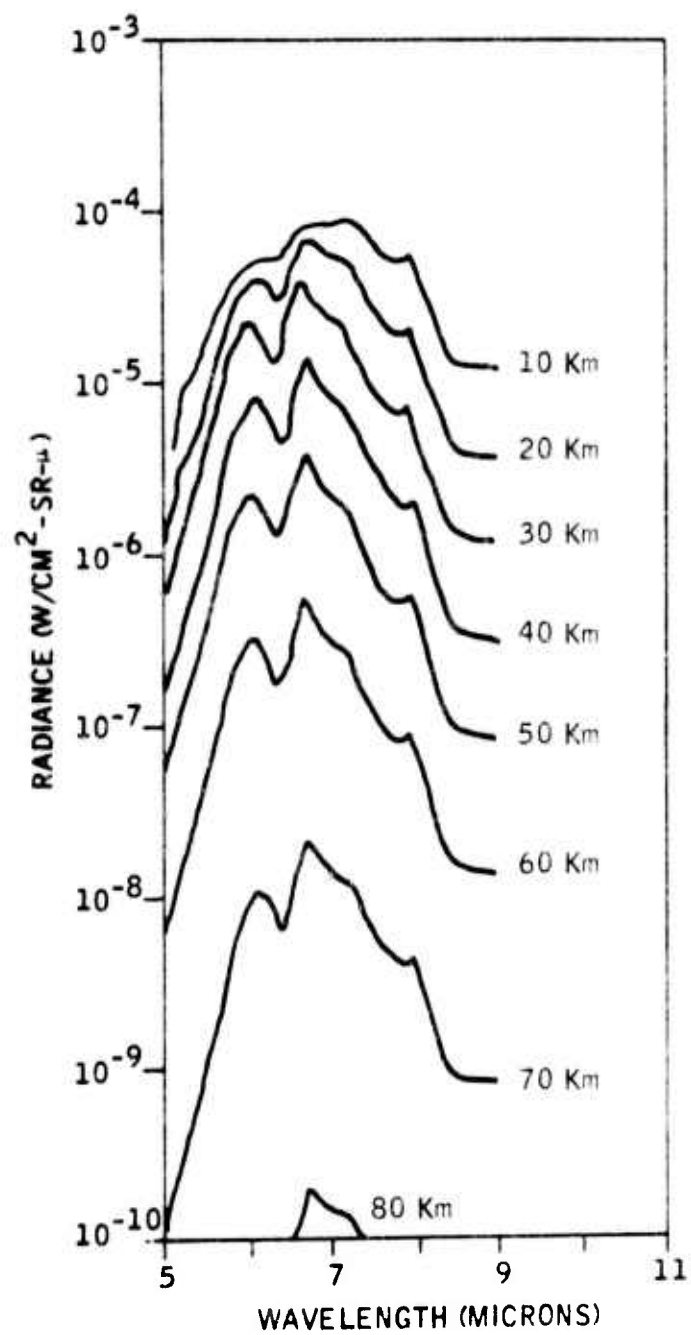(From 10.5 to 25 microns, see Model No. 6)

193
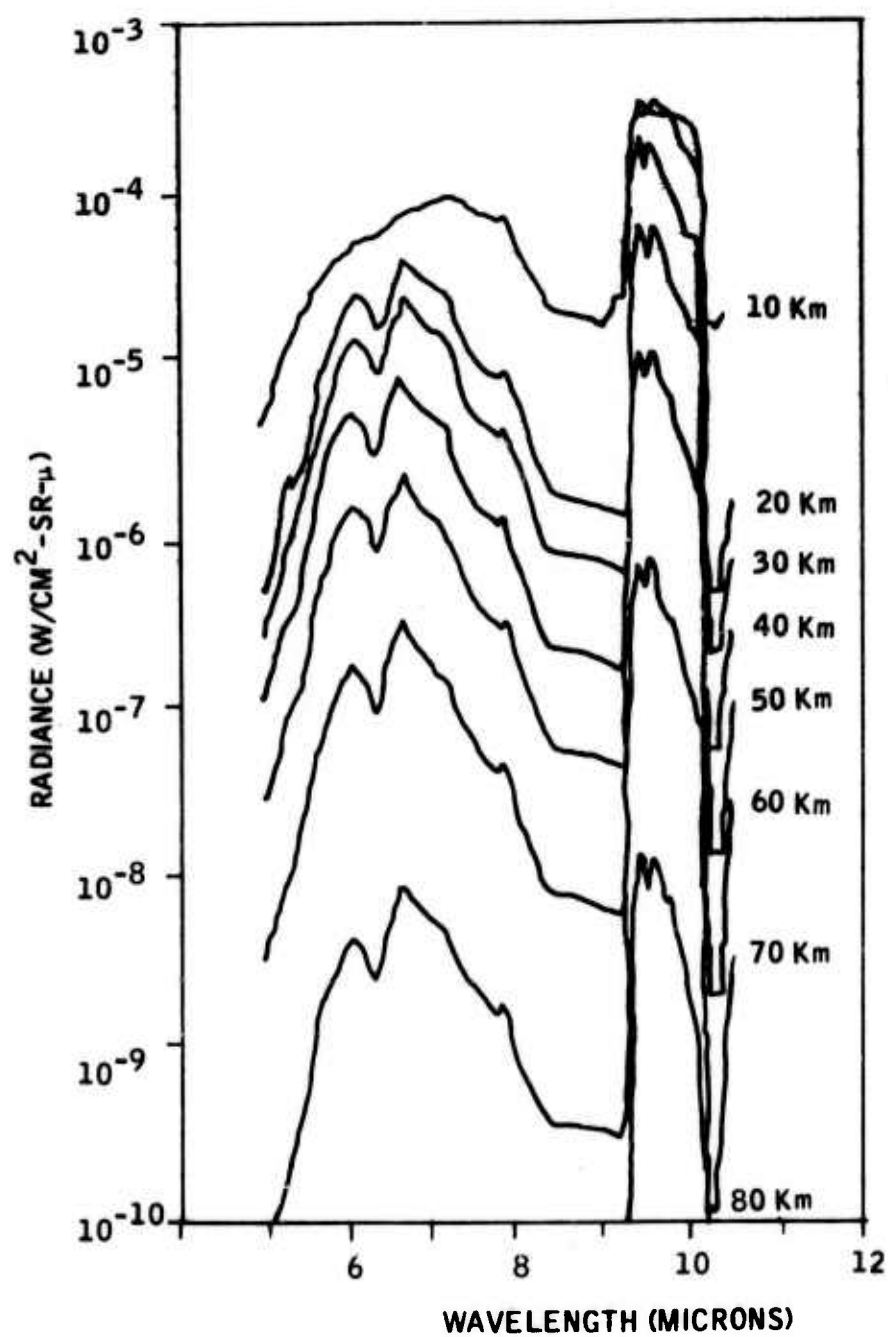
Figure E18

Atmospheric Model No. 18 (6-18-1-18)
Horizon Spectral Radiance
Arctic Summer - Moist Troposphere

(From 10.5 to 25 microns, see Model No. 6)
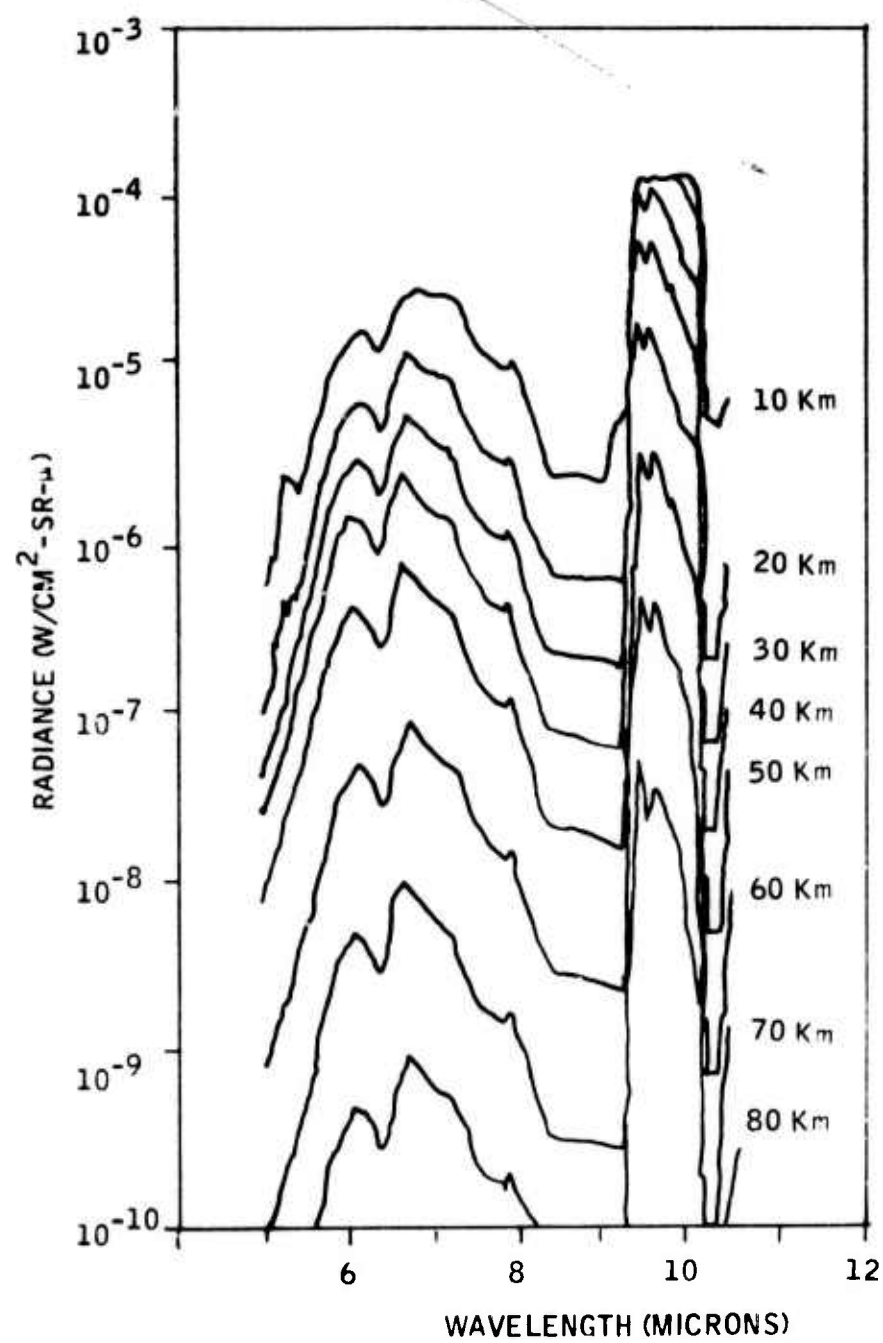
Figure E19

Atmospheric Model No. 19 (5-19-1-19)
Horizon Spectral Radiance
Arctic Winter - Dry Troposphere

(From 10.5 to 25 microns, see Model No, 5)

195
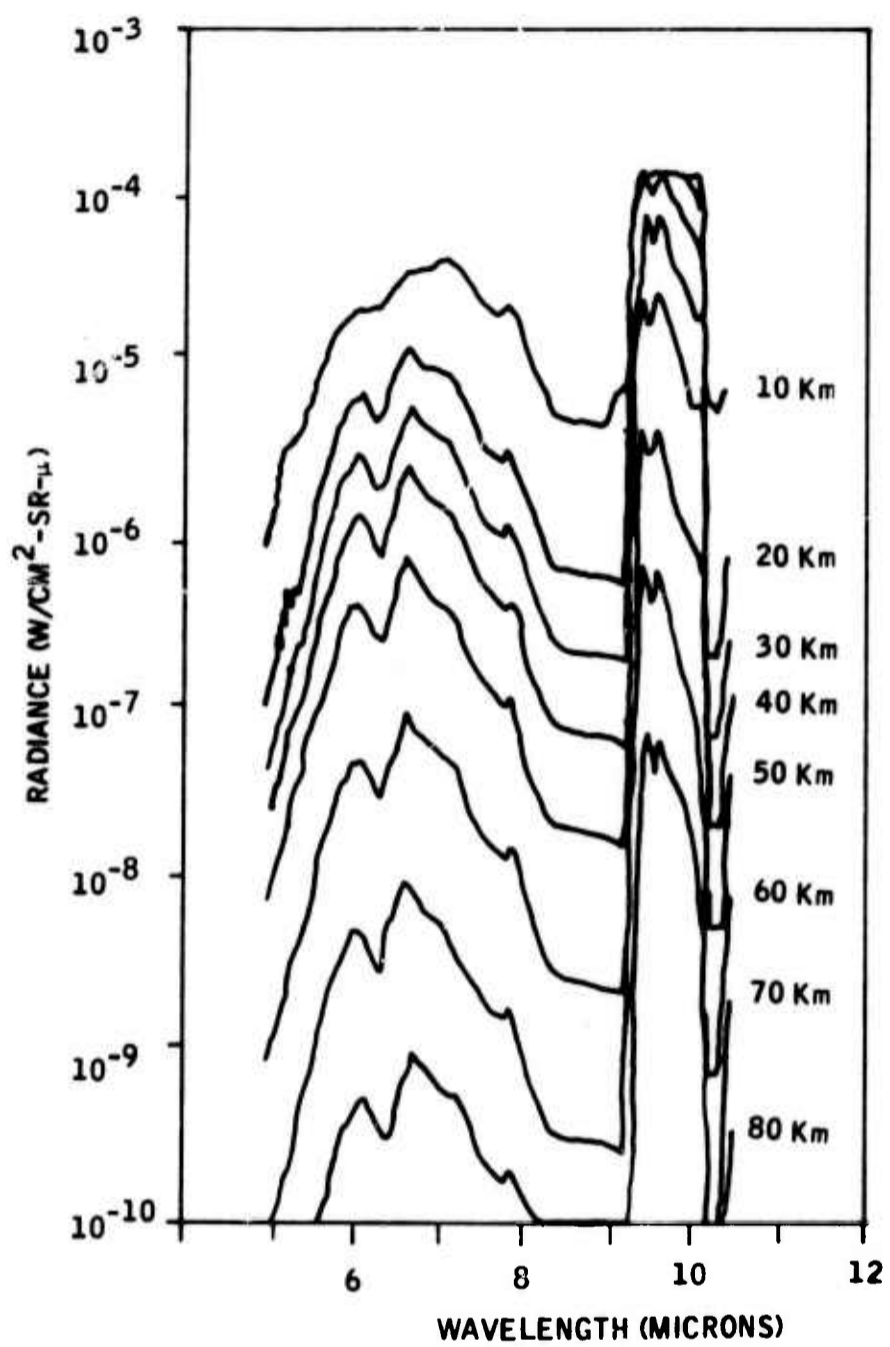
Figure E20

Atmospheric Model No. 20 (5-20-1-20)
Horizon Spectral Radiance
Arctic Winter - Moist Troposphere
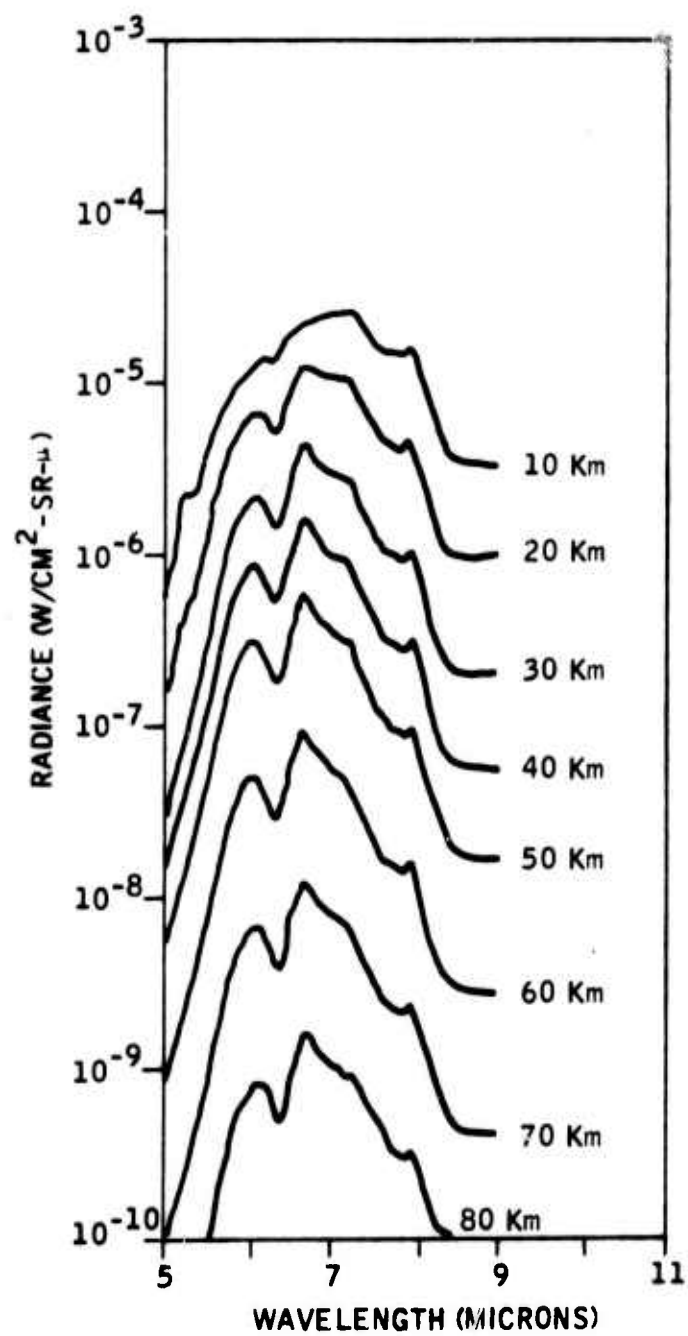
(From 10.5 to 25 microns, see Model No. 5)

196
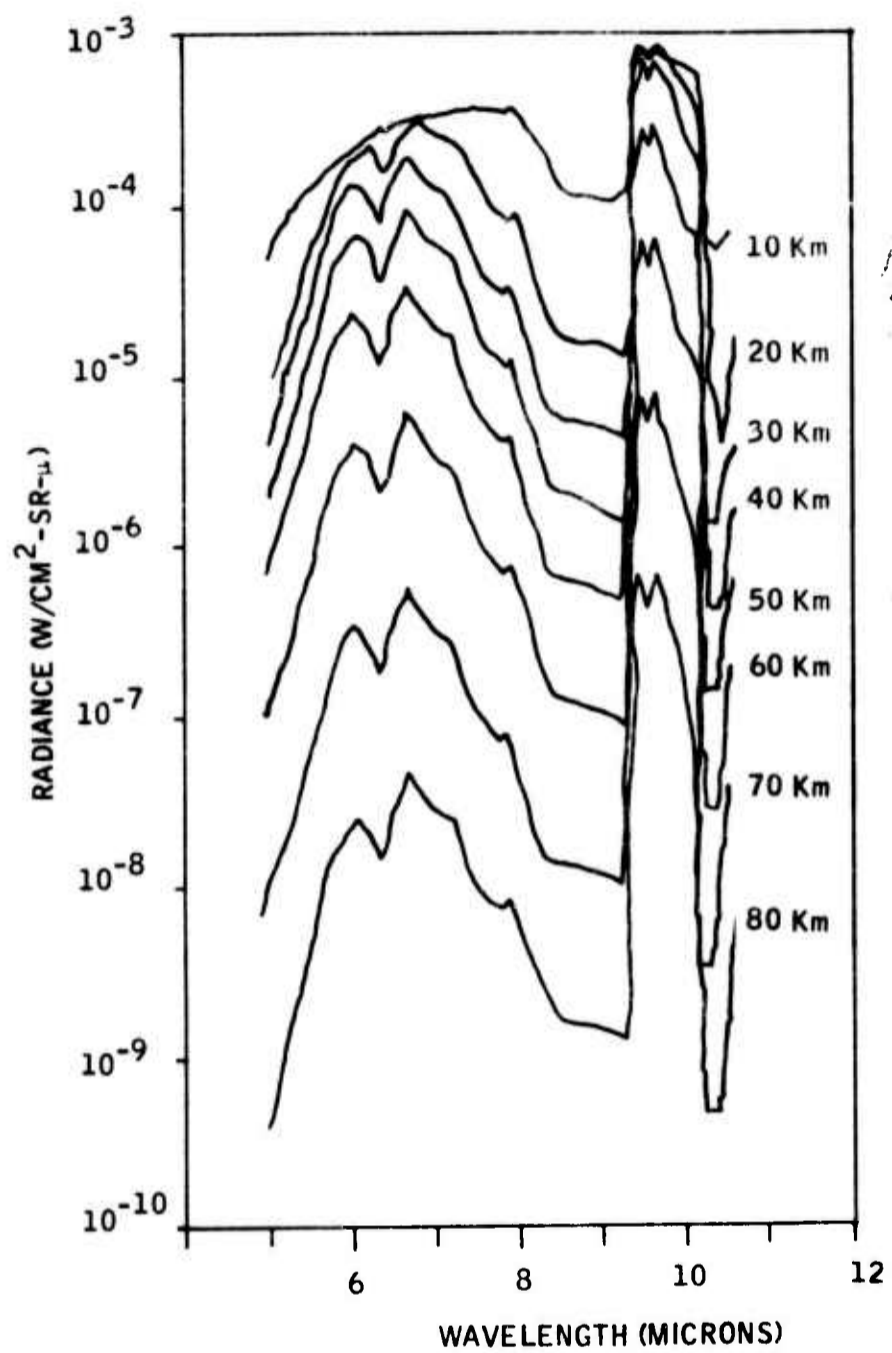
Figure E21

Atmospheric Model No. 21 (10-12-3-20)
Horizon Spectral Radiance
Extreme Conditions - Maximum Radiance

(From 10.5 to 25 microns, see Model No. 10)

197
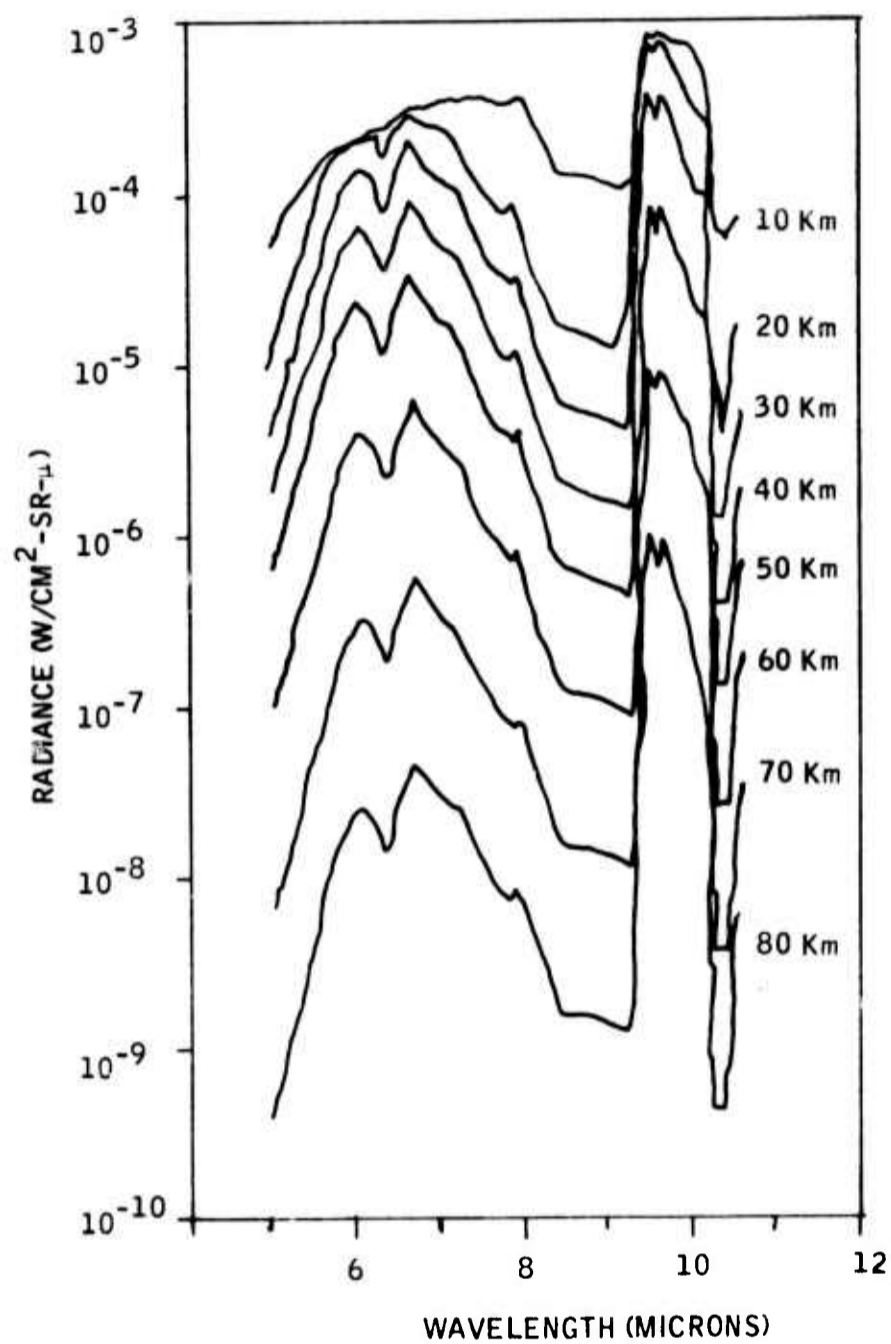
Figure E22

Atmospheric Model No. 22 (10-12-3-12)
Horizon Spectral Radiance
Extreme Conditions - Maximum Radiance

(From 10.5 to 25 microns, see Model No. 10)

198
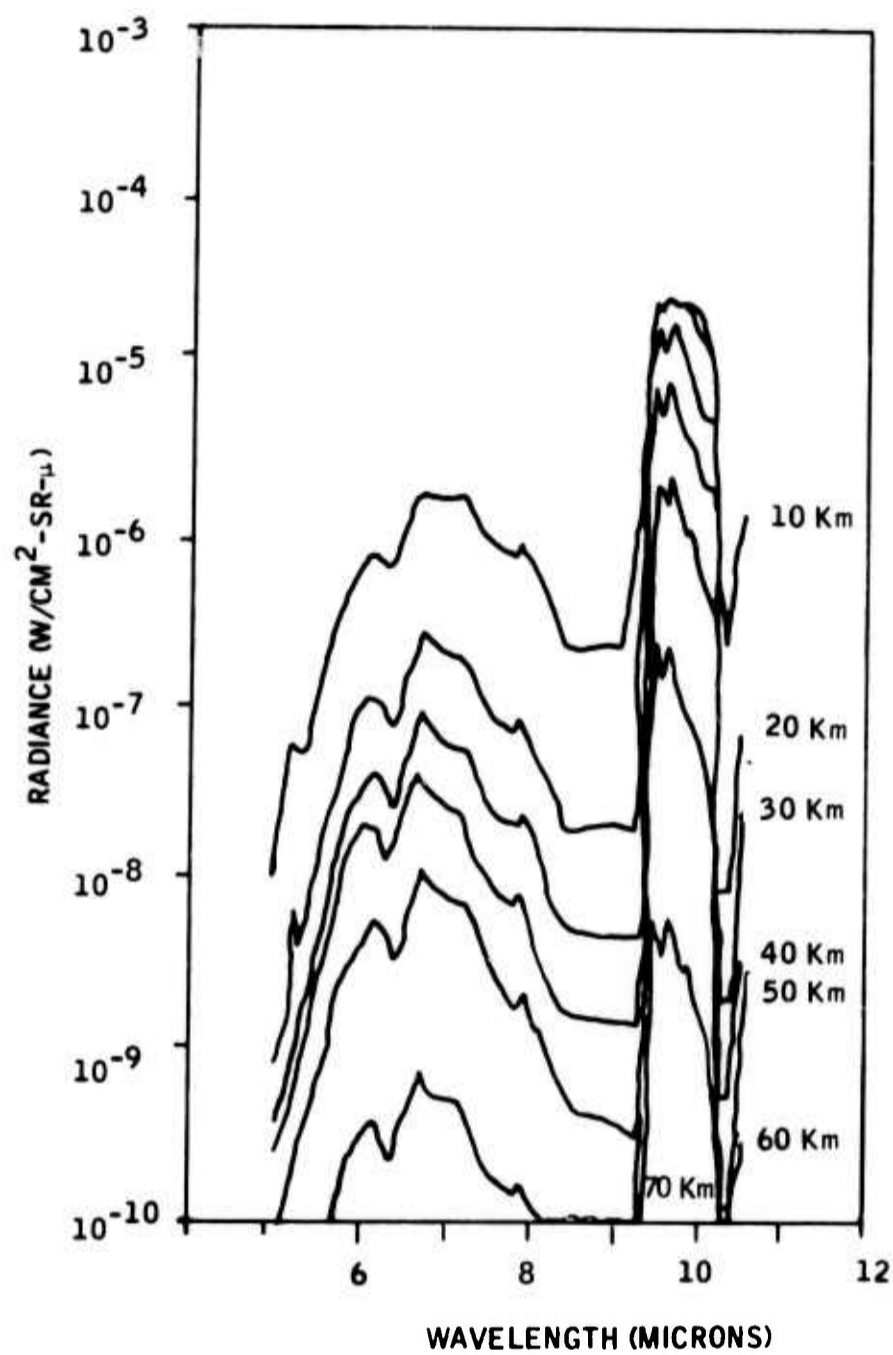
Figure E23

Atmospheric Model No. 23 (9-19-2-17)
Horizon Spectral Radiance
Extreme Conditions - Minimum Radiance
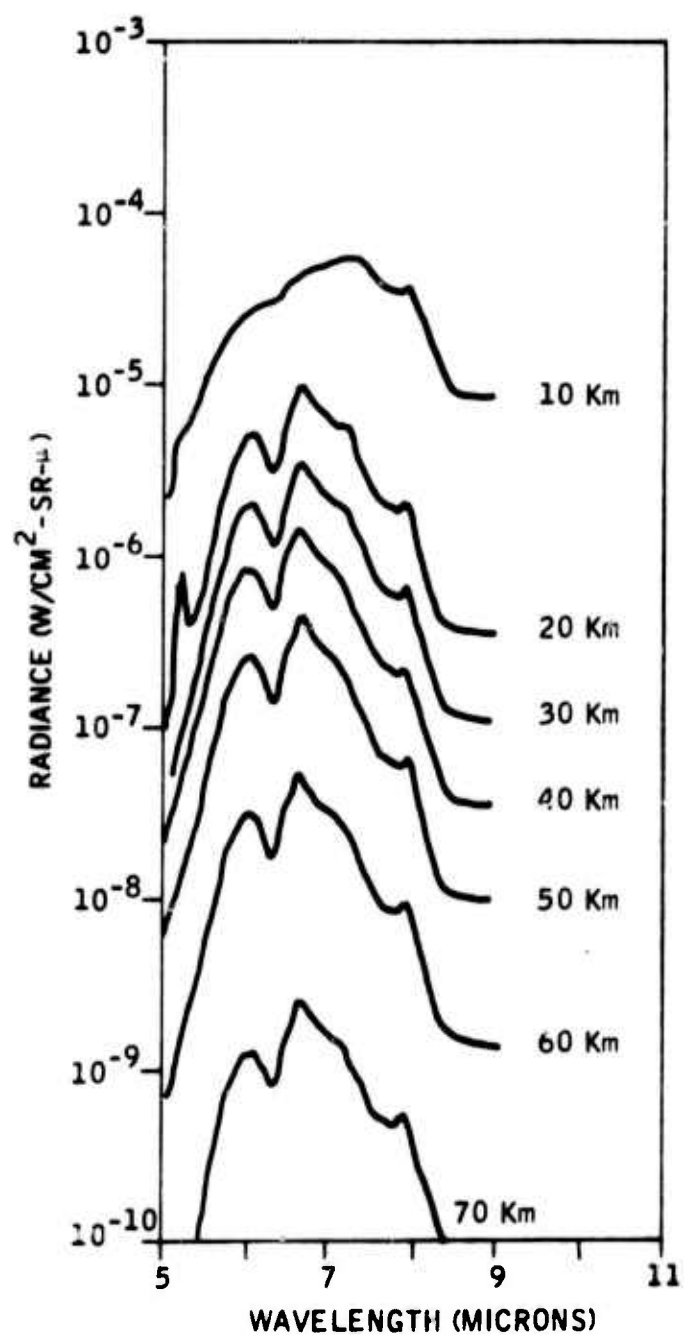
(From 10.5 to 25 microns, see Model No. 9)

199
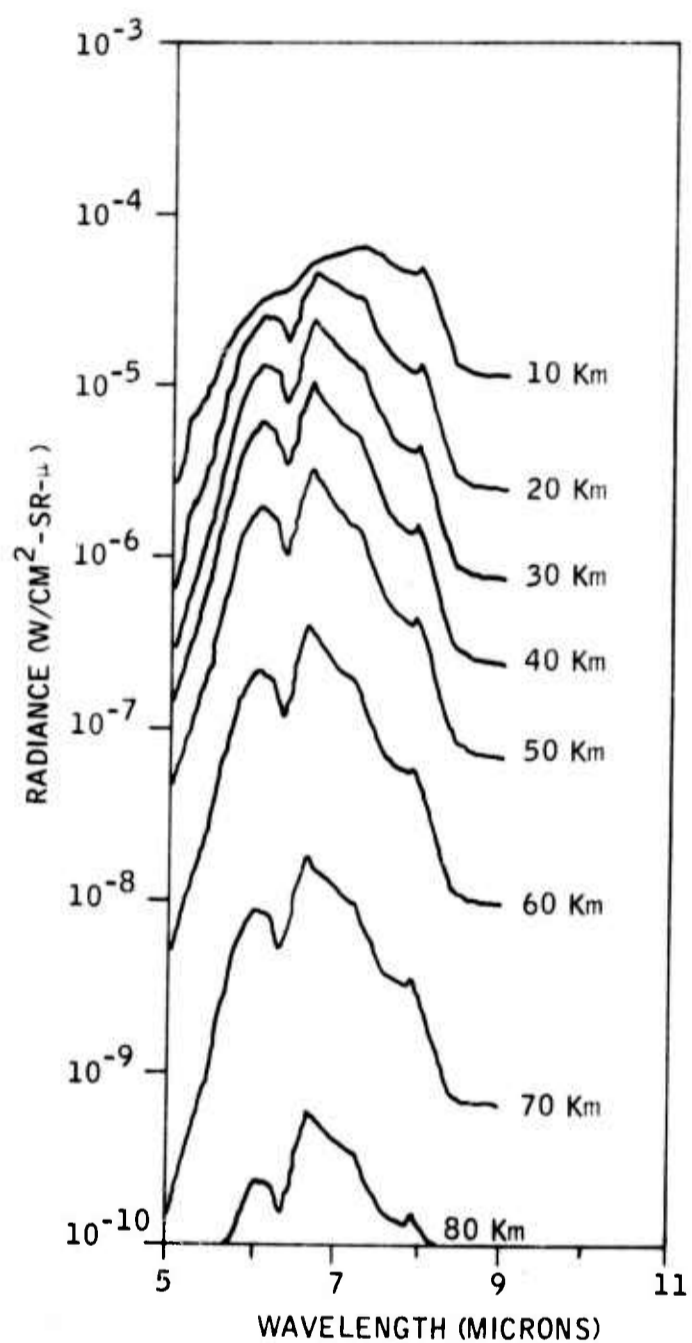
Figure E24

Atmospheric Model No. 24 (1-1-3-1)
Horizon Spectral Radiance
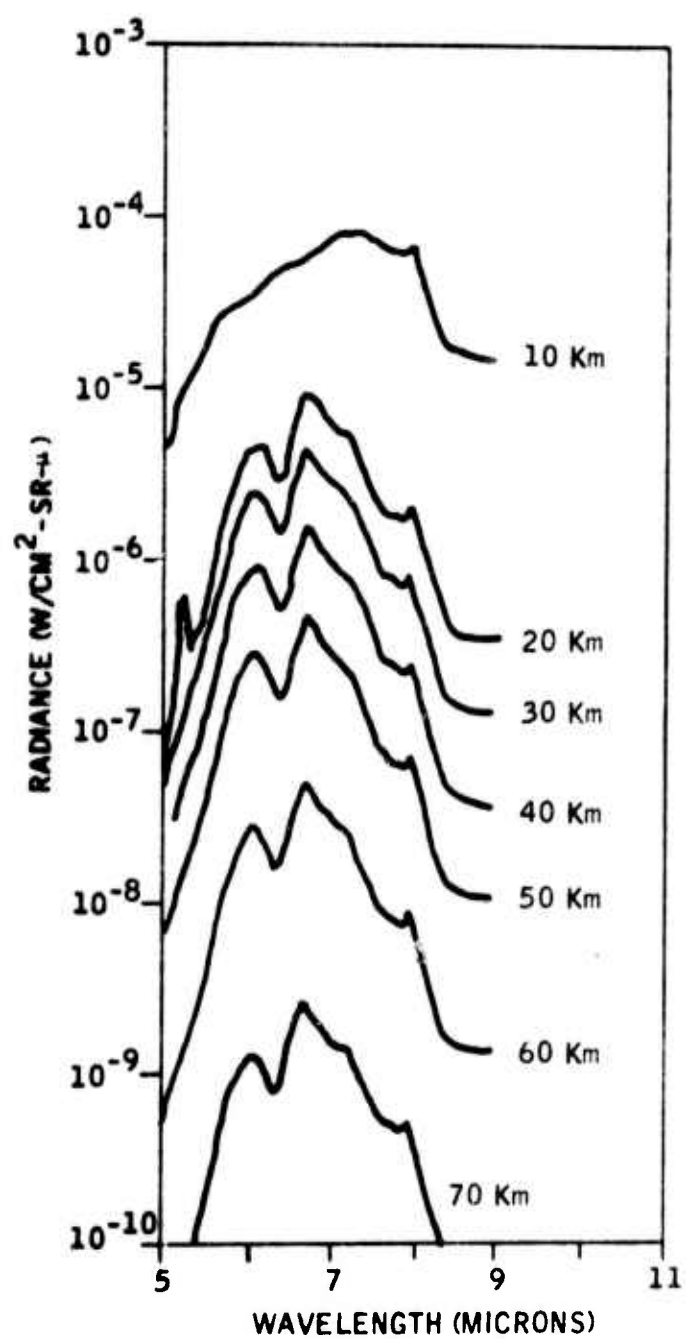U. S. Standard, Moist Stratosphere

(From 9 to 25 microns, see Model No. 1)

200

Figure E25

Atmospheric Model No. 25 (2-2-3-2)
Horizon Spectral Radiance
Tropical, Moist Stratosphere

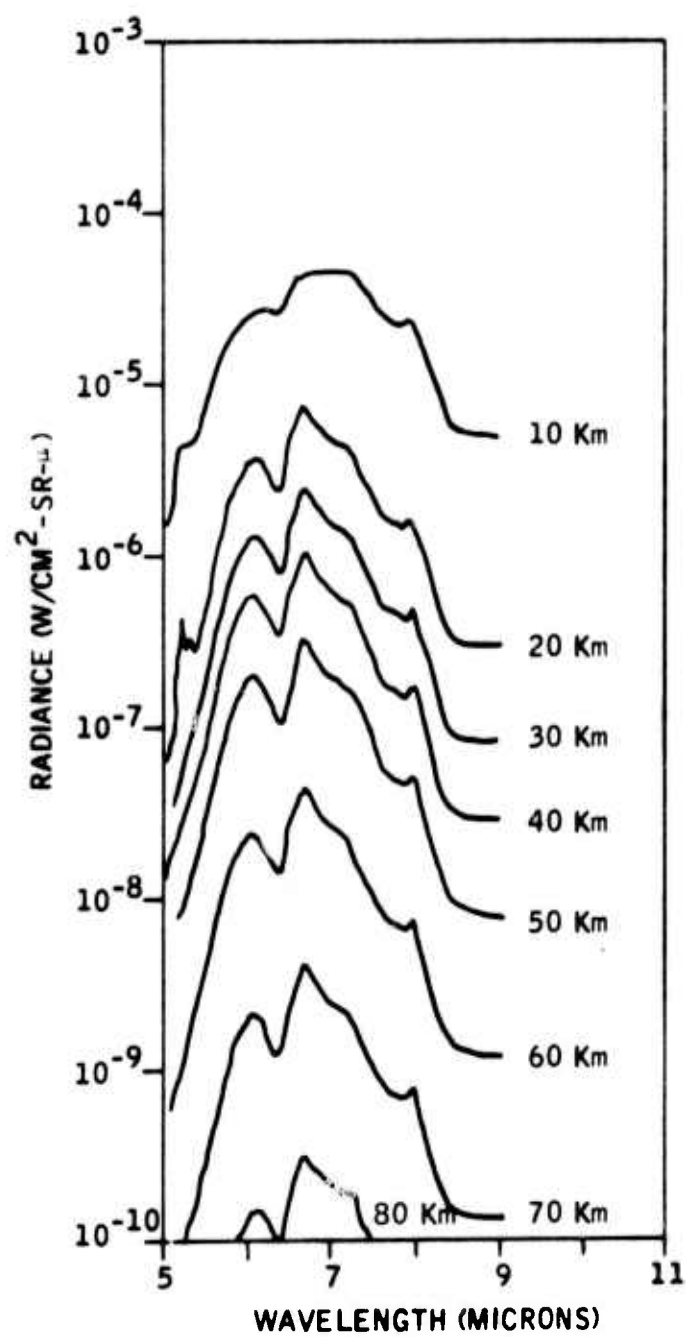(From 9 to 25 microns, see Model No. 2)

201
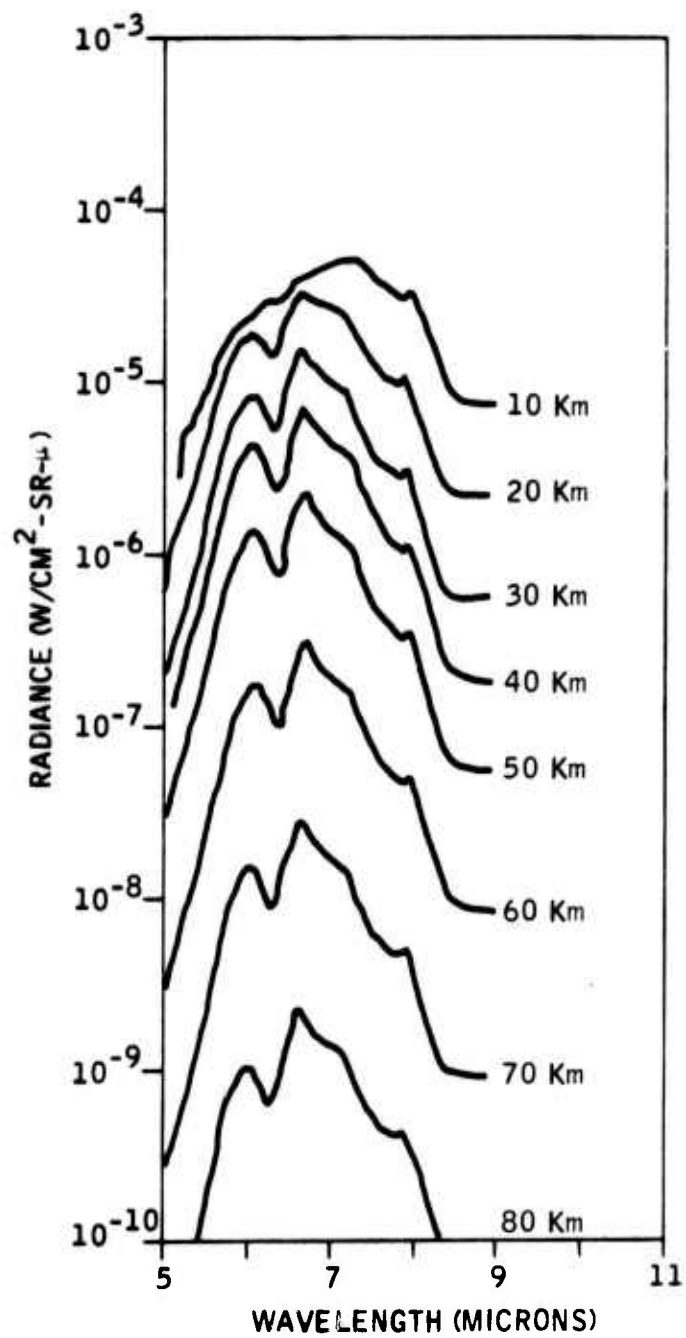
Figure E26

Atmospheric Model No. 26 (3-3-3-3)
Horizon Spectral Radiance
Mid-latitude Winter, Moist Stratosphere

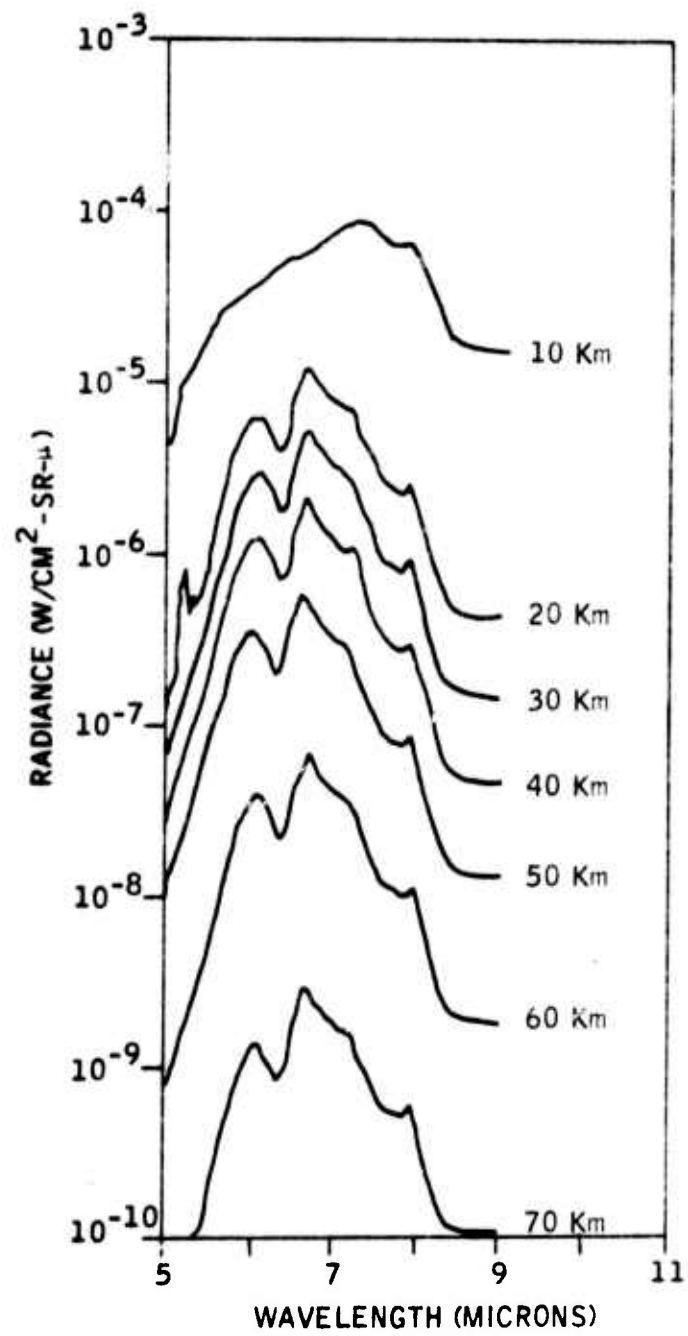(From 9 to 25 microns, see Model No. 3)

202

Figure E27

Atmospheric Model No. 27 (4-4-3-4)
Horizon Spectral Radiance
Mid-latitude Summer, Moist Stratosphere

(From 9 to 25 microns, see Model No. 4)

203

Figure E28

Atmospheric Model No. 28 (5-5-3-5)
Horizon Spectral Radiance
Arctic Winter, Moist Stratosphere

(From 9 to 25 microns, see Model No. 5)

204

Figure E29

Atmospheric Model No. 29 (6-6-3-6)
Horizon Spectral Radiance
Arctic Summer, Moist Stratosphere

(From 9 to 25 microns, see Model No. 6)

205

Figure E30

Atmospheric Model No. 30 (7-5-3-5)
Horizon Spectral Radiance
Arctic, Cold Moist Stratosphere
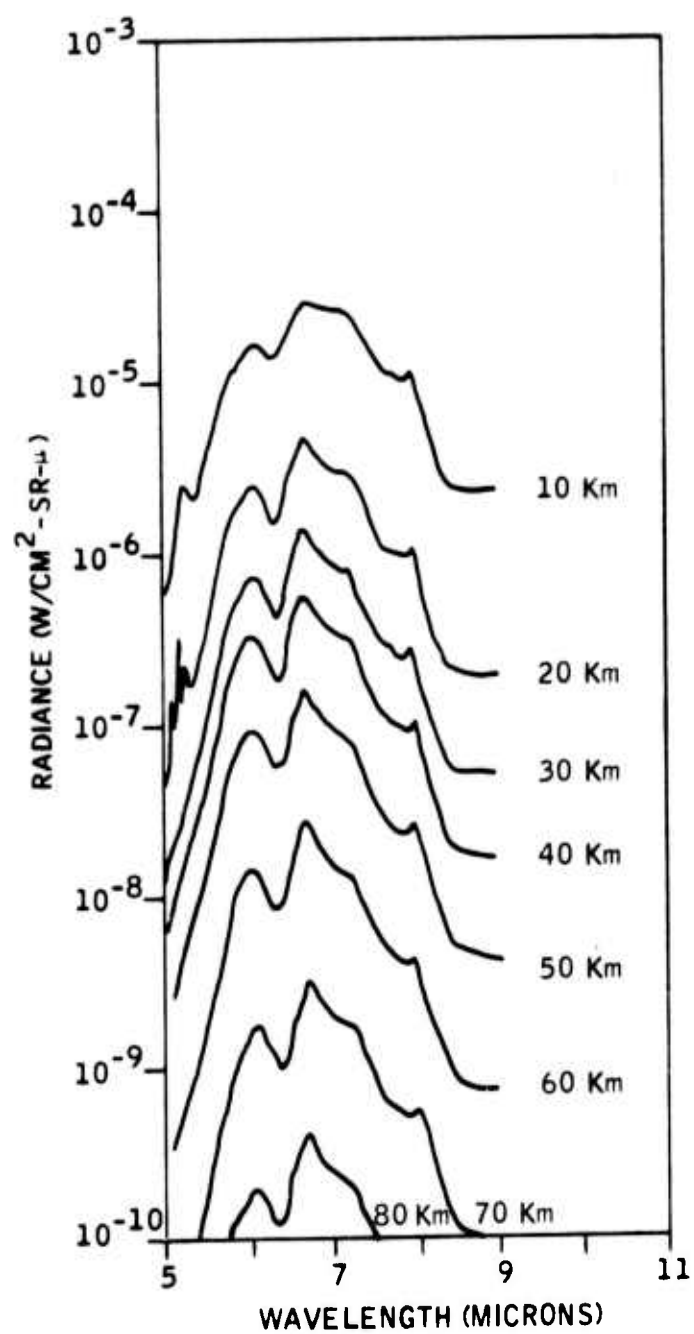
(From 9 to 25 microns, see Model No. 7)

206
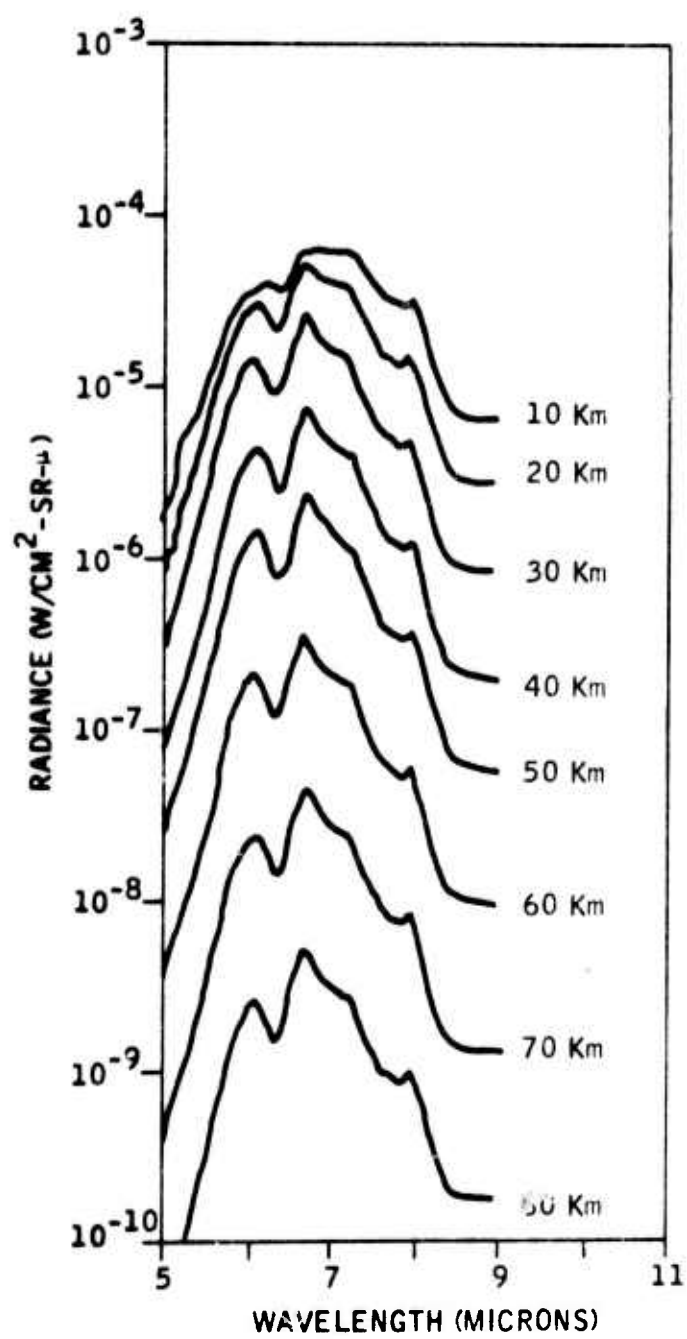
Figure E31

Atmospheric Model No. 31 (8-5-3-5)
Horizon Spectral Radiance
Arctic, Warm Moist Stratosphere

(From 9 to 25 microns, see Model No. 8)

207

Figure E32

Atmospheric Model No. 32 (1-1-2-1)
Horizon Spectral Radiance
U. S. Standard, Dry Stratosphere

(From 9 to 25 microns, see Model No. 1)

208

Figure E33

Atmospheric Model No. 33 (2-2-2-2)
Horizon Spectral Radiance
Tropical, Dry Stratosphere

(From 9 to 25 microns, see Model No. 2)

209

Figure E34

Atmospheric Model No. 34 (3-3-2-3)
Horizon Spectral Radiance
Mid-latitude Winter, Dry Stratosphere
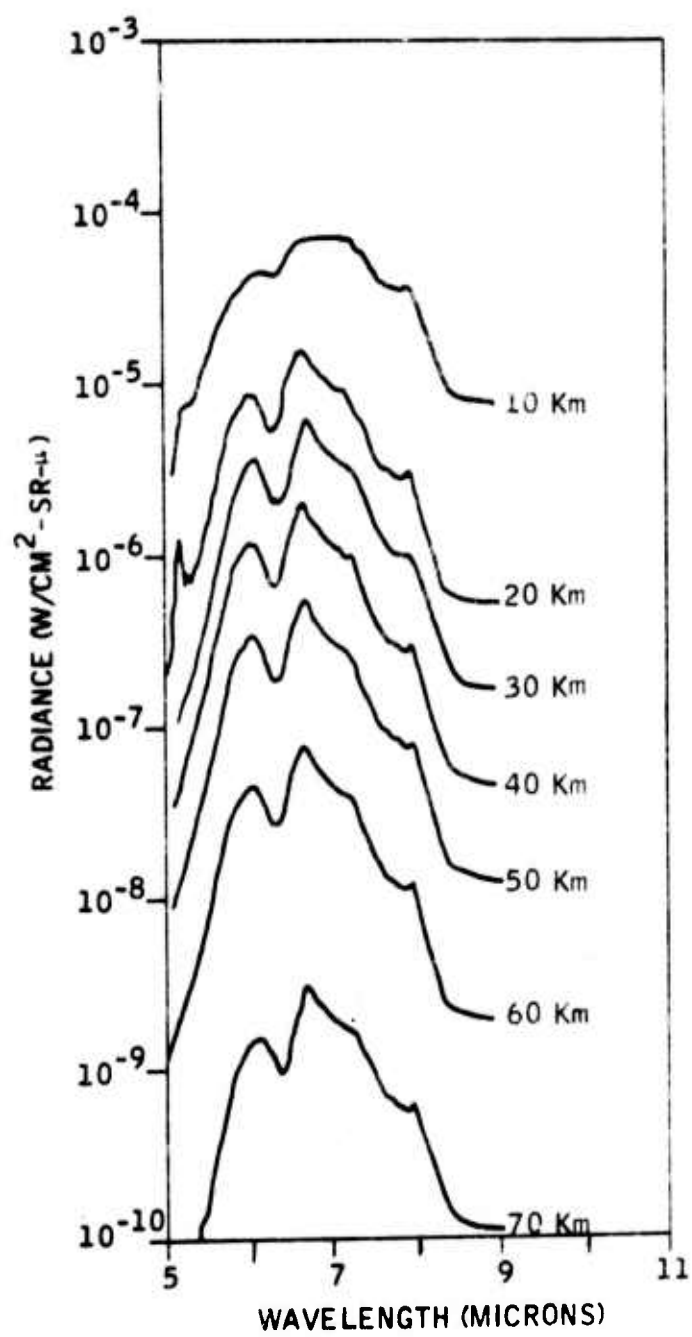
(From 9 to 25 microns, see Model No. 3)

210

Figure E35

Atmospheric Model No. 35 (4-4-2-4)
Horizon Spectral Radiance
Mid-latitude Summer, Dry Stratosphere

(From 9 to 25 microns, see Model No. 4)

211

Figure E36

Atmospheric Model No. 36 (5-5-2-5)
Horizon Spectral Radiance
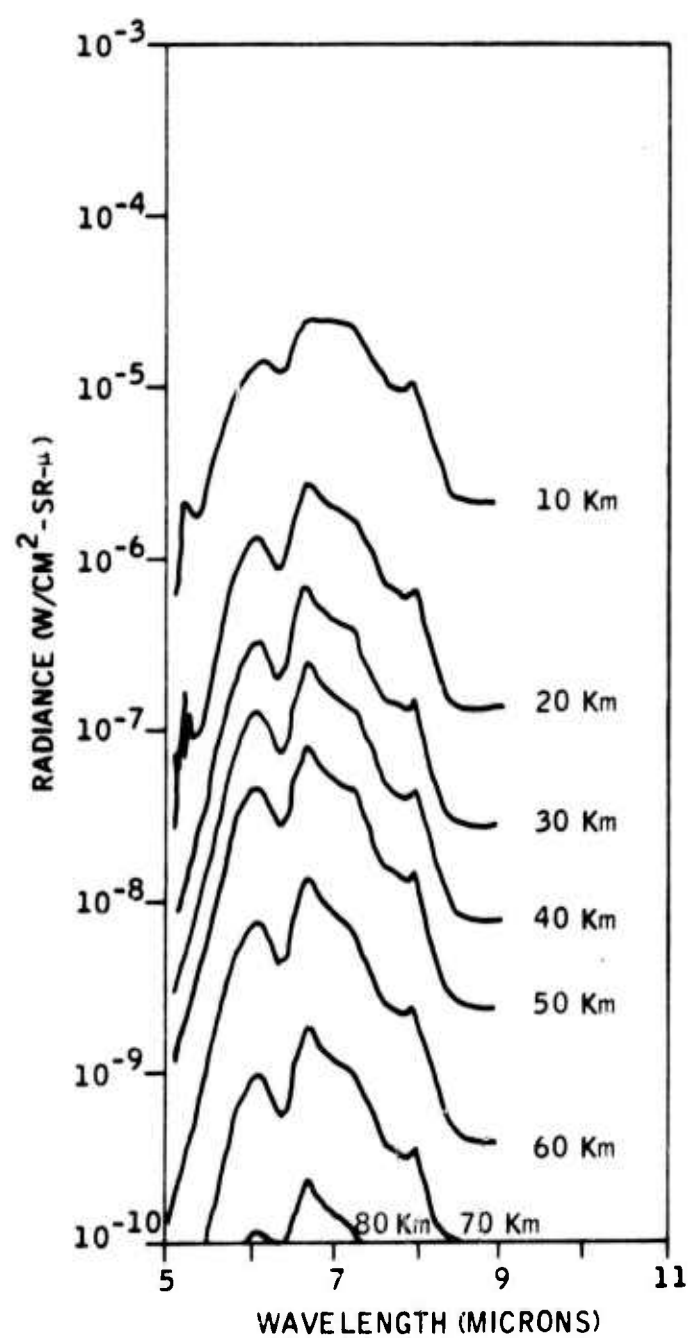Arctic Winter, Dry Stratosphere

(From 9 to 25 microns, see Model No. 5)

212

Figure E37

Atmospheric Model No. 37 (6-6-2-6)
Horizon Spectral Radiance
Arctic Summer, Dry Stratosphere

(From 9 to 25 microns, see Model No. 6)

213

Figure E38

Atmospheric Model No. 38 (7-5-2-5)
Horizon Spectral Radiance
Arctic, Cold Dry Stratosphere

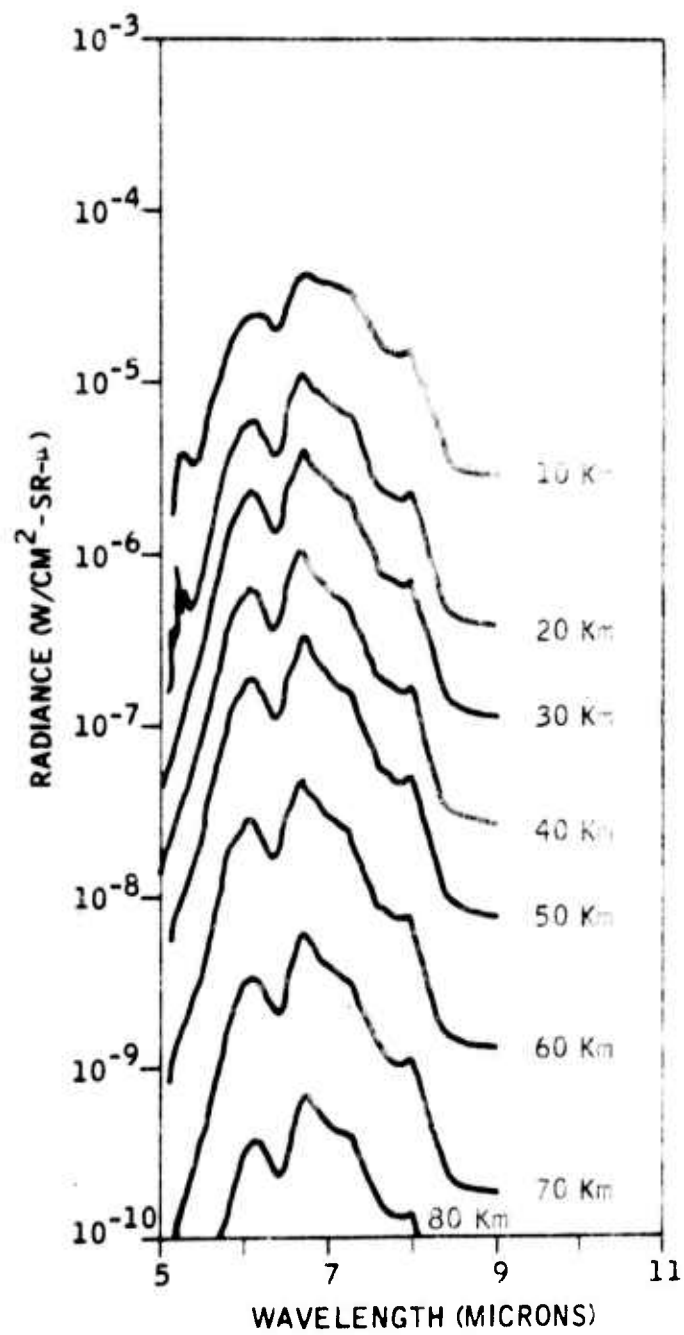(From 9 to 25 microns, see Model No. 7)

214

Figure E39

Atmospheric Model No. 39 (8-5-2-5)
Horizon Spectral Radiance
Arctic, Warm Dry Stratosphere

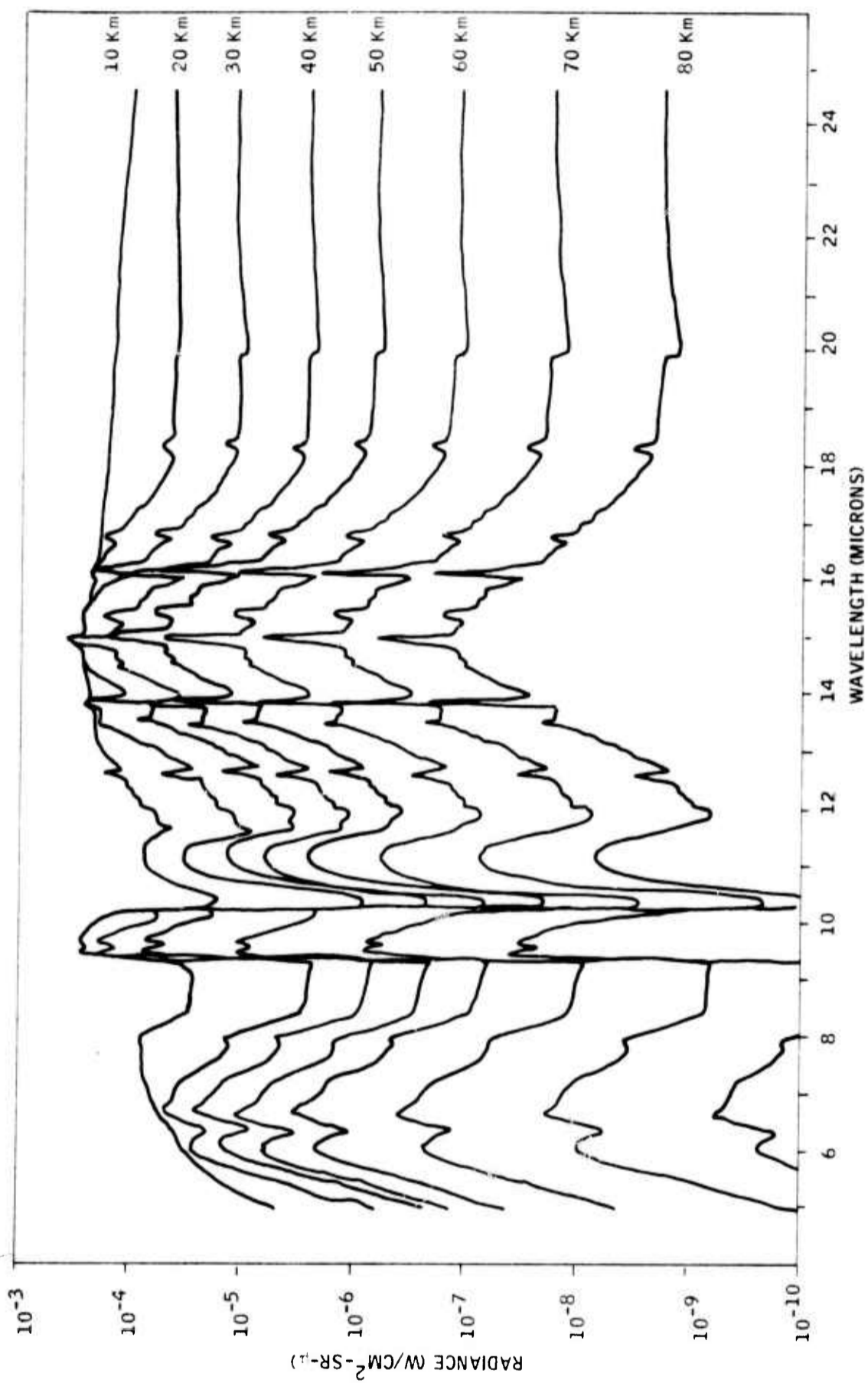(From 9 to 25 microns, see Model No. 8)

215

Figure E40

Atmospheric Model No. 40 (1-12-3-12)
Horizon Spectral Radiance
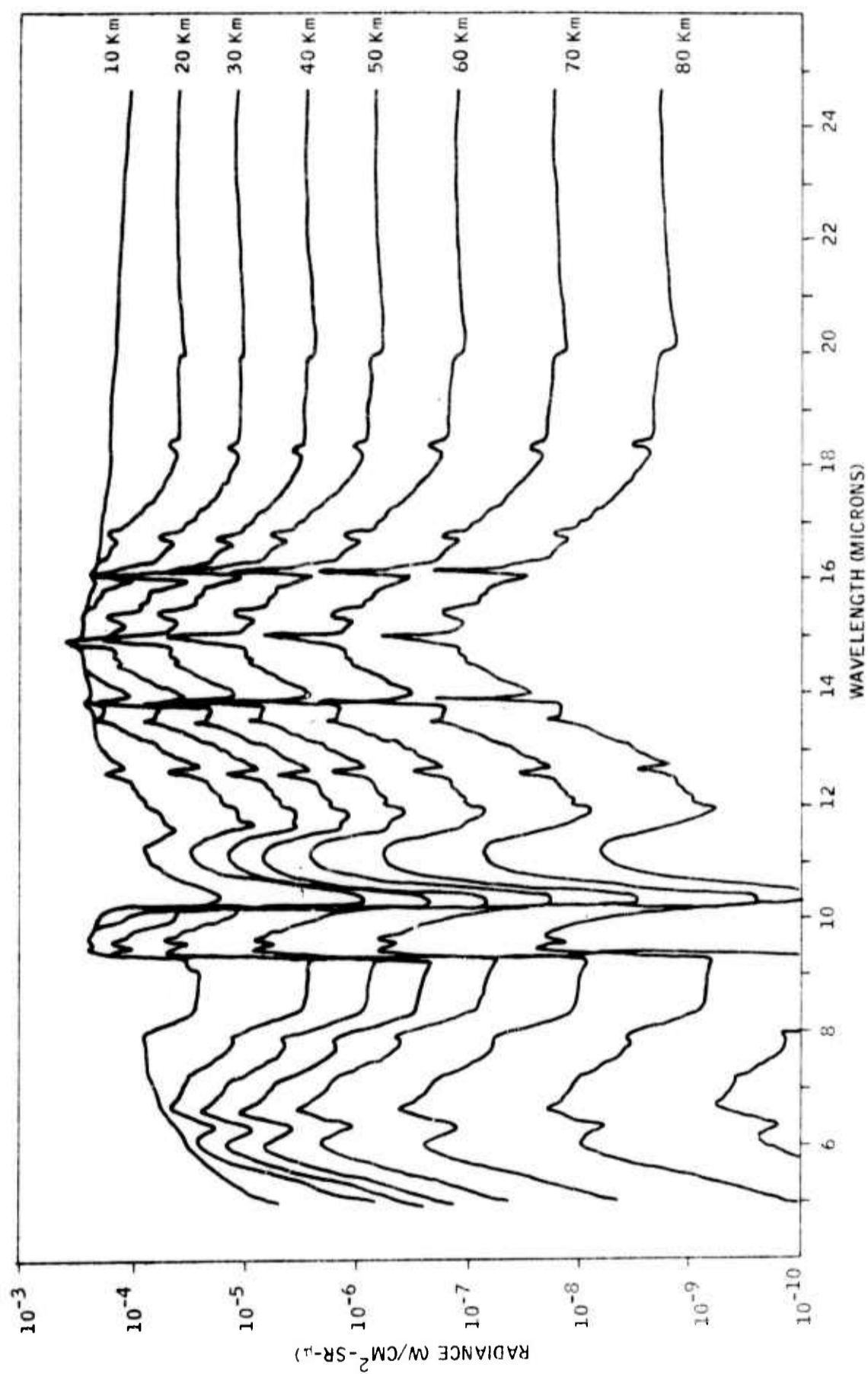U. S. Standard Atmosphere

216

Figure E41

Atmospheric Model No. 41 (1-12-3-20)
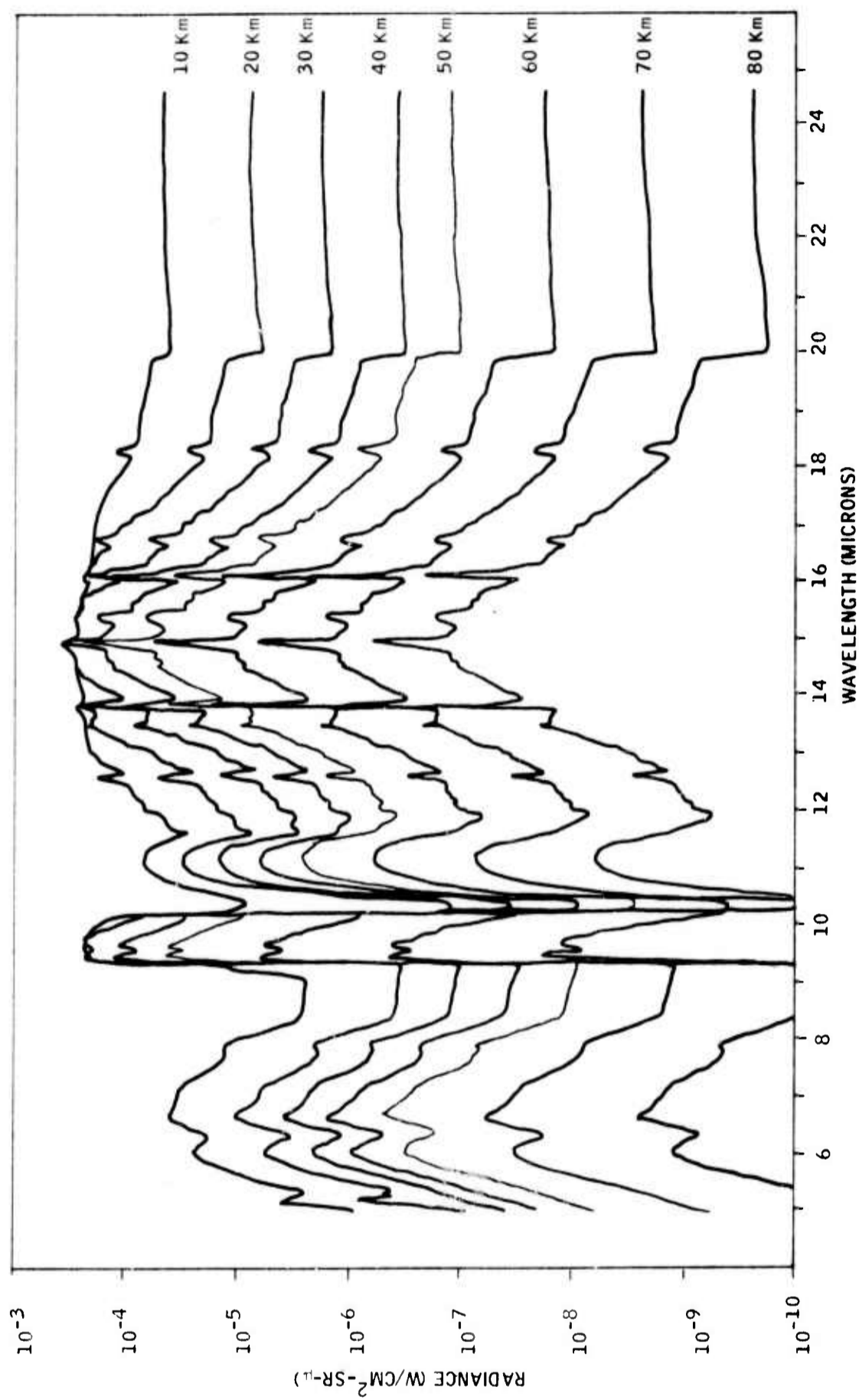Horizon Spectral Radiance
U. S. Standard Atmosphere

217

Figure E42

Atmospheric Model No. 42 (1-19-2-17)
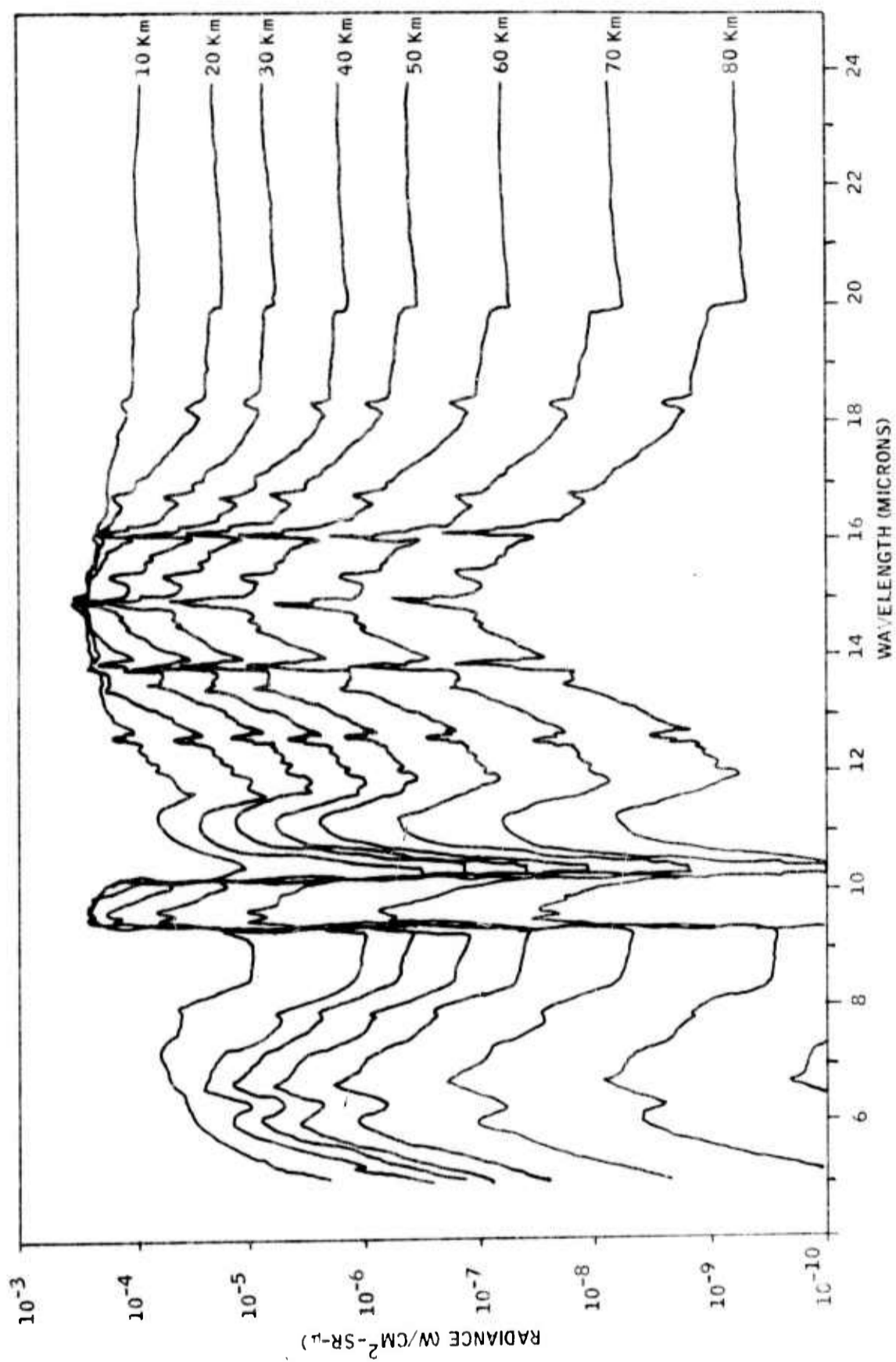Horizon Spectral Radiance
U. S. Standard Atmosphere

Figure E43

Atmospheric Model No. 43 (1-1-1-12)
Horizon Spectral Radiance
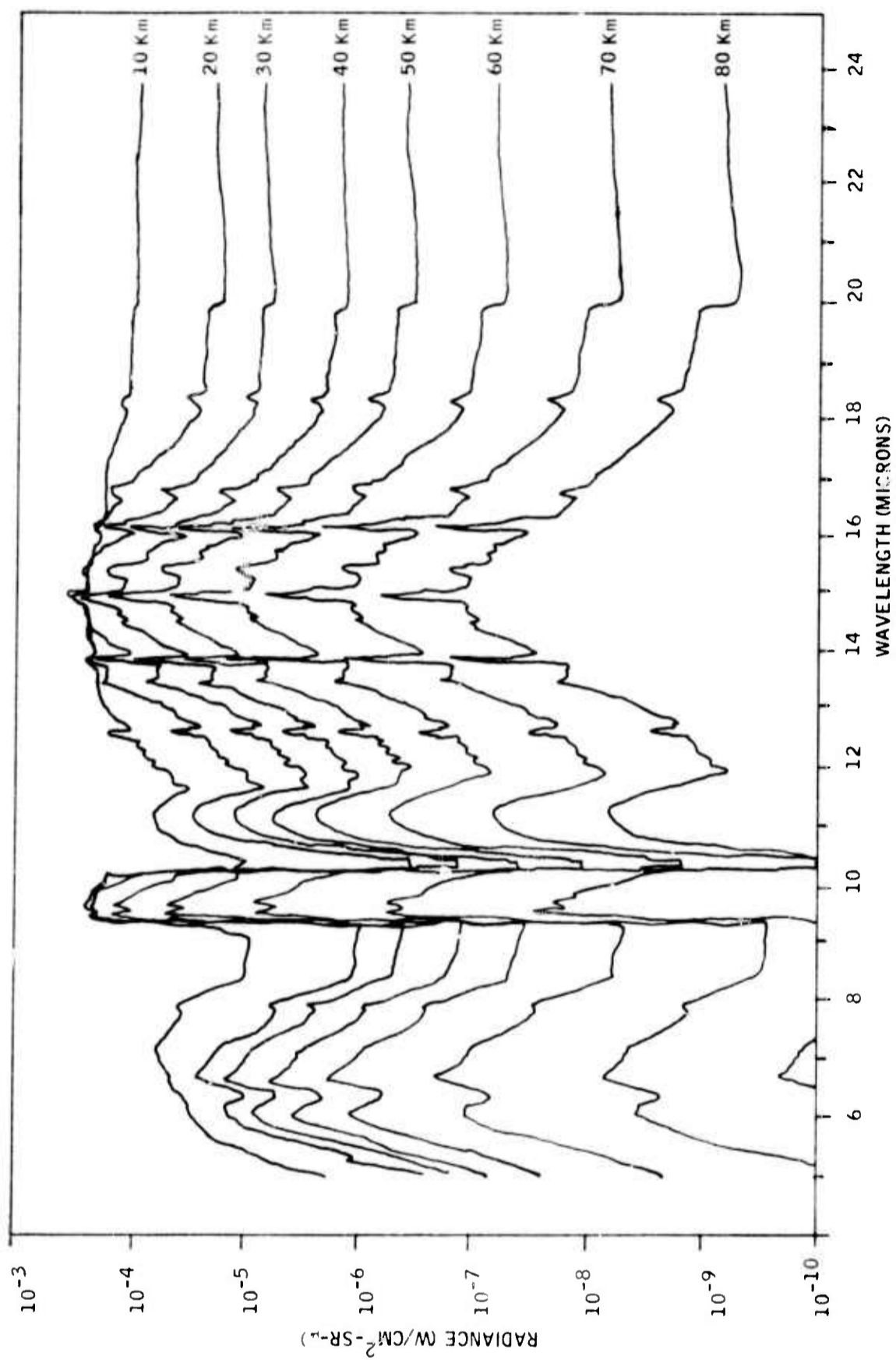U. S. Standard Atmosphere

219

Figure E44

Atmospheric Model No. 44 (1-1-1-20)
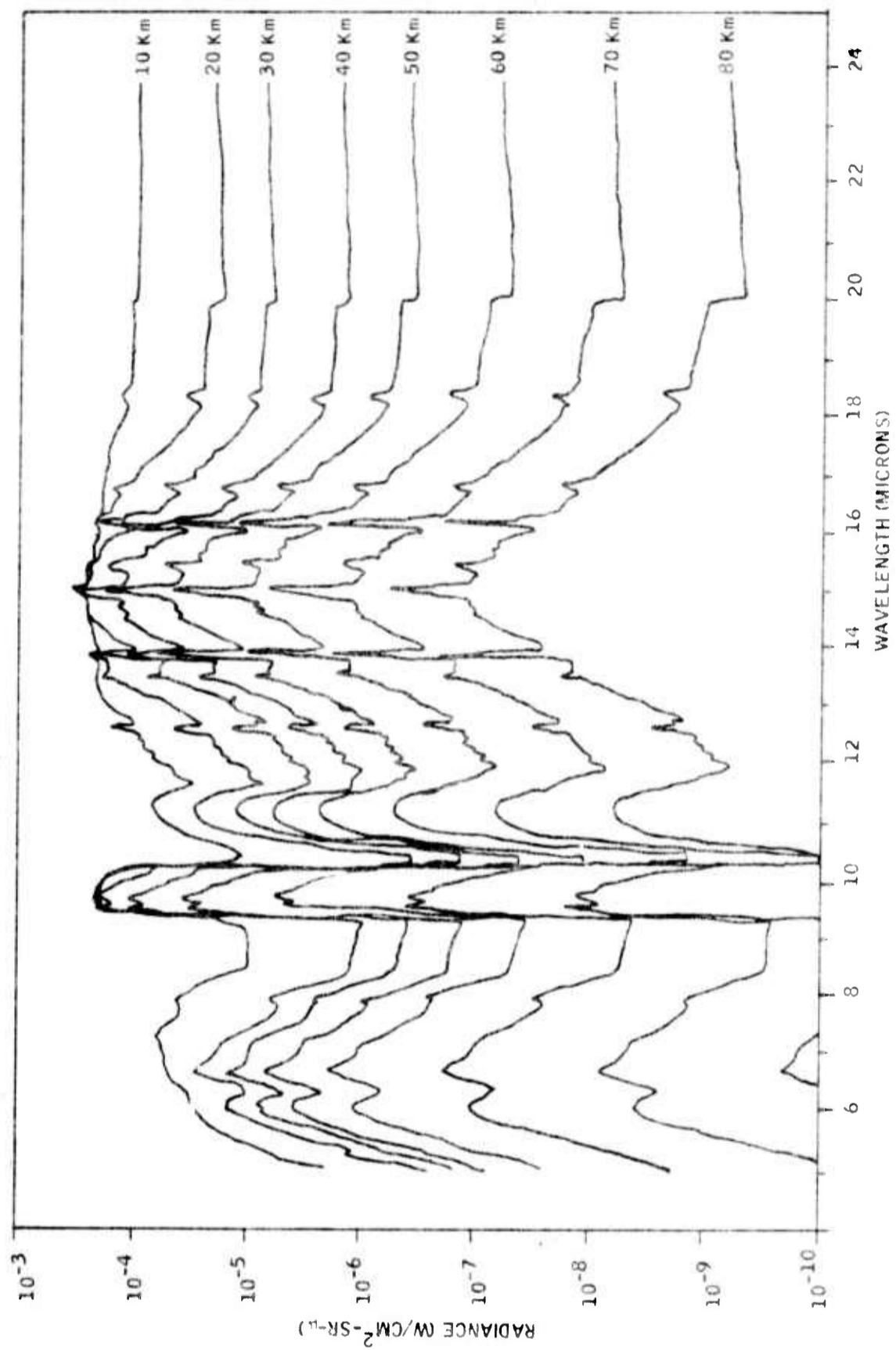Horizon Spectral Radiance
U. S. Standard Atmosphere

220

Figure E45

Atmospheric Model No. 45 (1-1-1-17)
Horizon Spectral Radiance
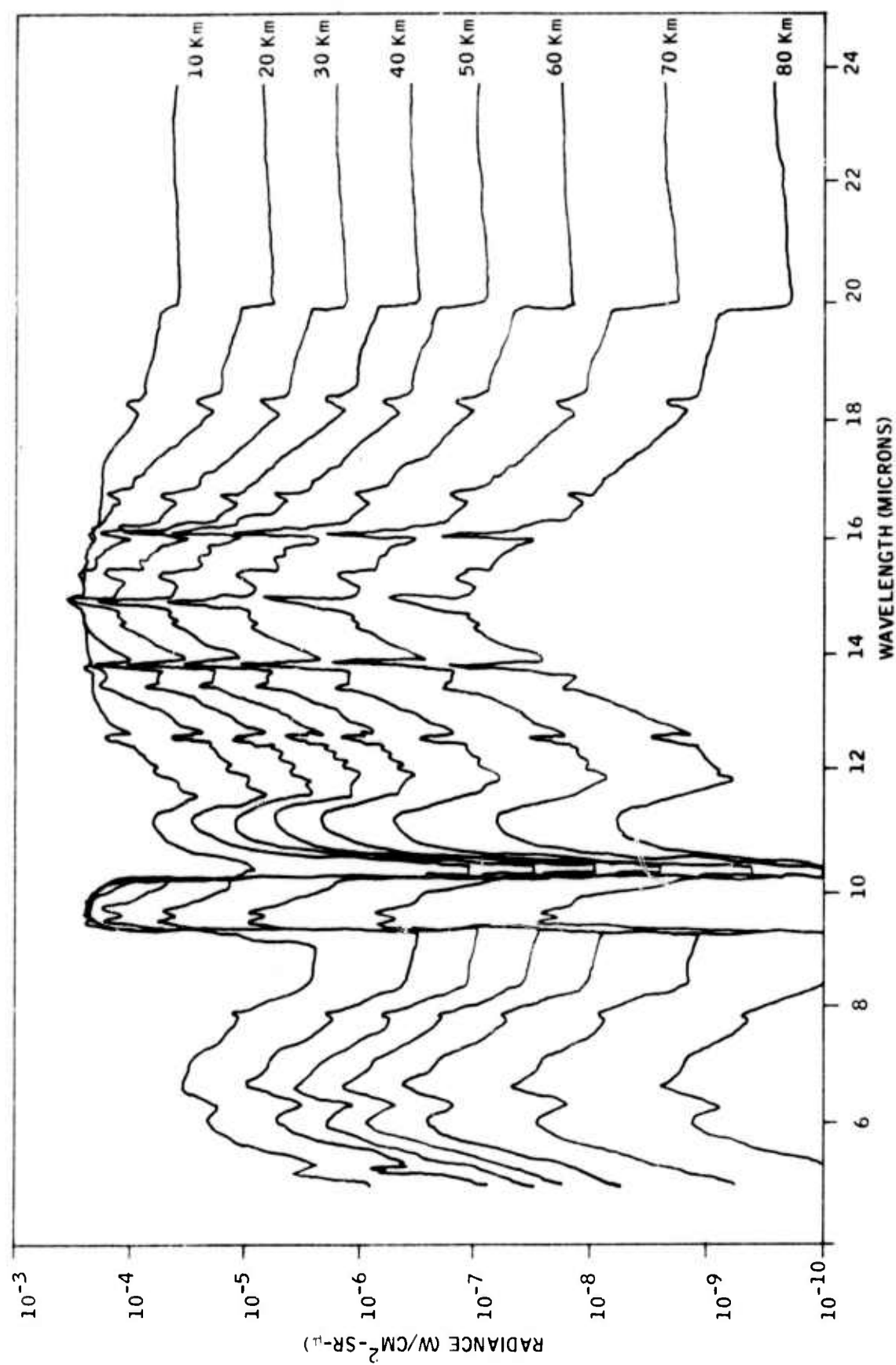U. S. Standard Atmosphere

221

Figure E46

Atmospheric Model No. 46 (1-19-2-1)
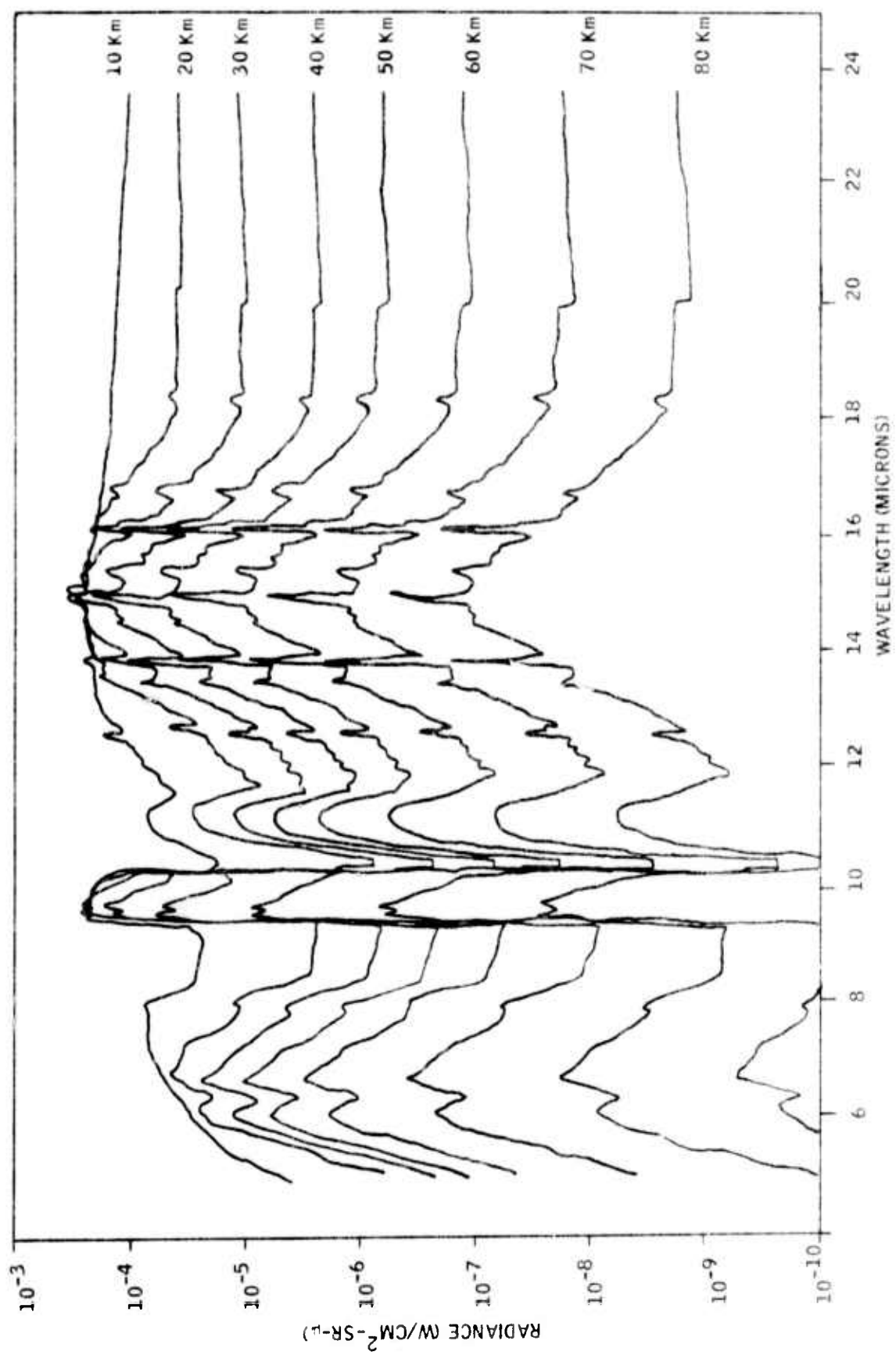Horizon Spectral Radiance
U. S. Standard Atmosphere

222

Figure E47

Atmospheric Model No. 47 (1-12-3-1)
Horizon Spectral Radiance
U. S. Standard Atmosphere

223

APPENDIX F
SPECTRAL RADIANCES FOR
UPPER ATMOSPHERE MODELS

The final goal of this study of upper atmosphere infrared radiance is the prediction of spectral radiance values at wavelengths between 5 and 25 μm for all species and for both exoatmospheric and endoatmospheric viewing. Figure F1 shows spectral limb radiances between 5 and 25 μm for tangent heights of 60 km, 80 km and 100 km. These radiances were computed by a program which is included as a subroutine in the final radiance model computer program.

For all contributions to the spectra from molecular vibration rotation bands, the total band radiances are spread out with the assumption that the rotational levels are in thermal equilibrium at a mean temperature computed for the line of sight determined by the populations of the lower vibrational level. Using this mean temperature, rotational populations are computed and wavelengths and relative intensities in emission of each line are computed. The effects of self-absorption for each line are determined from the optical thickness through Eq. 41. The sum of relative radiances corrected for optical thickness is normalized to the total band radiance and absolute line radiances computed. A further subroutine then computes the contribution of each line to the spectrum.

In the case of linear molecules, line positions are computed for 100 lines in each of the P, Q and R branches, neglecting the second rotational constant D_V, and any higher rotational constants. The effects of spin and ℓ doubling are neglected. In all cases, computed positions of lines are within 0.1 μm of accurate positions. For the water vapor 6.3 μm band, the positions and line lengths of about 450 of the strongest lines tabulated by Benedict and Calfee (1967) are used. For the ozone 9.6 μm band, mean line strengths at
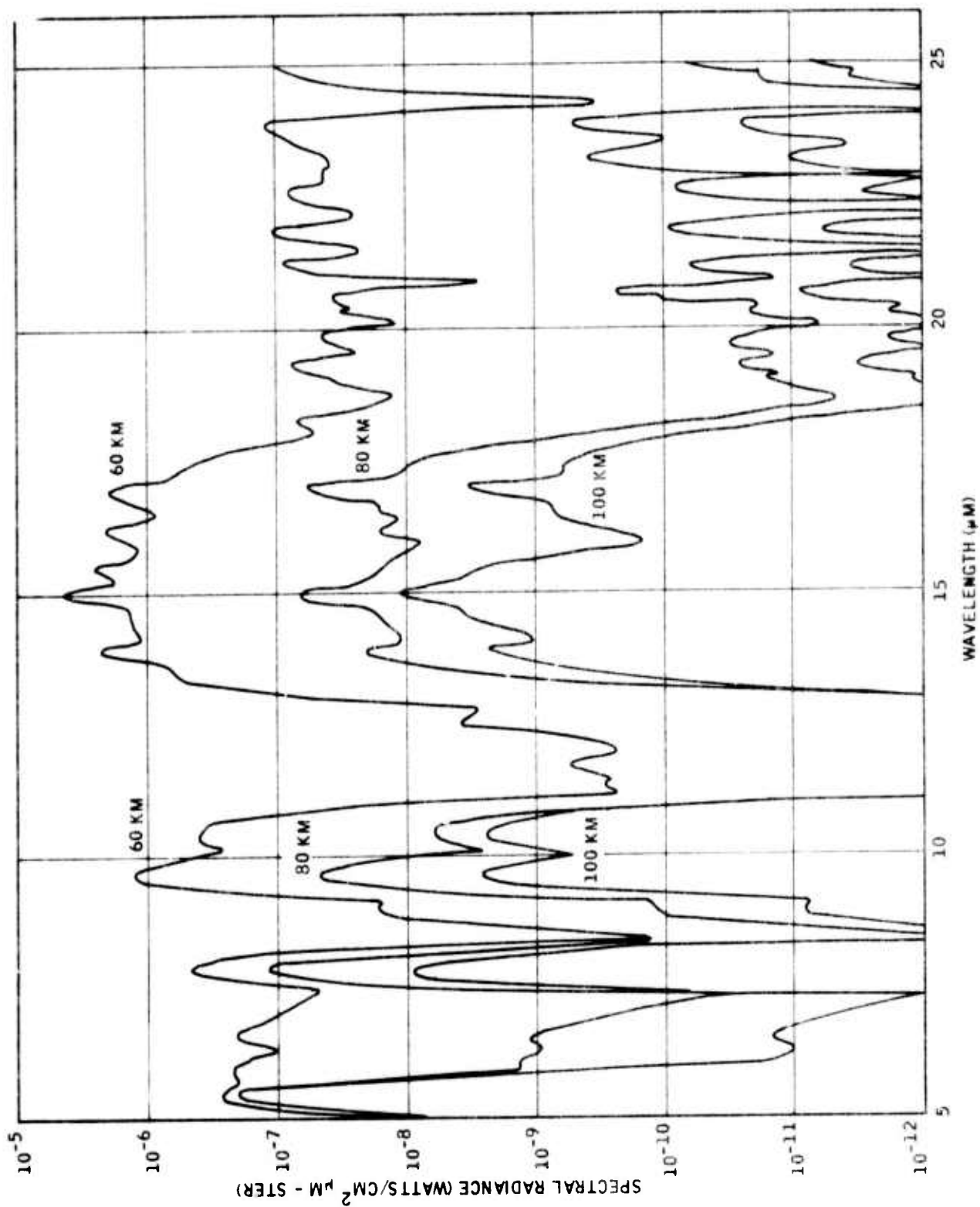
Figure F1. High Altitude Horizon Spectral Radiance

225

5 cm^{-1} determined from the tabulation of Clough and Kneizys (1965) are used, rather than attempting to include individual lines. The contribution to the spectra from water vapor rotational lines is determined from the dipole matrix elements and rotational level energies of about 250 lines between 10 and 25 μm.   Data for wavelengths longer than 12 μm were determined from the Tables of Gates, et al. (1964).   Those between 10 and 12 μm were determined from values of absorption coefficients supplied by Dr. R. McClatchey of AFCRL.

The present program computes spectra for a triangular slit function with a width at half maximum of 0.25 μm.   The appropriate subroutine may be re-written for any desired slit function.   The approximations made in the current computational model restrict computer resolution to about 0.1 μm.   At the expense of increased computation time and complexity, better resolution may be obtained.

DOCUMENT CONTROL DATA - R & D

(Security classification of title, body of abstract and indexing annotation must be entered when the overall report is classified)

1 ORIGINATING ACTIVITY *(Corporate author)*	2a. REPORT SECURITY CLASSIFICATION
Honeywell Inc. Aerospace Division Minneapolis, Minnesota 55413	Unclassified
	2b. GROUP

3 REPORT TITLE

ATMOSPHERIC RADIANCE MODELS FOR LIMB-VIEWING GEOMETRY IN THE FIVE TO TWENTY-FIVE MICRON SPECTRAL REGION (U)

4 DESCRIPTIVE NOTES *(Type of report and inclusive dates)*

Scientific Interim

5 AUTHOR(S) *(First name, middle initial, last name)*

Victor L. Corbin   Fred B. House   George E. Oppel
Alexander Dalgarno Pedro Lilienfeld
Thomas C. Deggs   George Ohring

6 REPORT DATE	7a. TOTAL NO. OF PAGES	7b. NO. OF REFS
March 1970	238	112

8a. CONTRACT OR GRANT NO. ARPA Order No	9a. ORIGINATOR'S REPORT NUMBER(S)
F19628-68-C-0258 1366	40244-SR1
b PROJECT, TASK, WORK UNIT NOS. 8692-n/a-n/a	
c DOD ELEMENT 62301D	9b. OTHER REPORT NO(S) *(Any other numbers that may be assigned this report)*
d. DOD SUBELEMENT 9E50	AFCRL-69-0552

10 DISTRIBUTION STATEMENT

Each transmittal of this document outside the Department of Defense must have prior approval of AFCRL (CROR), L.G. Hanscom Field, Bedford, Massachusetts 01730.

11 SUPPLEMENTARY NOTES	12 SPONSORING MILITARY ACTIVITY
This research was supported by Advanced Research Projects Agency.	Air Force Cambridge Research Laboratories (CRO), L.G. Hanscom Field, Bedford, Massachusetts 01730

13 ABSTRACT

The infrared radiance arising from the earth's limb for altitudes from sea level to 500 kilometers and within the spectral limits of 5 to 25 microns was determined from theoretical calculations. The atmosphere was divided into two altitude regimes: the lower atmosphere (below 70 kilometers) and the upper atmosphere (above 70 kilometers). The lower limb models were developed from the University of Michigan computer program with modifications, including the addition of a model for nitric acid. Spectral radiances were determined as a function of geometrical, geographical, and temporal parameters. Emphasis was placed on developing limb radiance models for the upper atmosphere, including identification of active molecular species in the infrared, the specification of their abundances, and their wavelengths of emission. In addition, particulate material sources, including infrared radiation arising from dust particles and noctilucent clouds, and uncertainties in atmospheric parameters, were considered.

DD FORM **1473** REPLACES DD FORM 1473, 1 JAN 54, WHICH IS OBSOLETE FOR ARMY USE.

14 KEY WORDS	LINK A		LINK B		LINK C	
	ROLE	WT	ROLE	WT	ROLE	WT
NONE						

KEY WORDS	LINK A		LINK B		LINK C	
	ROLE	WT	ROLE	WT	ROLE	WT